JULIUS-MAXIMILIANS-UNIVERSITÄT WÜRZBURG

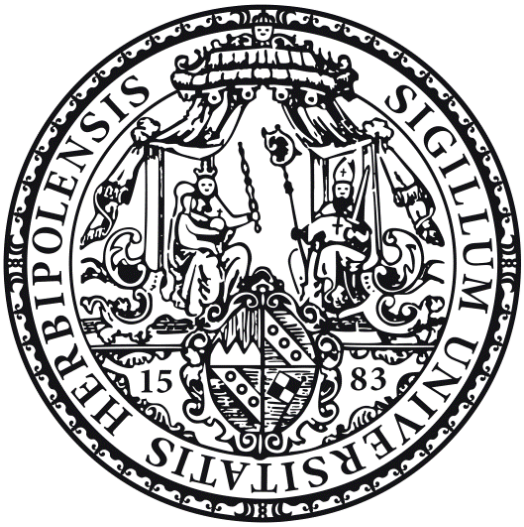

EARTH-ABUNDANT METAL-CATALYZED AND TRANSITION METAL-FREE BORYLATION OF ARYL HALIDES

Dissertation zur Erlangung des naturwissenschaftlichen Doktorgrades

der Julius-Maximilians-Universität Würzburg

vorgelegt von

Laura Kuehn

aus Hagen

Würzburg 2020

Eingereicht bei der Fakultät für Chemie und Pharmazie der Julius-Maximilians-Universität Würzburg am:

_____

Gutachter der schriftlichen Arbeit

1. Gutachter: Prof. Dr. Dr. h. c. Todd B. Marder

2. Gutachter: Prof. Dr. Udo Radius

Prüfer des öffentlichen Promotionskolloquiums

1. Prüfer: Prof. Dr. Dr. h. c. Todd B. Marder

2. Prüfer: Prof. Dr. Udo Radius

3. Prüfer: _____

Datum des öffentlichen Promotionskolloquiums:

_____

Die Experimente zur vorliegenden Arbeit wurden in der Zeit von November 2016 bis Juli 2020 am Institut für Anorganische Chemie der Julius-Maximilians-Universität Würzburg unter der Anleitung von Prof. Dr. Dr. h. c. Todd B. Marder und Prof. Dr. Udo Radius durchgeführt.

AFFIDAVIT

I hereby confirm that my thesis entitled “Earth-Abundant Metal-Catalyzed and Transition Metal-Free Borylation of Aryl Halides” is the result of my own work. I did not receive any help or support from commercial consultants. All sources and/or materials applied are listed and specified in the thesis.

Furthermore, I confirm that this thesis has not yet been submitted as part of another examination process neither in identical nor in similar form.

Würzburg, 01.07.2020 _____

EIDESSTATTLICHE ERKLÄRUNG

Hiermit erkläre ich an Eides statt, die Dissertation „Earth-Abundant Metal-Catalyzed and Transition Metal-Free Borylation of Aryl Halides“ eigenständig, d.h. insbesondere selbstständig und ohne Hilfe eines kommerziellen Promotionspartners angefertigt und keine anderen als die von mir angegebenen Quellen und Hilfsmittel verwendet zu haben.

Ich erkläre außerdem, dass die Dissertation weder in gleicher noch in ähnlicher Form bereits in einem anderen Prüfungsverfahren vorgelegen hat.

Würzburg, 01.07.2020 _____

LIST OF PUBLICATIONS

The publications listed below are partly reproduced in this dissertation with permission from the respective publisher. The table itemizes at which position in this work, each publication has been reproduced.

Publication	Position
L. Kuehn, D. G. Jammal, K. Lubitz, T. B. Marder, U. Radius, *Stoichiometric and Catalytic Aryl–Cl Activation and Borylation using NHC-stabilized Nickel(0) Complexes, Chem. Eur. J.* **2019***, 25,* 9514-9521.	Chapter 2
L. Kuehn, M. Huang, U. Radius, T. B. Marder, *Copper-Catalysed Borylation of Aryl Chlorides*, *Org. Biomol. Chem.* **2019**, *17*, 6601-6606.	Chapter 3

Further publications:

A. F. Eichhorn, L. Kuehn, T. B. Marder, U. Radius, *Facile Insertion of a Cyclic Alkyl(Amino) Carbene Carbon into the B–B Bond of Diboron(4) Reagents, Chem. Commun*. **2017**, *53*, 11694-11696.

L. Kuehn, A. F. Eichhorn, T. B. Marder, U. Radius, *Copper(I) Complexes of N-Alkyl-Substituted N-Heterocyclic Carbenes, J. Organomet. Chem.* **2019**, *881*, 25-33.

L. Kuehn, M. Stang, S. Würtemberger-Pietsch, A. Friedrich, H. Schneider, U. Radius, T. B. Marder, *FBpin and its Adducts and their Role in Catalytic Borylations*, *Faraday Discuss.* **2019**, *220*, 350-363.

J. H. J. Berthel, L. Tendera, M. W. Kuntze-Fechner, L. Kuehn, U. Radius, *NHC-Stabilized Nickel Olefin, Dialkyl, and Dicyanido Complexes*, *Eur. J. Inorg. Chem.* **2019**, 3061-3072.

L. Kuehn, A. F. Eichhorn, D. Schmidt, T. B. Marder, U. Radius, *NHC-Stabilized Copper(I) Aryl Complexes and their Transmetalation Reaction with Aryl Halides, J. Organomet. Chem.* **2020**, DOI: 10.1016/j.jorganchem.2020.121249.

TABLE OF CONTENTS

CHAPTER 1

NICKEL-CATALYZED BORYLATION REACTIONS

1 NICKEL-CATALYZED BORYLATION REACTIONS

1.1 C–X BOND BORYLATION OF ARYL AND BENZYLIC HALIDES AND PSEUDOHALIDES

In 2000, Tour and co-workers reported the first nickel-catalyzed borylation of aryl halides.[1] They modified the Pd-catalyzed borylation process developed by Miyaura *et al.*,[2] to use a less expensive nickel catalyst and HBpin for the bis- and trisborylation of aryl bromides. This multiborylation requires catalytic amounts of [Ni(dppp)$(Cl)_2$]/dppp, and NEt_3 as the base, in toluene at 100 °C.[1] Further investigations by Percec *et al.* on Ni-catalyzed monoborylation using these conditions as a starting point, led to a procedure for the pinacolborylation and the neopentylglycolborylation of aryl bromides and aryl iodides that utilizes *in situ* prepared HBpin and HBneop. The scope of this reaction was demonstrated with a wide range of substrates. The resulting aryl neopentylglycol boronic esters were subsequently applied in a [Ni(dppe)$(Cl)_2$]/dppe-catalyzed Suzuki-Miyaura cross-coupling reaction with aryl halides (X = I, Br, Cl), which led to biaryls in good to excellent yields (Scheme 1.1).[3]

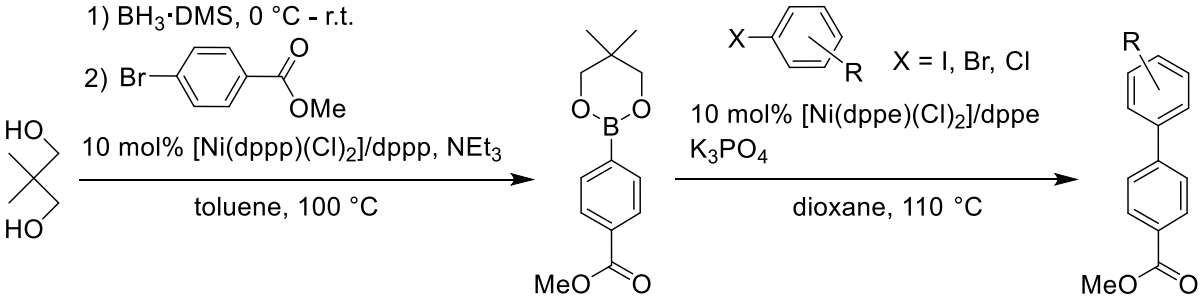

Scheme 1.1 $NiCl_2$(dppp)/dppp-catalyzed borylation of aryl bromides and a subsequent [Ni(dppe)$(Cl)_2$]/dppe-catalyzed Suzuki-Miyaura cross-coupling reaction with aryl halides.[3]

Further investigations revealed that a mixed ligand system consisting of a mixture of [$NiCl_2$(dppp)] and 1,2-bis(diphenylphosphino)ferrocene (dppf) as the co-ligand is very efficient for the borylation of aryl chlorides with *in situ* prepared HBneop (Scheme 1.2a).[4] Furthermore, this system as well as [Ni(dppp)$(Cl)_2$]/PPh_3 turned out to be an effective catalyst for the borylation of aryl iodides, bromides and chlorides bearing electron-rich and electron-deficient *ortho*-substituents.[5] The mixed-ligand system [Ni(dppp)$(Cl)_2$]/dppf combined with the reducing effect of zinc dust and of other metals

showed a considerable acceleration of the reaction rate and an increase of the yield. A variety of electron-rich and electron-deficient aryl halides, including aryl chlorides and pseudo halides (aryl mesylates and tosylates), were efficiently borylated in 1 h or less (Scheme 1.2b).[6, 7] It was proposed that the reduction of the precatalyst [Ni(dppp)(Cl)$_2$]/dppf and of the oxidative addition intermediate are rate-determining steps in this reaction, which explains the acceleration of the reaction with metallic reductants.[6]

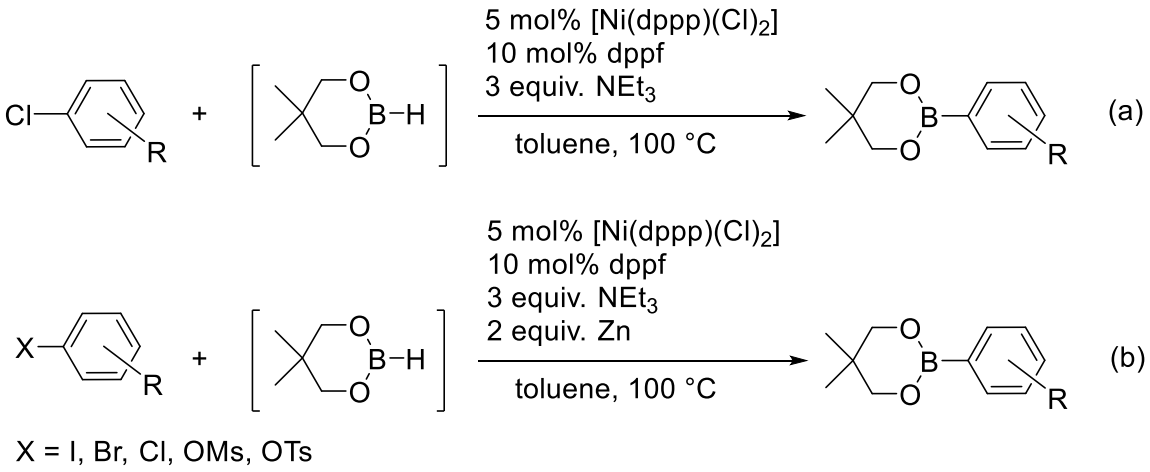

Scheme 1.2 (a) [Ni(dppp)(Cl)$_2$]/dppf-catalyzed borylation of aryl chlorides.[4] (b) [Ni(dppp)(Cl)$_2$]/dppf-catalyzed borylation of aryl halides and pseudo halides accelerated by zinc dust.[6, 7]

In the same year, Murata *et al.* reported a borylation of aryl chlorides using HBpin as the boron source and catalytic amounts of [Ni(dppp)(Cl)$_2$]/Bu$_4$NBr. However, this borylation is only successful for electron-deficient aryl chlorides.[8] In 2012, the same group introduced a nickel-catalyzed borylation of aryl iodides and bromides using the uncommon 4,4,6-trimethyl-1,3,2-dioxaborinane (neohexylglycolborane)[9] and *in situ* prepared 5-(*tert*-butyldimethyl-siloxymethyl)-5-methyl-1,3,2-dioxaborinane[10] as the boron sources (Scheme 1.3). In the presence of [Ni(dppp)(Cl)$_2$] as the catalyst and NEt$_3$ as the base, aryl bromides were borylated in yields up to 94%. However, the reaction suffered from the formation of small amounts of hydrodehalogenated arene byproducts. Utilizing an additional phosphine as a co-ligand (e.g. dppf) improved the yields and the selectivity, which is in line with the beneficial usage of the mixed ligand system reported earlier by Percec.[4] Interestingly, a [Ni(dppf)(Cl)$_2$]-based catalyst system provided poor yields, revealing that ligand exchange is limited and that the benefit of dppf is achieved only as a co-ligand.[4, 9] However, the role of the additional two equivalents of the second ligand remains unclear.

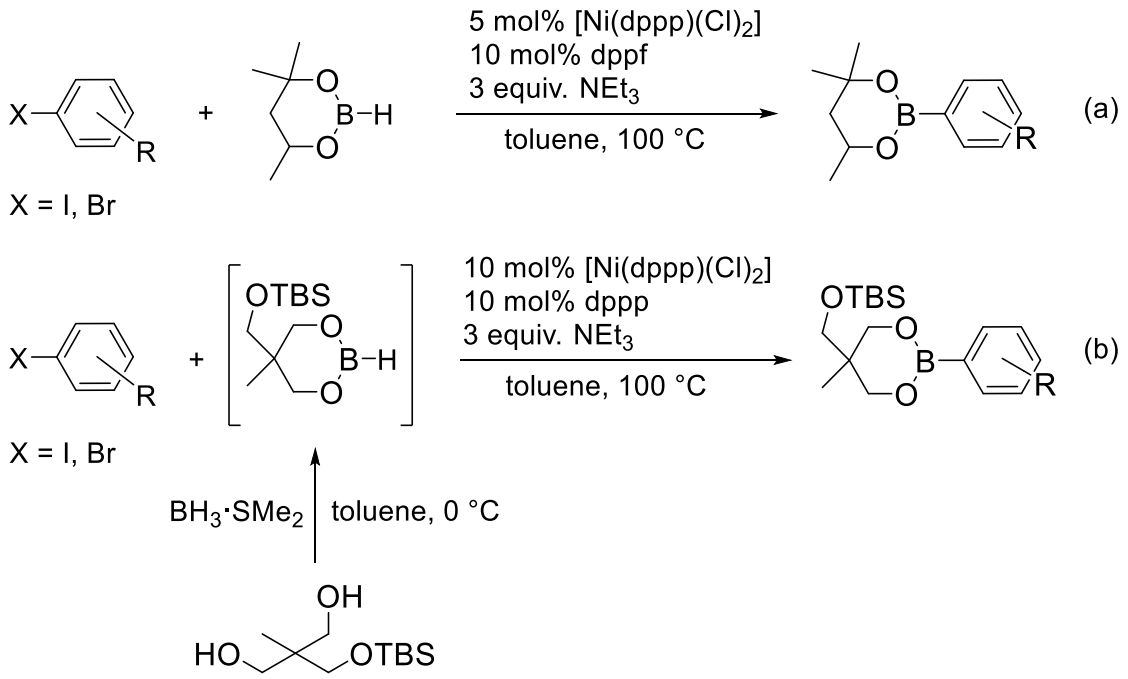

Scheme 1.3 (a) [Ni(dppp)(Cl)$_2$]/dppf-catalyzed borylation of aryl iodides and bromides using 4,4,6-trimetyl-1,3,2-dioxaborinane as the borylation reagent.[9] (b) [Ni(dppp)(Cl)$_2$]/dppp-catalyzed borylation of aryl iodides and bromides using *in situ* prepared 5-(*tert*-butyldimethylsiloxymethyl)-5-methyl-1,3,2-dioxaborinane as the borylation reagent.[10]

In the course of their studies on the pincer nickel-catalyzed borylation of bromobenzene, Mindiola and co-workers isolated and characterized the first nickel boryl complex [Ni(PNP)(Bcat)].[11] The boryl ligand of this complex was transferred to bromobenzene in the presence of $NaBH_4$ at 120 °C to yield Ph–Bcat. The mechanism proposed for this reaction is shown in Scheme 1.4. Starting from [Ni(PNP)(Br)] **1.4-III**, the reaction with $NaBH_4$ leads to the nickel hydride complex [Ni(PNP)(H)] **1.4-I** which is converted into the boryl complex [Ni(PNP)(Bcat)] **1.4-II** and hydrogen upon the treatment with HBcat. In the following step, the boryl fragment is transferred to bromobenzene yielding the aryl boronic ester and the corresponding nickel bromide **1.4-III**, which closes the catalytic cycle.[11]

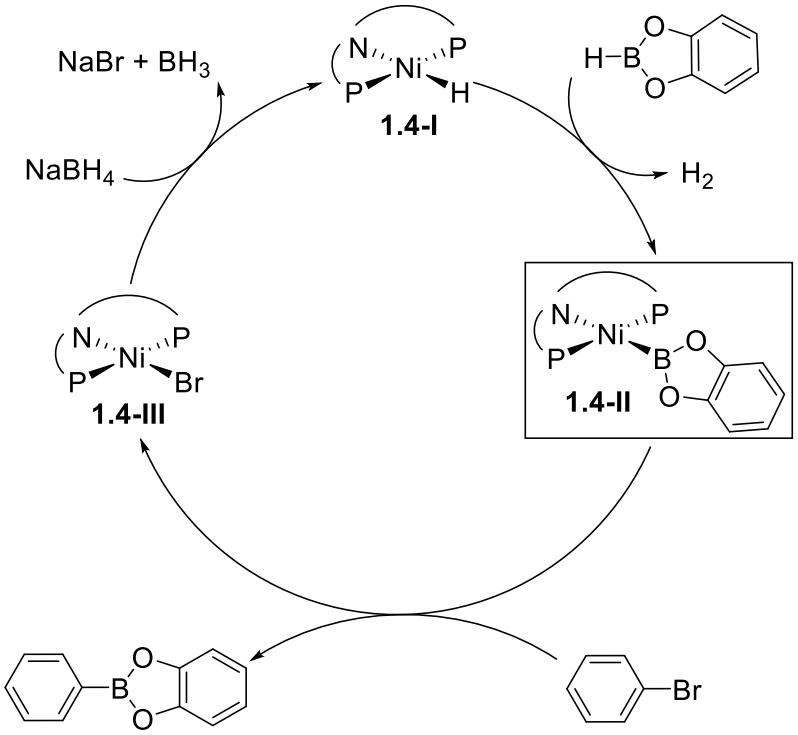

Scheme 1.4 Proposed catalytic cycle for the pincer nickel-catalyzed borylation of bromobenzene.[11]

Later on, Yamakawa *et al.* demonstrated that a combination of $[Ni(PMe_3)_2(Cl)_2]$, CsF and trimethyl(2,2,2-trifluoroethoxy)silane $SiMe_3(OCH_2CF_3)$ is an efficient catalytic system for the borylation of various aryl bromides and chlorides, including sterically challenging substrates as shown in Scheme 1.5.[12] As the addition of either CsF or $SiMe_3(OCH_2CF_3)$ alone afforded poor yields, it was concluded that *in situ* formed cesium-2,2,2-trifluoroethoxide $Cs^+[OCH_2CF_3]^-$ is required in the course of the reaction to obtain excellent yields.

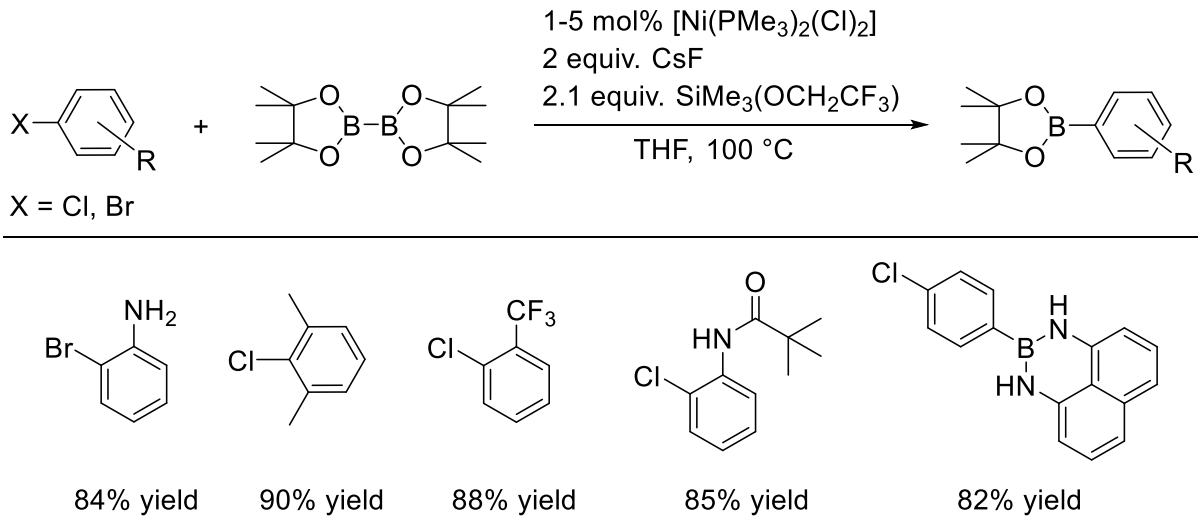

Scheme 1.5 [$Ni(PMe_3)_2(Cl)_2$]-catalyzed borylation of aryl bromides and chlorides.[12]

In 2013, Molander and co-workers reported the first effective Ni-catalyzed borylation of aryl halides at room temperature.[13] A combination of [$Ni(dppp)(Cl)_2$], PPh_3 and diisopropylethylamine (DIPEA) in ethanol catalyzed the borylation of aryl and heteroaryl halides as well as pseudo halides (mesylates, tosylates, triflates and sulfamates) with a wide functional group tolerance using $B_2(OH)_4$ as the boron source. Aryl bromides containing nitrile, ketone, ester, and aldehyde functional groups at *para*- and *meta*-position were efficiently borylated at room temperature (Scheme 1.6).

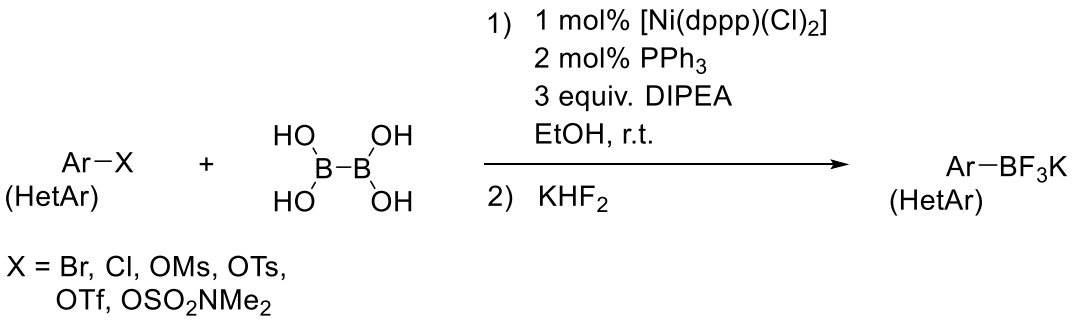

Scheme 1.6 [$Ni(dppp)(Cl)_2$]/PPh_3-catalyzed borylation of aryl and heteroaryl halides.[13]

As homocoupling products were observed for some of the substrates employed, the group proposed the occurrence of a secondary catalytic cycle parallel to borylation, i.e. a cross-coupling cycle wherein the aryl boronic acid formed may compete with $B_2(OH)_4$ in the transmetalation step following the oxidative addition of the aryl halide (Scheme 1.7).[13]

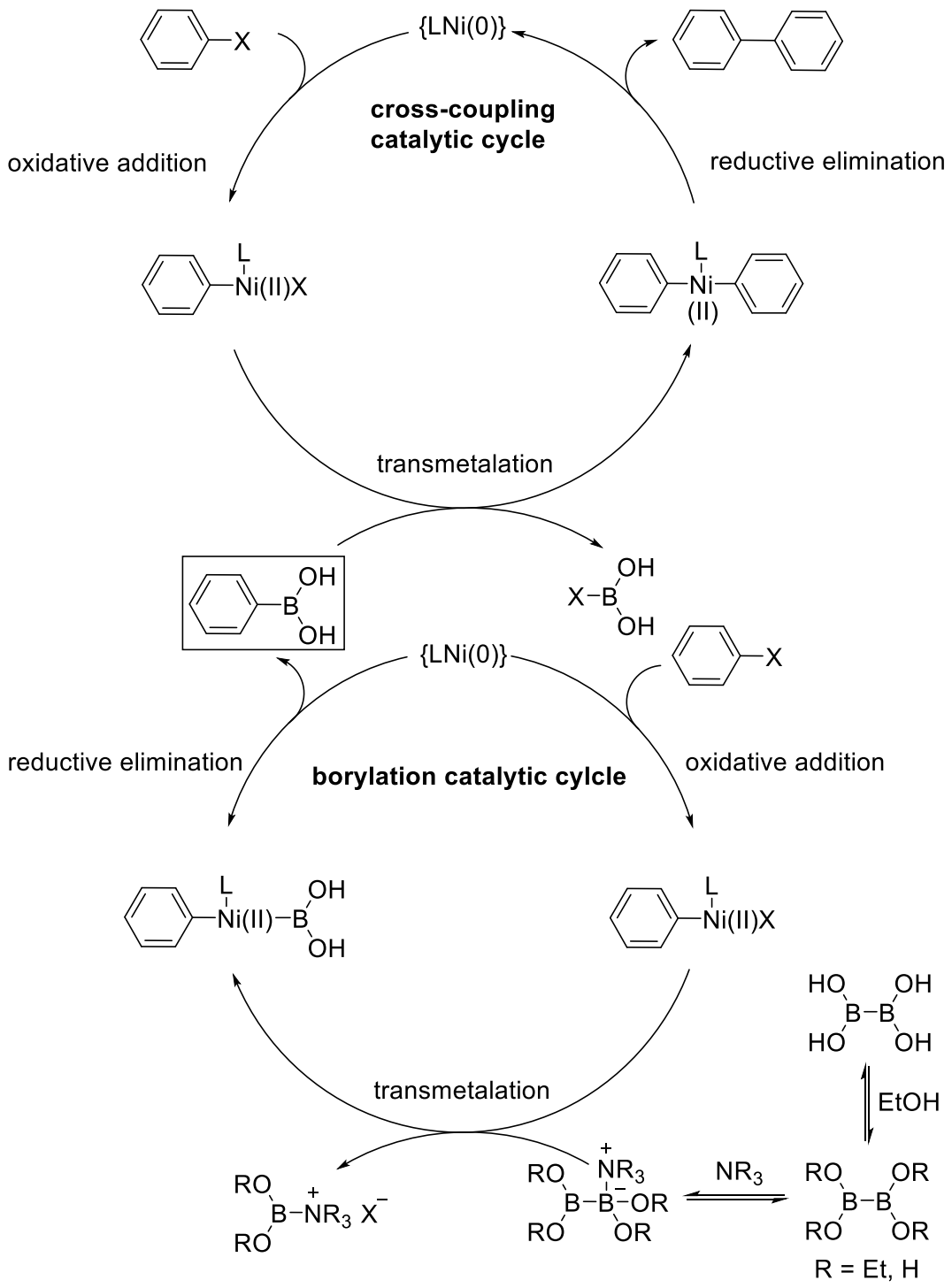

Scheme 1.7 Proposed mechanism for the [Ni(dppp)$(Cl)_2$]/PPh_3-catalyzed borylation of aryl and heteroaryl halides.[13]

Another room temperature borylation reaction of aryl tosylates was reported by Hu *et al*. generating the corresponding arylboronates with good functional group compatibility in yields of up to 92%.[14] Ni/PCy_3 complexes, generated from [Ni$(COD)_2$] and PCy_3, or air-stable [Ni$(PCy_3)_2$(OTs)(4-(MeO)-C_6H_4)], were found to be efficient catalysts in the presence of K_3PO_4 as the base and B_2pin_2 as the borylation reagent.

Darcel, Ghosh and co-workers synthesized a series of nickel complexes of 1,2,4-triazole-derived amido-functionalized *N*-heterocyclic carbene chelate ligands, which were found to be moderately active for the catalytic borylation of aryl bromide derivatives using B_2pin_2 as the borylation reagent and Cs_2CO_3 as the base (Scheme 1.8). The low to moderate yields are mainly due to a competitive hydrodehalogenation reaction leading to simple arenes.[15, 16]

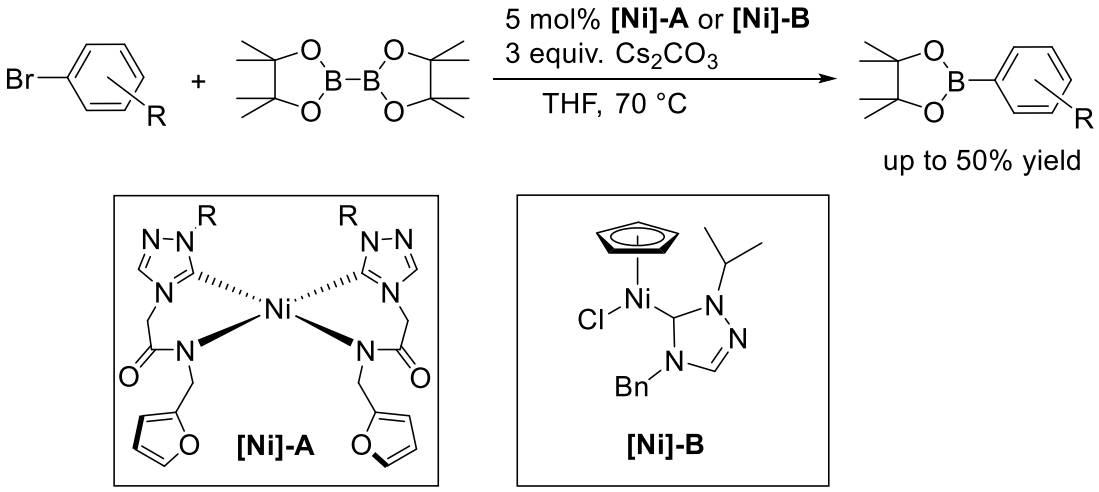

Scheme 1.8 Nickel complexes of 1,2,4-triazole-derived amido-functionalized *N*-heterocyclic carbene chelate ligands and their application in the borylation of aryl bromides.[15, 16]

Very recently, a standard workflow for the identification of nickel-catalyzed borylation reactions using high-throughput experimentation was developed by Wisniewski and co-workers.[17] The design of a 24-reaction screening platform provided insight into the borylation reaction using $B_2(OH)_4$ as the borylation reagent under various conditions. This general screening platform was applied to the borylation of a variety of aryl and heteroaryl halides (X = I, Br, Cl) as well as pseudo halides using commercial nickel nitrate hexahydrate as the metal source.

In 2015, Martin *et al.* reported the first example of a Ni-catalyzed defluoroborylation of unactivated fluoroarenes.[18] A variety of functionalized monofluoroarenes were borylated, in the presence of catalytic amounts of $[Ni(COD)_2]/PCy_3$ using B_2neop_2 as the boron source and NaOPh as the base. The borylation reaction was conducted in THF and required elevated temperatures of 110 °C (Scheme 1.9). The nature of the phosphine ligand played a crucial role, as other related phosphines (e.g. PPh_3) did not

show any conversion. Notably, inferior results were obtained when utilizing NHCs as ligands.

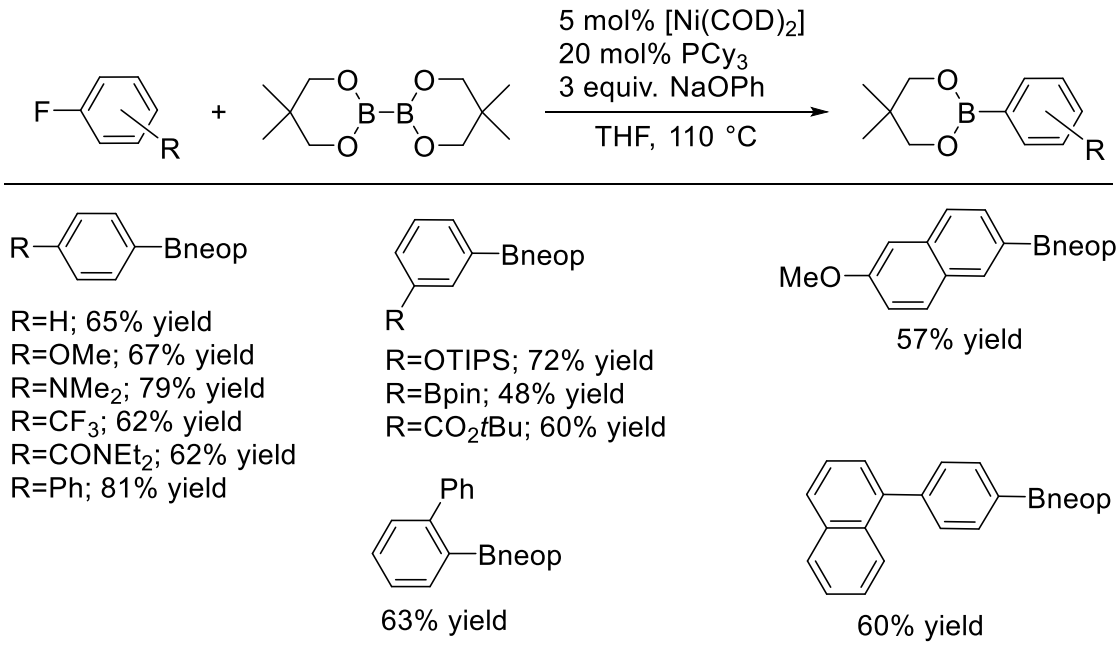

Scheme 1.9 [Ni(COD)$_2$]/PCy$_3$-catalyzed borylation of monofluoroarenes.[18]

At the same time, Niwa, Hosoya and co-workers reported an efficient nickel and copper co-catalyst system, which afforded a catalytic transformation of monofluoroarenes to arylboronic pinacol esters *via* C–F bond cleavage.[19] The co-catalyst system consisting of [Ni(COD)$_2$]/PCy$_3$, with catalytic amounts of CuI and CsF as additives in toluene at 80 °C gave the desired borylated products in nearly quantitative yields.

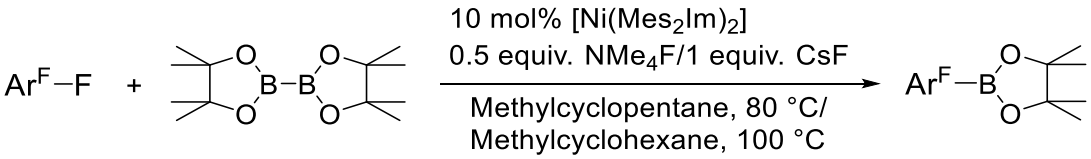

Scheme 1.10 [Ni(Mes$_2$Im)$_2$]-catalyzed borylation of partially fluorinated arenes.[20]

In 2016, Radius, Marder *et al.* developed an efficient procedure for the C–F bond borylation of mono- and polyfluoroarenes using a nickel/NHC catalyst system, NMe$_4$F or CsF as the base and B_2pin_2 as the boron source.[20] Based on C–F bond activation reactions reported earlier,[21-25] a variety of partially fluorinated arenes with different degrees of fluorination were converted into fluoroaryl boronic esters (Scheme 1.10).[20]

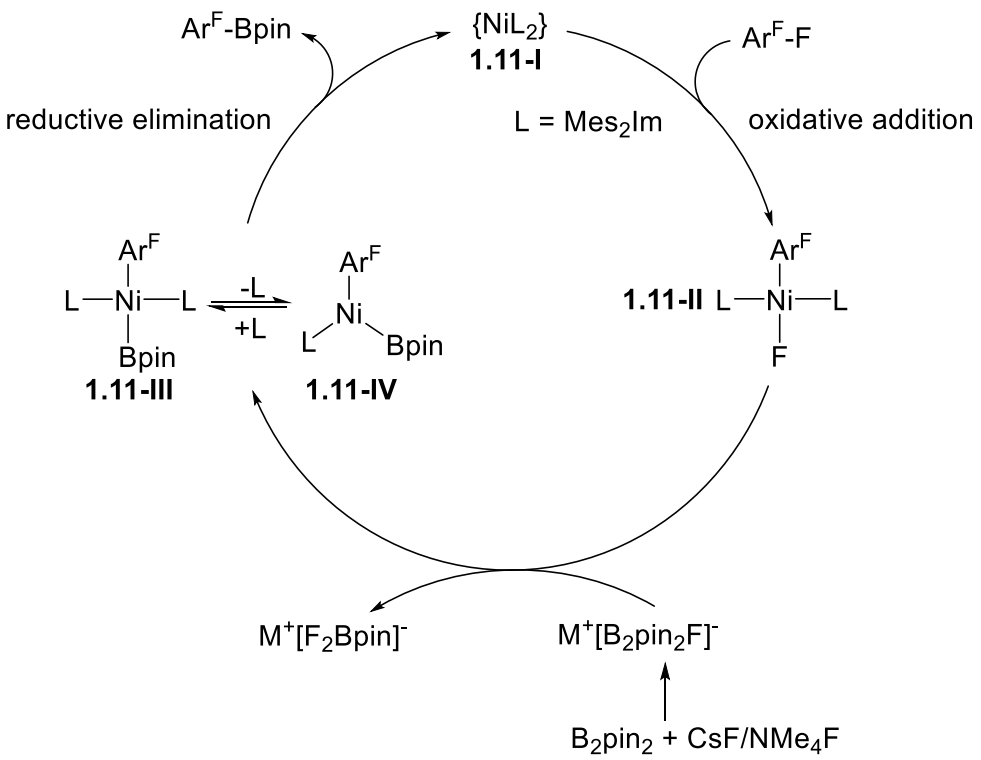

Scheme 1.11 Proposed mechanism for the [Ni(Mes$_2$Im)$_2$]-catalyzed borylation of partially fluorinated arenes.[20]

These fluorinated building blocks can be introduced into other organic molecules.[26] A mechanism was proposed (Scheme 1.11) where, in the first step, the reaction of [Ni(Mes$_2$Im)$_2$] **1.11-I** with the fluoroarene leads to an oxidative addition of the C–F bond with formation of *trans*-[Ni(Mes$_2$Im)$_2$(F)(Ar^F)] **1.11-II**. Although an initial "kinetic" C–H bond activation step would explain the regioselectivity of the borylation reaction (borylation occurs at a site adjacent to a hydrogen substituent), such a species could not be observed even at low temperatures. Complex **1.11-II** then reacts with M$^+$[B$_2$pin$_2$F]$^-$ in a boryl transfer to form *trans*-[Ni(Mes$_2$Im)$_2$(Bpin)(Ar^F)] **1.11-III** and M$^+$[F$_2$Bpin]$^-$. A final reductive elimination step gives the borylated fluoroarene and regenerates [Ni(Mes$_2$Im)$_2$] **1.11-I**.[20]

Two years later, the same group developed a highly selective photocatalytic C–F bond borylation protocol that employes a rhodium biphenyl complex as a triplet sensitizer and [Ni(Mes$_2$Im)$_2$] for the C–F bond activation and defluoroborylation process.[27] This tandem catalyst system operates with visible light (400 nm) yielding a wide range of borylated fluoroarenes at room temperature in good to excellent yields (Scheme 1.12).

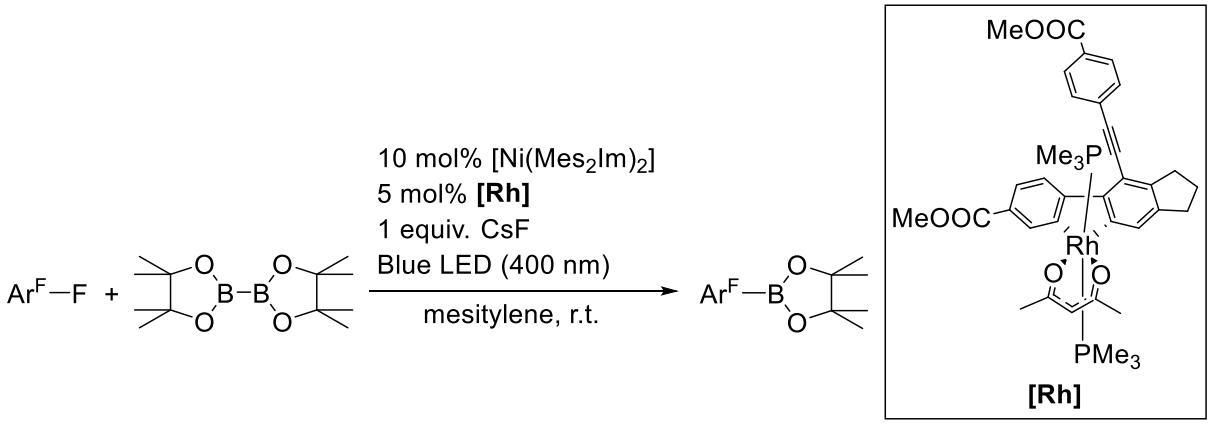

Scheme 1.12 Photocatalytic borylation of aryl fluorides by a [Rh]/[Ni(Mes$_2$Im)$_2$] tandem catalyst system.[27, 28]

As already demonstrated for the thermal version of this reaction (*vide supra*), [Ni(Mes$_2$Im)$_2$] undergoes very fast oxidative addition of the C(Ar^F)–F bond of the fluoroarene in the first step of the catalysis to yield *trans*-[Ni(Mes$_2$Im)$_2$(F)(Ar^F)], the resting state of the nickel catalyst. The following transmetalation step with B$_2$pin$_2$ is associated with a high energy barrier, which can be bypassed by indirect excitation of *trans*-[Ni(Mes$_2$Im)$_2$(F)(Ar^F)] in its triplet states *via* the photoexcited rhodium biphenyl complex. Irradiation (LED 400 nm) of the tandem catalytic system leads to excitation of the rhodium biphenyl complex into its S_1 state then giving an exceptionally long-lived triplet excited state after intersystem-crossing (ISC). Mechanistic studies suggest that this triplet excited state of the rhodium biphenyl complex is the active photosensitizer,[28] which allows efficient triplet energy transfer to *trans*-[Ni(Mes$_2$Im)$_2$(F)(Ar^F)], leading to dissociation of one of the NHC ligands and thus facilitating the borylation step (Scheme 1.13).[27] Transmetalation may also be facilitated by the formation of the ionic adduct [FB$_2$pin$_2$]$^-$ from B$_2$pin$_2$ and CsF, but a key role of added fluoride is to trap FBpin formed as [F$_2$Bpin]$^-$.[29, 30] Reductive elimination of Ar^F–Bpin is then fast, and the resulting Ni(0) species is stabilized by re-coordination of Mes$_2$Im to give [Ni(Mes$_2$Im)$_2$], the starting compound of the catalytic cycle. The triplet energy transfer (TET) proposed as the key step for this reaction contrasts with the majority of current photocatalytic transformations, which employ transition metals as excited state single electron transfer (SET) agents.

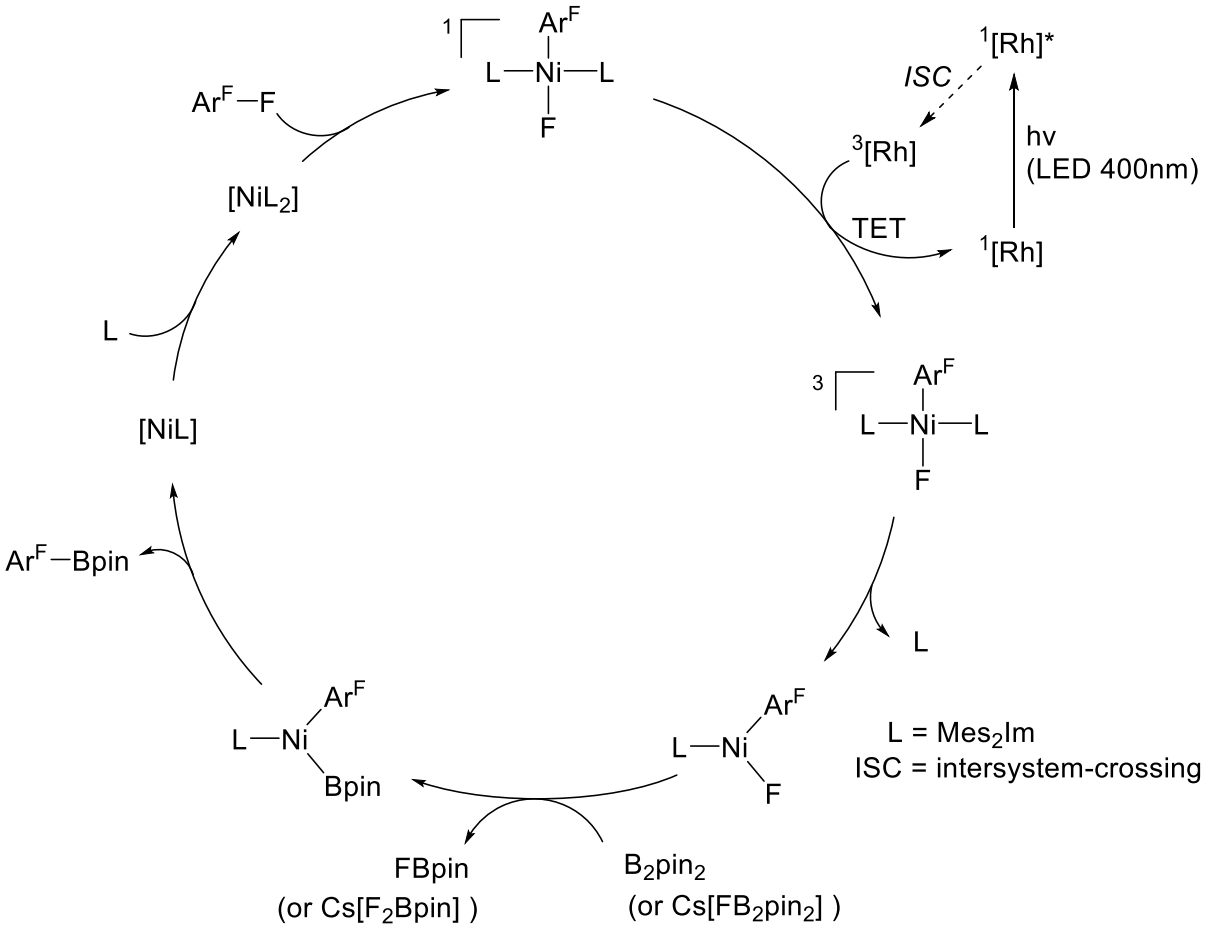

Scheme 1.13 Proposed mechanism for the photocatalytic borylation of fluoroarenes by a [Rh]/[Ni($Mes_2Im)_2$] tandem catalyst system using triplet energy transfer (TET).[27]

A procedure for an enantioconvergent borylation of racemic secondary benzylic chlorides, mediated by a chiral nickel catalyst, was reported by Fu and co-workers.[31] Utilizing a catalyst formed *in situ* from [Ni(DME)$(Cl)_2$] and a chiral pybox ligand, a variety of enantioenriched benzylic boronic esters were provided at room temperature (Scheme 1.14). The method displays good functional group compatibility being unimpeded by the presence of, for example, an indole, a ketone, or an unactivated aryl bromide. Moreover, both catalyst components are commercially available and the borylation reaction is neither highly water nor air sensitive.

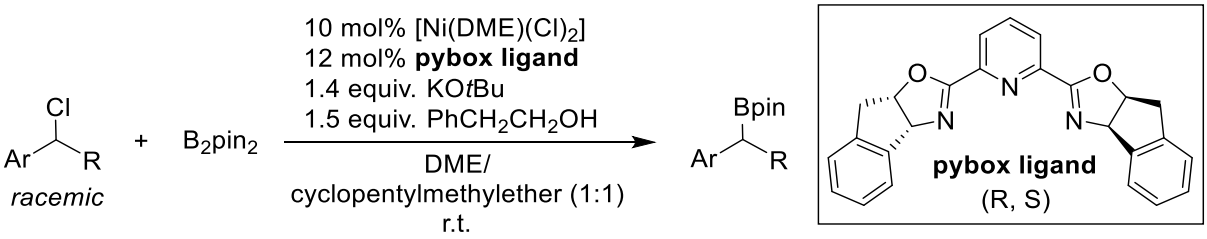

Scheme 1.14 [Ni(DME)(Cl)$_2$]/pybox-catalyzed enantioconvergent borylation of racemic benzylic chlorides.[31]

1.2 C–H BOND BORYLATION

In 2015, Itami and co-workers reported the first nickel-catalyzed aromatic C–H bond borylation.[32] A variety of benzene and indole derivates underwent borylation with B_2pin_2 at elevated temperatures in the presence of catalytic amounts of [Ni(COD)$_2$]/PCyp$_3$ and CsF as the base. Other phosphine ligands proved to be less effective or even completely inefficient, whereas the Dipp$_2$Im was found to show an efficiency similar to PCyp$_3$.

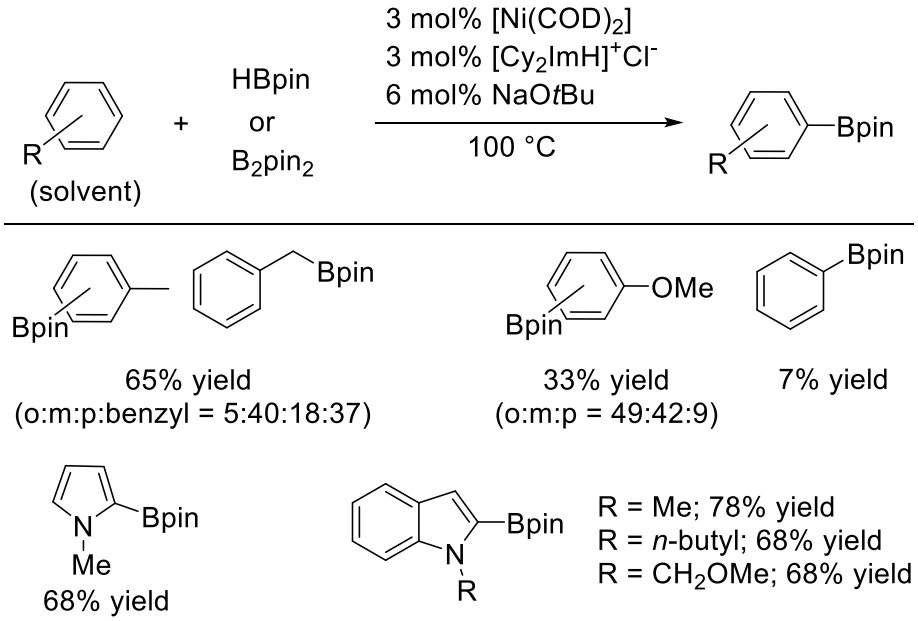

Scheme 1.15 [Ni(COD)$_2$]/Cy$_2$Im-catalyzed borylation of benzene and indole derivates *via* C–H bond activation.[33]

At the same time, Chatani, Tobisu *et al.* reported the nickel-catalyzed borylation of arenes and indole derivatives *via* C–H bond cleavage using Cy_2Im as the ligand without an extra base (Scheme 1.15). Besides B_2pin_2, HBpin was found to be a suitable borylation reagent. It is noteworthy that, in both cases, the arene served as the solvent and, thus, was used in large excess.[32, 33] Interestingly, the use of anisole as the substrate generated the *ortho*-borylated isomer as the major product.[33] This regioselectivity is in sharp contrast with that observed earlier in homogeneous Ir, Fe, and Co catalytic systems, wherein the *meta*- and *para*-isomers were the major products.[34-36]

1.3 HYDROBORATION OF *N*-HETEREOARENES

Recently, Findlater and co-workers found that a combination of $[Ni(acac)_2]$ and $PCyp_3$ as the ligand effectively catalyzed the 1,4-hydroboration of *N*-heteroarenes using HBpin as the boron source.[37] *N*-borylated 1,4-reduction products in excellent regioselectivity and broad functional group compatibility were generated in yields of up to 96% (Scheme 1.16).

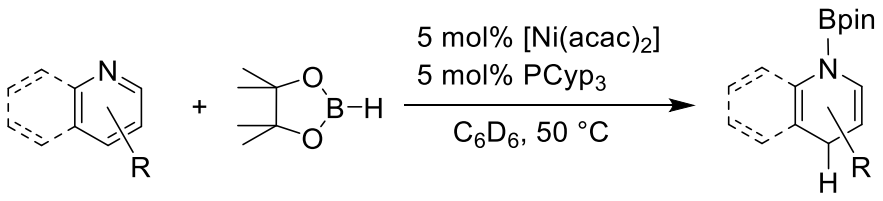

Scheme 1.16 $[Ni(acac)_2]/PCyp_3$-catalyzed 1,4-hydroboration of *N*-heteroarenes, affording *N*-borylated 1,4-reduction products.[37]

1.4 C–N BOND ACTIVATION AND BORYLATION (ARYL, BENZYLIC)

In 2014, Chatani, Tobisu and co-workers reported the first catalytic C(aryl)–N bond cleavage and further borylation of electronically neutral and structurally simple aryl amides and carbamates in the presence of a nickel catalyst.[38] The combination of $[Ni(COD)_2]$ and Mes_2Im in a ratio of 1:2 was found to be the optimal catalyst for this type of borylation with B_2neop_2 as the boron source and NaO*t*Bu as the base. However,

this reaction, performed in toluene, required a temperature of 160 °C to proceed in good yield (Scheme 1.17).

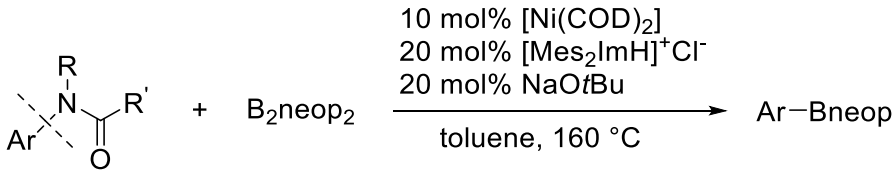

Scheme 1.17 [Ni(COD)$_2$]/Mes$_2$Im-catalyzed borylation of aryl amides and carbamates *via* C–N bond cleavage.[38]

Itami and co-workers reported an efficient C–N borylation reaction of aryl and benzylic ammonium salts, promoted by a nickel/phosphine catalyst.[39] The borylation of aryl ammonium salts to give arylboronic pinacol esters in good yields, was achieved in the presence of [Ni(COD)$_2$]/P*n*Bu$_3$ with NaO*t*Bu as the base (Scheme 1.18a). A variety of benzylic ammonium salts were also subjected to C–N bond borylation using [Ni(NO$_3$)$_2$·6H$_2$O]/P*n*Bu$_3$ as the catalyst, a system which is much more stable and much cheaper than [Ni(COD)$_2$] (Scheme 1.18b).

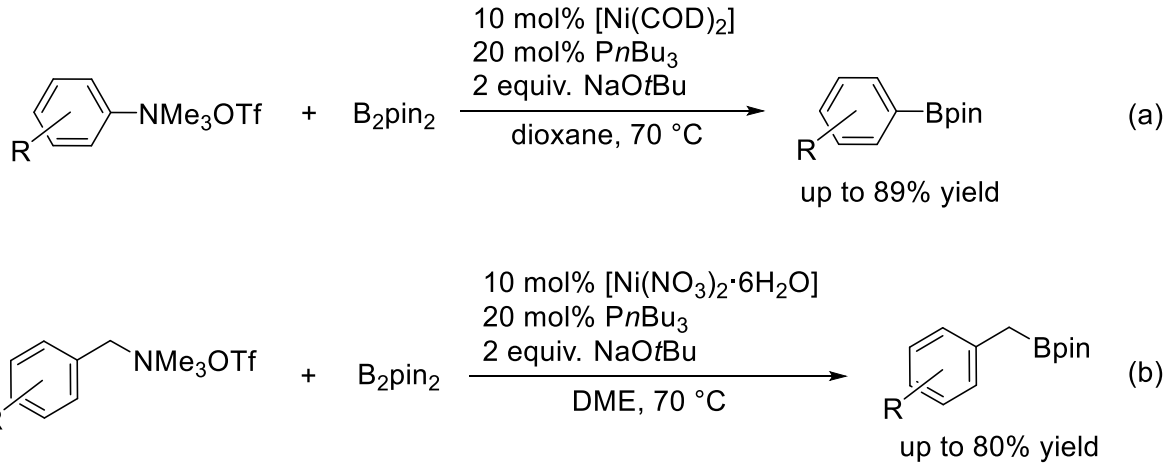

Scheme 1.18 (a) [Ni(COD)$_2$]/P*n*Bu$_3$-catalyzed borylation of aryl ammonium salts. (b) [Ni(NO$_3$)$_2$·H$_2$O]/P*n*Bu$_3$ catalyzed borylation of benzylic ammonium salts.[39]

In the same year, Watson and co-workers also reported the nickel-catalyzed borylation of chiral benzylic ammonium salts generating enantioenriched benzylic boronates.[40] [Ni(COD)$_2$]/PPh$_3$ turned out to be the optimal catalyst to obtain the highest levels of reactivity and enantio-specificity across a range of substrates. The reaction mechanism starts with an oxidative addition generating a benzylic nickel species, which further undergoes transmetalation and reductive elimination to yield the

enantioenriched borylated benzylic product. Higher reactivity is observed for substrates containing aryl substituents with an extended *π*-system. This observation and the overall inversion of configuration is consistent with oxidative addition occurring *via* an S_N2 mechanism with attack of the nickel catalyst at the *ortho*-position to form the nickel intermediate **19-I** or **19-II**, at least when the loss of aromaticity is not too costly (Scheme 1.19).

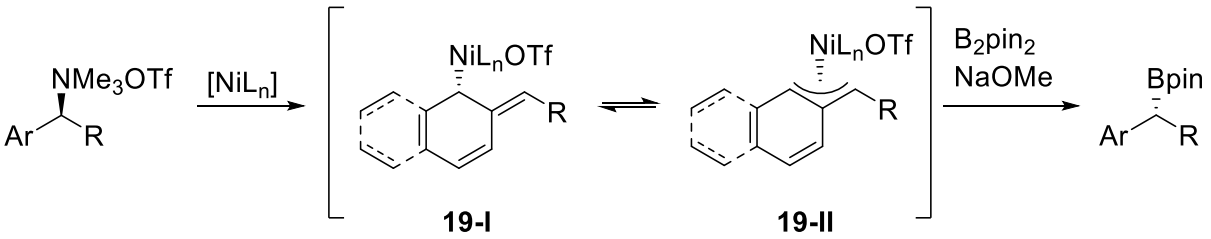

Scheme 1.19 Proposed mechanism for the $[Ni(COD)_2]/PPh_3$-catalyzed borylation of benzylic ammonium salts generating enantioenriched benzylic boronates.[40]

Another mild method, proceeding at 50 °C, for the borylation of sp^2 and sp^3 C–N bonds was developed by Shi and co-workers.[41] Using catalytic amounts of $[Ni(COD)_2]/[Cy_2ImH]^+Cl^-$, KO*t*Bu as the base and 2-ethoxyethanol/toluene as the solvent, aryl and benzyl ammonium salts were borylated with good functional group compatibility (Scheme 1.20).

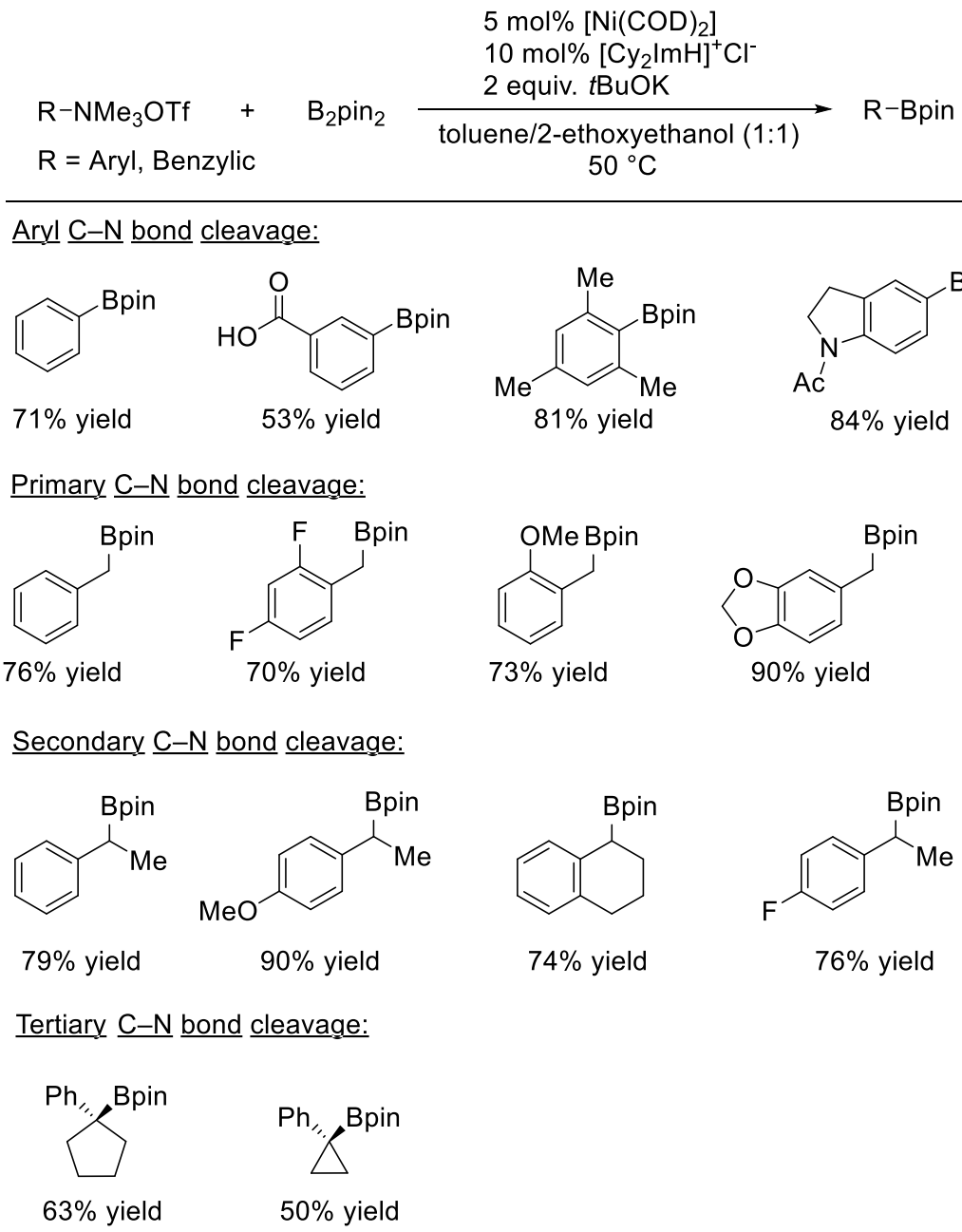

Scheme 1.20 $[Ni(COD)_2]/Cy_2Im$-catalyzed borylation of aryl and benzylic ammonium salts.[41]

The same group reported also the decarbonylative borylation of *N*-Boc-activated secondary amides by Ni-catalyzed C–N bond activation (Scheme 1.21).[42] This transformation, using $[Ni(OAc)_2{\cdot}4H_2O]$ as the catalyst precursor and $[Cy_2ImH]^+Cl^-$ as the ligand precursor, served as a powerful synthetic tool for the late-stage borylation of amide groups in complex compounds.

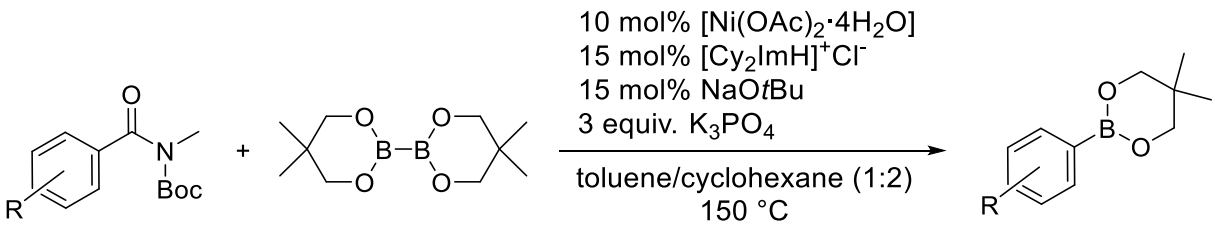

Scheme 1.21 [Ni(OAc)$_2$·4H$_2$O]/Cy$_2$Im-catalyzed decarbonylative borylation of *N*-Boc-activated secondary amides.[42]

Remarkably, the structure of an acyl nickel complex **1.22-III**, an important intermediate in the proposed mechanistic cycle (Scheme 1.22), was confirmed by X-ray analysis. The reaction was triggered by the insertion of the nickel(0) catalyst **1.22-I** into the imide C–N bond with formation of the *trans*-acyl-nickel(II) intermediate **1.22-II**. This complex is believed to undergo a ligand exchange with X$^-$ leading to the *trans*-acyl-nickel(II) species **1.22-III**. Decarbonylation of **1.22-III** to the aryl-nickel complex **1.22-IV**, followed by boryl transfer, assisted by the base, and subsequent reductive elimination yields the desired product and regenerates the nickel(0) catalyst **1.22-I**.[42]

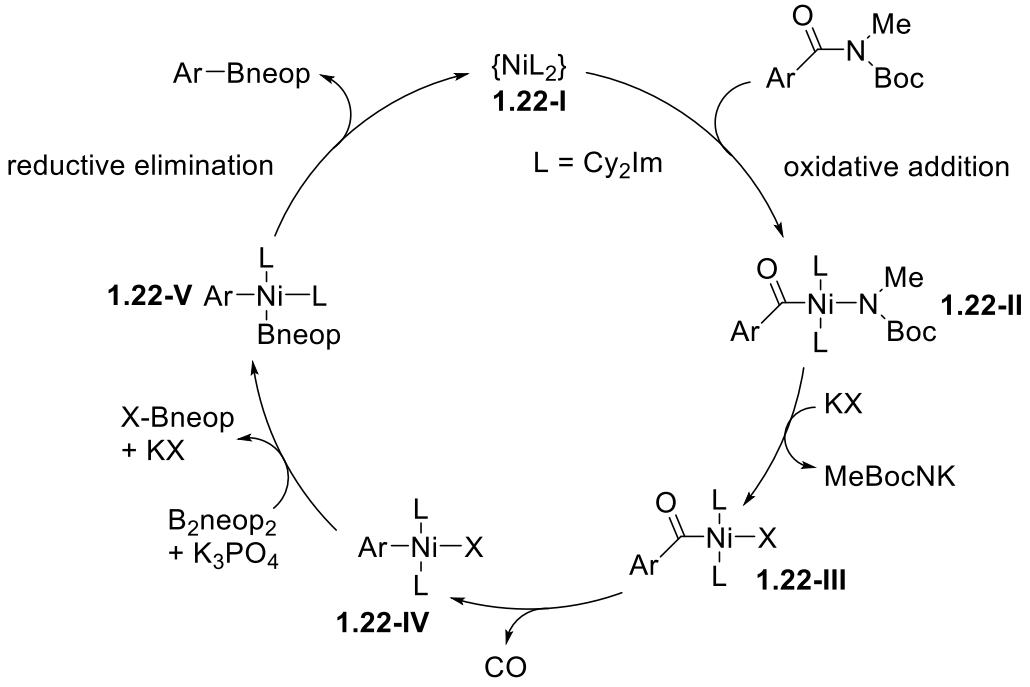

Scheme 1.22 Proposed mechanism for the [Ni(OAc)$_2$·4H$_2$O]/Cy$_2$Im-catalyzed decarbonylative borylation of *N*-Boc-activated secondary amides.[42]

1.5 C–O BOND ACTIVATION AND BORYLATION (ARYL, BENZYLIC)

In 2011, Shi *et al.* reported the borylation of aryl and alkenyl carbamates by a Ni-catalyzed C–O bond activation.[43] The borylation of 2-naphthol carbamate derivatives was accomplished using a $[Ni(PCy_3)_2(Cl)_2]/PCy_3$ catalyst with NaO*t*Bu as the base and B_2neop_2 as the boron source. The solvent was critical for this conversion; when toluene was used as a solvent, the yields were moderate, while use of the solvent DME completely inhibited the reaction. However, a mixture of toluene and DME in a 1:1 ratio enhanced the yields drastically (Scheme 1.23). As this method was rather ineffective for phenyl carbamates, the group found that K_2PO_4 is a better base without the addition of PCy_3 as a ligand. This borylation was also extended to alkenyl carbamates.

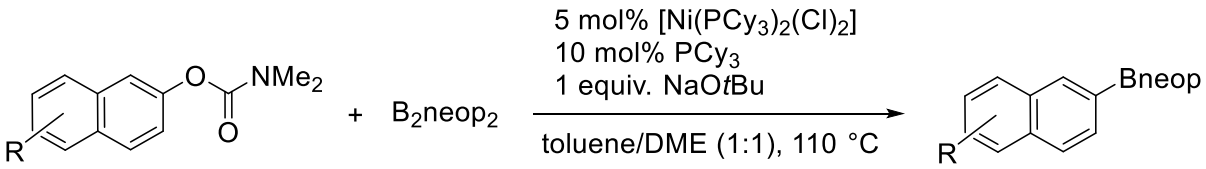

Scheme 1.23 $[Ni(PCy_3)_2(Cl)_2]/PCy_3$-catalyzed borylation of aryl and alkenyl carbamates *via* C–O bond activation.[43]

Later on, the same group described the nickel-catalyzed decarbonylative borylation and silylation of esters by acyl C–O bond cleavage.[44] The borylation was accomplished with good functional group compatibility using a $[Ni(COD)_2]/Cy_2Im$ catalyst system and B_2neop_2 as the boron source with Na_2CO_3 and NaCl as additives in dioxane with harsh conditions of 160 °C (Scheme 1.24).

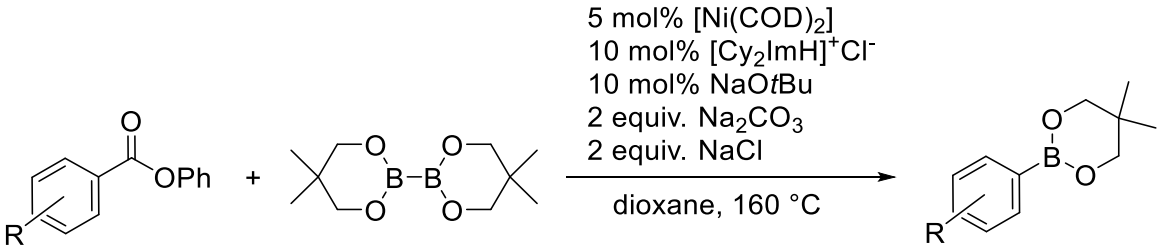

Scheme 1.24 $[Ni(COD)_2]/Cy_2Im$-catalyzed decarbonylative borylation of esters by acyl C–O bond cleavage.[44]

At the same time, Rueping and co-workers reported another efficient nickel-catalyzed decarboxylative borylation of esters using B_2pin_2 as the boron source.[45] This transformation generated structurally diverse aryl as well as alkenyl and alkyl boronate esters with a high functional group tolerance in the presence of catalytic amounts of $[Ni(COD)_2]$/P*n*Bu_3 with Li_2CO_3 as the base.

A nickel-catalyzed borylation of aryl ethers *via* C(sp^2)– and C(sp^3)–OMe cleavage was reported by Martin and co-workers.[46] They found $[Ni(COD)_2]$/PCy_3 with sodium formate or CsF as the base as the most efficient catalytic system (Scheme 1.25).

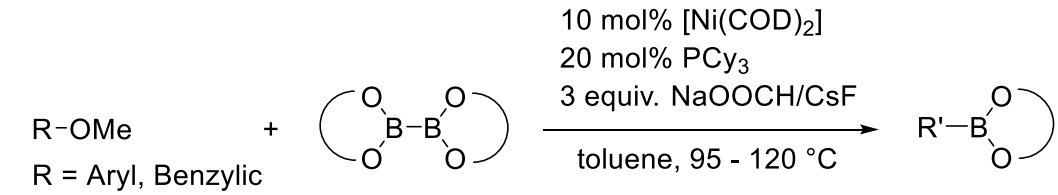

Aryl C–OMe bond cleavage:

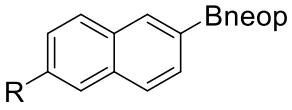

R = H; 80% yield
R = $SiEt_3$; 73% yield
R = TIPSO; 65% yield

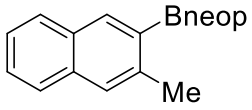

67% yield

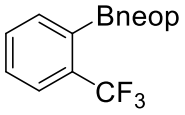

56% yield

Benzylic C–OMe bond cleavage:

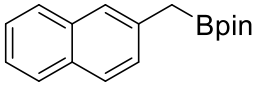

61% yield

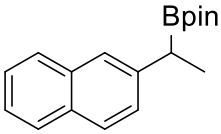

81% yield

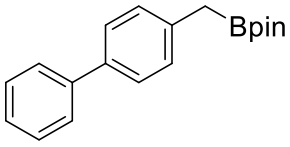

57% yield

Scheme 1.25 $[Ni(COD)_2]$/PCy_3-catalyzed borylation of aryl and benzylic ethers.[46]

Interestingly, the use of B_2pin_2 instead of B_2neop_2 as the boron source for the borylation of naphthyl ethers did not provide any product, but it was found that B_2pin_2 could be utilized to effect the C(sp^2)–OMe bond cleavage in regular arenes, and the C(sp^3)–OMe bond cleavage in naphthyl benzylic ethers. They concluded that the nature of the boron reagent might not be entirely innocent in the reaction outcome. One year later, Chatani, Tobisu *et al.* reported a $[Ni(DME)(Cl)_2]$/PCy_3-catalyzed borylation of aryl and benzylic 2-pyridyl ethers *via* the loss of a 2-pyridyloxy group (OPy).[47] This method

allowed the OPy group to be used as a convertible directing group for *ortho* C–H bond functionalization reactions. This nickel-system was also applied in the borylation of more challenging secondary benzylic substrates, for which the reaction proceeded with retention of configuration at the benzylic stereocenter (Scheme 1.26).

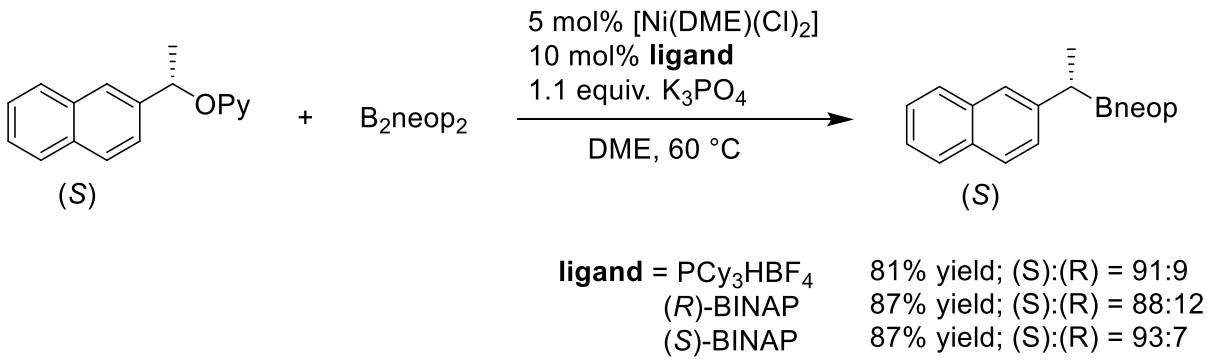

Scheme 1.26 [Ni(DME)(Cl)$_2$]/PCy$_3$-catalyzed borylation of aryl and benzylic 2-pyridyl ethers.[47]

Watson *et al.* developed a stereospecific, nickel-catalyzed borylation of allylic pivalates, which provided highly enantioenriched *α*-stereogenic *γ*-aryl allylboronates in good yields and regioselectivities.[48] Their complementary sets of conditions using [Ni(COD)$_2$] as the catalyst precursor and either *t*Bu-XantPhos (XantPhos = 4,5-bis(diphenylphosphino)-9,9-dimethylxanthene) or BnPPh$_2$ as the ligand enabled access to both enantiomers of allylboronates from a single initial isomer (Scheme 1.27).

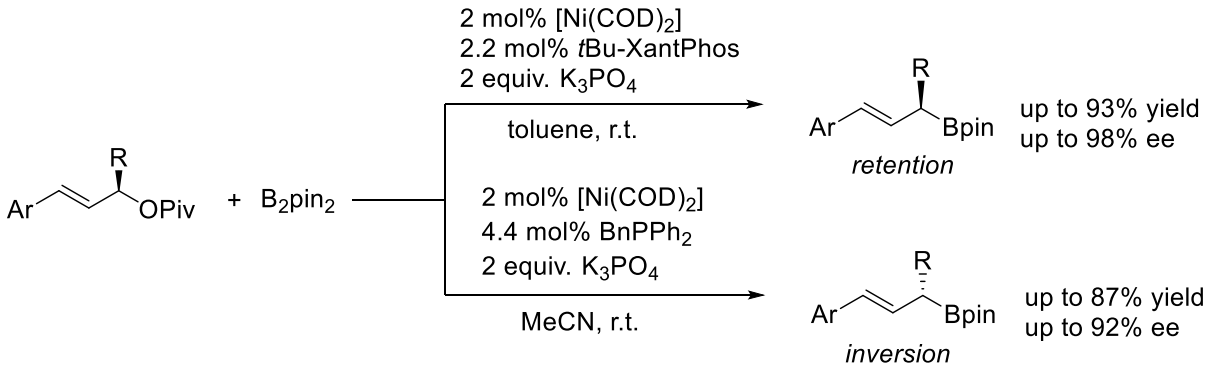

Scheme 1.27 [Ni(COD)$_2$]/*t*Bu-XantPhos and [Ni(COD)$_2$]/BnPPh$_2$-catalyzed borylation of allylic pivalates with access to both enantiomers.[48]

In 2017, Turculet and co-workers introduced nickel and palladium hydride complexes bearing a new bis(indolylphosphino)silyl pincer ligand (*i*Pr-PSiP^{Ind}).[49] These complexes were found to exhibit divergent selectivity in the catalytic hydroboration of CO_2 using HBpin as the boron source. While the palladium analogous only showed moderate catalytic activity for the hydroboration of CO_2 to the formate level, the nickel species revealed high selectivity for the hydroboration to the formaldehyde level generating the bis(boryl)acetal $(pinBO)_2CH_2$ in high yield. The reaction proceeds under mild conditions at room temperature without any additives (Scheme 1.28).

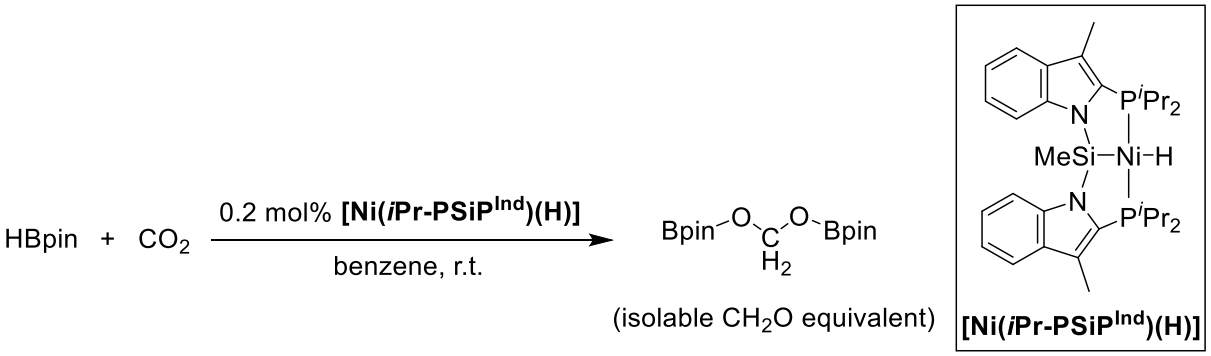

Scheme 1.28 Selective [Ni(*i*Pr-PSiP^{Ind})(H)]-catalyzed hydroboration of CO_2 to the formaldehyde level.[49]

1.6 BORYLATION OF ALKYNES

In 1996, Suginome *et al.* introduced the addition of a B–Si bond across a carbon-carbon triple bond, which is effectively catalyzed by palladium and platinum complexes and leads to the selective formation of *ß*-silylalkenylboronates in high yields (Scheme 1.29).[50]

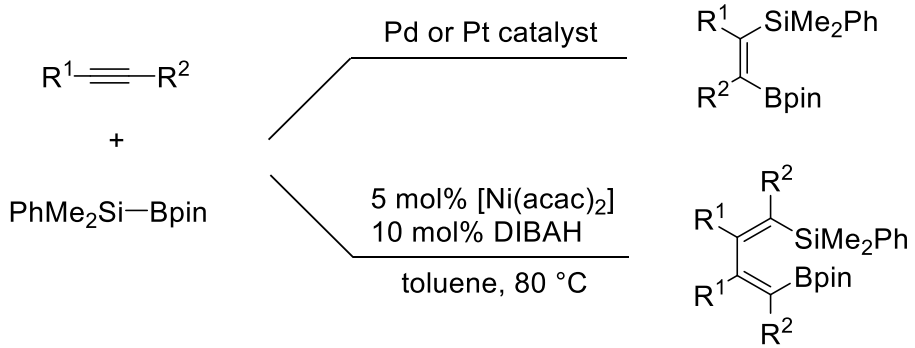

Scheme 1.29 Pd/Pt *versus* [Ni(acac)$_2$]-catalyzed reaction of an alkyne with PhMe$_2$Si**–**Bpin.[50, 51]

In contrast, utilizing a nickel catalyst resulted in the selective formation of 1-silyl-4-boryl-1,4-dienes *via* subsequent insertion of two alkynes into the Si–B bond (Scheme 1.29).[51] The same group reported the first cyanoboration of alkynes catalyzed by nickel- and palladium-complexes.[52, 53] Their initial attempt at carrying out the intermolecular reaction of bis(dialkylamino)cyanoboranes with phenylacetylene in the presence of a palladium-catalyst failed. However, the intramolecular reaction using readily prepared homopropargylic cyanoboryl ethers in the presence of catalytic amounts of a palladium or nickel complex formed the cyclization products in good yields. [Ni(COD)$_2$] was found to be more effective than a palladium catalyst for the cyanoboration of terminal alkynes derived from primary and secondary homopropargylic alcohols (Scheme 1.30a).

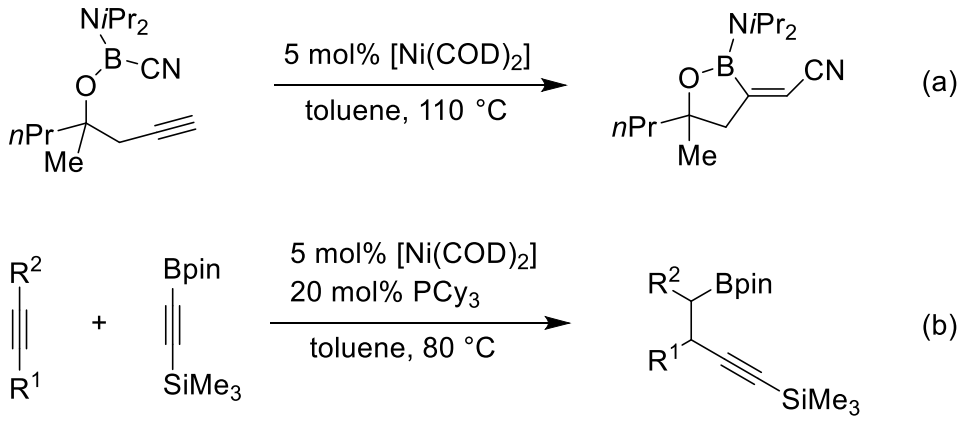

Scheme 1.30 (a) [Ni(COD)$_2$]-catalyzed cyanoboration of terminal alkynes.[52, 53] (b) [Ni(COD)$_2$]/PCy$_3$ catalyzed addition of alkynylboranes to alkynes.[54]

In 2006, the same group reported the addition of alkynylboranes to alkynes.[54] Initial attempts utilizing palladium/phosphine catalysts failed. Replacing the catalyst by a [Ni(COD)$_2$]/phosphine catalyst system turned out to be promising. The *cis*-alkynylboration products are best obtained using PCy$_3$ or PCy$_2$Ph as the ligands (Scheme 1.30b). Cheng *et al.* reported a [Ni(COD)$_2$]/P*n*Bu$_3$ catalyzed borylative coupling of alkynes with enones using B$_2$pin$_2$ as the boron source (Scheme 1.31).[55] They provided synthetically useful, highly substituted alkenyl boronates in good to excellent yields and demonstrated their application in coupling reactions and functional-group transformations.

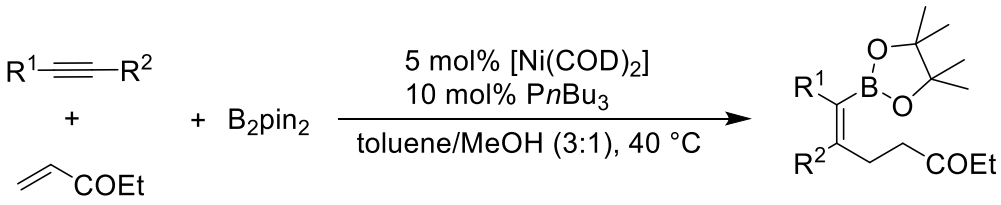

Scheme 1.31 [Ni(COD)$_2$]/P*n*Bu$_3$ catalyzed borylative coupling of alkynes with enones.[55]

A possible catalytic reaction mechanism for this three-component coupling reaction is shown in Scheme 1.32. A highly chemoselective coordination of the alkyne and the enone to the Ni(0)-center **1.32-I** is followed by a regioselective oxidative cyclometalation step. A nickel-acyclopentene intermediate **1.32-II** is generated, which gets selectively protonated by MeOH and affords an alkenyl(methoxy)nickel species **1.32-III**. This species undergoes a transmetalation with B_2pin_2 to yield the alkenyl-nickel-boryl intermediate **1.32-IV** and MeO–Bpin. A final reductive elimination of **1.32-IV** generates the desired borylation product and regenerates the Ni(0)-catalyst **1.32-I**.[55]

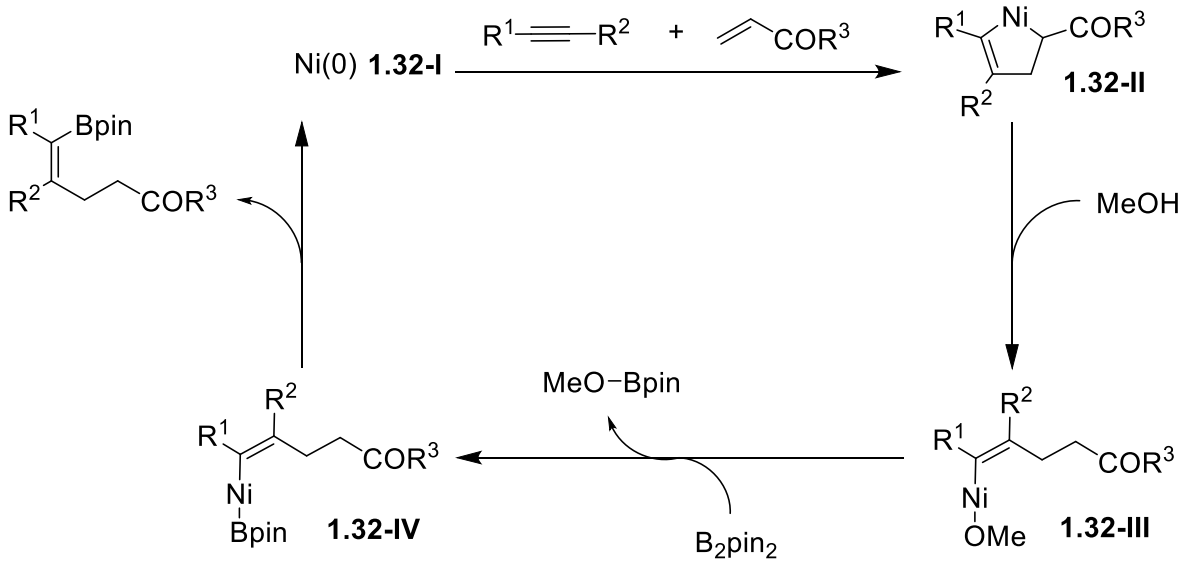

Scheme 1.32 Proposed mechanism for the three-component coupling reaction catalyzed by [Ni(COD)$_2$]/P*n*Bu$_3$.[55]

In 2013, Suginome and co-workers reported a cyclizative alkynyl- and alkenylboration of carbon-carbon triple bonds using a nickel-catalyst.[56] A chloroborane bearing a tethered alkyne moiety was treated with an alkynylstannane in the presence of a [Ni(COD)$_2$]/PPh$_3$ catalyst at elevated temperatures (Scheme 1.33a). The efficiency of this reaction was significantly affected by the phosphine ligand, as bulky aryl groups

on the phosphorus atom significantly inhibited the reaction. Testing of alternative organometallic reagents revealed that alkenylzirconium compounds are also suitable as transmetalation reagents (Scheme 1.33b).

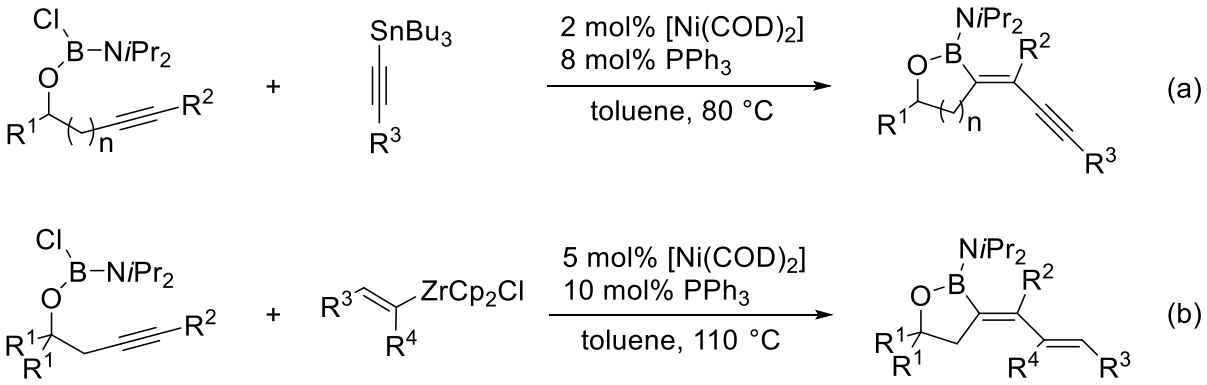

Scheme 1.33 $[Ni(COD)_2]/PPh_3$-catalyzed borylation of chloroboranes with (a) alkynylstannanes and (b) alkenylzirconium compounds, respectively.[56]

A mechanism was proposed in which the B–Cl bond of the chloroborane is activated by the nickel(0)-catalyst **1.34-I**, resulting in the formation of a nickel(boryl)chloro intermediate **1.34-II**. This B–Ni bond further undergoes an intramolecular insertion of the carbon-carbon triple bond. Furthermore, it is presumed that the *trans*-addition intermediate **1.34-IV** may be formed by *cis-trans* isomerization of an initially formed *cis*-addition intermediate **1.34-III**. The large steric repulsion in **1.34-III** between the $\{Ni(L)_2(Cl)\}$-moiety and the di-*iso*-propylamino group may be the thermodynamic reason for the formation for the *cis-trans* isomerization (Scheme 1.34).[56]

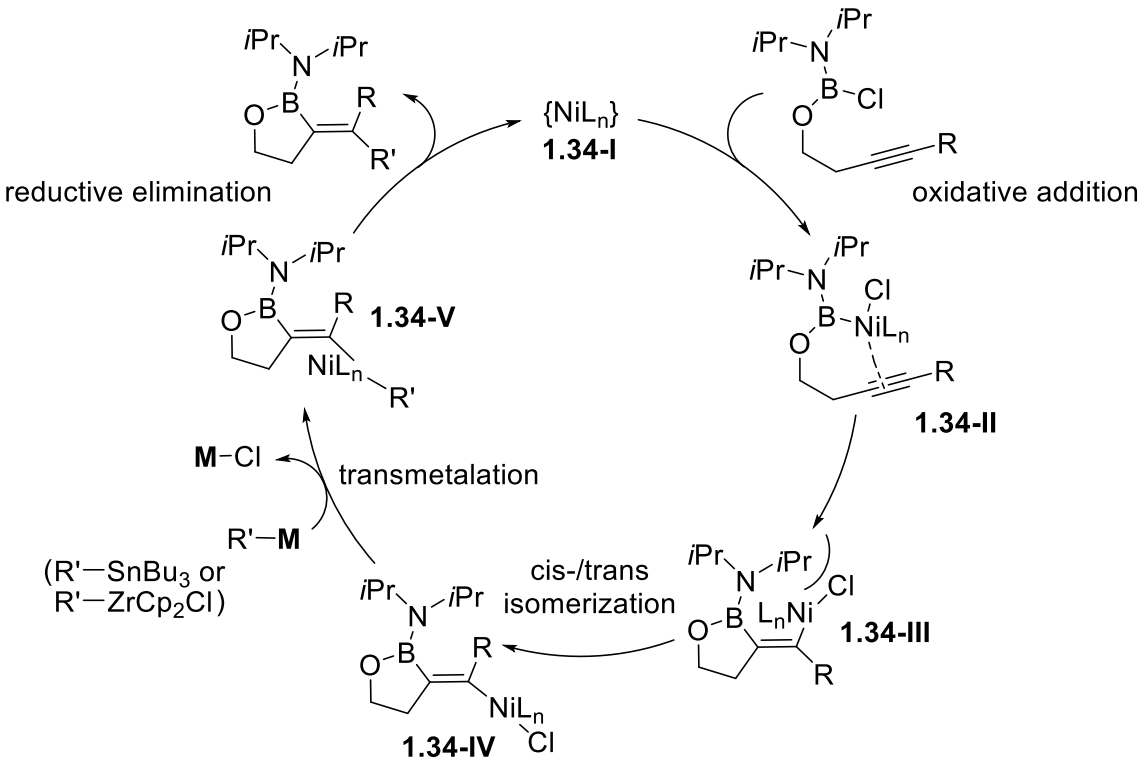

Scheme 1.34 Proposed mechanism for the Ni-catalyzed borylation of chloroboranes with alkynylstannanes or alkenylzirconium compounds.[56]

1.7 BORYLATION OF ALKENES AND DIENES

In 2003, Suginome *et al.* reported the regio- and stereo-controlled synthesis of boryl-substituted allylsilanes *via* a [Ni(acac)$_2$]/DIBAH-catalyzed silaborylation of 1,3-dienes.[57] Applying the successful silaborylation to cyclic 1,3-dienes failed, but modification of the catalytic system by adding the phosphine ligand PCyPh$_2$ provided the *cis*-silaborylation product stereoselectively in high yields. Furthermore, a catalytic stereoselective 1,4-diborylation of conjugated dienes with B$_2$pin$_2$ as the boron source was accomplished with a [Ni(COD)$_2$]/PCy$_3$ catalyst, as reported by Morken and co-workers.[58] This reaction enlarged the substrate scope for catalytic diene diborylation, especially concerning internal and sterically hindered dienes (Scheme 1.35).

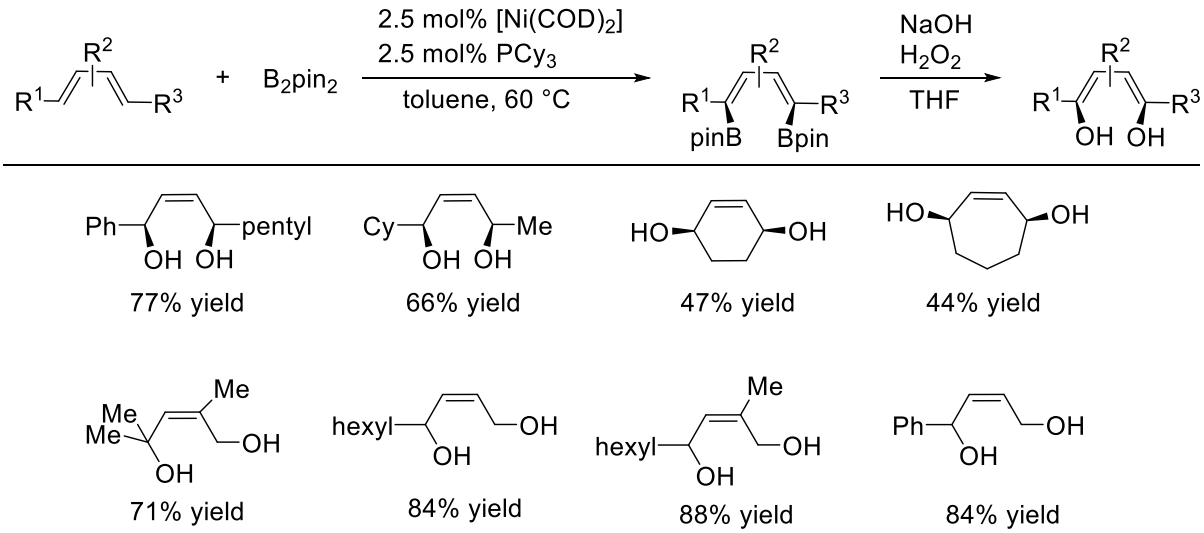

Scheme 1.35 $[Ni(COD)_2]/PCy_3$-catalyzed stereoselective 1,4-diborylation of conjugated dienes.[58]

Morken *et al.* also reported a stereoselective diborane(4)-promoted diene-aldehyde coupling reaction catalyzed by $[Ni(COD)_2]/PCy_3$.[59] Mechanistic studies by Ogoshi *et al.* gave the first structural evidence that such a nickel-promoted reductive coupling of dienes and aldehydes is initiated by cyclometalation of the substrates.[60] A subsequent *σ*-bond metathesis and reductive elimination formed the unsaturated reaction product in the presence of a metal hydride (Scheme 1.36a). Diborane(4) reagents may participate in an analogous *σ*-bond metathesis reaction, thereby providing access to organoboronic esters as the reaction product (Scheme 1.36b).[59]

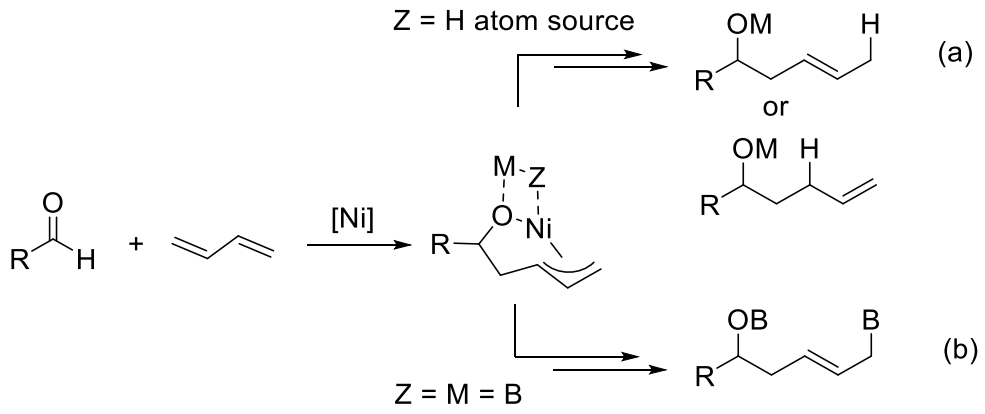

Scheme 1.36 Ni-catalyzed reductive coupling of dienes and aldehydes.[59, 60]

Two years later, the same group described a remarkable change in regioselectivity of the borylative diene/aldehyde coupling reaction when the ligand PCy_3 was replaced by $P(SiMe_3)_3$ (Scheme 1.37).[61] They proposed that the regioselectivity observed with this ligand must arise from electronic rather than steric differences, as the cone angle of e.g. P*t*Bu$_3$ is similar to that of $P(SiMe_3)_3$, but the ratio of the products generated in the catalytic reaction is reversed (**A**:**B** = >20:1 and 1:12, respectively). Later, when using the sterically similar phosphine P*t*Bu$_3$ as the ligand, a stereoselective borylative coupling reaction between dienes and ketones was achieved by utilizing $[Ni(COD)_2]$ as the precatalyst.[62]

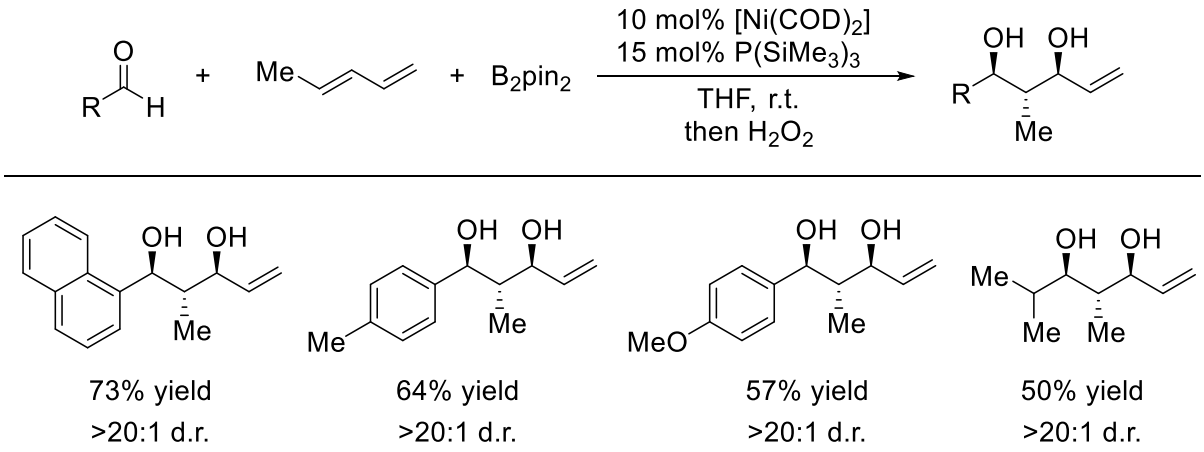

Scheme 1.37 $[Ni(COD)_2]/P(SiMe_3)_3$-catalyzed diene/aldehyde coupling reaction.[61]

In 2012, Morken *et al.* also reported a highly efficient method for the synthesis of functionalized and substituted allylic boronates.[63] They demonstrated that allylic acetates were converted to allylic boronates in high yields with a high level of functional group compatibility when catalyzed by $[Ni(COD)_2]$ with PCy_3 or PPh_3 as the ligand, using B_2pin_2 as the boron source.

Recently, the group of Turculet introduced a first-row transition metal-catalyzed isomerization-hydroboration of alkenes as depicted in Scheme 1.38.[64] The group described computational and experimental studies of reactions involving (*N*-phosphinoamidinate)metal($N(SiMe_3)_2$) precatalysts for the isomerization-hydroboration of 1-octene, *cis*-4-octene, or *trans*-4-octene with HBpin as the boron source. While, for example, the use of an Fe or Co precatalyst showed high catalytic activity and selectivity for the terminal hydroboration product (*n*-octyl)Bpin, the Ni and Mn analogues revealed only poor hydroboration yields.

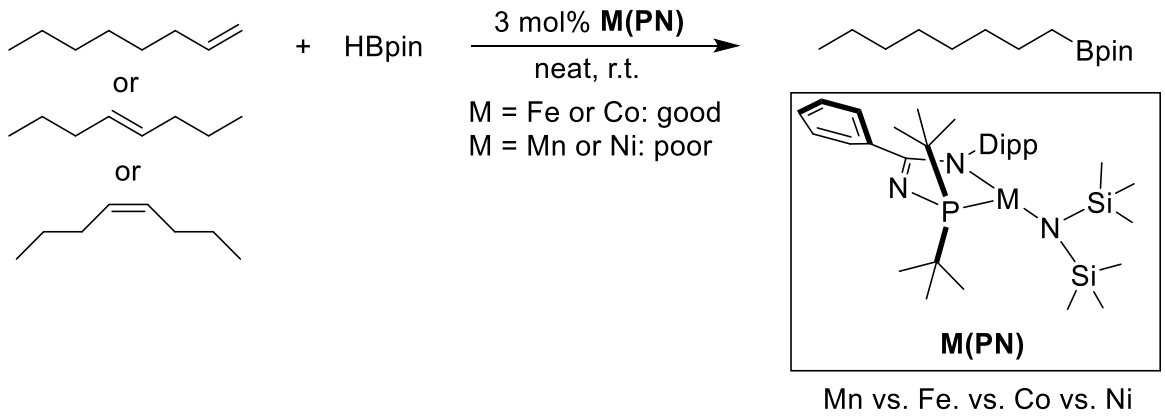

Scheme 1.38 First-row transition metal-catalyzed isomerization-hydroboration of octenes with HBpin.[64]

Furthermore, Suginome *et al.* reported the silaborylative ring-opening reaction of a variety of vinylcyclopropanes (VCPs) catalyzed by a [Ni(acac)$_2$]/PCy$_3$/DIBAH system.[65] This silaborylation yielded 5-borylallylsilane compounds *via* selective cleavage of the proximal C–C bond in the cyclopropane ring (Scheme 1.39a). While P*n*Bu$_3$ is only a little less effective than PCy$_3$, other phosphine ligands, such as PPh$_3$, PCyPh$_2$, P*t*Bu$_3$ generated the silaborylation product in less than 10% yield. This silaborylative C–C bond cleavage was also successfully applied to vinylcyclobutanes (VCBs) giving 6-borylallylsilanes simply by using [Ni(acac)$_2$] as the catalyst without any phosphine ligand (Scheme 1.39b). Based on the exclusive formation of the *E*-allylsilanes, the authors proposed that the silaborylation of VCBs proceeds *via* a mechanism analogous to that of VCPs.

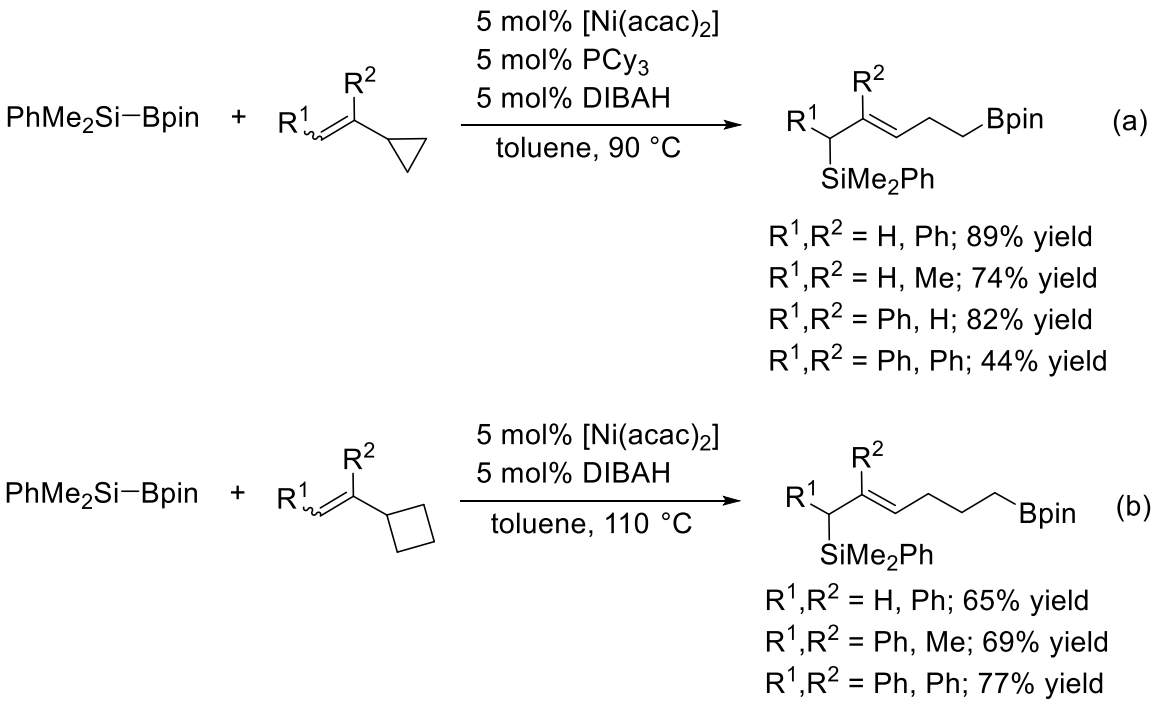

Scheme 1.39 (a) $[Ni(acac)_2]/PCy_3$/DIBAH-catalyzed silaborylative ring-opening reaction of VCPs. (b) $[Ni(acac)_2]$/DIBAH-catalyzed silaborylative ring-opening reaction of VCBs.[65]

Oshima, Yorimitsu and co-workers also reported a ring-opening reaction of VCPs in the presence of $K_3PO_4 \cdot H_2O$ and catalytic amounts of $[Ni(COD)_2]/PCyp_3$ forming allylic boronates in high yields with high *E*-selectivity.[66] With increasing size of the EWGs attached to the cyclopropane ring, the *E*/*Z* ratios were slightly improved, but the reaction required higher catalyst loadings to provide high yields. One year later, the same group reported another nickel-catalyzed borylative ring-opening reaction of aryl cyclopropyl ketones forming synthetically useful 4-oxoalkylboronates.[67] The application of the previously reported standard conditions using a $[Ni(COD)_2]/PCyp_3$ catalyst gave only low yields. The use of the NHC ligand, Mes_2Im, provided higher activity and improved the yields to 95% (Scheme 1.40).

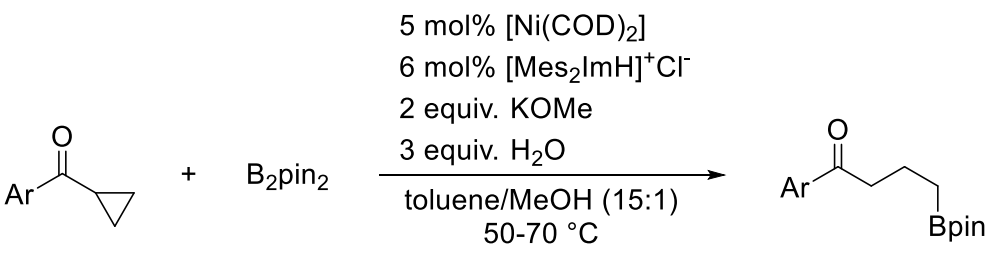

Scheme 1.40 $[Ni(COD)_2]/Mes_2Im$-catalyzed borylative ring-opening reaction of VCPs.[67]

Pineschi *et al.* demonstrated that [Ni(COD)$_2$]/BINAP (BINAP = 2,2'-bis(diphenyl-phosphino)-1,1'-binaphthyl) is a useful catalyst for the regio- and stereoselective ring-opening of vinyl epoxides and aziridines with B_2pin_2 at ambient temperature.[68] The functionalized allylic boronate derivatives obtained from this reaction can easily be oxidized to synthetically useful bis-allylic 1,4-amino alcohols (Scheme 1.41). The reaction was carried out in a toluene/methanol mixture (30:1). It is worth noting that the reaction did not proceed without the addition of methanol; however, with increased amounts of this solvent, side products were observed derived from the methanolysis of the initial vinyl epoxide.

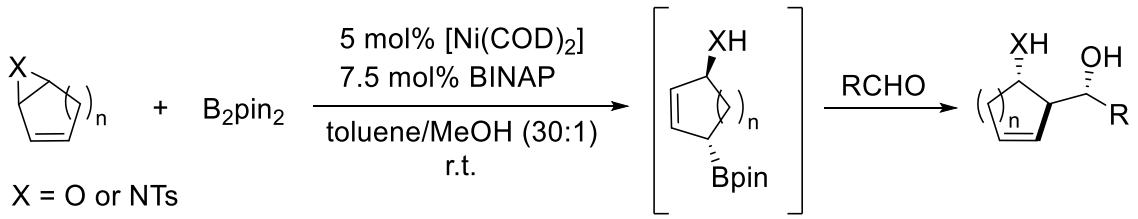

Scheme 1.41 [Ni(COD)$_2$]/BINAP-catalyzed borylative ring-opening reaction of vinyl epoxides and further oxidation to bis-allylic 1,4-amino alcohols.[68]

1.8 *α,ß*-BORYLATION OF *ß*-UNSATURATED COMPOUNDS

Oshima, Yorimitsu and co-workers reported the *ß*-borylation of *α,ß*-unsaturated esters and amines.[69] The catalyst system [Ni(COD)$_2$]/PCy$_3$ with Cs_2CO_3 as the base in toluene/methanol gave the borylation of di-, tri- and tetrasubstituted substrates at room temperature in good yields (Scheme 1.42).

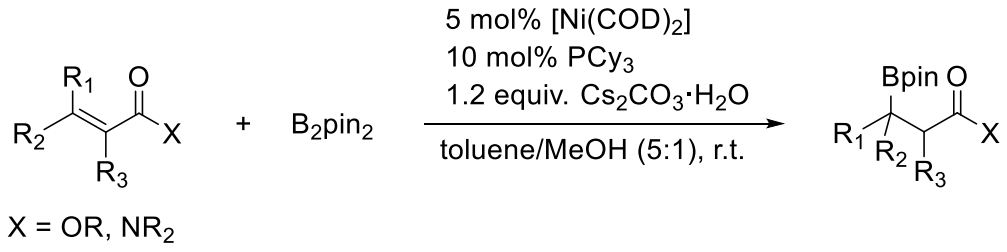

Scheme 1.42 [Ni(COD)$_2$]/PCy$_3$ catalyzed *ß*-borylation of *α,ß*-unsaturated esters and amines.[69]

Two years later Westcott, Fernandez *et al.* reported a catalyst system based on nickel complexes modified with chiral P-P ligands, which can be applied for the enantioselective borylation of the *ß*-position of *α*,*ß*-unsaturated esters.[70]

1.9 C(ALKYL)–X BOND BORYLATION

Recent efforts have focused on C(sp^3)–C(sp^3) cross-coupling reactions of unactivated alkyl halides. These investigations reveal that it may only be successfully applied to secondary and primary alkyl halides, as exemplified by a report by Fu and Zhou on the nickel-catalyzed alkyl-alkyl cross-coupling reactions.[71] The same group observed the opposite trend for closely related C–B bond formation reactions, and achieved the first example of borylation reactions of unactivated tertiary alkyl electrophiles. In this case, the reactivity of unactivated alkyl bromides towards B_2pin_2 was the highest for a tertiary alkyl bromide, using a catalyst formed *in situ* from [Ni(Br)$_2$·diglyme] and a pybox ligand (Scheme 1.43).[71-73]

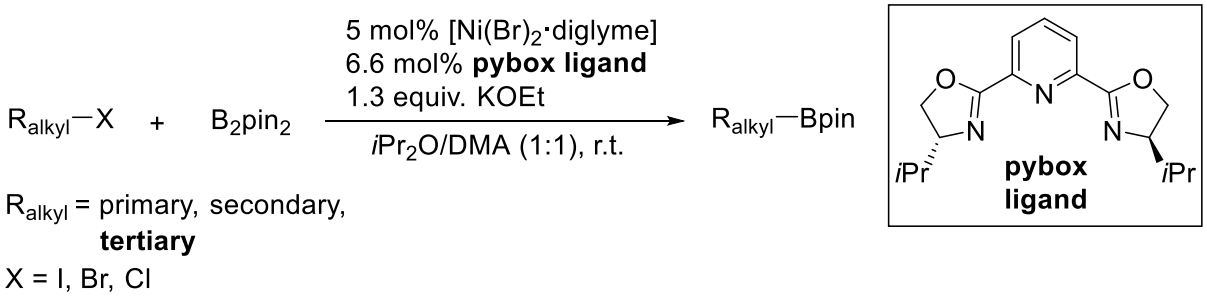

Scheme 1.43 [Ni(Br)$_2$·diglyme]/pybox-catalyzed borylation of unactivated primary, secondary and tertiary alkyl halides.[71-73]

In 2015, Lin, Marder and co-workers provided computational insight into the nickel-catalyzed carbon-carbon versus carbon-boron coupling reactions of unactivated alkyl bromides.[74] The reactions are characterized by opposite reactivity orders regarding primary, secondary, and tertiary alkyl bromides. According to DFT-calculations, reductive elimination is the rate-determining step for the carbon-carbon cross-coupling reaction, whereas in the borylation case, the rate is determined largely by the atom-transfer step. The boryl ligand involved in the borylation process possesses an empty p-orbital, which greatly accelerates the reductive elimination process. Thus, the difficulty for non-activated tertiary alkyl halides to undergo alkyl-alkyl cross-coupling lies mainly in the high barrier for the final reductive elimination step.

CHAPTER 2

STOICHIOMETRIC AND CATALYTIC ARYL–CL ACTIVATION AND BORYLATION USING NHC-STABILIZED NICKEL(0) COMPLEXES

2 STOICHIOMETRIC AND CATALYTIC ARYL–CL ACTIVATION AND BORYLATION USING NHC-STABILIZED NICKEL(0) COMPLEXES

2.1 INTRODUCTION

Aryl boronic acids and esters represent important precursors for modern organic synthesis.[75-77] Transition metal-catalyzed borylations of aryl C–H[78-81] and C–X bonds[2, 82-90] have become especially attractive and mild routes to aryl boronates. In 1995, Miyaura and co-workers demonstrated the first catalytic synthesis of an arylboronic ester, that is, the [Pd(dppf)$(Cl)_2$]-catalyzed borylation of aryl iodides and bromides[2] using B_2pin_2 as the boron source.[76] Given that early borylation reactions were often based on precious metal catalysts, first row "earth abundant" metal catalysts have become of increasing interest, due to their low cost and toxicity.[91-97] Zhu and Ma reported the copper-catalyzed borylation of aryl iodides with HBpin in the presence of CuI and NaH at room temperature, but this reaction does not work with aryl bromides.[84] Later, the groups of Lin and Marder reported the first copper-catalyzed borylation of aryl bromides, including electron-rich and hindered examples, under mild conditions (room temperature) using a phosphine Cu(I) catalyst and KO*t*Bu.[85] Marder *et al.* also reported two efficient systems, active at room temperature, using $ZnBr_2$ and Mes_2Im, or a combination of $ZnCl_2$ and 4,4'-di-*tert*-butyl-2,2'-bipyridine (dtbpy) for the catalytic borylation of aryl iodides and bromides.[86, 87] One example was demonstrated for an electron-poor aryl chloride at elevated temperatures of 50 °C, resulting in only a poor yield of 18%.[86] Nakamura and co-workers reported an iron-catalyzed borylation reaction that effectively transforms biaryl chlorides into the corresponding boronate esters using [Fe$(acac)_3$] and KO*t*Bu in toluene at 130 °C.[88] However, the borylation of aryl chlorides such as chlorobenzene or 4-chloroanisole gave only 27% and 46% yields, respectively, of borylated products. Using biaryl iodides or bromides as substrates, the reaction suffers from large quantities of hydrodehalogenation byproducts. A cobalt-catalyzed borylation of aryl halides and pseudohalides, also including aryl chlorides, was reported utilizing expensive oxazolinylferrocenyl-phosphine ligands and MeLi, a reactive organometallic reagent.[89] Another milder method for the borylation of aryl chlorides, employing an NHC-stabilized Co(II) catalyst and KOMe as the base at 50 °C, was recently introduced by Geetharani and co-workers.[90] Since Tour *et al.* demonstrated the first nickel-catalyzed borylation of aryl halides,[1] various borylation reactions of aryl halides based on [Ni$(PR_3)_2(Cl)_2$]

complexes were reported.[3-9, 12, 13] A mixed-ligand system developed by the group of Percec consisting of [Ni(dppp)Cl_2] and dppf as the co-ligand turned out to be very efficient for the borylation of aryl chlorides (Scheme 1.2).[4-6] Furthermore, this system, as well as [Ni(dppp)$(Cl)_2$] with PPh_3 as the additional ligand, turned out to be effective catalysts for the borylation of aryl iodides, bromides and chlorides bearing electron-rich and electron-deficient *ortho*-substituents in toluene at 100 °C.[5] These borylation reactions involve the use of *in situ* prepared HBneop as the boron source formed by adding BH_3·DMS to a toluene solution of neopentylglycol, as well as NEt_3 as an additive, which has to be freshly distilled from CaH_2 for a satisfying catalytic conversion.[4-6] In the same year, Murata *et al.* reported the borylation of aryl chlorides using HBpin as the boron source and catalytic amounts of [Ni(dppp)$(Cl)_2$] with Bu_4NBr and NEt_3 as additives in dioxane at 100 °C.[8] Yamakawa and co-workers also effectively borylated a variety of aryl bromides and chlorides in THF at 100 °C using the phosphine-stabilized nickel complex [Ni$(PMe_3)_2(Cl)_2$]; however, the reaction requires the addition of CsF and $SiMe_3(OCH_2CF_3)$ (Scheme 1.5).[12] Molander and co-workers achieved room temperature borylation for some electron-poor aryl chlorides by the combination of [Ni(dppp)$(Cl)_2$] and PPh_3 in ethanol using $B_2(OH)_4$ as the boron source and DIPEA as an additive (Scheme 1.6).[13] However, using 4-chloroanisole, temperatures of 80 °C were required to give a 66% yield of the borylated product. The borylation of 4-bromotoluene using the same catalyst system only proceeds at elevated temperatures of 80 °C yielding 84% of the borylated arene. The new catalytic system, described in the following, has the advantage of a readily prepared catalyst requiring no additional ligands. NaOAc as the additive is mild, inexpensive, nontoxic, and easier to use compared with DIPEA and NEt_3 employed by the groups of Percec, Murata, and Molander.[4-6, 8, 13]

Radius and co-workers have demonstrated the reactivity of the NHC-stabilized nickel(0) complex [Ni_2(*i*Pr_2Im)$_4$(μ-(η^2:η^2)-COD)] towards organic halides[21-26, 98-104] and other substrates[105-107] in stoichiometric element–element bond activation reactions. The use of this complex as a catalyst made C–F bonds in per- and polyfluorinated arenes accessible for Suzuki-Miyaura cross-coupling reactions.[22] Oxidative addition of aryl chlorides to [Ni_2(*i*Pr_2Im)$_4$(μ-(η^2:η^2)-COD)] affords complexes of the type *trans*-[Ni(*i*Pr_2Im)$_2$(Cl)(Ar)].[100] The application of [Ni_2(*i*Pr_2Im)$_4$(μ-(η^2:η^2)-COD)] as a catalyst for Suzuki-Miyaura cross-coupling reactions of aryl chlorides and bromides revealed high catalytic activity without needing additional ligands.[100, 102, 103] Furthermore, in

2016, the groups of Radius and Marder reported efficient C–F bond borylation of a variety of fluoroarenes catalyzed by the related complex [Ni($Mes_2Im)_2$], bearing a sterically more demanding NHC, in the presence of NMe_4F or CsF as an additive and B_2pin_2 as the boron source (Scheme 1.10).[20] The same groups have recently shown that this reaction can take place at ambient temperatures using visible light in the presence of a novel rhodium-biphenyl photocatalyst (Scheme 1.12).[27] In the following section, the first NHC-nickel-catalyzed borylation of aryl chloride C–Cl bonds and the stoichiometric oxidative addition of aryl–Cl bonds to [$Ni_2(Cy_2Im)_4$(μ-(η^2:η^2)-COD)] **1** is described.

2.2 RESULTS AND DISCUSSION

The catalytic investigation was initiated using 4-chlorobenzotrifluoride **4-Cl** (1.0 equiv.) as the substrate, B_2pin_2 (1.5 equiv.) as the boron source, NMe_4F (1.5 equiv.) as the base and [$Ni_2(Cy_2Im)_4(\mu\text{-}(\eta^2\text{:}\eta^2)\text{-COD})$] **1** (2.5 mol%) as the catalyst (for synthesis and characterization of complex **1** see below). Methylcyclohexane was chosen as the solvent, as earlier studies demonstrated that these conditions are excellent for C–F bond borylation.[20] From this initial reaction, the C–Cl bond borylation product **4** was obtained in 67% yield (Table 2.1, entry 1). With this promising first result, different bases, solvents, catalysts, and boron sources were screened using standard conditions (100 °C, 24 h). First of all, the studies revealed the importance of the base, as when no base was used the borylated product was observed in only 31% yield (Table 2.1, entry 8), whereas the use of NaOAc or K_3PO_4 increased the yields of **4** to 99% and 95%, respectively (Table 2.1, entries 2, 5). Decreasing the amount of NaOAc and B_2pin_2 from 1.5 to 1.0 equivalents each only lowered the yield of **4** to 74% (Table 2.1, entry 3). The bases CsF and Li*O*t*Bu worked well (Table 1, entries 6-7), whereas KF gave **4** in only 17% yield (Table 2.1, entry 3). Using Li*O*t*Bu, CsF, or KF, trace amounts of the biaryl homocoupling byproduct were observed by GC-MS. Running the reaction at 80 °C gave only traces of borylation product **4** (Table 2.1, entry 9).

Table 2.1 Screening of different bases and solvents for the borylation of 4-chlorobenzotrifluoride **4-Cl**.

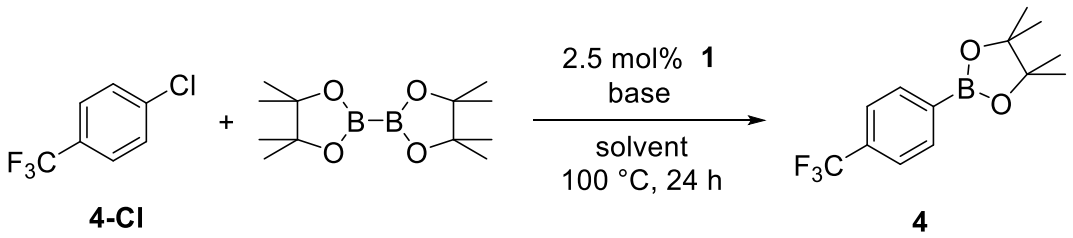

Entry	Substrate	Base	Solvent	Yield [%][a]
1	**4-Cl**	NMe_4F	methylcyclohexane	67
2	**4-Cl**	NaOAc	methylcyclohexane	>99
3	**4-Cl**	NaOAc	methylcyclohexane	74[b]
4	**4-Cl**	KF	methylcyclohexane	17
5	**4-Cl**	K_3PO_4	methylcyclohexane	95
6	**4-Cl**	LiO*t*Bu	methylcyclohexane	65
7	**4-Cl**	CsF	methylcyclohexane	59
8	**4-Cl**	-	methylcyclohexane	34
9	**4-Cl**	NaOAc	methylcyclohexane	4[c]
10	**4-Cl**	NaOAc	*n*-hexane	37
11	**4-Cl**	NaOAc	toluene	>99
12	**4-Cl**	NaOAc	acetonitrile	23
13	**4-Cl**	NaOAc	MTBE	33
14	**4-Cl**	NaOAc	THF	29

[a] Reaction conditions: $[Ni_2(Cy_2Im)_4(\mu\text{-}(\eta^2{:}\eta^2)COD)]$ **1** (2.5 mol%), 4-chlorobenzotrifluoride **4-Cl** (368 mmol, 1.0 equiv.), B_2pin_2 (1.5 equiv.), base (1.5 equiv.), solvent (5 mL), 100 °C, 24 h. The yields were determined by GC-MS of a diluted and filtered aliquot of the reaction mixture using biphenyl as an internal standard. [b] B_2pin_2 (1.0 equiv.), base (1.0 equiv.). [c] 80 °C

With the optimized base in hand, the influence of the solvent on the reaction was investigated. Yields of **4** decreased to 37% (*n*-hexane), 23% (acetonitrile) 33% (MTBE) and 29% (THF) (Table 2.1, entries 10,12-14), whereas toluene as the solvent gave a 99% yield of the borylated product **4** (Table 2.1, entry 11). Thus, the best solvents are hydrocarbons with a reasonably high boiling point. The competitive C–H bond borylation of toluene, reported by Chatani *et al.*,[33] was not observed in the presence of an aryl chloride.

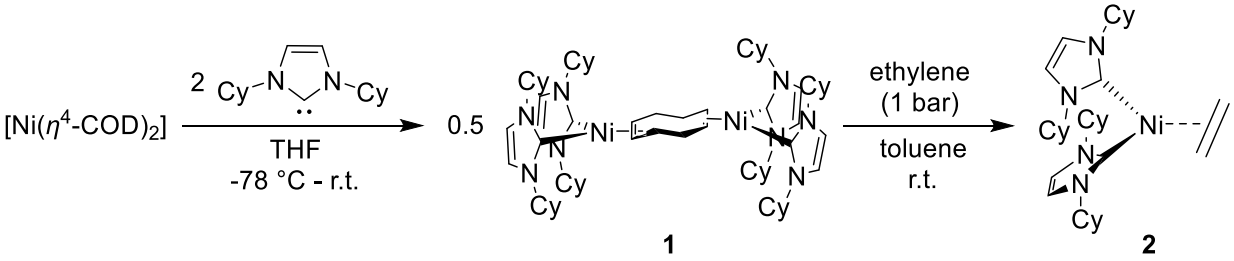

Scheme 2.1 Synthesis of the dinuclear, COD-bridged complex $[Ni_2(Cy_2Im)_4(\mu\text{-}(\eta^2\text{:}\eta^2)\text{-COD})]$ **1**, which was further reacted with ethylene forming $[Ni(Cy_2Im)_2(\eta^2\text{-}C_2H_4)]$ **2**.

The reaction of $[Ni(\eta^4\text{-COD})_2]$ with two equivalents of the free carbene Cy_2Im in THF afforded the dinuclear, COD-bridged complex $[Ni_2(Cy_2Im)_4(\mu\text{-}(\eta^2\text{:}\eta^2)\text{-COD})]$ **1** (Scheme 2.1). Given that a significant amount of the mononuclear compound $[Ni(Cy_2Im)_2(\eta^4\text{-COD})]$ **1a** arises as a side product in this preparation (this was also observed while preparing $[Ni_2(i\text{Pr}_2Im)_4(\mu\text{-}(\eta^2\text{:}\eta^2)\text{-COD})]$[105]), **1** was further reacted with ethylene, cleanly forming $[Ni(Cy_2Im)_2(\eta^2\text{-}C_2H_4)]$ **2** (Scheme 2.1). Complex **2** was characterized by NMR spectroscopy, HRMS, and elemental analysis. To verify that the borylation reaction is actually mediated by the $\{Ni(Cy_2Im)_2\}$-complex fragment and not by any intermediate caused by the side product **1a**, the screening reactions were reproduced using $[Ni(Cy_2Im)_2(\eta^2\text{-}C_2H_4)]$ **2** as the catalyst. The yields of the borylated compounds generated by catalyst **2** are in very good agreement with those observed using catalyst **1** (Table 2.2, entry 2).

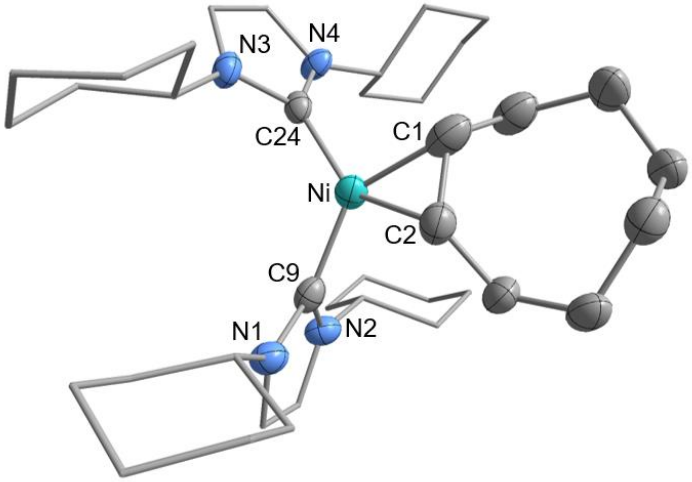

Figure 2.1 Molecular structure of [Ni(Cy$_2$Im)$_2$(η^2-COE)] **3** with thermal ellipsoids drawn at the 50% probability level; hydrogen atoms are omitted for clarity. Selected bond distances [Å] and angles [°]: Ni-C15 1.891(6), Ni-C26 1.892(5), Ni-C1 1.984(6), Ni-C8 1.953(6), Ni-(η^2–COE)$_{Centroid}$ 1.225(8), C1-C8 1.414(9), C15-Ni-(η^2-COE)$_{Centroid}$ 119.1(2), C26-Ni-(η^2-COE)$_{Centroid}$ 123.4(1).

Furthermore, the catalytic activity of other NHC-nickel complexes for C–Cl bond borylation was investigated. The complex [Ni(Cy$_2$Im)$_2$(η^2-COE)] **3** was prepared by reaction of [Ni(Cy$_2$Im)$_2$(Br)$_2$] with COE under reductive conditions (Scheme 2.2) and was characterized by NMR spectroscopy, HRMS, elemental analysis, and X-ray diffraction (Figure 2.1). Complex **3** also formed the borylation product **4** in excellent yields of 99% (Table 2.2, entry 3).

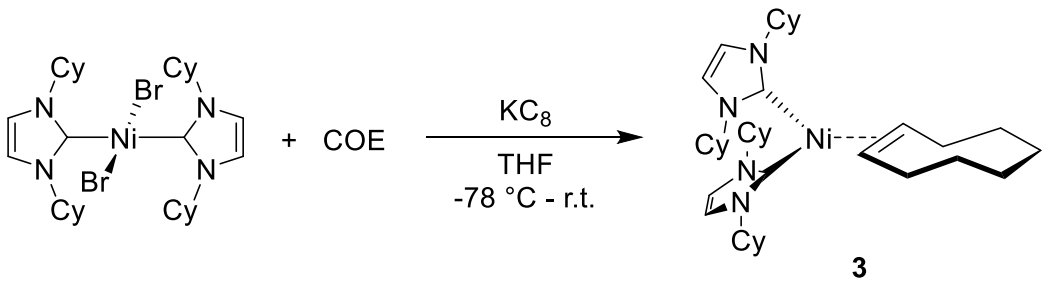

Scheme 2.2 Synthesis of [Ni(Cy$_2$Im)$_2$(η^2-COE)] **3** by reacting [Ni(Cy$_2$Im)$_2$(Br)$_2$] with COE under reductive conditions.

Using [Ni(η^4-COD)$_2$] and one equivalent of the chelating phosphine ligand dppf as a catalyst, borylation was only achieved in moderate yields of 50% (Table 2.2, entry 5). In previous work, Radius *et al.* have shown that [Ni$_2$(*i*Pr$_2$Im)$_4$(μ-(η^2:η^2)-COD)] catalyzes the Suzuki-Miyaura coupling reaction of chlorobenzene with phenylboronic acid.[100] Using this catalyst in the standard reaction afforded the borylated compound **4** in a very good yield of 91% (Table 2.2, entry 4). Moreover, the carbonyl complex [Ni(Me$_2$Im)$_2$(CO)$_2$], bearing the smaller methyl-substituted carbene ligand, revealed poor catalytic activity under the standard conditions (Table 2.2, entry 6). The application of [Ni(Mes$_2$Im)$_2$], with the sterically more demanding NHC Mes$_2$Im, which turned out to be an efficient catalyst for the C–F bond borylation of fluoroarenes in previous work,[20, 27] revealed only moderate catalytic activity (44% yield) for the borylation of C–Cl bonds under the current conditions (Table 2.2, entry 7). When the Ni(II)-complex [Ni(Cy$_2$Im)$_2$(Br)$_2$] was employed in the standard reaction, only traces of borylated product **4** were detected.

Table 2.2 Screening of different nickel-catalyst for the borylation of 4-chlorobenzotrifluoride **4-Cl**.

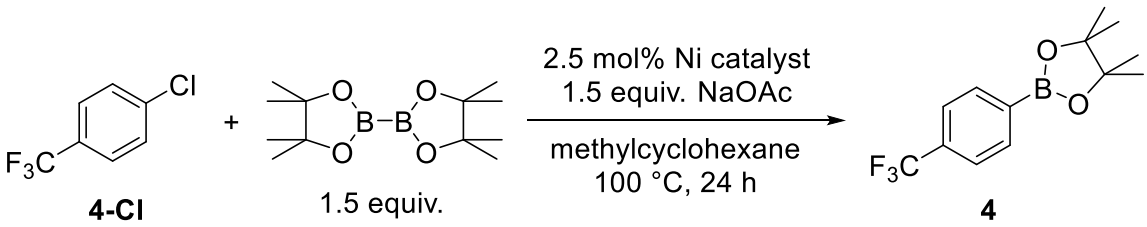

Entry	Catalyst (2.5 mol%)	Substrate	Yield [%][a]
1	$[Ni_2(Cy_2Im)_4(\mu\text{-}(\eta^2{:}\eta^2)\text{-COD})]$ **1**	**4-Cl**	>99
2	$[Ni(Cy_2Im)_2(\eta^2\text{-}C_2H_4)]$ **2**	**4-Cl**	>99[b]
3	$[Ni(Cy_2Im)_2(\eta^2\text{-COE})]$ **3**	**4-Cl**	>99[b]
4	$[Ni_2(i\text{Pr}_2Im)_4(\mu\text{-}(\eta^2{:}\eta^2)\text{-COD})]$	**4-Cl**	91
5	$[Ni(\eta^4\text{-COD})_2]$ + dppf	**4-Cl**	50[b]
6	$[Ni[(Me_2Im)_2(CO)_2]$	**4-Cl**	24[b]
7	$[Ni(Mes_2Im)_2]$	**4-Cl**	44[b]
8	$[Ni(Cy_2Im)_2(Br)_2]$	**4-Cl**	traces
9	*trans*-$[Ni(Cy_2Im)_2(Cl)(4\text{-}(F_3C)C_6H_4)]$ **11**	**4-Cl**	88

[a] Reaction conditions: Ni-catalyst (2.5 mol%), 4-chlorobenzotrifluoride **4-Cl** (368 mmol, 1.0 equiv.), B_2pin_2 (1.5 equiv.), NaOAc (1.5 equiv.), methylcyclohexane (5 mL), 100 °C, 24 h. The yields were determined by GC-MS of a diluted and filtered aliquot of the reaction mixture using biphenyl as an internal standard. [b] Ni catalyst (5.0 mol%)

Using the optimized conditions, the scope of the nickel-catalyzed C–Cl bond borylation was explored using different chloroarenes (**4-Cl**-**10-Cl**). As shown in Table 2.3, the borylation of chloroarenes containing either electron-withdrawing or -donating groups was achieved in good to excellent yields. For example, using simple chlorobenzene **7-Cl**, the borylated compound **7** was generated in 97% yield (Table 2.3, entry 4). The borylation of 4-chlorotoluene **5-Cl** gave **5** in 80% yield (Table 2.3, entry 2), whereas 4-chloroanisole **6-Cl** generated the borylated product **6** in nearly quantitative yield (Table 2.3, entry 3). Borylations of 3,5-difluorochlorobenzene **8-Cl** and 4-fluorochlorobenzene **9-Cl** gave good yields of 76% and 90%, respectively, without any competitive C–F

bond borylation product (Table 2.3, entries 5-6). Furthermore, the heteroarene 3-chloropyridine **10-Cl** was employed which provided the borylated product **10** in quantitative yields (Table 2.3, entry 7).

Table 2.3 Scope of the nickel-catalyzed C–Cl borylation.

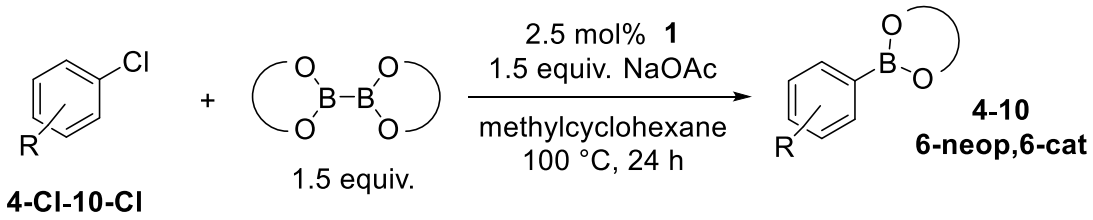

Entry	Substrate	Product	Boron Source	Yield [%][a]
1	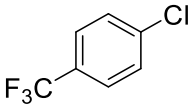	**4**	B_2pin_2	>99 (85)[b]
2	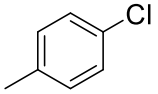	**5**	B_2pin_2	80 (61)[b]
3	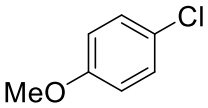	**6**	B_2pin_2	>99 (88)[b]
4	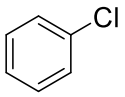	**7**	B_2pin_2	97 (79)[b]
5	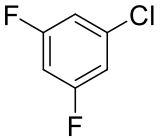	**8**	B_2pin_2	76 (63)[b]
6	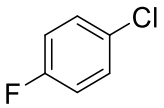	**9**	B_2pin_2	90 (77)[b]
7	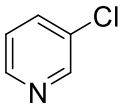	**10**	B_2pin_2	99
8	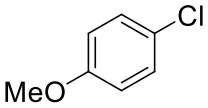	**6-cat**	B_2cat_2	traces
9	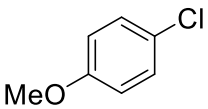	**6-neop**	B_2neop_2	76 (59)[b]

[a]Reaction conditions: $[Ni_2(Cy_2Im)_4(\mu\text{-}(\eta^2{:}\eta^2)\text{-COD})]$ **1** (2.5 mol%), aryl chloride (1.0 equiv.), boron source (1.5 equiv.), NaOAc (1.5 equiv.), methylcyclohexane (5 mL), 100 °C, 24 h. The yields were determined by GC-MS of a diluted and filtered aliquot of the reaction mixture using biphenyl as an internal standard. [b]Isolated yield after chromatographic workup.

Next, the influence of the nature of the boron source was tested by using B_2neop_2 instead of B_2pin_2. The reaction using 4-chloroanisole **6-Cl** as the model substrate yielded the borylated species **6-neop** in 76% (Table 2.3, entry 9). Notably, only traces of borylation product **6-cat** were detected utilizing B_2cat_2 as the boron source (Table 2.3, entry 8).

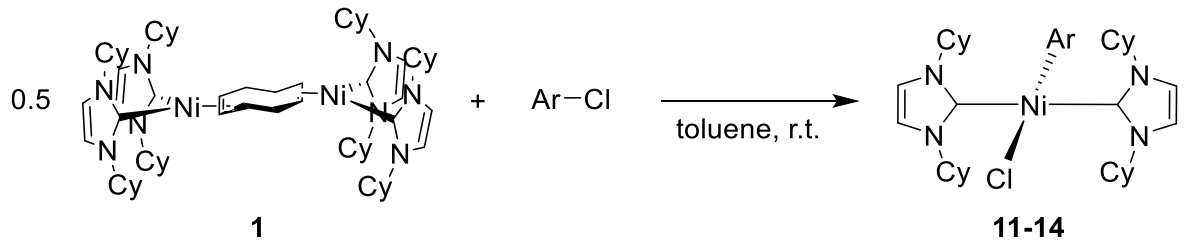

Scheme 2.3 Synthesis of the oxidative addition products of the type *trans*-[Ni(Cy_2Im)$_2$(Cl)(Ar)]. Ar = 4-F_3C-C_6H_4 **11**, 4-MeO-C_6H_4 **12**, C_6H_5 **13**, and 3,5-$F_2C_6H_3$ **14**.

In previous work, Radius and co-workers have shown that NHC-stabilized nickel complexes readily insert into C–X bonds of aryl,[20, 27, 100, 103] benzyl[102] and aroyl (C(O)Ar)[104] halides. Using [$Ni_2(Cy_2Im)_4$(μ-(η^2:η^2)-COD)] **1**, the aryl chloride C–Cl bond activation occurs cleanly (Scheme 2.3). The stoichiometric reaction of 4-chlorobenzotrifluoride **4-Cl** with **1** afforded *trans*-[Ni(Cy_2Im)$_2$(Cl)(4-F_3C-C_6H_4)] **11** in 70% isolated yield. In analogous reactions utilizing 4-chloroanisole **6-Cl** and 4-chlorobenzene **7-Cl**, the oxidative addition products *trans*-[Ni(Cy_2Im)$_2$(Cl)(4-(MeO)-C_6H_4)] **12** and *trans*-[Ni(Cy_2Im)$_2$(Cl)(C_6H_5)] **13** were isolated, respectively. Applying 3,5-difluorochlorobenzene **8-Cl** resulted in the formation of the C–Cl activation product *trans*-[Ni(Cy_2Im)$_2$(Cl)(3,5-$F_2C_6H_3$)] **14** exclusively, revealing a singlet at -115.9 ppm in the aryl fluoride region of the $^{19}F\{^1H\}$ NMR spectrum, and no signal in the range characteristic for Ni–F bonds (ca. -350 ppm). Complexes **11-14** were characterized by NMR and, IR spectroscopy, HRMS, elemental analysis and, for **14**, by X-ray diffraction (Figure 2.2). The structure obtained from X-ray analysis confirms a distorted square planar coordinated nickel(II) complex.

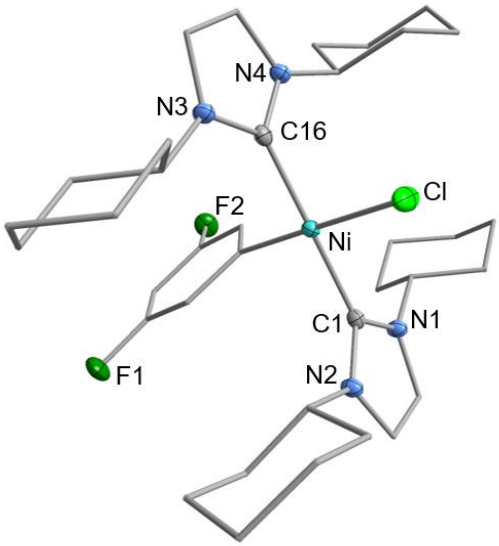

Figure 2.2 Molecular structure of *trans*-[Ni(Cy$_2$Im)$_2$(Cl)(3,5-F$_2$C$_6$H$_3$)] **14** with thermal ellipsoids drawn at the 50% probability level; hydrogen atoms are omitted for clarity. Selected bond distances [Å] and angles [°]: Ni-C1 1.889(3), Ni-C16 1.901(3), Ni-C31 1.888(2), Ni-Cl 2.226(7), C1-Ni-C16 178.4(1), C1-Ni-C31 89.88(1), C16-Ni-C31 88.83(1), C1-Ni-Cl 89.99(7), C16-Ni-Cl 91.35(7), C31-Ni-Cl 177.06(7).

The reaction using B$_2$pin$_2$, NaOAc, 4-chlorobenzotrifluoride **4-Cl** under standard conditions in the presence of catalytic amounts of the C–Cl bond activation product [Ni(Cy$_2$Im)$_2$(Cl)(4-F$_3$C-C$_6$H$_4$)] **11** generated the desired borylated product **4** (Table 2.2, entry 9). Concerning the mechanism, the reaction of [Ni$_2$(Cy$_2$Im)$_4$(μ-(η^2:η^2)-COD)] **1** with an aryl chloride leads to rapid oxidative addition of the C–Cl bond with formation of *trans*-[Ni(Cy$_2$Im)$_2$(Cl)(Ar)]. Interestingly, the reaction of **1** with stoichiometric amounts of B$_2$pin$_2$ at room temperature indicated the formation of a nickel-boryl complex (Figure 2.3 and Figure 2.4). The ^{11}B{^{1}H} NMR spectrum reveals, in addition to free B$_2$pin$_2$, a broad signal at a chemical shift of 44.5 ppm characteristic of transition metal-boryl complexes.[11, 108-110] HRMS indicates the formation of a [Ni(Cy$_2$Im)$_2$(Bpin)$_2$] species. However, the reaction does not proceed to completion as it appears to be an equilibrium process, so there is always free B$_2$pin$_2$ observed in the NMR spectra. The proposed nickel-boryl complex also has limited stability in common deuterated-solvents such as C$_6$D$_6$, d$_8$-THF and d$_8$-toluene, making further characterization extremely difficult.

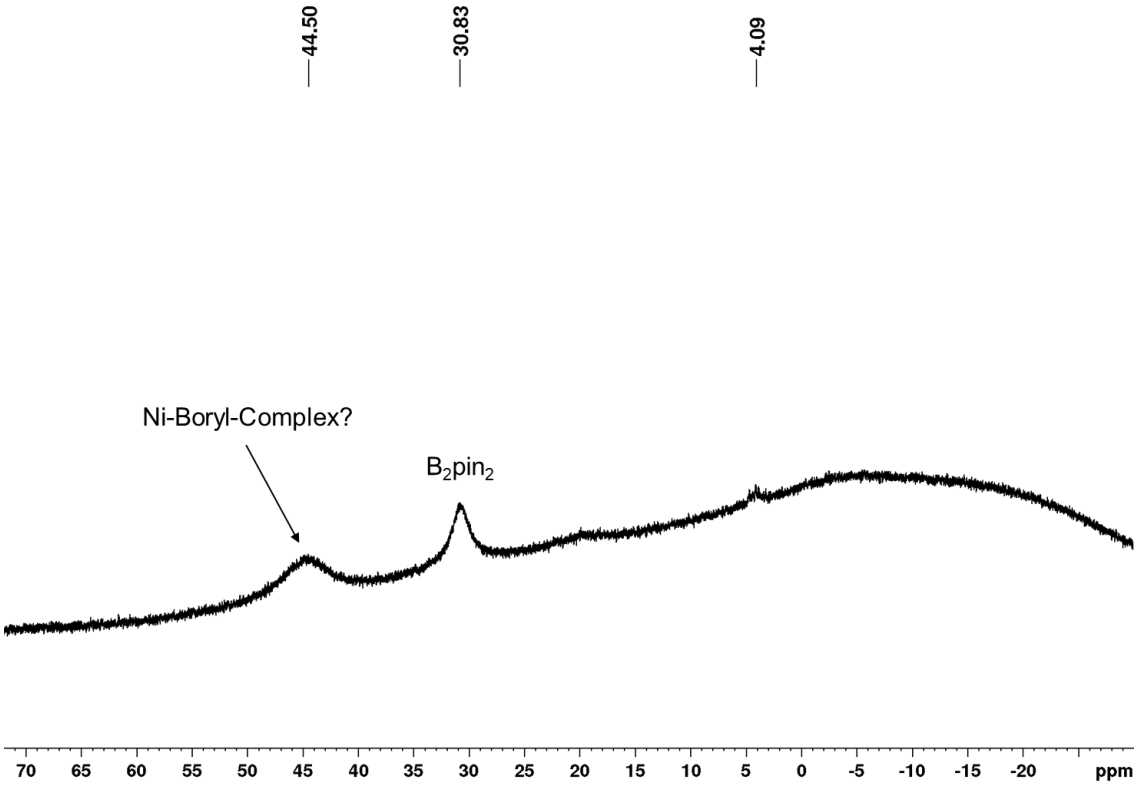

Figure 2.3 $^{11}B\{^1H\}$ NMR spectrum (recorded in methylcyclohexane; 128 MHz) of the stoichiometric reaction of $[Ni_2(Cy_2Im)_4(\mu\text{-}(\eta^2\text{:}\eta^2)\text{-COD})]$ **1** with B_2pin_2 in methylcyclohexane at room temperature.

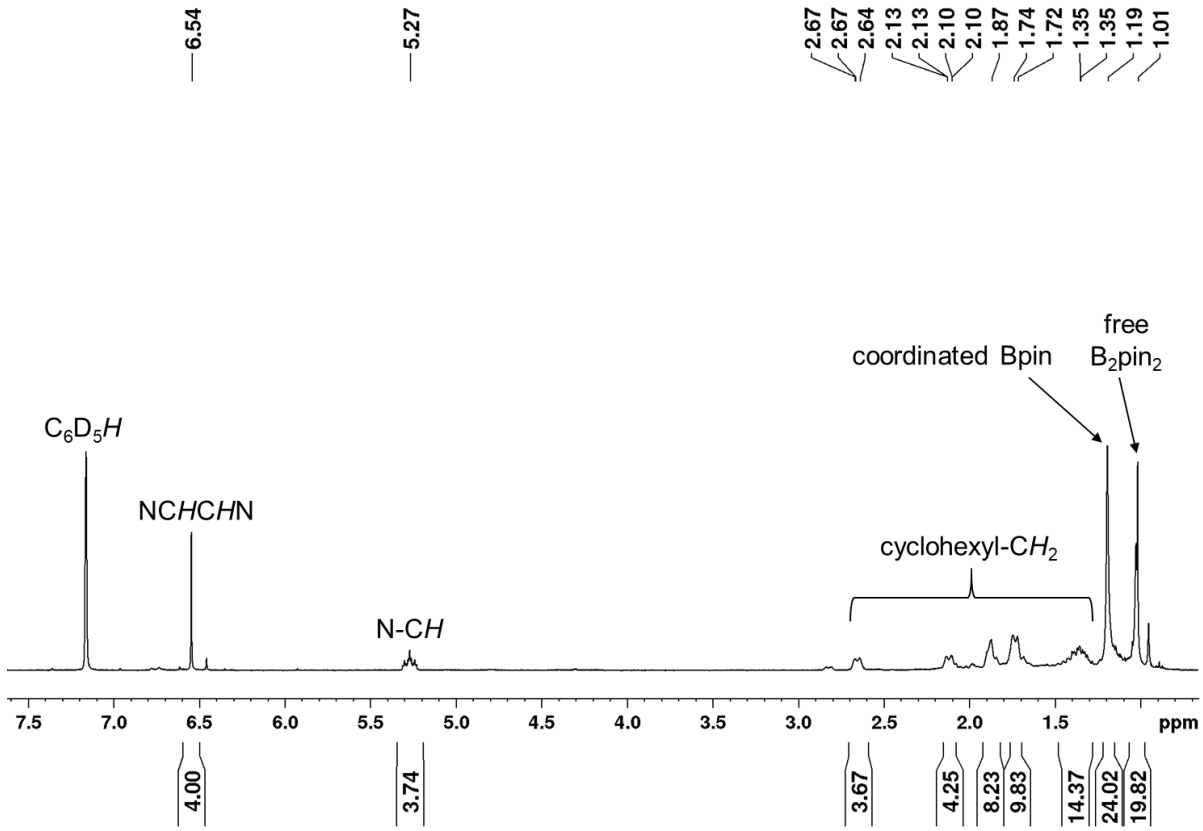

Figure 2.4 ^1H NMR spectrum of the proposed nickel-boryl complex (recorded in C_6D_6; 400 MHz).

However, the formation of the nickel-boryl species does not compete effectively with oxidative addition of a C–Cl bond to [$Ni_2(Cy_2Im)_4(\mu\text{-}(\eta^2{:}\eta^2)\text{-COD})$] **1**, as the latter shows a much higher reaction rate. It is clear that the oxidative addition product *trans*-[$Ni(Cy_2Im)_2(Cl)(Ar)$] is the resting state of the catalytic cycle. The borylation of *trans*-[$Ni(Cy_2Im)_2(Cl)(Ar)$] (i.e. transmetalation of boron to Ni) seems to be the rate-limiting process in this catalytic cycle,[20] as **11** is observed as the resting state in the reaction mixture under catalytic conditions with 50 mol% catalyst loading. It was not possible to isolate or observe *trans*-[$Ni(Cy_2Im)_2(Bpin)(Ar)$].

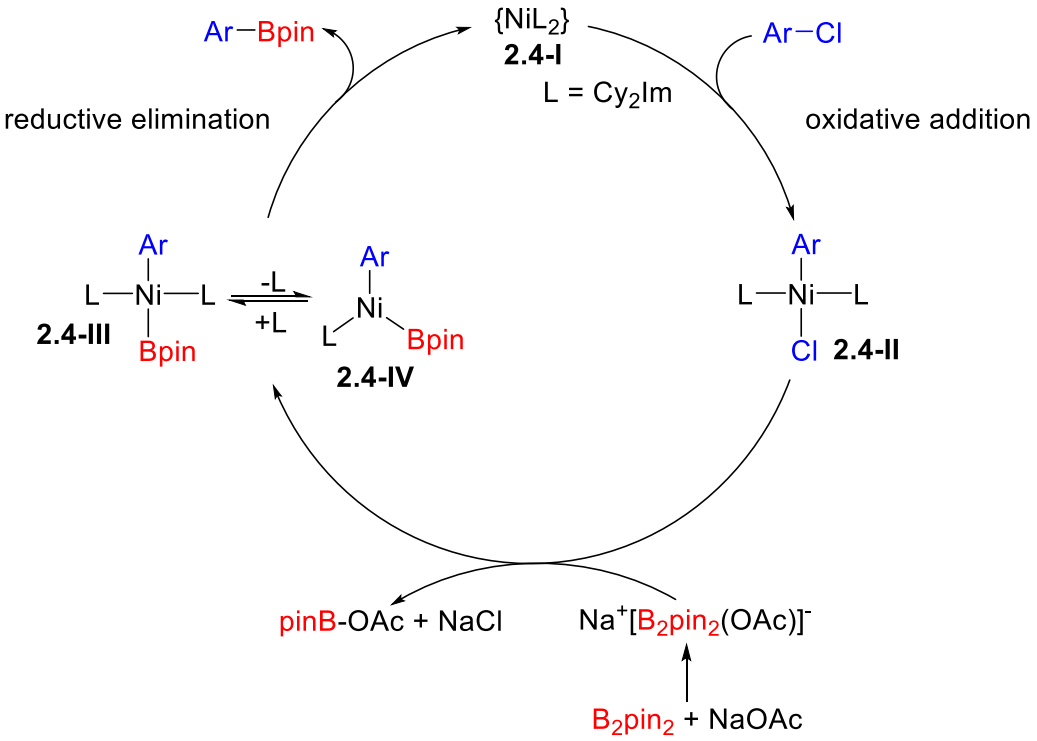

Scheme 2.4 Proposed mechanism for the NHC-nickel catalyzed borylation of aryl chlorides.

The boryl transfer reagent is either B_2pin_2, which would react with a Ni–OAc species or, possibly, its adduct Na[$B_2pin_2(OAc)$].[29] However, the treatment of **11** with NaOAc did not reveal the formation of a Ni-acetate complex, in contrast with what the group of Miyaura observed for the analogous *trans*-[$Pd(PPh_3)_2(Br)(Ph)$] complex.[2] Furthermore, no reaction or interaction was observed between B_2pin_2 and stoichiometric amounts of NaOAc either at room temperature or at 100 °C, although KOAc is capable of activating B_2pin_2 for the metal-free borylation of aryldiazonium salts.[29] A proposed mechanism is shown in Scheme 2.4. In the first step, the reaction of the {$Ni(Cy_2Im)_2$}-moiety **2.4-I** with the aryl chloride leads to oxidative addition of the

C–Cl bond forming *trans*-[Ni(Cy_2Im)$_2$(Cl)(Ar)] **2.4-II**. The acetate anion coordinates to B_2pin_2 forming the very weakly bound adduct Na[B_2pin_2(OAc)] with an activated B–B bond.[29] Complex **2.4-II** then reacts with Na[B_2pin_2(OAc)] by boryl transfer to give *trans*-[Ni(Cy_2Im)$_2$(Bpin)(Ar)] **2.4-III**, pinB–OAc and NaCl. A final reductive elimination step, after ligand dissociation, from a three coordinate species **2.4-IV** gives the desired borylated product Ar–Bpin and regenerates {Ni(Cy_2Im)$_2$} **I**.

2.3 CONCLUSION

An efficient procedure for the C–Cl bond borylation of aryl chlorides was developed using [Ni_2(Cy_2Im)$_4$(μ-(η^2:η^2)-COD)] **1** as the catalyst precursor, NaOAc as the base and B_2pin_2 as the boron source. [Ni_2(iPr$_2$Im)$_4$(μ-(η^2:η^2)-COD)] is also an efficient catalyst for this borylation reaction. The catalysts compare well with other nickel catalysts reported so far[3-9, 12, 13] with the advantage that no further ligand or additive is required other than the very mild base NaOAc. This is the first example of an NHC-nickel-mediated borylation of aryl chlorides. Furthermore, stoichiometric reactions of **1** with different aryl chlorides were demonstrated generating C–Cl oxidative addition products of the type *trans*-[Ni(Cy_2Im)$_2$(Cl)(Ar)] **11**-**14**.

CHAPTER 3

COPPER-CATALYZED BORYLATION OF ARYL CHLORIDES

3 COPPER-CATALYZED BORYLATION OF ARYL CHLORIDES

3.1 INTRODUCTION

Arylboronic acids and their derivatives represent an interesting and versatile class of compounds.[75-77] Due to their stability, low toxicity, and ease of handling, they have become important building blocks in organic synthesis, in particular as substrates for the Suzuki-Miyaura cross-coupling reaction.[75, 111, 112] As their conventional multi-step preparation,[75, 113] *via* reactive magnesium or lithium alkyl reagents, is limited by functional group compatibility, there has been an increasing interest in the development of one-step transition metal-catalyzed methods for the generation of arylboronic esters. Therefore, transition metal-catalyzed borylation has become especially attractive as a mild and powerful approach for the generation of arylboronic esters. As direct C–H bond borylation reactions of arenes[78-80, 114, 115] as well as highly selective metal-catalyzed borylation reactions of aryl halides[2, 82, 83, 94, 116-136] are often based on precious metal catalysts, first row “earth-abundant” metal catalysts have become of increasing interest due to their low cost and toxicity.[91-95, 97, 137] One of the earliest examples was the nickel-catalyzed borylation of aryl bromides using a phosphine nickel catalyst and NEt_3 as the base at elevated temperatures, demonstrated by Tour and co-workers in 2000.[1] Subsequently, a variety of nickel-catalyzed borylations of aryl halides based on $[Ni(PR_3)_2(Cl)_2]$ complexes were reported.[3-9, 12, 13] A mixed-ligand system developed by Percec *et al.* consisting of $[Ni(dppp)(Cl)_2]$ and dppf as the co-ligand was found to catalyze the borylation of aryl chlorides.[4, 5] By applying a readily prepared NHC-stabilized nickel(0) complex $[Ni_2(Cy_2Im)_4(\mu\text{-}(\eta^2\text{:}\eta^2)\text{-COD})]$ and the very mild base NaOAc, the C–Cl bond borylation of a variety of aryl chlorides was demonstrated (cf. chapter 2). The group of Radius also investigated the reactivity of the analogous NHC-stabilized nickel(0) complex $[Ni_2(i Pr_2Im)_4(\mu\text{-}(\eta^2\text{:}\eta^2)\text{-COD})]$ towards organic halides[21-26, 100-104] and other substrates[105-107] in stoichiometric element–element bond activation reactions. The application of $[Ni_2(i Pr_2Im)_4(\mu\text{-}(\eta^2\text{:}\eta^2)\text{-COD})]$ as a catalyst for Suzuki-Miyaura cross-coupling reactions of aryl chlorides and bromides revealed high catalytic activity in these transformations without additional ligands.[100, 102, 103] Recently, Radius, Marder *et al.* reported an efficient thermal[20] as well as a photocatalytic[27] procedure for the borylation of C–F bonds in aryl fluorides in the presence of $[Ni(Mes_2Im)_2]$ (Mes_2Im = 1,3-dimesitylimidazolin-2-ylidene) and a Ni/Rh tandem catalyst system, respectively.

Zhu and Ma first demonstrated that aryl iodides were borylated in the presence of CuI and NaH at room temperature; however, the conversion of aryl bromides was very poor under these conditions.[84] Later, Marder, Lin and co-workers reported the first Cu-catalyzed borylation of aryl bromides, including electron-rich and hindered examples, under mild conditions (room temperature) using a CuI/P*n*Bu$_3$ catalyst, although one example of an electron-poor aryl chloride was only borylated in low yield.[85] In 2015, a copper-catalyzed borylation of aryl iodides and bromides mediated by a bicyclic NHC-stabilized Cu-complex was reported by Ishizuka.[138] Furthermore, the group of Marder developed two efficient processes proceeding at room temperature, using ZnBr$_2$ and Mes$_2$Im, or a combination of ZnCl$_2$ and dtbpy for the catalytic borylation of aryl iodides and bromides.[86, 87] One example was reported for an electron-poor aryl chloride at elevated temperatures of 50 °C, generating the aryl boronic ester in only a poor yield of 18%. Feasible methods for the borylation of inexpensive and widely available aryl chlorides using first-row transition metals other than nickel are still rare. In 2016, Hu, Huang *et al.* developed the first Co-catalyzed borylation of aryl halides and pseudohalides, including aryl chlorides, utilizing oxazolinyl-ferrocenylphosphine ligands and MeLi, a reactive organometallic reagent.[89] Another milder method, for the borylation of aryl chlorides, employing a Co(II)-NHC catalyst and KOMe as the base at 50 °C, was recently introduced by Geetharani and co-workers.[90] Nakamura, Ilies *et al.* reported an Fe-catalyzed borylation which effectively transforms biaryl chlorides into the corresponding boronate esters using [Fe(acac)$_3$] and KO*t*Bu in toluene at 130 °C.[88] However, the use of simple aryl chlorides such as chlorobenzene or 4-chloroanisole as substrates gave only 27% and 46% yields, respectively, of borylated products. The borylation of biaryl iodides or bromides suffers from large quantities of hydrodehalogenation byproducts. Recently, Radius, Marder and co-workers described synthetic routes to and characterization of a variety of Cu(I)-complexes of the type [Cu(NHC)(Cl)],[139] some of which are shown herein to catalyze effectively the C–Cl bond borylation of a wide range of aryl chlorides.

3.2 RESULTS AND DISCUSSION

The NHC-stabilized Cu(I) complexes [Cu(*i*Pr$_2$Im)(Cl)] **15**,[139] [Cu(Me$_2$Im^{Me})(Cl)] **16**,[139] and [Cu(Cy$_2$Im)(Cl)] **17**[140] were synthesized in good yields by reacting copper(I) chloride and the corresponding free NHC at low temperatures (-78 °C) in THF (Scheme 3.1).

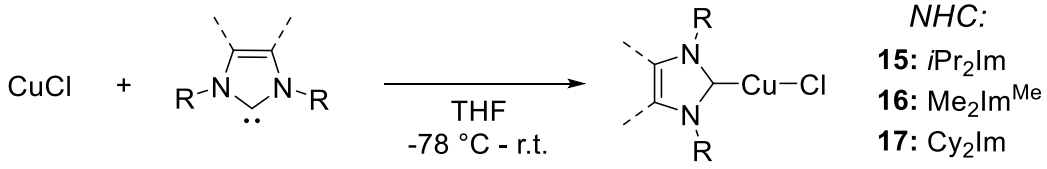

Scheme 3.1 Reaction of CuCl with free NHCs forming complexes of the type [Cu(NHC)(Cl)] **15**-**17**.

The catalytic investigation was initiated using 4-chlorobenzotrifluoride **4** (1.0 equiv.) as the model substrate, B_2pin_2 (1.5 equiv.) as the boron source, [Cu(*i*Pr$_2$Im)(Cl)] **15** (10 mol%) as the catalyst, KO*t*Bu as the base (1.5 equiv.) and methylcyclohexane (Me-Cy) as the solvent at 90 °C. Methylcyclohexane was the solvent of choice as earlier studies demonstrated it is very suitable for C–Cl (cf. chapter 2) as well as C–F[20] bond borylation reactions, avoiding competing aromatic C–H bond activations and allowing elevated reaction temperatures. From the initial approach, the C–Cl bond borylation product **4** was obtained in 73% yield (Table 3.1, entry 5). With this promising first result, a range of catalysts, bases, solvents and boron sources were screened to determine the scope and limitations of this reaction (Table 3.1). First, the influence of the NHC ligand was investigated (Figure 3.1).

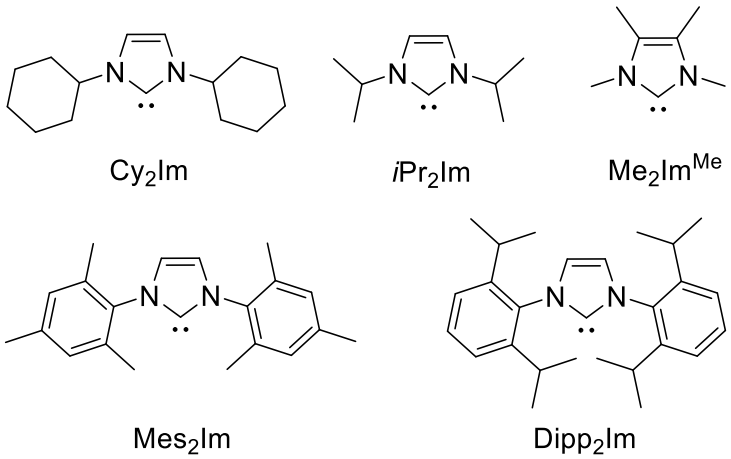

Figure 3.1 Structures of the utilized NHC ligands.

While [Cu(Me_2Im^{Me})(Cl)] **16**, bearing the small backbone methylated NHC Me_2Im^{Me}, only provided the desired product **4** in a poor yield of 25%, [Cu(Cy_2Im)(Cl)] **17** revealed a significantly higher catalytic activity than **15** and thus increased the yield to 84% (Table 3.1, entry 4 and 7). Utilizing [(Mes_2Im)CuCl] and [($Dipp_2$Im)CuCl], bearing sterically more demanding NHCs, under the standard conditions, the borylated product **4** was only obtained in traces and 12% yield, respectively (Table 3.1, entry 1-2). Employing the *in situ* formed catalyst from Cu(I) chloride and the imidazolium salt $[Cy_2ImH]^+Cl^-$ provided a slighty lower yield (Table 3.1, entry 10). Generally, inferior results were observed when using a phosphine ligand instead of an NHC ligand. Applying [(PCy_3)Cu(μ-I_2)Cu(PCy_3)] as well as the copper-XantPhos-chloro complex (XantPhos = 4,5-bis(diphenylphosphino)-9,9-dimethylxanthene) did not provide even traces of **4** (Table 3.1, entry 11-12).

Table 3.1 Screening of reaction conditions for the Cu-catalyzed borylation of **4-Cl**.[a]

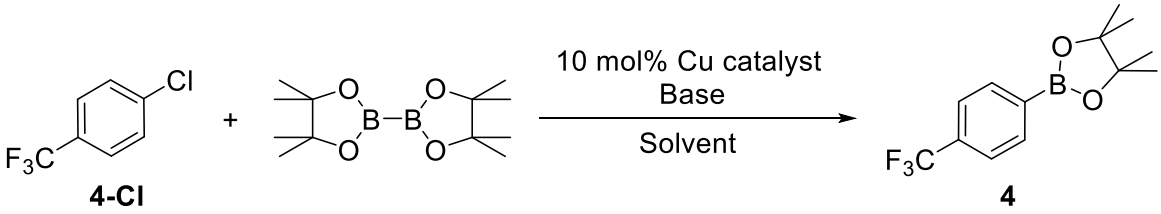

Entry	Base	Catalyst	Solvent	Yield of **4** (%)[b]
1	KO*t*Bu	[Cu(Mes$_2$Im)(Cl)]	Me-Cy	trace
2	KO*t*Bu	[Cu(Dipp$_2$Im)(Cl)]	Me-Cy	12
3	KO*t*Bu	[Cu(CaaC^{Me})(Cl)]	Me-Cy	trace
4	KO*t*Bu	[Cu(Me$_2$Im^{Me})(Cl)]	Me-Cy	25
5	KO*t*Bu	[Cu(*i*Pr$_2$Im)(Cl)]	Me-Cy	73
6	KO^{t}Bu	[Cu(Cy$_2$Im)(Cl)]	Me-Cy	69[c]
7	**KO*t*Bu**	**[Cu(Cy$_2$Im)(Cl)]**	**Me-Cy**	**84 (80)[d]**
8	KO*t*Bu	[Cu(Cy$_2$Im)(Cl)]	Me-Cy	59[e]
9	KO*t*Bu	CuCl/Cy$_2$Im	Me-Cy	78[f]
10	KO*t*Bu	CuCl/[Cy$_2$ImH]$^+$Cl$^-$	Me-Cy	74[g]
11	KO*t*Bu	[(PCy$_3$)Cu(μ-I$_2$)Cu(PCy$_3$)]	Me-Cy	0[h]
12	KO*t*Bu	[Cu(XantPhos)(Cl)]	Me-Cy	0
13	KOMe	[Cu(Cy$_2$Im)(Cl)]	Me-Cy	55
14	LiO*t*Bu	[Cu(Cy$_2$Im)(Cl)]	Me-Cy	16
15	NaOMe	[Cu(Cy$_2$Im)(Cl)]	Me-Cy	0
16	CsF	[Cu(Cy$_2$Im)(Cl)]	Me-Cy	0
17	NMe$_4$F	[Cu(Cy$_2$Im)(Cl)]	Me-Cy	39
18	-	[Cu(Cy$_2$Im)(Cl)]	Me-Cy	0
19	KO*t*Bu	[Cu(Cy$_2$Im)(Cl)]	toluene	53
20	KO*t*Bu	[Cu(Cy$_2$Im)(Cl)]	acetonitrile	trace
21	KO*t*Bu	[Cu(Cy$_2$Im)(Cl)]	1,4-dioxane	0
22	KO*t*Bu	[Cu(Cy$_2$Im)(Cl)]	THF	0
23	KO*t*Bu	[Cu(Cy$_2$Im)(Cl)]	DMF	trace
24	KO*t*Bu	[Cu(Cy$_2$Im)(Cl)]	MTBE	trace

[a] Reaction conditions, unless otherwise stated: [Cu]-catalyst (10 mol%), 4-chlorobenzotrifluoride **4-Cl** (0.5 mmol, 1.0 equiv.), B_2pin_2 (1.5 equiv.), base (1.5 equiv.), solvent (3 mL), 90 °C, 42 h. [b] The yields were determined by GC-MS of a diluted and filtered aliquot of the reaction mixture using biphenyl as an internal standard. [c] Reaction time 36 h. [d] Isolated yield. [e] B_2pin_2 (1.0 equiv.), KO*t*Bu (1.0 equiv.). [f] CuCl (10 mol%), Cy$_2$Im (10 mol%). [g] CuCl (10 mol%), [Cy$_2$ImH]$^+$Cl$^-$ (20 mol%). [h] [(PCy$_3$)Cu(μ-I$_2$)Cu(PCy$_3$)] (5 mol%).

With the optimal catalyst [Cu(Cy_2Im)(Cl)] **17** in hand, the impact of the base was further investigated. When KO*t*Bu was omitted from the reaction, no aryl boronate **4** was formed (Table 3.1, entry 18). Decreasing the amount of KO*t*Bu and B_2pin_2 from 1.5 to 1.0 equivalents each lowered the yield of **4** to 59% (Table 3.1, entry 8). Employing KOMe instead of KO*t*Bu decreased the yield to 55% (Table 3.1, entry 13), whereas no borylation occurred when NaOMe or CsF was used as the base (Table 3.1, entry 15-16). The replacement of KO*t*Bu with NMe_4F resulted in moderate yields of 39% (Table 3.1, entry 17). Methylcyclohexane proved to be the most effective among the solvents studied, whereas the aromatic hydrocarbon, toluene, provided the borylated product **4** in a moderate yield of 53% (Table 3.1, entry 19). Polar solvents, such as THF, MTBE, acetonitrile, 1,4-dioxane, and DMF were not suitable for this borylation reaction (Table 3.1, entry 20-24).

Table 3.2 Screening of aryl chlorides and diborane reagents for the Cu-catalyzed borylation reaction.[a]

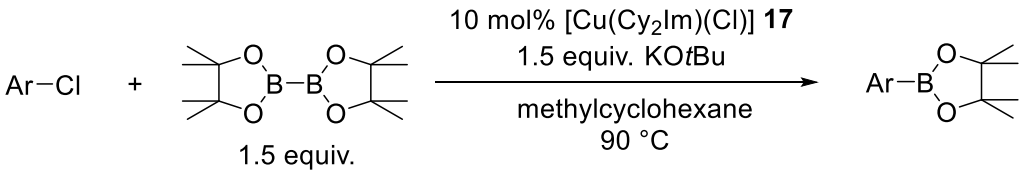

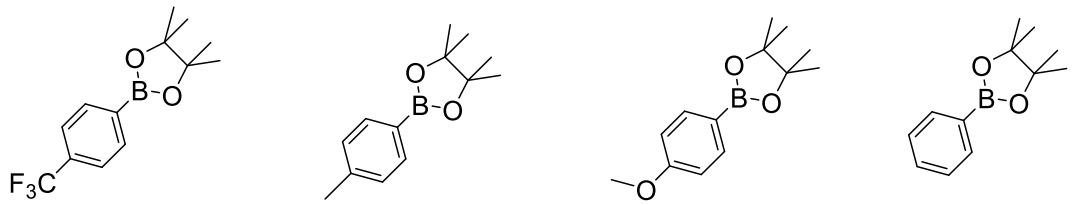

4, 80%

5, 74%

6, 50%

7, 58%

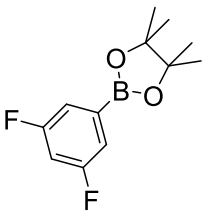

8, 72%

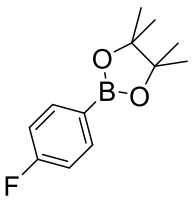

9, 78%

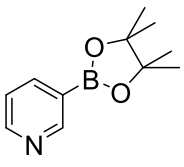

10, 68%[b]

[a] Reaction conditions, unless otherwise stated: aryl chloride (500 µmol, 1.0 equiv.), [Cu(Cy_2Im)(Cl)] **17** (10 mol%), diboron reagent (1.5 equiv.), KO*t*Bu (1.5 equiv.), methylcyclohexane (3 mL), 90 °C, 42 h. Isolated yield after chromatographic workup. [b] The yield was determined by GC-MS of a diluted and filtered aliquot of the reaction mixture using biphenyl as an internal standard.

Having identified the optimized conditions with 4-chlorobenzotrifluoride **4-Cl** as the standard substrate, various aryl chlorides with different electronic properties were screened as depicted in Table 3.2. Electron neutral chlorobenzene **7-Cl** was converted into the corresponding arylboronic ester **7** in good yields of 58%, and 4-chlorotoluene **5-Cl** and 4-chloroanisole **6-Cl**, bearing electron-donating substituents, gave the borylated products in yields of 74 and 50%, respectively. For **6-Cl** borylative cleavage of the C–O bond was not observed under these standard conditions. Beside the standard substrate **4-Cl**, the electron-poor aryl chlorides 3,5-difluorochlorobenzene **8-Cl** and 4-fluorochlorobenzene **9-Cl** were borylated in good yields of 72 and 78%, respectively. Substrate **8-Cl** and **9-Cl** were exclusively converted into the mono-borylated products **8** and **9** without any competitive C–F bond borylation. This copper-catalyzed method was also applicable for the heteroarene 3-chloropyridine **10-Cl** providing the borylated product **10** in 68% yields. When using B_2neop_2 instead of B_2pin_2 as the boron reagent, the yields are slightly lower to those observed for B_2pin_2. However, B_2cat_2, B_2eg_2, and diboronic acid were unreactive under the standard conditions, possibly due to solubility problems.

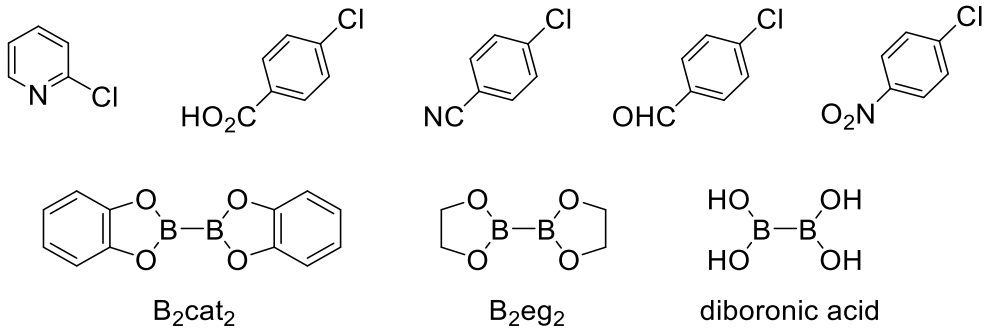

Figure 3.2 Examples of unreactive substrates and boron reagents in the copper-catalyzed borylation reaction.

Although the reaction shows a broad scope, there are certain functional groups which were not tolerated, as shown in Figure 3.2. Thus, 2-chloropyridine as well as carboxylic acid- and cyano-substituted substrates failed to provide borylated products, and the starting materials were recovered. It is possible that borylation of the pyridine or CO_2H groups occurred, but rapid and facile hydrolysis reforms the starting materials. When 4-chlorobenzaldehyde was used, no borylated product was generated. Using a substrate containing a nitro moiety under the conditions employed, generated 4,4'-dichloroazoxybenzene as the product.[141, 142]

Based on a previously postulated[85] catalytic cycle for the Cu-catalyzed borylation of aryl iodides and bromides by Marder, Lin, and co-workers, a proposed mechanism for the Cu-catalyzed borylation of aryl chlorides is shown in Scheme 3.2. In an initial step, a copper boryl complex **3.2-I** and *t*BuO–Bpin is formed by the reaction of the Cu-catalyst precursor [Cu(L)(Cl)] with the alkoxyl activated [*t*BuOB$_2$pin$_2$]$^-$ anion[29, 76] or by the reaction of [Cu(L)(O*t*Bu)] **3.2-IV** with B$_2$pin$_2$. The copper boryl complex **3.2-I** further reacts with the aryl chloride generating the desired aryl boronate and [Cu(L)(Cl)] **3.2-III**, which subsequently reacts with the base forming [Cu(L)(O*t*Bu)] **3.2-IV**. This complex regenerates the copper boryl species **3.2-I** by reaction with B$_2$pin$_2$ forming *t*BuO–Bpin. The slow step of this process is the activation of the aryl chloride by the Cu-boryl complex **3.2-I**.[143-145]

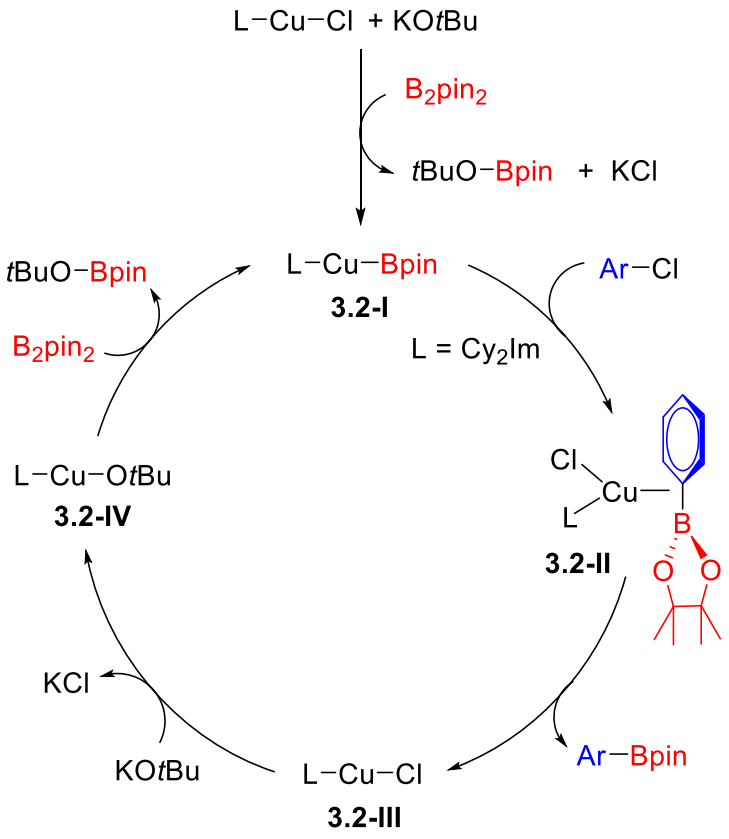

Scheme 3.2 Proposed mechanism for the NHC-copper catalyzed borylation of aryl chlorides.

While the Ni-catalyzed borylation, introduced in chapter 2, starts with an oxidative addition of the C–Cl bond to {Ni(Cy$_2$Im)$_2$} generating *trans*-[Ni(L)$_2$(Cl)(Ar)], which further reacts with the (activated) boron reagent (Scheme 2.4), the Cu-catalyzed borylation is proposed to proceed *via* the initial formation of a Cu-boryl complex **3.2-I**, followed by C–B bond formation through *σ*-bond metathesis with the aryl chloride forming the aryl boronic ester.

3.3 CONCLUSION

In summary, the first Cu-catalyzed borylation of various aryl chlorides with different electronic properties has been developed using a readily prepared NHC-stabilized Cu-catalyst and KO*t*Bu as the base. This is a simple procedure using an inexpensive, low toxicity metal, for the borylation of aryl chlorides, which are inexpensive and broadly available building blocks compared to other aryl halides.

CHAPTER 4

LEWIS BASE ADDUCTS OF BORON COMPOUNDS

4 LEWIS BASE ADDUCTS OF BORON COMPOUNDS

4.1 INTRODUCTION

Transition metal-free systems for activating the B–B bond of diborane(4) compounds have been attracting increased attention, bearing the advantage of lower costs and the avoidance of heavy metal contamination in the final product.[77] Lewis adducts of sp^2–sp^3 hybridized diborane(4) compounds activate the B–B bond and therefore show a higher reactivity, due to the change in hybridization, increased bond length and polarity.[146, 147] In 1995 and 1997, Marder and Norman reported the addition of one equivalent of the Lewis base 4-methyl-pyridine (mpy) to B_2cat_2 introducing an early example of an sp^2–sp^3 diborane(4) mpy·B_2cat_2 **4.1-I**, that takes advantage of the significant stabilizing effect of the *π*-donating cyclic boronate ester moiety.[148, 149] This was the first example of a structurally characterized sp^2–sp^3 diborane(4), in which the boron atoms are not linked in a cyclic system.[150] The latter is a key distinction, as acyclic sp^2–sp^3 diboranes do not provide a ‘‘chelate effect’’ to favor stable coordination of the Lewis base to the boron atom. The molecular structure of mpy·B_2cat_2 **4.1-I** enabled structural comparison of an sp^2–sp^3 diborane(4) with its corresponding free diborane(4) for the first time, revealing an increased B–B bond length due to quarternization at one boron atom.[148] NMR studies of mpy·B_2cat_2 **4.1-I** indicate a dynamic equilibrium in solution (Scheme 4.1).[148, 149] The fast equilibrium between the mono-pyridine adduct **4.1-I** and free B_2cat_2 and mpy, together with an exchange of mpy between the two boron atoms in **4.1-I**, leads to a broad averaged resonance at ca. 20.0 ppm in the ^{11}B NMR spectrum. The presence of the bis-pyridine adduct $(mpy)_2$·B_2cat_2 **4.1-II** leads to a resonance at ca. 6.00 ppm, i.e. in the typical region for sp^3-B atoms. It is formed *via* a comparatively slow (on the NMR time scale) dismutation process of **4.1-I**.

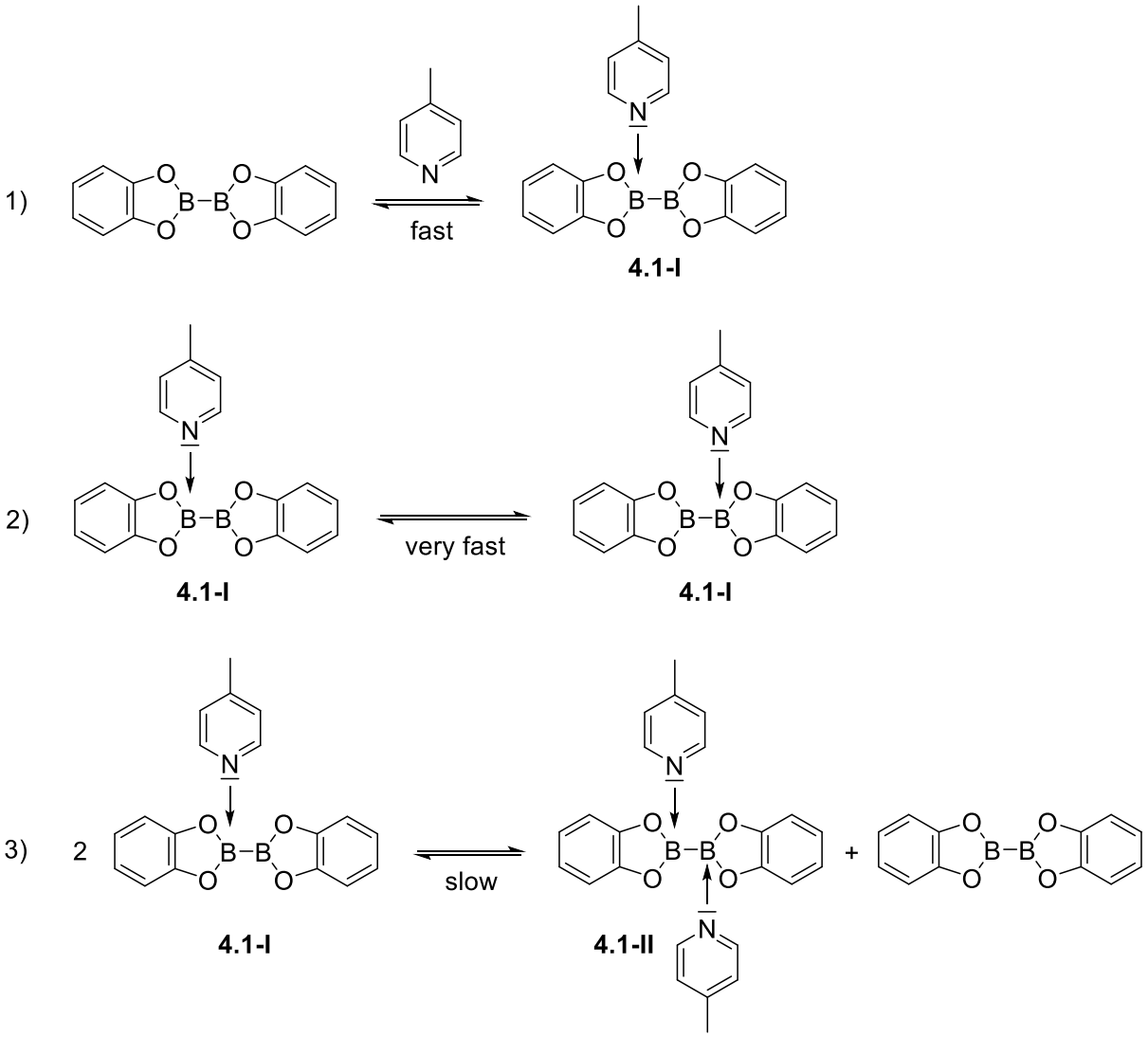

Scheme 4.1 Dynamic equilibrium of mpy·B_2cat_2 **4.1-I** in solution, revealing: 1) a fast equilibrium between the mono-pyridine adduct **4.1-I** and free B_2cat_2 and mpy; 2) a very fast intramolecular exchange of mpy between the two boron atoms in **4.1-I**; 3) a slow (on the NMR time scale) dismutation process of **4.1-I** forming the bis-pyridine adduct $(mpy)_2$·B_2cat_2 **4.1-II** and free B_2cat_2.

When the concentration of mpy was increased successively, the average resonance at 20.0 ppm, was shifted upfield, and decreased relative to the signal at 6.00 ppm, arising from **4.1-II**. The latter signal dominates, once the B_2cat_2:pyridine ratio reaches 1:2.

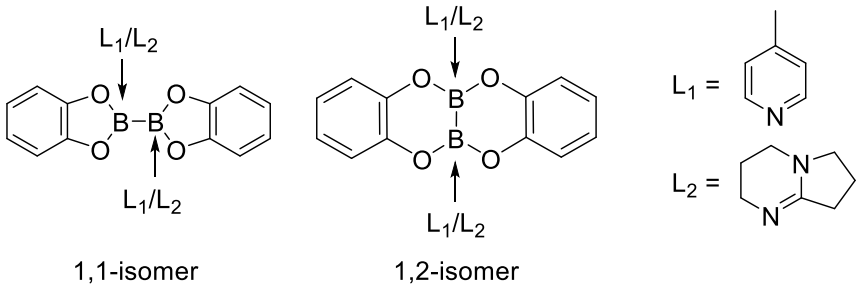

Figure 4.1 Structures of the two isomers of $(mpy)_2 \cdot B_2cat_2$ and $(DBN)_2 \cdot B_2cat_2$

Further studies by Ingleson *et al.* on the bis-pyridine adduct $(mpy)_2 \cdot B_2cat_2$ demonstrated that, under specific solvent conditions, the 1,2-isomer of $(mpy)_2 \cdot B_2cat_2$ could be crystallized and isolated (Figure 4.1).[151] For the analogous reaction of B_2cat_2 with two equivalents of DBN as the Lewis base, the same group observed resonances due to two different 4-coordinate boron environments in the ^{11}B NMR spectrum in solution at 12.3 and 4.00 ppm.[151] X-ray diffraction analysis confirmed the formation of the 1,1- and 1,2-isomers of $(DBN)_2 \cdot B_2cat_2$ (Figure 4.1). DFT calculations demonstrated that the two isomers are energetically similar, but they show a significant difference in the calculated dipole moments, which explains the observed solvent dependence of the isomerization.

The reaction of the strongly Lewis acidic bis(dithiocatecholato)diborane(4) $B_2(1,2\text{-}S_2C_6H_4)_2$ with phosphines in a 1:1 and 1:2 ratio yielded the corresponding mono-phosphine and bis-phosphine adducts, respectively.[149] In solution the same equilibrium as for B_2cat_2 and mpy was observed, with the difference that all the exchanging processes involved happen with similar rates. For B_2cat_2, phosphine adduct formation was only observed for the small and basic phosphine PMe_3.[152] Marder and co-workers have attempted unsuccessfully to reproduce it. Notably, no interaction was observed between B_2pin_2 and pyridines or phosphines.

The groups of Norman, Orpen, and Marder reported the formation of TCNQ (7,7,8,8-tetracyano-p-quinodimethane) and TCNE (tetracyanoethene) co-crystals with B_2cat_2 and $B_2(1,2\text{-}S_2C_6H_4)_2$, which were structurally characterized. However, no adduct formation was evidenced at room temperature by solution NMR spectroscopy.[153]

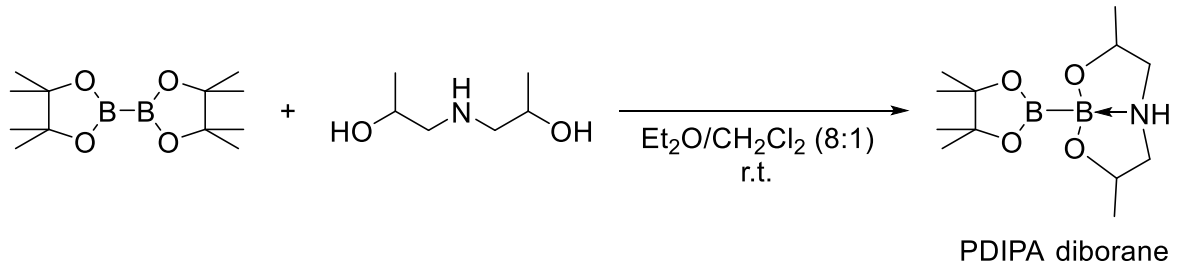

Scheme 4.2 Synthesis of PDIPA diborane by reacting B_2pin_2 with di-*iso*-propanolamine.[154]

In 2009, Santos *et al.* introduced the novel sp^2–sp^3 hybridized mixed PDIPA diborane, which can be considered as an intramolecular version of an sp^2–sp^3 diborane adduct.[154] The reaction of B_2pin_2 with di-*iso*-propanolamine with loss of one pinacol moiety led to the formation of the PDIPA diborane, which contains a dative N→B bond (Scheme 4.2). The ^{11}B NMR spectrum of the PDIPA diborane in solution revealed one signal at 35.5 ppm for the sp^2-B atom of the Bpin unit and one for the sp^3-B atom of the di-*iso*-propanol-aminato moiety at 8.95 ppm. This "preactivated" diborane reagent was applied in the catalytic regioselective borylation of *α*,*β*-unsaturated conjugated compounds.[154-156]

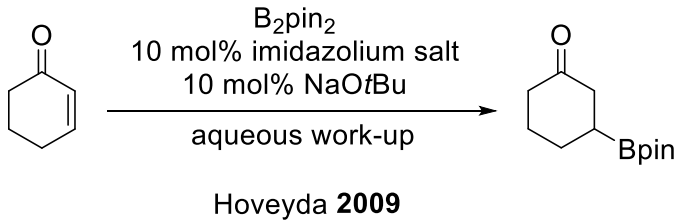

Scheme 4.3 NHC promoted *β*-borylation reaction of cyclohexanone with B_2pin_2.[157]

The activation of B_2pin_2 *via* an sp^2–sp^3 adduct of an NHC was first introduced by the group of Hoveyda in 2009.[157, 158] They claimed that the *in situ* generated adduct of the type NHC·B_2pin_2 from the corresponding imidazolium salt, NaO*t*Bu, and B_2pin_2, functions as an organocatalyst in *β*-borylation reactions of *α*,*β*-unsaturated compounds (Scheme 4.3). However, the originally reported conclusions from the NMR data were incorrect, and the observed $^{11}B\{^1H\}$ NMR signals did not match the expected region for sp^2–sp^3 hybridized diborane(4) compounds. Later, the groups of Hodgkinson, Lin, and Marder investigated the proposed adduct in detail and reported the synthesis and full characterization of the mono-NHC adduct Cy_2Im·B_2pin_2.[146] While the adduct was crystallographically confirmed by X-ray diffraction analysis, the binding of the NHC to B_2pin_2 was shown to be very weak in solution. This results in a fast dynamic exchange

of the NHC between the two boron centers of B_2pin_2 (Scheme 4.4). Thus, no signal was detected at 20 °C in the $^{11}B\{^1H\}$ NMR due to a broadening of the signal close to the coalescence temperature. At elevated temperatures of 50 °C one averaged signal at 20.4 ppm was observed. Decreasing the temperature to 5 °C led to the appearance of two signals as expected for an NHC sp^2–sp^3 diborane(4) adduct, one for the sp^2-B atom at 37.2 ppm and one for the sp^3-B atom at 2.40 ppm.[146] Notably, bis-NHC adducts of B_2pin_2 were not observed so far.

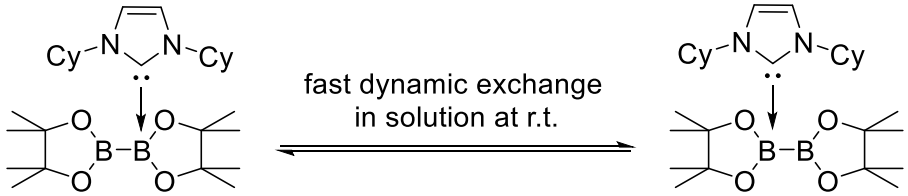

Scheme 4.4 Fast dynamic exchange of the NHC between the two boron centers in $Cy_2Im{\cdot}B_2pin_2$ in solution at room temperature.[146]

Further studies on NHC adducts of B_2cat_2 by the groups of Marder, Radius, and Ingleson demonstrated that, depending on the stoichiometry, mono-NHC and bis-NHC adducts are accessible (Scheme 4.5).[159] The mono-NHC adduct $Me_2Im^{Me}{\cdot}B_2cat_2$ was isolated and characterized and, unlike the mono-NHC adduct of B_2pin_2, no dynamic exchange of the NHC between the two boron atoms was observed on the NMR time scale, presumably due to the higher Lewis acidity of B_2cat_2 compared to B_2pin_2. Thus, one signal was observed at 36.8 ppm for the sp^2-B atom and one for the sp^3-B atom at 7.11 ppm. The corresponding bis-NHC adduct $(Me_2Im^{Me})_2{\cdot}B_2cat_2$ was characterized by solid-state (SS) NMR spectroscopy, due to solubility problems. As expected for a bis-NHC adduct with both boron atoms coordinated by an NHC, the ^{11}B SS NMR spectrum revealed one signal at 2.72 ppm in the typical region for sp^3-B atoms.[159]

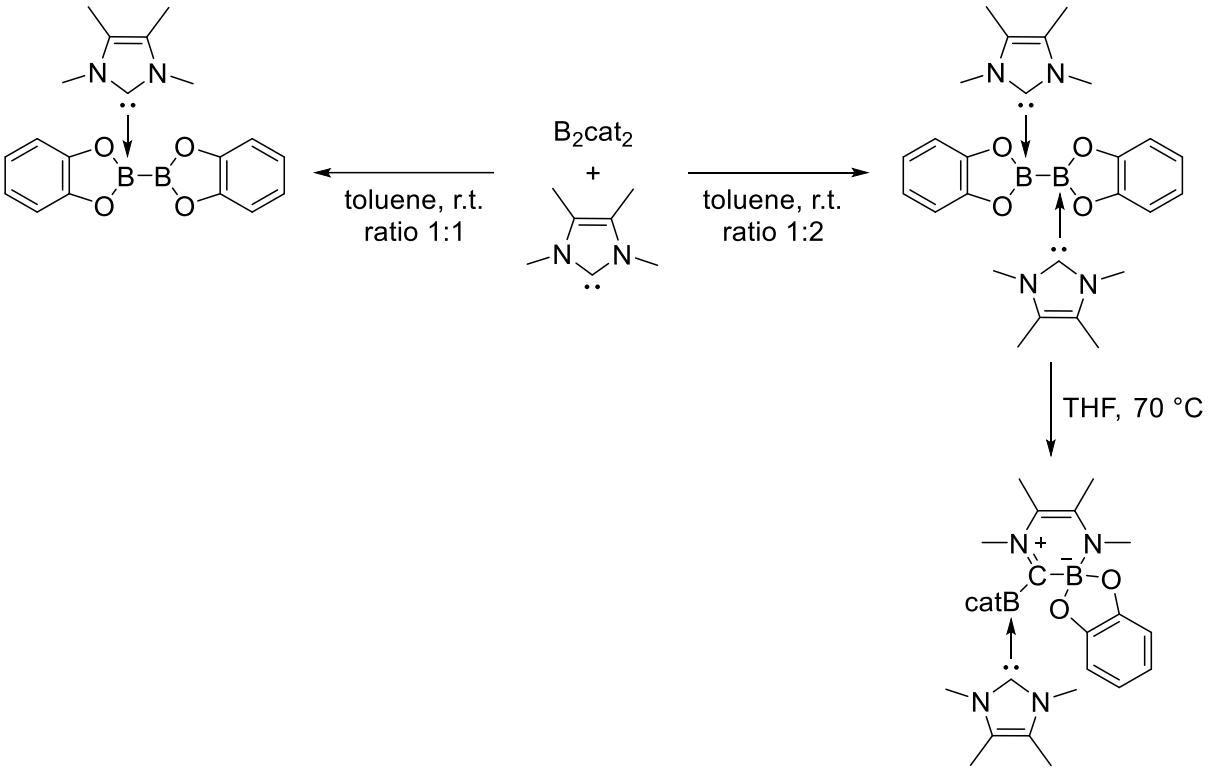

Scheme 4.5 Synthesis of the mono-NHC adduct $Me_2Im^{Me}{\cdot}B_2cat_2$ (left) and the bis-NHC adduct $(Me_2Im^{Me})_2{\cdot}B_2cat_2$ (right), which forms a ring expanded product at temperatures of 70 °C.[159]

Unlike $Me_2Im^{Me}{\cdot}B_2cat_2$, the corresponding bis-NHC adduct $(Me_2Im^{Me})_2{\cdot}B_2cat_2$ is thermally unstable and undergoes a ring expansion reaction (RER) *via* the insertion of one Bcat moiety into the C–N bond of one NHC. A second exo Bcat moiety binds to the former carbene carbon atom and its boron atom is saturated by the coordination of a second NHC (Scheme 4.5). This ring expansion product is soluble and the solution $^{11}B\{^1H\}$ NMR spectrum revealed two sharp signals at 6.23 and 7.20 ppm, indicating two different four coordinate boron centers.[159]

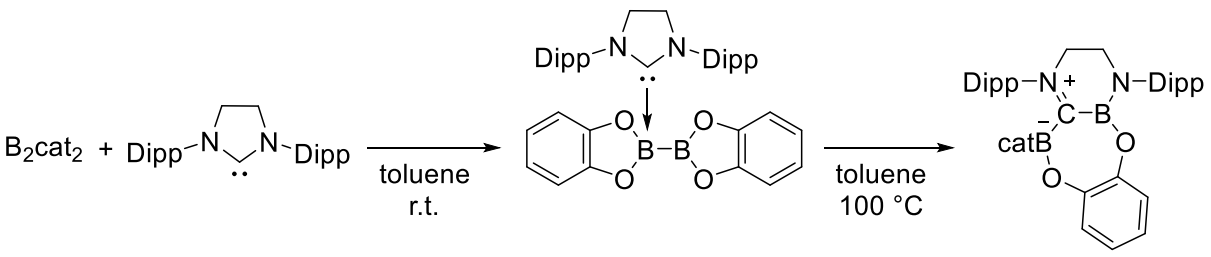

Scheme 4.6 Room temperature reaction of B_2cat_2 with one equivalent of $Dipp_2SIm$ to yield $Dipp_2SIm{\cdot}B_2cat_2$, which undergoes a RER at temperatures of 100 °C.[160]

The reaction of B_2cat_2 with one equivalent of $Dipp_2Im$ (unsaturated NHC backbone) or $Dipp_2SIm$ (saturated NHC backbone) leads, in both cases, to the mono-NHC adducts.[160] However, while $Dipp_2Im{\cdot}B_2cat_2$ is stable with regard to RER, the NHC adduct with the backbone-saturated NHC $Dipp_2SIm{\cdot}B_2cat_2$ is thermally unstable, generating a ring expansion product (Scheme 4.6).

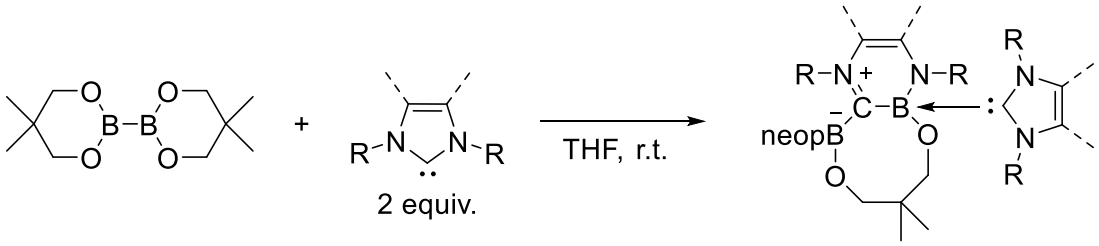

Scheme 4.7 Reaction of B_2neop_2 with two equivalents of NHC at room temperature forming a ring expansion product.[159, 160]

For the reaction of B_2neop_2 with two equivalents of sterically less demanding NHCs (Me_2Im^{Me}, Me_2Im, and $n Pr_2Im$) no bis-NHC adduct could be isolated. Instead, RERs occurred at room temperature (Scheme 4.7).[159, 160] A ring expansion product was isolated, in which one Bneop moiety inserted into the C–N bond of one NHC and the endocyclic neop substituent opened and is bound to the exocyclic boron atom, forming an 8-membered heterocyclic ring with the second NHC coordinated to the endocyclic boron atom.

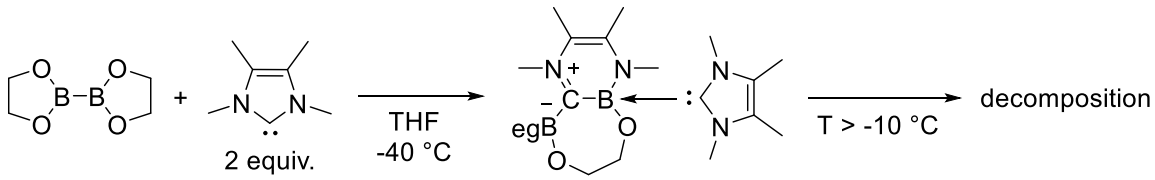

Scheme 4.8 Reaction of B_2eg_2 with two equivalents of NHC forming a ring expanded product at temperatures as low as -40 °C, which decomposes above a temperature of -10 °C.[160]

In the case of the more reactive diborane(4) compound B_2eg_2 with an unsubstituted ethylene glycolato backbone, adduct formation was only observed for the sterically demanding NHC Mes_2Im, which led to the mono-NHC adduct $Mes_2Im{\cdot}B_2eg_2$.[160] The $^{11}B\{^1H\}$ NMR spectrum in solution showed one broad signal at 22.6 ppm due to the dynamic exchange of the NHC between the two boron centers. The SS NMR spectrum

revealed two signals at chemical shifts of 35.1 and 3.90 ppm for the sp^2-B and the sp^3-B atom, respectively, as expected for mono-NHC adducts. $Mes_2Im{\cdot}B_2eg_2$ was stable at room temperature and did not undergo a RER, even at elevated temperatures. For the reaction of B_2eg_2 with 2 equivalents of the small NHCs Me_2Im^{Me} and iPr_2Im, respectively, ring expansion products were observed at temperatures as low as -40 °C by *in situ* NMR spectroscopy, which decomposed at temperatures above -10 °C (Scheme 4.8).[160] For iPr_2Im, the ring expansion product was isolated by crystallization at -30 °C and fully characterized. Redissolving the compound at room temperature led to decomposition.

4.2 PYRIDINE AND NHC ADDUCTS OF DIBORANE(4) ESTERS

4.2.1 Synthesis of Pyridine Adducts of B_2cat_2

According to the procedure for (mpy)·B_2cat_2 by Marder and Norman,[148] the sp^2–sp^3 diborane(4) adducts pyridine·B_2cat_2 **18** and DMAP·B_2cat_2 **19** were synthesized by reaction of B_2cat_2 with pyridine and DMAP, respectively, in dichloromethane at room temperature, followed by precipitation with *n*-hexane (Scheme 4.9). Compounds **18** and **19** were obtained as pale yellow solids in very good yields of 70 and 92%, respectively, and were characterized by NMR spectroscopy, HRMS, and elemental analysis.

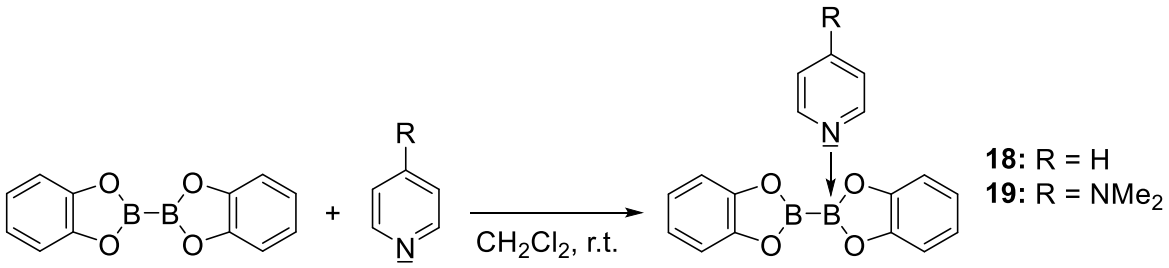

Scheme 4.9 Synthesis of the mono-pyridine adducts pyridine·B_2cat_2 **18** and DMAP·B_2cat_2 **19**.

The $^{11}B\{^1H\}$ NMR spectrum of **18** gives rise to two broad signals at chemical shifts of 22.2 and 6.60 ppm (Figure 4.2). The former is an averaged signal explained by a fast equilibrium in solution between pyridine·B_2cat_2 **18** and B_2cat_2 and pyridine, and by pyridine exchanging between the two boron atoms in pyridine·B_2cat_2 **18**. The latter is explained by the presence of the bis-pyridine adduct in solution, formed *via* a comparatively slow (on the NMR timescale) dismutation process (cf. Scheme 4.1). This observation is in accordance with the previous findings by Marder and Norman.[148, 149]

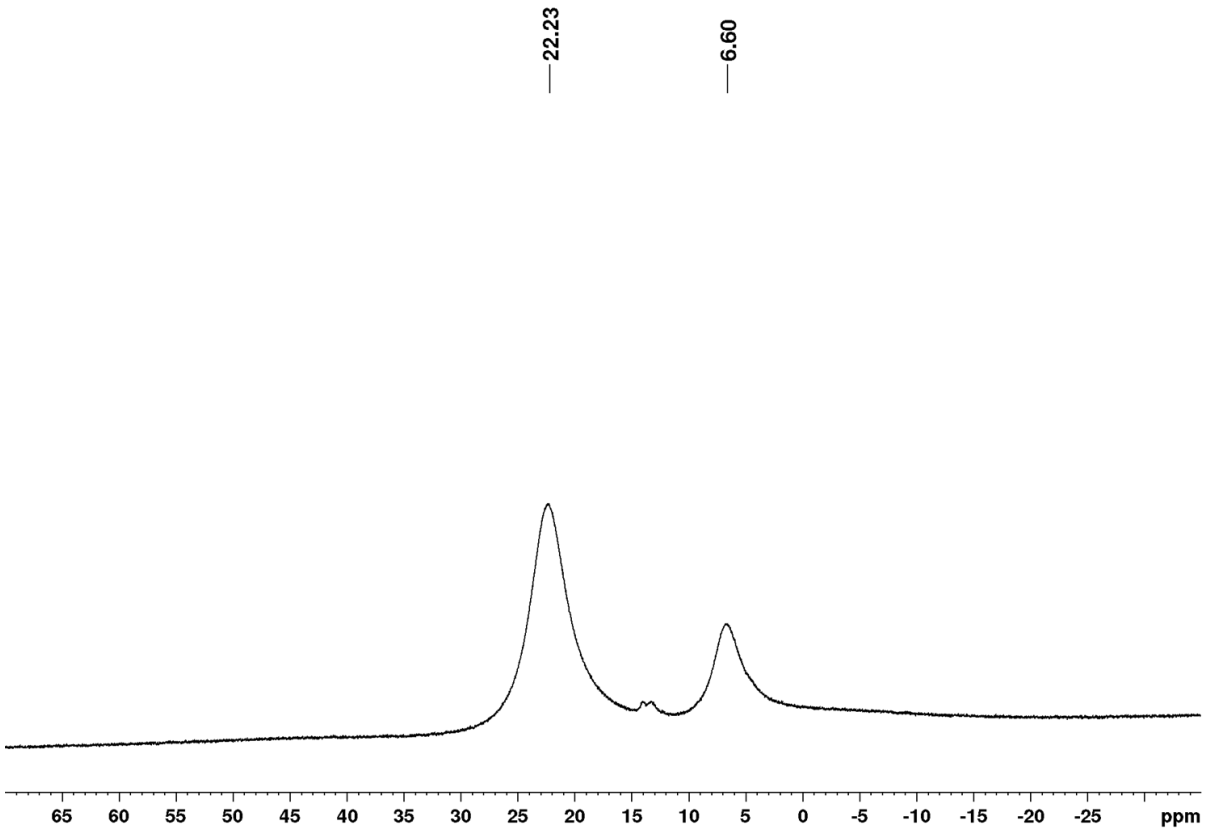

Figure 4.2 $^{11}B\{^{1}H\}$ NMR spectrum of pyridine·B_2cat_2 **18** recorded in CD_2Cl_2 (128 MHz) revealing a fast equilibrium in solution between pyridine·B_2cat_2 **18** and free B_2cat_2 and pyridine, and a very fast exchange of pyridine between the two boron atoms in pyridine·B_2cat_2 **18** (δ = 22.2 ppm), as well as the presence of the bis-pyridine adduct (δ = 6.60 ppm), formed *via* a comparatively slow (on the NMR timescale) dismutation process of **18**.

Single crystals suitable for X-ray diffraction were obtained from a saturated solution of pyridine·B_2cat_2 **18** in *n*-hexane/CH_2Cl_2 (3:1) at -30 °C (Figure 4.3). The molecular structure of **18** is in accordance with that previously reported for (mpy)·B_2cat_2 by Marder and Norman.[148] While the boron atom B1 is trigonal planar substituted, the sp^3-hybridized boron atom B2 is tetrahedrally coordinated by the bidentate catecholato unit, the second Bcat moiety, and pyridine. The B1−B2 distance of 1.7106(18) Å is similar to that found in (mpy)·B_2cat_2 (B1−B2 1.706(3) Å). The B–B bond distances in both mono-pyridine adducts are elongated compared to that found in uncoordinated B_2cat_2 (1.678(3) Å).[161] The B2−N bond length (1.6439(15) Å) is similar to that found in (mpy)·B_2cat_2 (1.644(2) Å).[148]

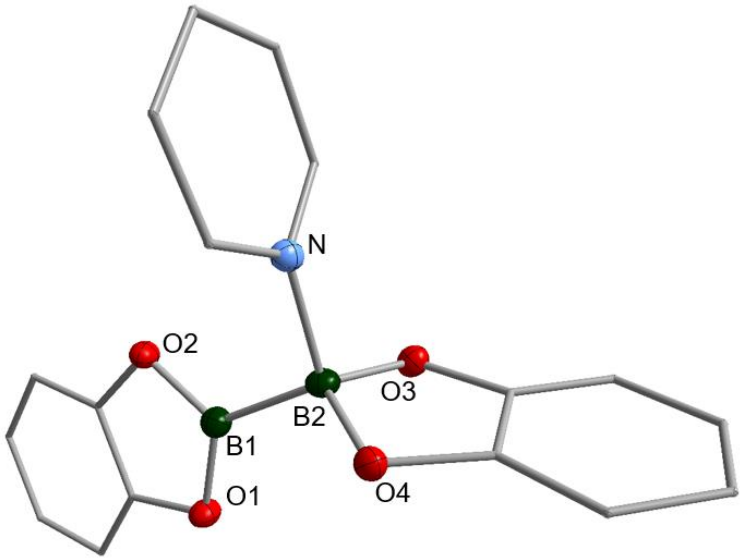

Figure 4.3 Molecular structure of pyridine·B_2cat_2 **18**. Hydrogen atoms are omitted for clarity and the thermal ellipsoids are drawn at 50% probability. Selected bond lengths [Å] and angles [°]: B2−N 1.6439(15), B1−B2 1.7106(18), B1−O1 1.3943(15), B1−O2 1.3954(15), B2−O3 1.4793(15), B2−O4 1.4750(15), N-B2-B1 106.62(9), N-B2-O3 106.47(9), N-B2-O4 106.48(9).

In the $^{11}B\{^1H\}$ NMR spectrum of DMAP·B_2cat_2 **19** one broad signal at 21.7 ppm was detected, arising from the fast dynamic exchange of DMAP between the two boron atoms of B_2cat_2 (Figure 4.4). However, no formation of the bis-pyridine adduct, was observed, possibly due to the fact that DMAP is a better σ-donor than unsubstituted pyridine and mpy, and therefore a stronger Lewis base, which leads to a stronger interaction with the boron centers of B_2cat_2 and thus to a more stable mono-pyridine adduct.

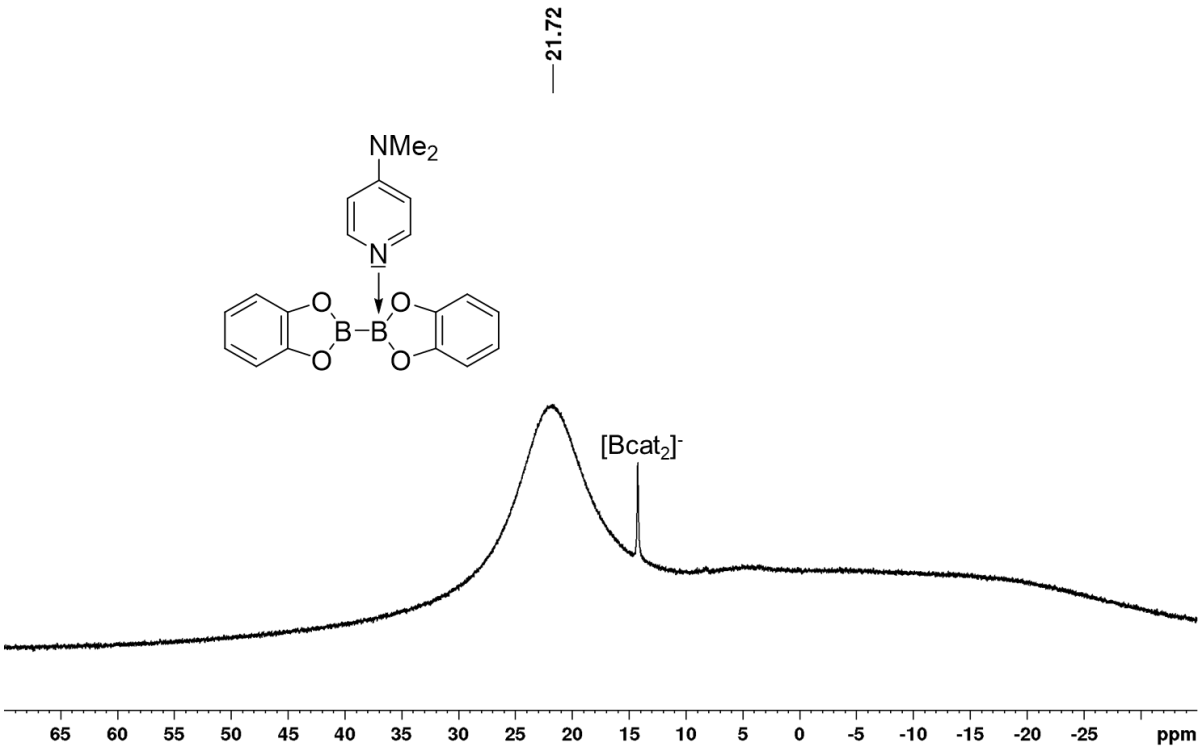

Figure 4.4 $^{11}B\{^{1}H\}$ NMR spectrum of DMAP·B_2cat_2 **19** recorded in CD_2Cl_2 (128 MHz).

The ^{1}H NMR spectrum of **19** shows only one set of multiplets for the catechol units, which proves the formation of a stable mono-pyridine adduct in solution. The signals detected for the aromatic protons of DMAP are broadened, as a result of the fast dynamic exchange in solution (Figure 4.5).

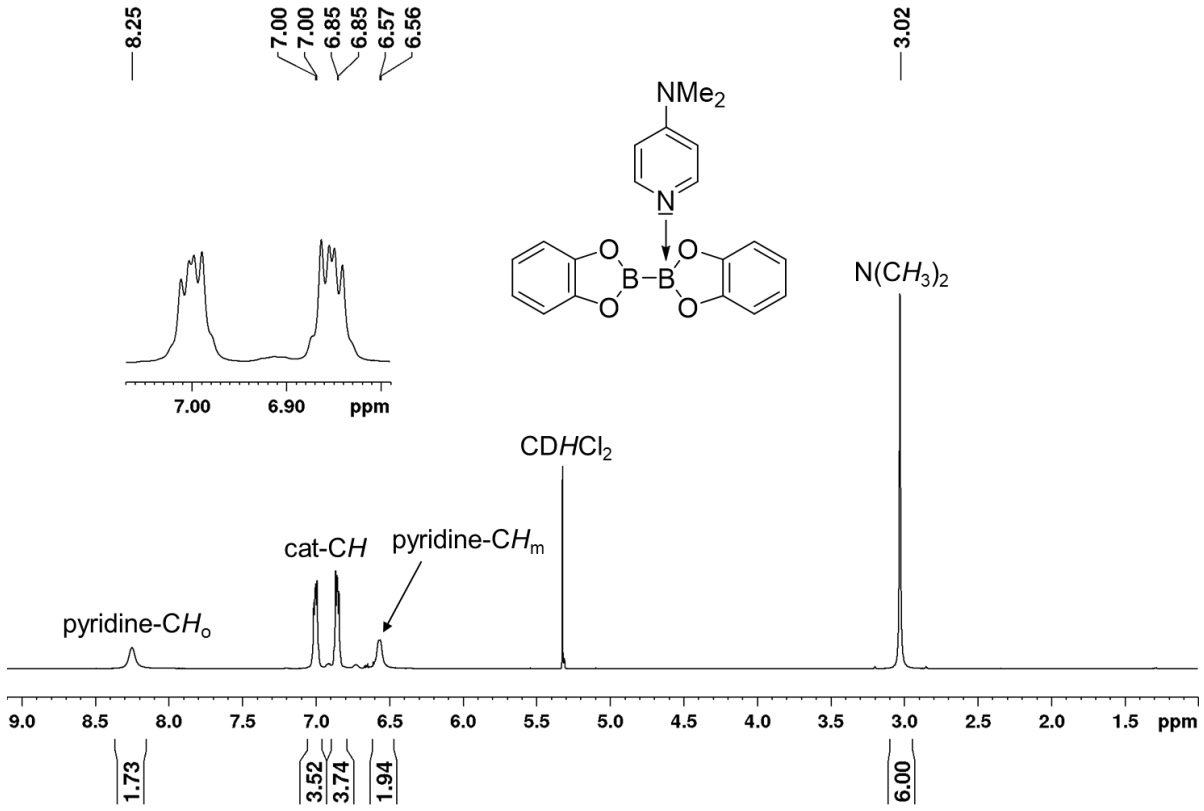

Figure 4.5 ^{1}H NMR spectrum of DMAP·B_2cat_2 **19** recorded in CD_2Cl_2 (400 MHz).

4.2.2 Synthesis of Mono-NHC Adducts of the Type NHC·$B_2(OR)_4$

Based on the procedure of the mono-NHC adduct Cy_2Im·B_2pin_2,[146] Me_2Im^{Me}·B_2pin_2 **20** and *i*Pr_2Im^{Me}·B_2pin_2 **21** were accordingly synthesized by reacting B_2pin_2 with one equivalent of the free NHC in toluene at room temperature (Scheme 4.10).

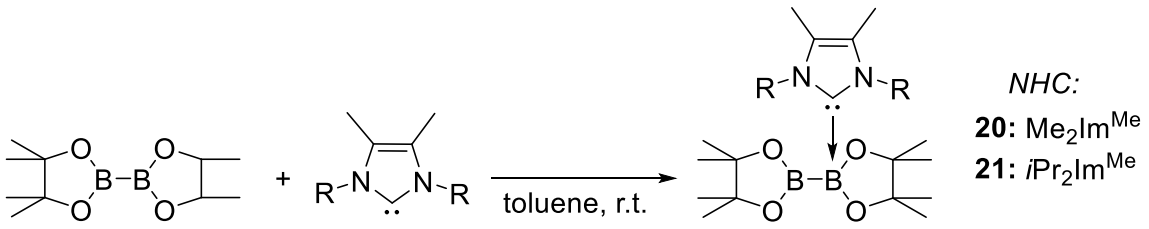

Scheme 4.10 Synthesis of the mono-NHC adducts Me_2Im^{Me}·B_2pin_2 **20** and *i*Pr_2Im^{Me}·B_2pin_2 **21**.

The mono-NHC adducts **20** and **21** were obtained as colorless solids in good yields of 73 and 91%, respectively, and were characterized *via* NMR spectroscopy, HRMS, and elemental analysis. In the ^{1}H NMR spectra, the signals detected do not show any significant shift compared to those of the starting material, apart from the methine

protons of the *iso*-propyl moiety in *i*Pr$_2$Im^{Me}·B$_2$pin$_2$ **21** at 6.23 ppm, which are significantly downfield shifted compared to that observed for the free NHC (3.96 ppm). The ^{1}H NMR spectrum of Me$_2$Im^{Me}·B$_2$pin$_2$ **20** is shown in Figure 4.6.

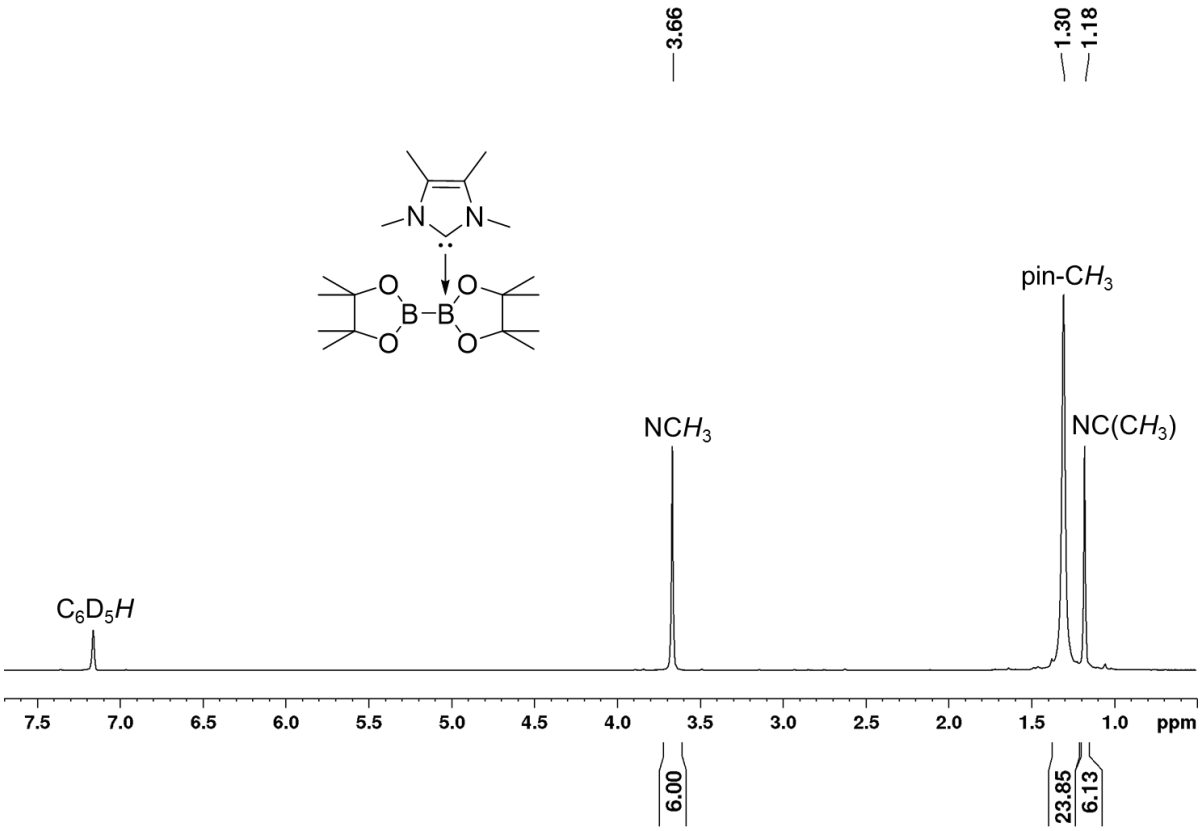

Figure 4.6 ^{1}H NMR spectrum of Me$_2$Im^{Me}·B$_2$pin$_2$ **20** recorded in C$_6$D$_6$ (400 MHz).

The signals for the carbene carbon atom in the ^{13}C{^{1}H} NMR spectra of **20** and **21** are significantly upfield-shifted at 168.1 and 169.8 ppm, respectively, compared to those of the free NHCs Me$_2$Im^{Me} (213.0 ppm) and *i*Pr$_2$Im^{Me} (207.6 ppm). The ^{11}B{^{1}H} NMR spectra of both compounds, reveal only one broad resonance at ca. 20 ppm at room temperature, which can be explained by the fast dynamic exchange of the NHC between the two boron atoms of B$_2$pin$_2$. A low temperature ^{11}B NMR spectrum of **20** recorded at 0 °C shows one broad signal at 36.5 ppm for the sp^2-B atom and one at 2.94 ppm for the sp^3-B atom (Figure 4.7), and for **21** at 36.9 and 2.91 ppm, respectively.

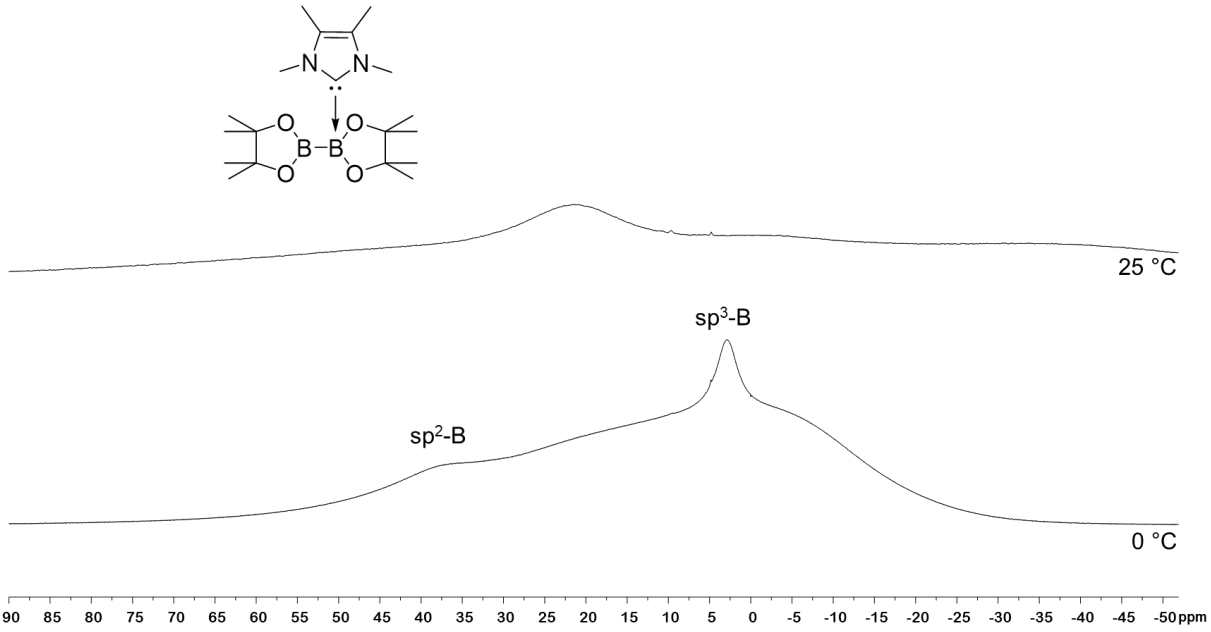

Figure 4.7 ^{11}B NMR spectrum (160 MHz) of Me_2Im^{Me}·B_2pin_2 **20** recorded in d_8-toluene at 25 °C (top) and 0 °C (bottom).

Furthermore, the diborane(4) compound $B_2(OMe)_4$ featuring a more flexible structure compared to those of B_2pin_2, B_2cat_2, B_2neop_2, and B_2eg_2 (which have a rigid backbone), was reacted with various NHCs in toluene at room temperature. No evidence for any interaction between the NHC and $B_2(OMe)_4$ was observed when using the sterically demanding $Dipp_2Im$. The *in situ* $^{11}B\{^1H\}$ NMR of the reaction of $B_2(OMe)_4$ and Mes_2Im, shows one averaged signal at 25.1 ppm, presumably arising from a dynamic exchange of the NHC between the two boron atoms. However, the isolation of the observed NHC adduct failed, as the compound was not stable during work up under reduced pressure. Only the NHC was isolated, presumably due to a weak interaction of the sterically demanding Mes_2Im with the boron atom of volatile $B_2(OMe)_4$. Upon evaporation, an equilibrium between Mes_2Im, $B_2(OMe)_4$, and the adduct Mes_2Im·$B_2(OMe)_4$ (Scheme 4.1) is shifted to the side of the starting material, as volatile $B_2(OMe)_4$ is removed. The work up *via* precipitation was not successful either due to the very good solubility of the compound in all solvents in which mono-NHC adducts are commonly stable (*n*-hexane, THF etc.). The mono-NHC adducts iPr_2Im^{Me}·$B_2(OMe)_4$ **22** and Cy_2Im·$B_2(OMe)_4$ **23** were isolated from the reaction of the smaller and more nucleophilic NHCs Cy_2Im and iPr_2Im^{Me} with $B_2(OMe)_4$, as colorless solids in moderate yields of 45 and 49%, respectively (Scheme 4.11).

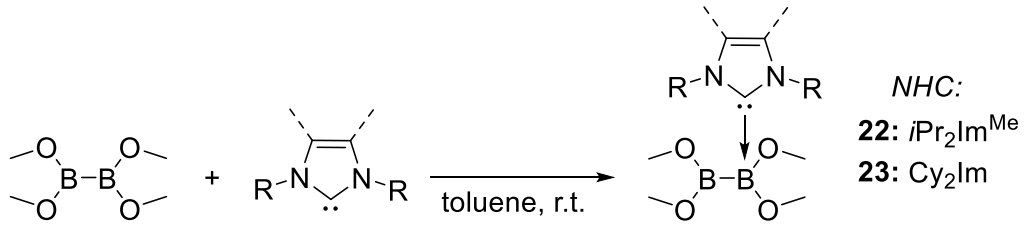

Scheme 4.11 Synthesis of *i*Pr$_2$Im^{Me}·B$_2$(OMe)$_4$ **22** and Cy$_2$Im·B$_2$(OMe)$_4$ **23**.

The compounds **22** and **23** were characterized *via* NMR spectroscopy, HRMS, and elemental analysis. For *i*Pr$_2$Im^{Me}·B$_2$(OMe)$_4$ **22,** the ^{1}H NMR spectrum reveals a characteristic downfield shift of the methine protons of the *iso*-propyl moiety, detected at 6.22 ppm, compared to the starting material (3.96 ppm). In the ^{1}H NMR spectrum of Cy$_2$Im·B$_2$(OMe)$_4$ **23** the signal of the C*H*-unit of the cyclohexyl substituent is detected at 5.81 ppm, significantly downfield shifted compared to that observed for the free NHC (4.11 ppm). In the ^{11}B{^{1}H} NMR spectra of both compounds, two signals are observed for the mono-NHC adducts. For *i*Pr$_2$Im^{Me}·B$_2$(OMe)$_4$ **22** the signal for the sp^3-B atom is detected at 4.05 ppm and the signal for the sp^2-B atom at 35.0 ppm (Figure 4.8), for Cy$_2$Im·B$_2$(OMe)$_4$ **23** at 4.34 and 36.4 ppm, respectively.

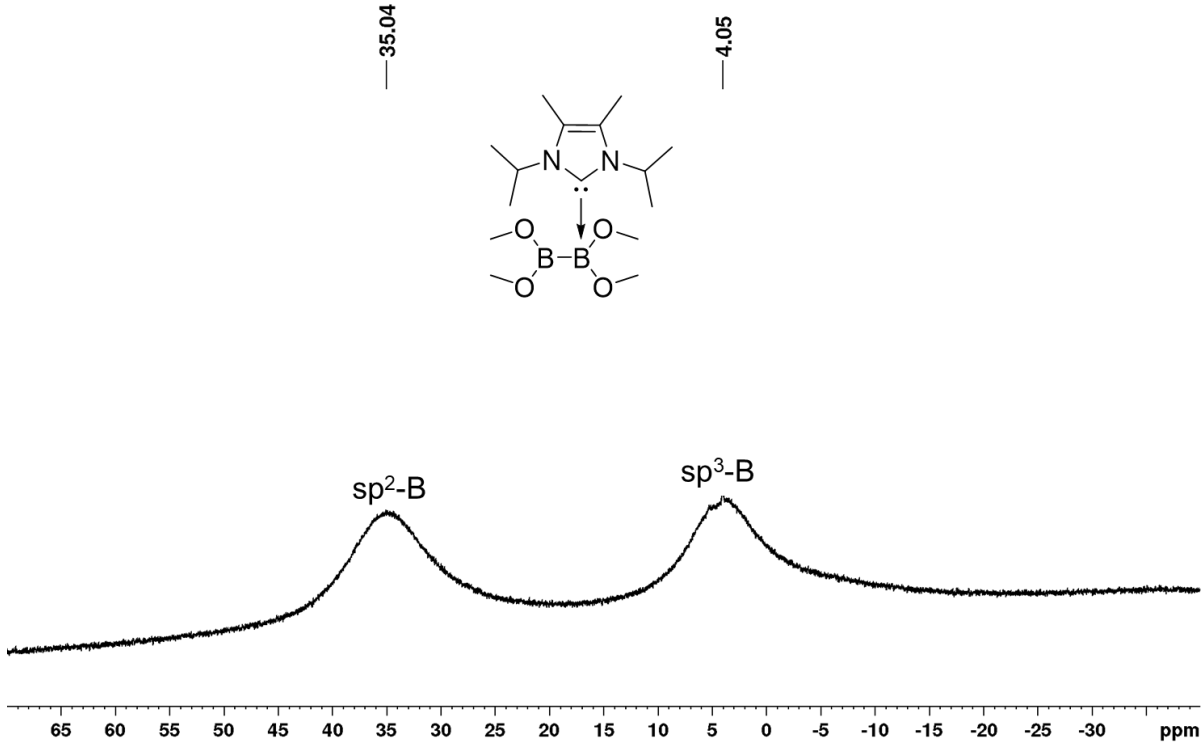

Figure 4.8 ^{11}B{^{1}H} NMR spectrum of *i*Pr$_2$Im^{Me}·B$_2$(OMe)$_4$ **22** recorded in C$_6$D$_6$ (160 MHz).

The resonances for the carbene carbon atom in the $^{13}C\{^1H\}$ NMR spectra of **22** and **23** are detected significantly upfield-shifted at 166.2 and 167.3 ppm, respectively, compared to those of the free carbenes at 207.6 and 212.7 ppm. Additionally, single crystals of *i*Pr$_2$Im^{Me}·B$_2$(OMe)$_4$ **22** suitable for X-ray diffraction were obtained from slow evaporation of the solvent of a saturated solution of **22** in benzene (Figure 4.9).

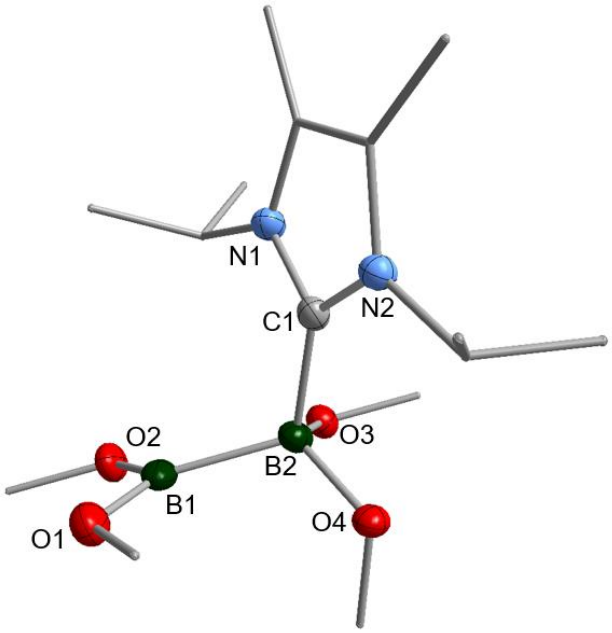

Figure 4.9 Molecular structure of *i*Pr$_2$Im^{Me}·B$_2$(OMe)$_4$ **22**. Hydrogen atoms are omitted for clarity and the thermal ellipsoids are drawn at 50% probability. Selected bond lengths [Å] and angles [°]: B2−C1 1.6864(19), B1−B2 1.759(2), B1−O1 1.3811(19), B1−O2 1.3756(19), B2−O3 1.4806(17), B2−O4 1.4785(17), C1-B2-B1 109.61(10), C1-B2-O3 107.37(10), C1-B2-O4 107.86(10).

The molecular structure of **22** is in accordance with the structures previously reported for mono-NHC adducts.[146, 159, 160] The boron atom B1 is trigonal planar, while the sp^3-hybridized boron atom B2 is tetrahedrally coordinated. The B1−B2 and B2−C1 bond lenghts of 1.759(2) and 1.6864(19) Å, are similar to those found for the mono-NHC adduct Cy$_2$Im·B$_2$pin$_2$ (B1−B2 1.743(2) and B2−C1 1.673(2) Å).[146]

4.2.3 Synthesis of Bis-NHC Adducts of the type $(NHC)_2{\cdot}B_2cat_2$

Previous studies of Ingleson, Radius, Marder *et al.*[159] on bis-NHC adducts demonstrated that this class of compounds is thermally unstable in solution towards ring expansion reactions, which occur with insertion of one boryl moiety into the C−N bond of the NHC. This process strongly depends on the diborane(4) compound employed; the bis-NHC adducts of B_2cat_2 are stable up to temperatures of 70 °C, whereas for B_2neop_2 ring expansion occurs at room temperature.[159] Using the small diborane(4) reagent B_2eg_2, RER was observed at temperatures as low as -40 °C,[160] while for the well-known representative B_2pin_2, there are no reports of bis-NHC adduct formation or ring expansion reaction to date. So far, the only accessible and room temperature stable bis-NHC adduct is $(Me_2Im^{Me})_2{\cdot}B_2cat_2$, reported by Marder and Radius in 2015.[159] Thus, the synthesis of further bis-NHC adducts was investigated, using B_2cat_2 as the diborane(4) compound. Under the same conditions as employed for the synthesis of the mono-NHC adducts, the reaction of B_2cat_2 and the corresponding NHC, in a 1:2 ratio, afforded the bis-NHC adducts $(Cy_2Im)_2{\cdot}B_2cat_2$ **24** and $(i Pr_2Im^{Me})_2{\cdot}B_2cat_2$ **25** as colorless solids in good yields of 74 and 84%, respectively (Scheme 4.12).

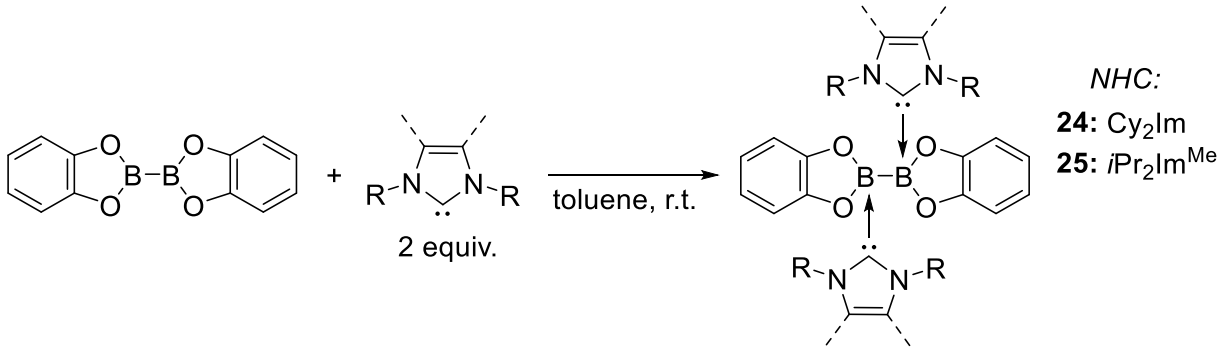

Scheme 4.12 Synthesis of the bis-NHC adducts $(Cy_2Im)_2{\cdot}B_2cat_2$ **24** and $(i Pr_2Im^{Me})_2{\cdot}B_2cat_2$ **25**.

Compounds **24** and **25** were characterized by NMR spectroscopy, HRMS, and elemental analysis. Due to the poor solubility of $(Cy_2Im)_2{\cdot}B_2cat_2$ **24** in common deuterated solvents, the adduct was not characterized in solution, but instead by solid-state NMR spectroscopy. The ^{11}B RSHE/MAS NMR spectrum reveals one signal with an isotopic shift of 12.4 ppm arising from the two equivalent sp^3-B atoms (Figure 4.10). In the ^{15}N NMR spectrum of **24**, one signal for the nitrogen atoms of the NHCs is detected at -182.1 ppm, which also confirms the formation and symmetry of the bis-

NHC adduct $(Cy_2Im)_2{\cdot}B_2cat_2$ **24**. The data obtained match those reported earlier for $(Me_2Im^{Me})_2{\cdot}B_2cat_2$, which was also characterized by solid-state NMR spectroscopy, due to solubility problems.[159]

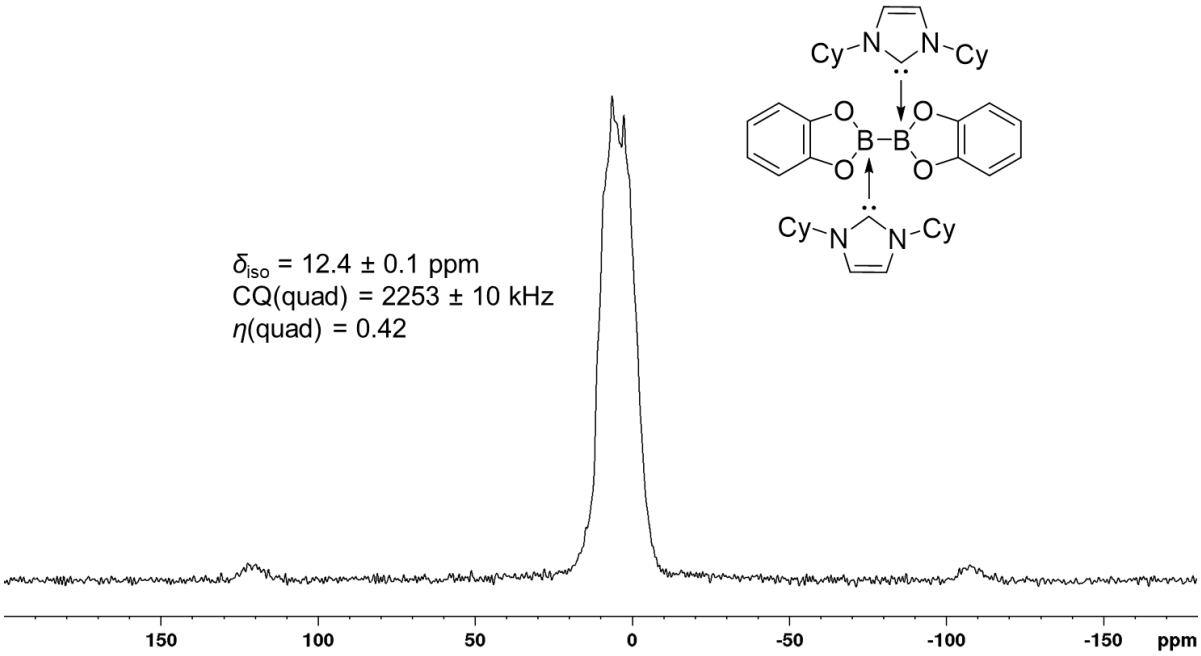

Figure 4.10 ^{11}B RSHE/MAS NMR spectrum of the bis-NHC adduct $(Cy_2Im)_2{\cdot}B_2cat_2$ **24** (128 MHz, 25 °C, *v* rot = 14800 Hz).

As $(i Pr_2Im^{Me})_2{\cdot}B_2cat_2$ **25** is moderately soluble in deuterated benzene, it was possible to record NMR spectra in solution. The ^1H NMR spectrum confirms the symmetric constitution of **25** with only one set of signals for the NHCs and one for the Bcat units (Figure 4.11). The septet detected for the methine protons of the *iso*-propyl group at 6.27 ppm shows a significant shift compared to that of the free NHC at 3.96 ppm. In the ^{11}B NMR spectrum one signal is detected at 11.5 ppm in the expected region for sp^3-B atoms (Figure 4.11). The ^1H NMR spectrum also reveals toluene in a 1:1 ratio (**25**:toluene), which could not be removed, either under high vacuum or by washing the compound with *n*-hexane/*n*-pentane. This was also found for $(Me_2Im^{Me})_2{\cdot}B_2cat_2$.[159]

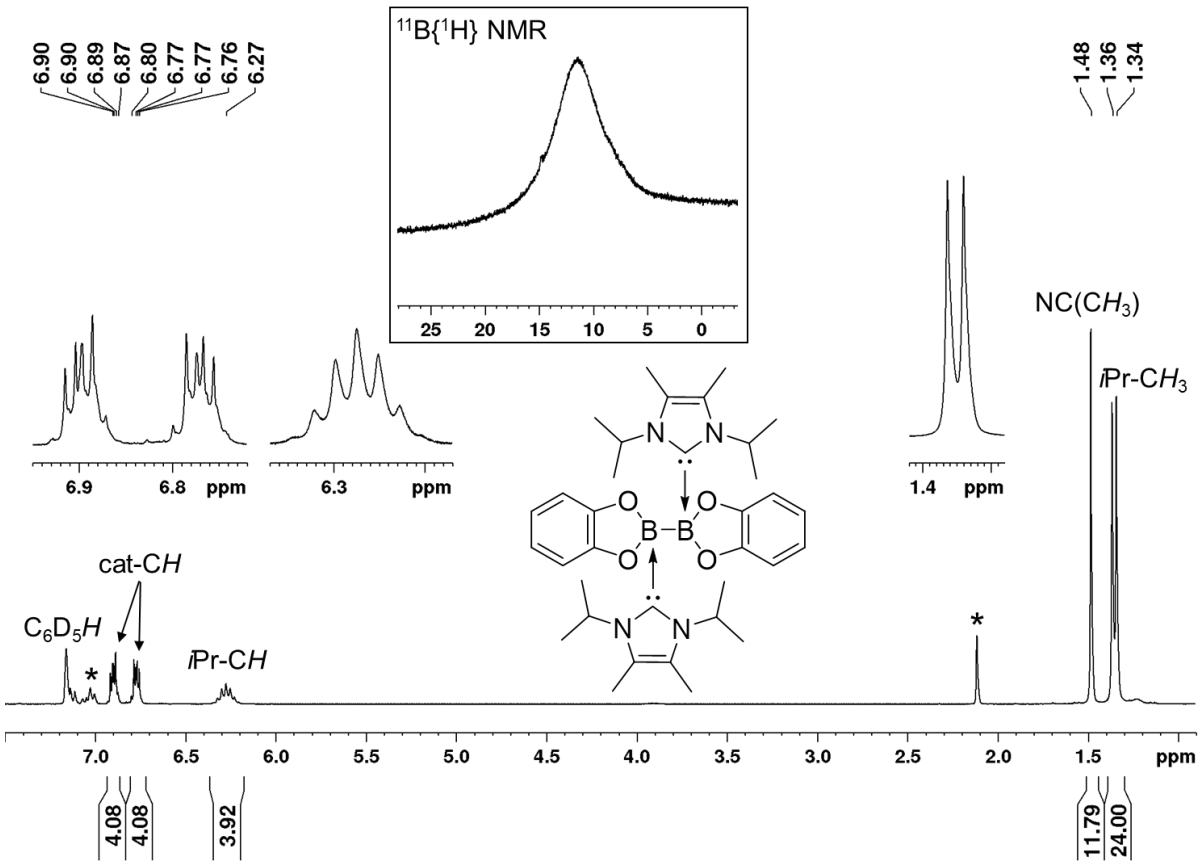

Figure 4.11 ^1H NMR and $^{11}B\{^1H\}$ NMR (inlay) spectra of (*i*Pr$_2$Im^{Me})$_2$·B$_2$cat$_2$ **25** recorded in C_6D_6 (400 MHz; asterisk: toluene in a 1:1 ratio (**25**:toluene)).

Single crystals suitable for X-ray diffraction were obtained from slow evaporation of the solvent of a saturated solution of (*i*Pr$_2$Im^{Me})$_2$·B$_2$cat$_2$ **25** in benzene. The molecular structure of **25** matches that previously reported for (Me$_2$Im^{Me})$_2$·B$_2$cat$_2$,[159] with both boron atoms being sp^3-hybridized and tetrahedrally coordinated (Figure 4.12). The B1–B1' bond distance of 1.732(6) Å is slightly longer compared to that observed for the bis-NHC adduct (Me$_2$Im^{Me})$_2$·B$_2$cat$_2$ (1.710(8) Å).[159] The B–B distances in both bis-NHC adducts are elongated compared to that in uncoordinated B$_2$cat$_2$ (1.678(3) Å).[161] The B1–C1 bond length (1.656(4) Å) is similar to that found in (Me$_2$Im^{Me})$_2$·B$_2$cat$_2$ (1.658(9) Å).[159] Two benzene molecules are present in the lattice, but no specific molecular interactions are observable.

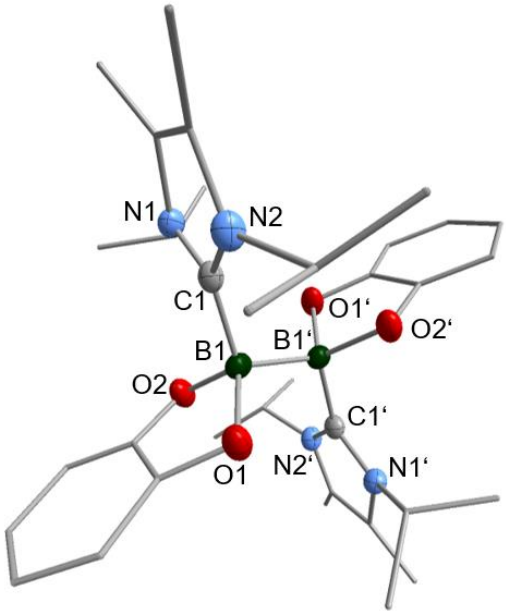

Figure 4.12 Molecular structure of (*i*Pr$_2$Im^{Me})$_2$·B$_2$cat$_2$ **25**. Hydrogen atoms are omitted for clarity and the thermal ellipsoids are drawn at 50% probability. Selected bond lengths [Å] and angles [°]: B1−C1 1.656(4), B1−B1’ 1.732(6), B1−O1 1.541(3), B1−O2 1.564(3), C1-B1-O1 112.1(2), C1-B1-O2 112.4(3).

The groups of Curran, Lacôte, and Lalevée have extensively studied radicals of the type NHC–BH$_2$˙,[162, 163] generated from the corresponding borane adducts by photo-induced homolytic B–H bond cleavage, and applied them as efficient co-initiators in radical photopolymerization reactions.[164-168] As the bis-NHC adducts **24**, **25**, and (Me$_2$Im^{Me})$_2$·B$_2$cat$_2$ might also be used as potential precursors for radical photopolymerization reactions by photo-induced homolytic B–B bond cleavage in a cooperation with the groups of Lacôte and Lalevée, absorption spectra were recorded in toluene (Figure 4.13). Despite the solubility issues, toluene solutions of the compounds were sufficiently concentrated to obtain meaningful spectra. The bis-NHC adducts **24**, **25**, and (Me$_2$Im^{Me})$_2$·B$_2$cat$_2$ all show an absorption maximum at ca. 300 nm, revealing a bathochromic shift compared to uncoordinated B$_2$cat$_2$. Compounds **24** and **25** are colorless compounds absorbing until ca. 400 nm. The absorbance of (Me$_2$Im^{Me})$_2$·B$_2$cat$_2$ is detectable until ca. 450 nm and, thus, it appears pale yellow. The absorption maximum for B$_2$cat$_2$ was not detectable, as it is hypsochromatically shifted with respect to the solvent cut-off of toluene.

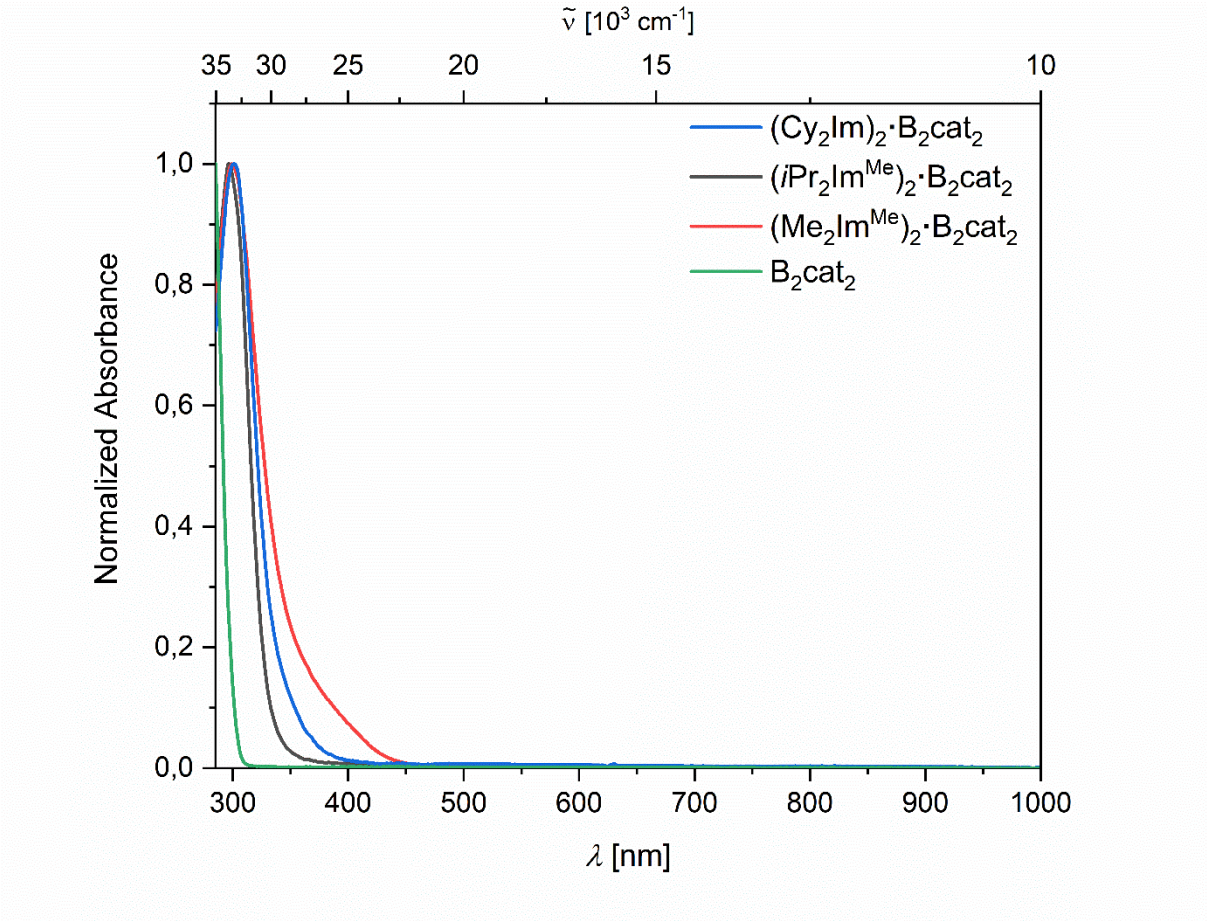

Figure 4.13 UV/VIS spectra of (Cy$_2$Im)$_2$·B$_2$cat$_2$ **24**, (*i*Pr$_2$Im^{Me})$_2$·B$_2$cat$_2$ **25**, (Me$_2$Im^{Me})$_2$·B$_2$cat$_2$, and B$_2$cat$_2$ recorded in toluene.

4.3 NHC Adducts of Pinacolborane and Aryl Boronic Esters

The reaction of NHCs with HBcat leads to adduct formation, whereas the more nucleophilic and simultaneously more electrophilic cyclic alkyl amino carbenes (cAACs) activate the borane by insertion of the cAAC carbene carbon atom into the B–H bond (Figure 4.14).[169] These findings are in accordance with studies by Bertrand *et al.* who activated HBpin upon reaction with the sterically more demanding cAAC^{Cy} and cAAC^{Menthyl}.[170] In 2017, the groups of Marder and Radius demonstrated that the reaction of NHCs with aryl boronic esters leads to the formation of adducts of the type Ar–B(OR)$_2$·NHC, while cAAC^{Me} activates the aryl boronic ester with cleavage of the B–C bond (Figure 4.14).[171] The insertion of the cAAC carbene carbon atom into the B–C bond is a reversible, temperature dependent process. Analogously, the reaction of cAACs with diborane(4) compounds leads to the insertion of the carbene carbon atom into the B–B bond; however, in this case, the process is irreversible (Figure 4.14).[172]

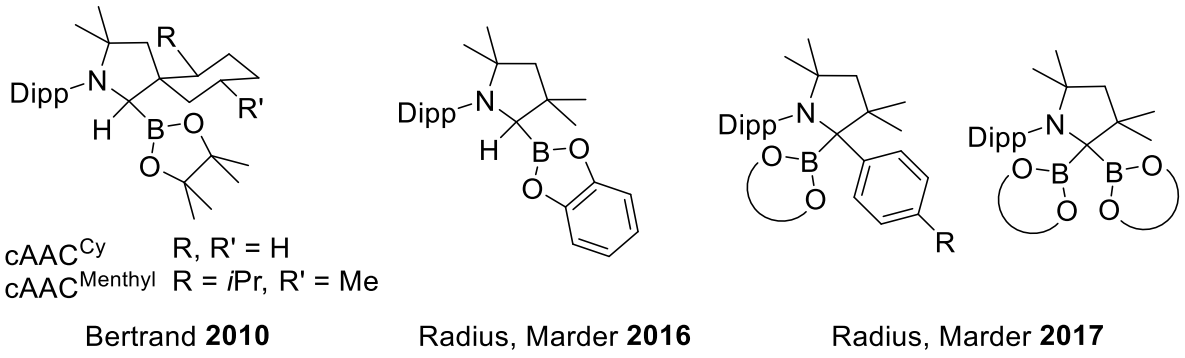

Figure 4.14 Examples of recently reported oxidative addition of B**–**E bonds (E = H, C, B) at cAAC.[169-172]

Based on the synthesis of a variety of NHC adducts of HBcat demonstrated by the groups of Marder and Radius in 2016,[169] HBpin was reacted with one equivalent of the free NHCs Cy_2Im, iPr_2Im^{Me}, and Me_2Im^{Me} in toluene at room temperature to afford the corresponding adducts Cy_2Im·HBpin **26,** iPr_2Im^{Me}·HBpin **27**, and Me_2Im^{Me}·HBpin **28** (Scheme 4.13).

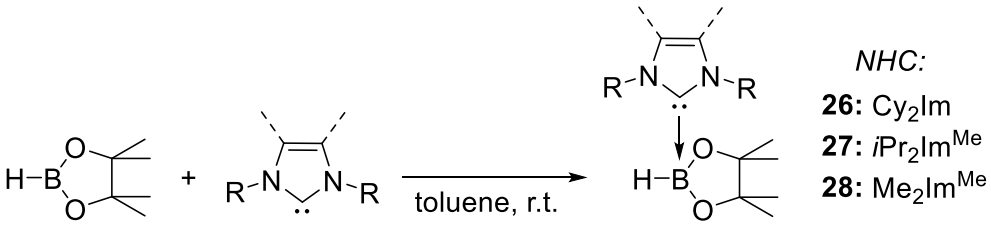

Scheme 4.13 Synthesis of the NHC adducts of pinacolborane Cy_2Im·HBpin **26**, iPr_2Im^{Me}·HBpin **27**, and Me_2Im^{Me}·HBpin **28**.

The compounds **26**-**28** were obtained as colorless solids in moderate yields up to 64% and were characterized *via* NMR spectroscopy, HRMS, and elemental analysis. While the ^{11}B NMR spectra show a sharp doublet with a coupling constant of $^1J_{BH}$ = 109 Hz in the expected region for sp^3-hybridized boron atoms (ca. 2.50 ppm), a corresponding broad quartet ($^1J_{BH}$ = 109 Hz) is observed in the ^1H NMR spectra. For Me_2Im^{Me}·HBpin **28** the ^1H and ^{11}B NMR spectra are depicted in Figure 4.15.

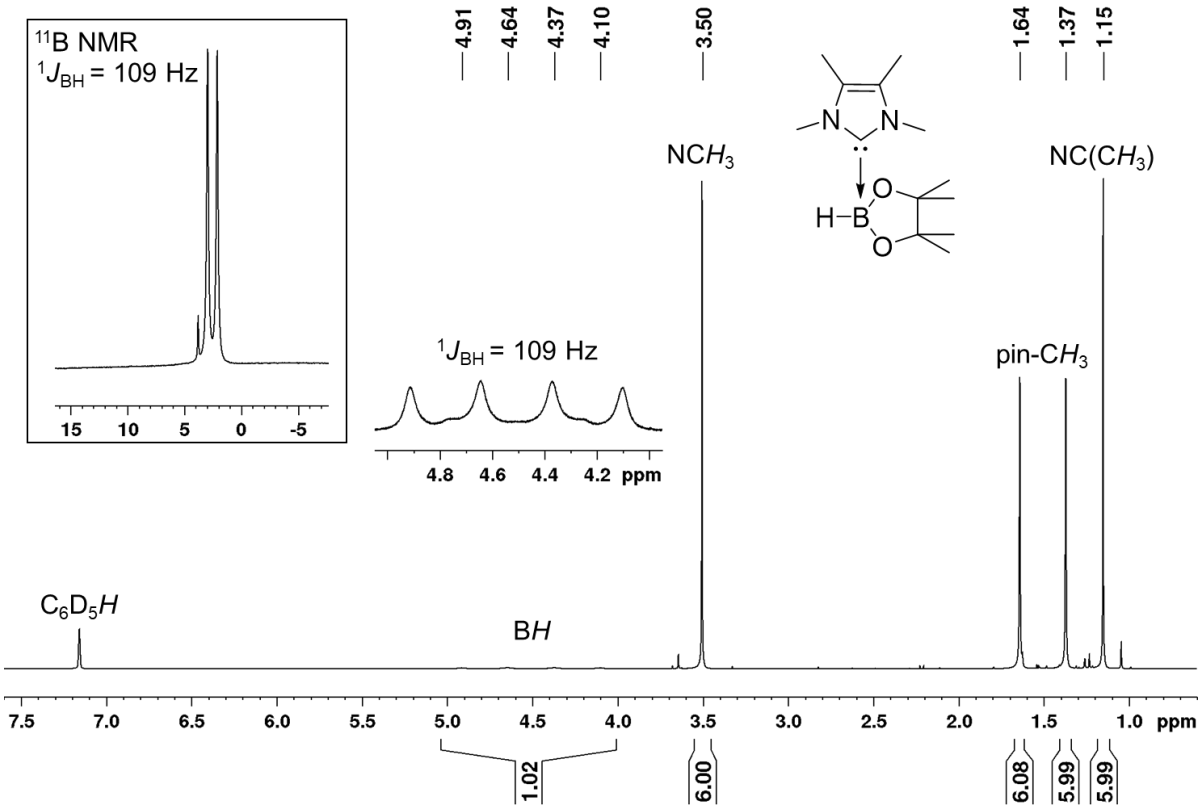

Figure 4.15 ^{1}H NMR and ^{11}B NMR (inlay) spectra of Me_2Im^{Me}·HBpin **28** recorded in C_6D_6 (500 MHz/160 MHz).

In the $^{13}C\{^{1}H\}$ NMR spectra of **26**-**28**, the signals do not show any significant shift compared to the starting material, apart from that of the carbene carbon atoms. These resonances are observed at 166.8, 166.6, and 165.8 ppm, respectively, significantly up-field shifted compared to those of the free NHCs (Me_2Im^{Me}: 213.0 ppm, iPr_2Im^{Me}: 207.6 ppm and Cy_2Im: 212.7ppm). This is in accordance with the observations made for the NHC adducts of diborane(4) compounds **20**-**25**.

When pinacolborane was reacted with the more nucleophilic and simultaneously more electrophilic $cAAC^{Me}$, an activation of HBpin occurred *via* insertion of the $cAAC^{Me}$ carbene carbon atom into the B–H bond (Scheme 4.14). While for HBpin, this B–H oxidative addition process at the $cAAC^{Me}$ carbene carbon atom readily takes place in toluene at room temperature, for HBcat the reaction mixture requires heating overnight at 100 °C.

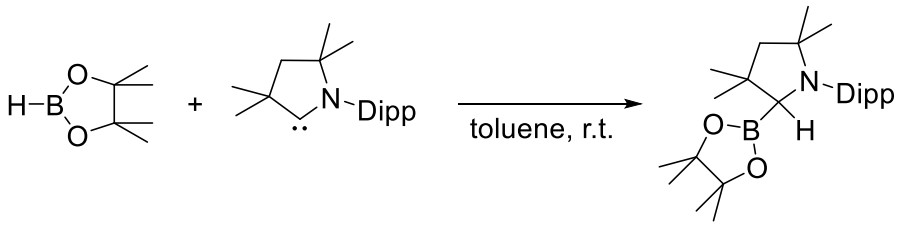

Scheme 4.14 Synthesis of cAAC^{Me}(H)Bpin **29**.

The B–H activation product cAAC^{Me}(H)Bpin **29** was obtained as a colorless solid in 72% yield and was characterized by NMR spectroscopy, HRMS, elemental analysis, and X-ray diffraction. The ^{1}H NMR spectrum reveals the C*H* proton at the former cAAC^{Me} carbene carbon atom at a chemical shift of 3.73 ppm, whereas two septets were detected for the *iso*-propyl methine protons of the Dipp-moiety, which indicates the loss of symmetry at the former cAAC^{Me} carbene carbon atom (Figure 4.16). In both ^{11}B and ^{11}B{^{1}H} NMR spectra, one broad singlet appears at 32.3 ppm as the former carbene carbon atom has inserted into the B–H bond. In the ^{13}C{^{1}H} NMR spectrum, this now sp^{3}-hybridized carbon atom gives rise to a broad resonance at 62.9 ppm, which is significantly up-field shifted compared to that of the carbene carbon atom in the free cAAC^{Me} (313.5 ppm).

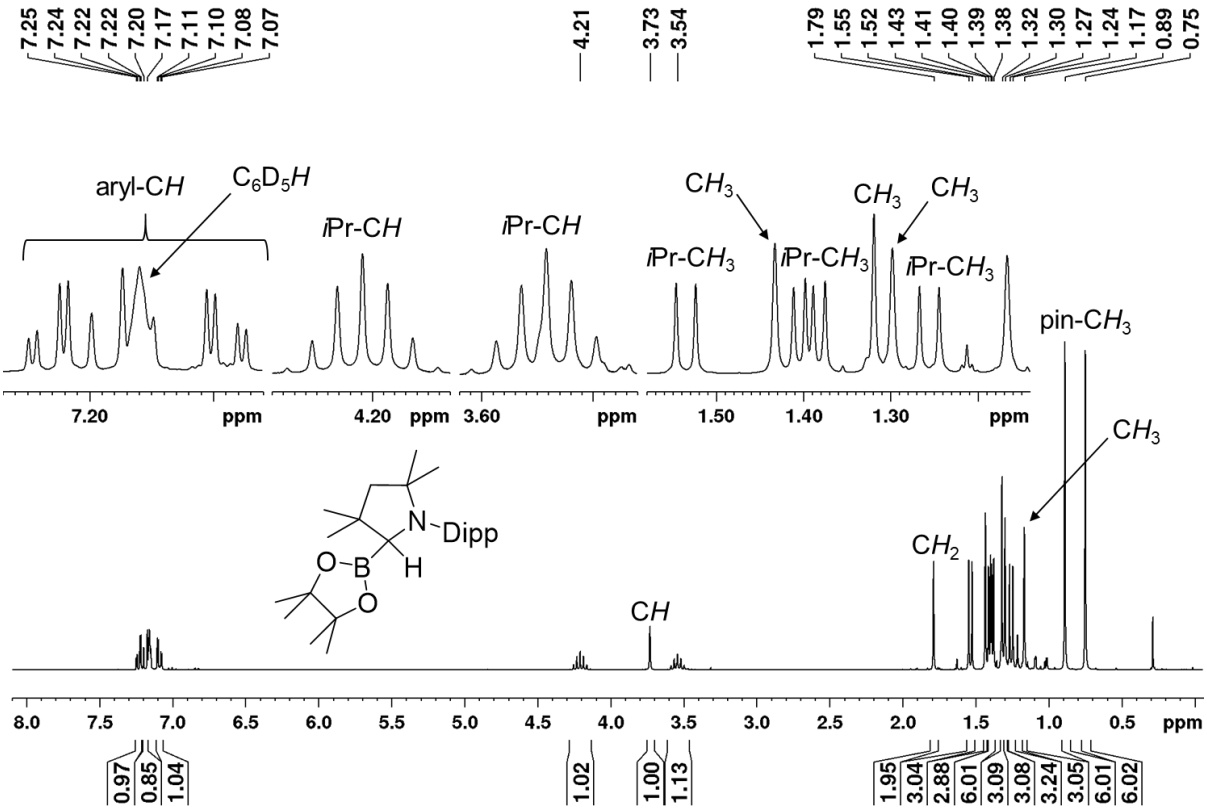

Figure 4.16 ^{1}H NMR spectrum of cAAC^{Me}(H)Bpin **29** recorded in C_6D_6 (400 MHz).

Single crystals suitable for X-ray diffraction were obtained from slow evaporation of the solvent of a saturated solution of cAAC^{Me}(H)Bpin **29** in benzene. The molecular structure of **29** confirms the formation of an oxidative addition product with a stereo center at the former cAAC carbene carbon atom. The molecule is disordered with both enantiomers being present (ca. 69% S-enantiomer and 31% R-enantiomer). As the crystal structure is centrosymmetric, the entire molecule is inverted at the inversion center and as a result there are just as many molecules with the inverse disorder (ca. 69% R-configuration and 31% S-configuration). In total, both enantiomers are present in the crystal by the same amount. The molecular structure of (S)-cAAC^{Me}(H)Bpin **29** is shown in Figure 4.17. The B–C1 bond distance of 1.567(3) Å is similar to that observed for cAAC^{Me}(H)Bcat (1.550(2) Å),[169] but significantly shorter than those observed for NHC adducts of the type NHC·HBcat (e.g. *i*Pr$_2$Im^{Me}·HBcat: 1.646(2) Å)[169] and for the previously mentioned NHC adducts of diborane(4) compounds (**22:** 1.6864 (19) Å; **25:** 1.656(4) Å).

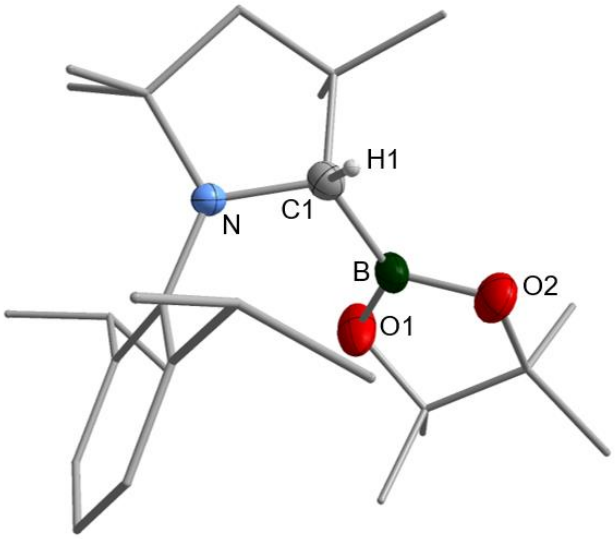

Figure 4.17 Molecular structure of (S)-cAAC^{Me}(H)Bpin **29**. Hydrogen atoms are omitted for clarity except at the former cAAC carbene carbon atom, and the thermal ellipsoids are drawn at 50% probability. Selected bond lengths [Å] and angles [°]: B−C1 1.567(3), B−O1 1.361(3), B−O2 1.370(3), C1-B-O1 125.1(2), C1-B-O2 122.3(2).

In 1999, Marder and co-workers first reported an adduct of mpy with phenylcatecholborane.[173] Later, the groups of Marder and Radius demonstrated the reactivity of NHCs towards aryl boronic esters.[171] The analogous principle of B–E bond activation as observed for NHC adducts of diborane(4) compounds can be applied to aryl boronic esters and NHCs. Similar to sp^2–sp^2 diborane(4) compounds,

aryl boronic esters offer an sp^2-hybridized boron atom bound to an sp^2-hybridized carbon atom. The coordination of an NHC quarternizes the boron atom and, thus, weakens the B–C bond, potentially enabling the transfer of the aryl moiety in a transition metal-free C–C bond forming process.

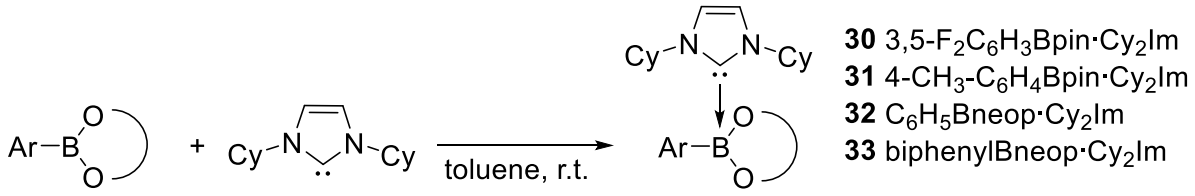

Scheme 4.15 Synthesis of NHC adducts of aryl boronic esters using Cy_2Im.

As sterically less demanding, alkyl substituted NHCs showed adduct formation with various aryl boronic esters preferentially,[171] in the following the cyclohexyl substituted NHC Cy_2Im was investigated for adduct formation.

The reaction of various functionalized aryl boronic esters of pinacolato and neopentyl glycolato with stoichiometric amounts of Cy_2Im in toluene at room temperature led to the isolation of 3,5-$F_2C_6H_3$Bpin·Cy_2Im **30**, 4-CH_3-C_6H_4Bpin·Cy_2Im **31**, C_6H_5Bneop·Cy_2Im **32**, and biphenylBneop·Cy_2Im **33** as colorless solids in moderate yields between 42 and 51% (Scheme 4.15). The compounds were characterized *via* NMR spectroscopy, HRMS, and elemental analysis. In the $^{11}B\{^1H\}$ NMR spectra an upfield shift is observed due to the quaternization of the boron atom. The signals for the boron atom of the NHC adducts are detected in a range between 2.94 and 4.88 ppm, while the boron atoms of the starting compounds give rise to resonances at ca. 30.0 ppm.

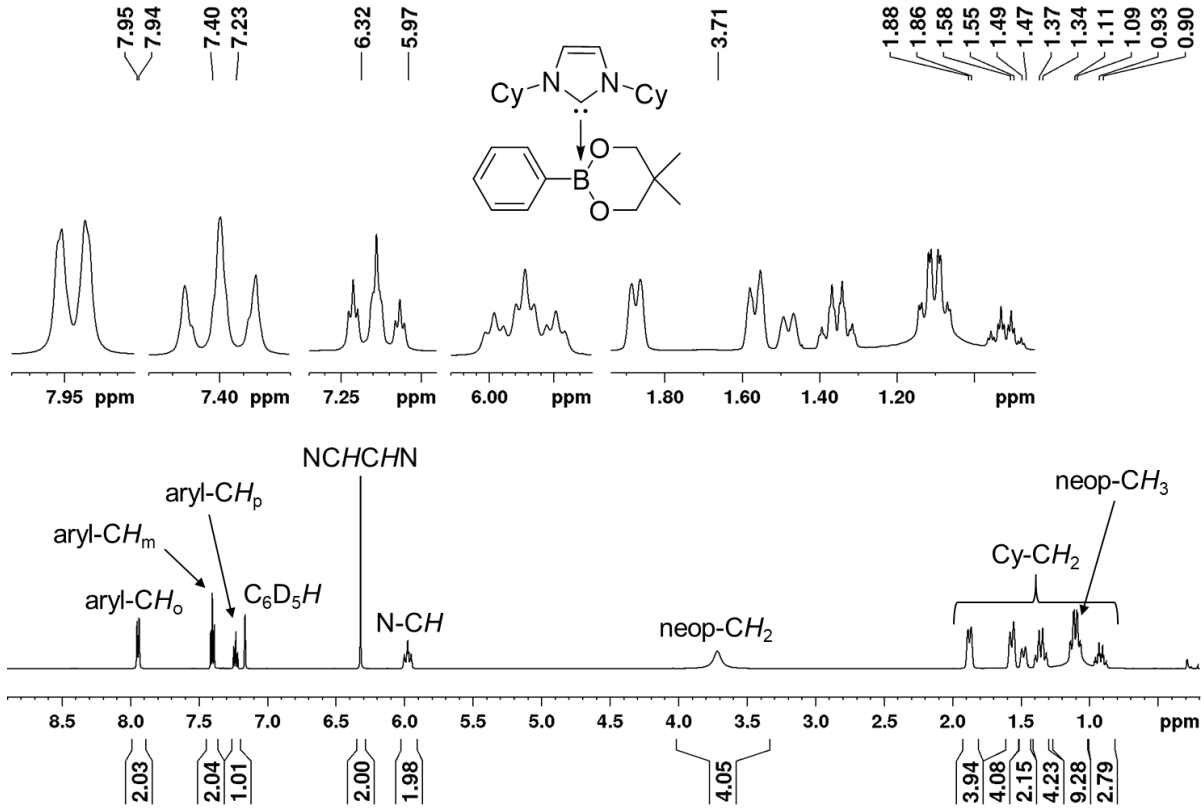

Figure 4.18 ^{1}H NMR spectrum of C_6H_5Bneop·Cy_2Im **32** recorded in C_6D_6 (400 MHz).

The ^{1}H NMR spectra reveal a significant downfield shift of the multiplet arising from the protons of the C*H*-unit of the cyclohexyl substituent, compared to that observed in the free NHC. The ^{1}H NMR spectrum of C_6H_5Bneop·Cy_2Im **32** is depicted in Figure 4.18. In the ^{13}C{^{1}H} NMR spectra, the detected signals do not show any significant shift compared to the starting material, apart from the signal of the carbene carbon atom, which is observed characteristically upfield shifted compared to that in free Cy_2Im. In addition, the fluorine atoms in **30** give rise to a singlet at -112.9 ppm in the ^{19}F{^{1}H} NMR spectrum.

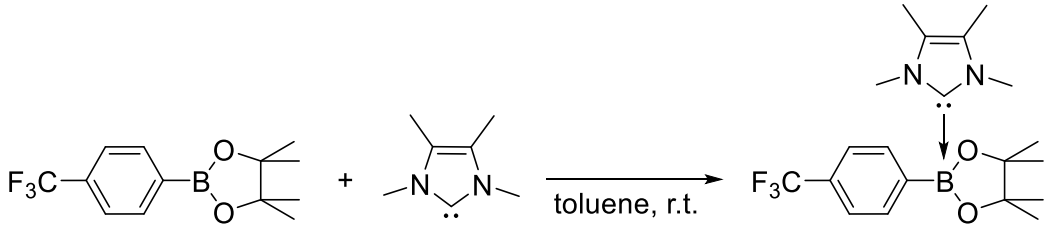

Scheme 4.16 Synthesis of 4-F_3C-C_6H_4Bpin·Me_2Im^{Me} **34**.

Additionally, 4-F_3C-C_6H_4Bpin·Me_2Im^{Me} **34** was obtained as a colorless solid in good yields of 68% by reacting 4-F_3C-C_6H_4Bpin **4** with one equivalent of Me_2Im^{Me} in toluene at room temperature (Scheme 4.16). Adduct **34** was characterized *via* NMR spectroscopy, HRMS, and elemental analysis. In the $^{11}B\{^1H\}$ NMR, a signal is observed at 4.13 ppm, as expected for sp^3-hybridized boron atoms. Instead of one signal for the pinacol unit, as detected in the starting material, two signals are observed in the ^1H NMR spectrum (Figure 4.19).

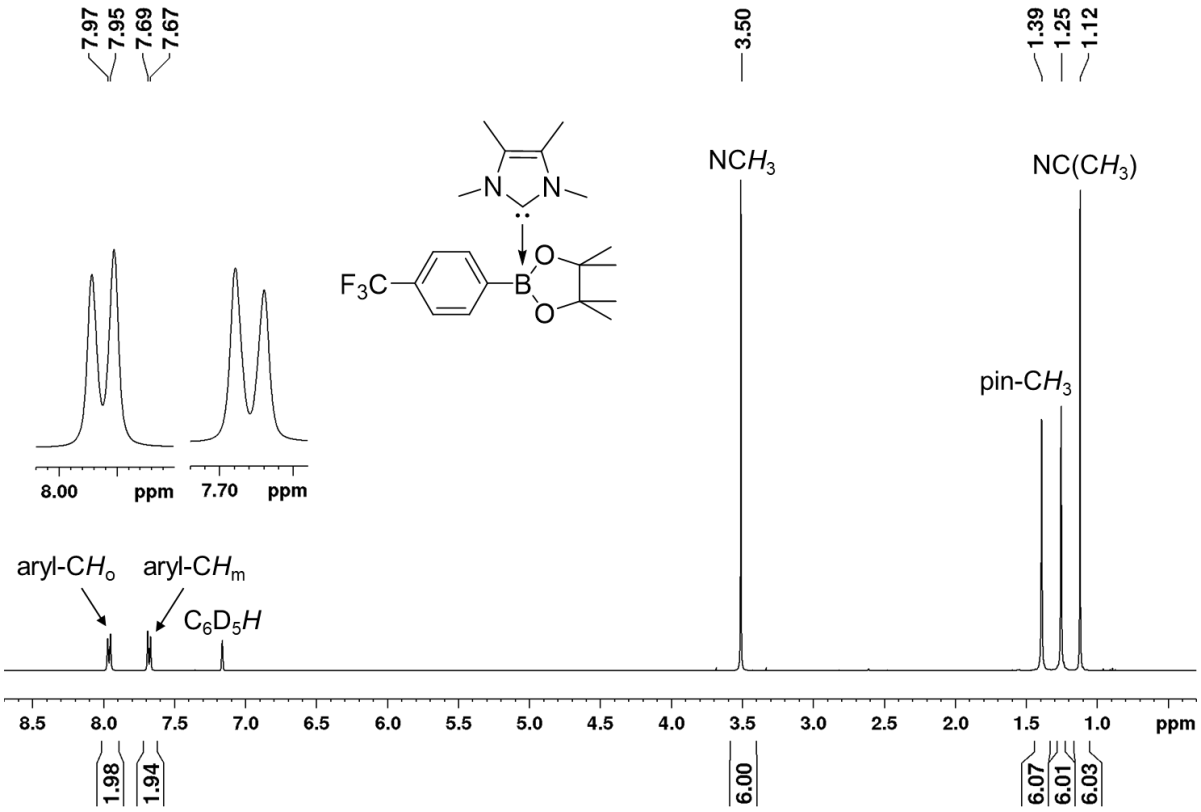

Figure 4.19 ^1H NMR spectrum of 4-F_3C-C_6H_4Bpin·Me_2Im^{Me} **34** recorded in C_6D_6 (400 MHz).

Compared to the starting material (213.0 ppm), the carbene carbon atom shows a significant upfield-shift at 165.7 ppm in the $^{13}C\{^1H\}$ NMR spectrum. The quaternary carbon atom of the aryl unit bound to boron, resonates as a hardly detectable and very broad signal at 160.8 ppm, due to the quadrupole moment of the boron. The $^{19}F\{^1H\}$ NMR spectrum reveals a singlet for the fluorine atoms of the CF_3-moiety at a chemical shift of -61.4 ppm.

A comparison of the $^{11}B\{^1H\}$ NMR shifts, the $^{13}C\{^1H\}$ NMR shifts of the carbene carbon atom, and of the B–B and B–C or B–N bond lengths of the compounds synthesized **18**-**34** is given in Table 4.1.

Table 4.1 Comparison of the $^{11}B\{^1H\}$ NMR shifts [ppm], the $^{13}C\{^1H\}$ NMR shifts of the carbene carbon atom (C_{NHC}) [ppm], and of the B**–**B and B**–**C or B**–**N bond lengths [Å].

Compound	δ ($^{11}B\{^1H\}$)	δ (C_{NHC})	B–B	B–C / B–N
pyridine·B_2cat_2 **18**	22.2/6.60[a]	-	1.7106(18)	1.6439(15)
DMAP·B_2cat_2 **19**	21.7[b]	-	-	-
Me_2Im^{Me}·B_2pin_2 **20**	2.94/36.5	168.1	-	-
iPr_2Im^{Me}·B_2pin_2 **21**	2.91/36.9	169.8	-	-
iPr_2Im^{Me}·$B_2(OMe)_4$ **22**	4.05/35.0	166.2	1.759(2)	1.6864(19)
Cy_2Im·$B_2(OMe)_4$ **23**	4.34/36.4	167.3	-	-
$(Cy_2Im)_2$·B_2cat_2 **24**	12.4[c]	164.5	-	-
(*i*Pr_2Im^{Me})$_2$·B_2cat_2 **25**	11.5	166.5	1.732(6)	1.656(4)
Cy_2Im·HBpin **26**	2.50	166.8	-	-
iPr_2Im^{Me}·HBpin **27**	2.65	166.6	-	-
Me_2Im^{Me}·HBpin **28**	2.50	165.8	-	-
cAAC^{Me}(H)Bpin **29**	32.3	-	-	1.567(3)
3,5-$F_2C_6H_3$Bpin·Cy_2Im **30**	4.02	165.7	-	-
4-CH_3-C_6H_4Bpin·Cy_2Im **31**	4.88	168.3	-	-
C_6H_5Bneop·Cy_2Im **32**	2.94	165.8	-	-
BiphenylBneop·Cy_2Im **33**	3.29	165.6	-	-
4-F_3C-C_6H_4Bpin·Me_2Im^{Me} **34**	4.13	165.7	-	-

[a] Equilibrium in solution between pyridine·B_2cat_2 **18** and free B_2cat_2 and pyridine, and a very fast exchange of pyridine between the two boron atoms in pyridine·B_2cat_2 **18** (δ = 22.2 ppm), as well as the presence of the bis-pyridine adduct (δ = 6.60 ppm), formed via a comparatively slow (on the NMR timescale) dismutation process of **18**. [b] Averaged signal, due to dynamic exchange of DMAP between the two boron atoms. [c] Indicated by SS NMR spectroscopy.

4.4 REACTIVITY OF ADDUCTS OF THE TYPE L·$B_2(OR)_4$ WITH ARYL HALIDES

In 2009, during the studies on the Cu-catalyzed borylation reaction of aryl iodides and bromides, an uncatalyzed background reaction was observed by Marder and co-workers, forming the desired aryl boronic ester in low yields.[85] The *in situ* formed anionic sp^2–sp^3 adduct $[B_2pin_2(OtBu)]K$ was detected, which was assumed to be the active nucleophilic species, enabling the transfer of a boryl moiety to the aryl iodide without the necessity of a transition metal catalyst. In 2013, Wu and Zhang reported a similar transition metal-free borylation of aryl iodides with B_2pin_2 and B_2neop_2 in methanol with Cs_2CO_3.[174] Later, the groups of Radius, Lin, Kleeberg, and Marder described the syntheses and characterization of various anionic sp^2–sp^3 diborane(4) adducts of the type $[B_2pin_2(OR)]K(L)$ (R = *t*Bu, Me; L = 18-crown-6) and $[B_2pin_2(F)][NR_4]$ (R = *n*Bu, Me), which were investigated as potential nucleophilic boron sources for borylation reactions of aryl iodides and diazonium tetrafluoroborates.[29, 175] For aryl iodides, merely the use of $[B_2pin_2(OtBu)]K$ gave the desired borylated product in 29% yield after long reaction times of 3 weeks at 60 °C. Utilizing aryl diazonium tetrafluoroborates as the substrate, which offer an increased electrophilicity compared to aryl iodides, the anionic sp^2–sp^3 diborane(4) adducts, were shown to serve as effective sources of nucleophilic boryl moieties. This transition metal-free borylation reaction was further studied in detail for a variety of aryl diazonium tetrafluoroborates using $[B_2pin_2(F)][NMe_4]$ as the anionic adduct of B_2pin_2 (Scheme 4.17).[175]

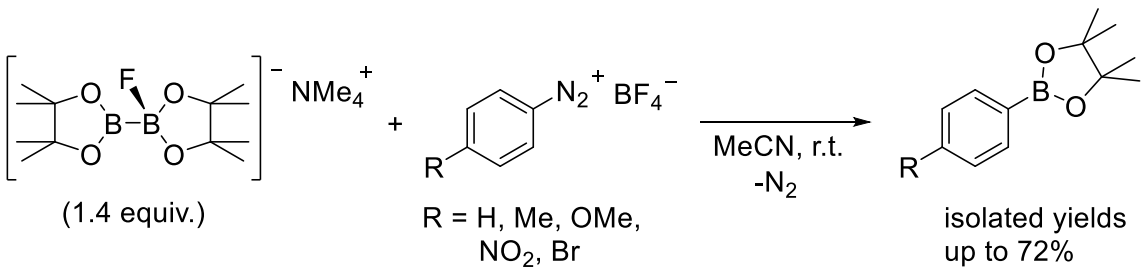

Scheme 4.17 Reaction of the anionic sp^2–sp^3 diborane(4) compound $[B_2pin_2(F)][NMe_4]$ with diazonium tetrafluoroborates in acetonitrile at room temperature forming the corresponding aryl boronates.[175]

Based on these studies, neutral adducts of the type pyridine·B_2cat_2 **18**-**19** and NHC·$B_2(OR)_4$ **20**-**23**, as well as Cy_2Im·B_2pin_2[146] and Me_2Im^{Me}·B_2cat_2,[169] were examined for their ability to transfer a boryl moiety to an aryl iodide. In a standard procedure, the adduct to be examined and 4-iodotoluene **5-I** were reacted in a 1:1 stoichiometry in C_6D_6 for 16 h at 80 °C in a sealed Young's tap NMR tube and the reactions were monitored by NMR spectroscopy and GC-MS.

The reaction of 4-iodotoluene **5-I** with the pyridyl adducts pyridine·B_2cat_2 **18** and DMAP·B_2cat_2 **19** in C_6D_6 did not show any conversion of the starting material, either at room temperature or at an elevated temperature of 80 °C. As **18** and **19** only show moderate solubility in benzene, the reaction was repeated in CD_2Cl_2 at temperatures up to 60 °C. Despite the better solubility in dichloromethane, only starting material was detected. The reaction of 4-iodotoluene with the mono-NHC adducts *i*Pr_2Im^{Me}·$B_2(OMe)_4$ **22** and Cy_2Im·$B_2(OMe)_4$ **23** gave only traces of borylation product according to GC-MS. Applying the mono-NHC adduct Me_2Im^{Me}·B_2cat_2,[169] traces of the aryl iodide were also converted to the corresponding aryl boronic ester, as evidenced by GC-MS. However, extending the reaction time or adding another 0.5 equivalents of the respective mono-NHC adduct did not lead to the formation of a noteworthy amount of the desired borylation product. When the mono-NHC adducts of B_2pin_2, Cy_2Im·B_2pin_2[146] and *i*Pr_2Im^{Me}·B_2pin_2 **21** were also treated with 4-iodotoluene **5-I**, again, only traces of borylation product were detected by GC-MS. However, when monitoring the stoichiometric reaction of Me_2Im^{Me}·B_2pin_2 **20** with 4-iodotoluene **5-I** in C_6D_6 at 80 °C, the first new signals arising from the desired borylation product appeared within 1 h (Figure 4.20). Full conversion of **5-I** was achieved after the addition of 2.5 equivalents of **20**. The new signals match those reported for the desired C–I bond borylated product **5**,[118, 122] which was additionally verified by GC-MS and HRMS.

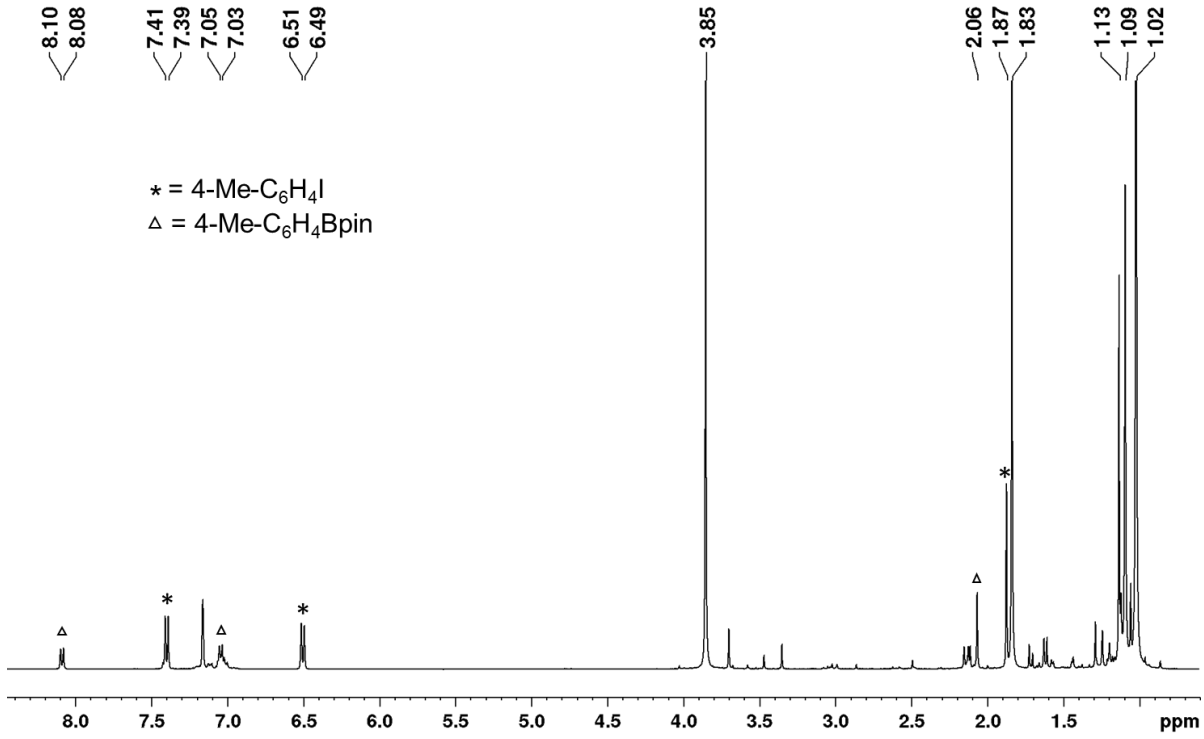

Figure 4.20 *In situ* ^{1}H NMR spectrum of the 1:1 stoichiometric reaction of 4-iodotoluene and Me_2Im^{Me}·B_2pin_2 **20** in C_6D_6 after 16 h at 80 °C (400 MHz).

Interestingly, the C–C coupling product of the aryl halide with the solvent C_6D_6 was detected as a byproduct **5a** in ca. 25% yield (Scheme 4.18). Compound **5a**, as well as the coupling product **5a-H**, which was obtained by running the reaction in non-deuterated benzene, were isolated and characterized *via* NMR spectroscopy, GC-MS, and HRMS.

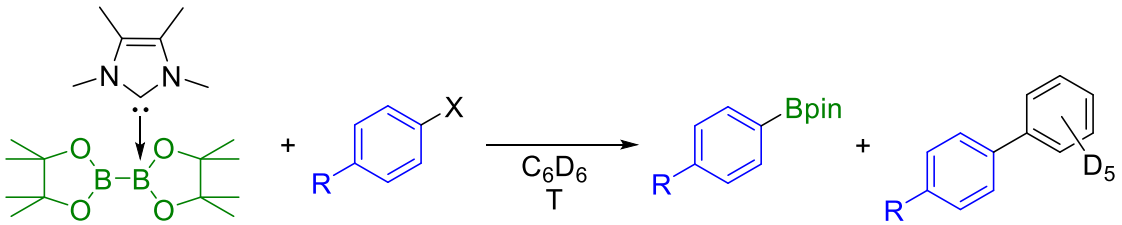

X = I, R = CF_3 **4-I**
X = I, R = CH_3 **5-I**
X = I, R = OCH_3 **6-I**
X = Br, R = CF_3 **4-Br**
X = Br, R = CH_3 **5-Br**
X = Cl, R = CF_3 **4-Cl**
X = Cl, R = CH_3 **5-Cl**

Scheme 4.18 Reaction of the mono-NHC adduct Me_2Im^{Me}·B_2pin_2 **20** with aryl halides (X = I, Br, Cl) forming the corresponding C–X bond borylation products **4**-**6** and the C–C coupling products **4a**-**6a** between the substrate and the solvent C_6D_6.

Further reactivity studies were conducted for the reaction of **20** with different *para*-substituted aryl iodides, bromides, and chlorides (Scheme 4.18). Full conversion was achieved for the aryl iodides **4-I** - **6-I** and the aryl bromides **4-Br** and **5-Br**. The ratio of the borylated arene and the C–C coupling side product strongly depends on the reaction temperature (Table 4.2). Lower temperatures (50 °C) diminish the formation of the byproduct from 25 to 7% (cf. Table 4.2, entry 3 and 4), but also decrease the reaction rate. For example, in the case of 4-iodo-benzotrifluoride **4-I** starting material was no longer detectable after 1.5 h at 80 °C, whereas at a reaction temperature of 50 °C full conversion was achieved only after 16 h (Figure 4.21). For **4-I** and **4-Br**, the borylated arene was obtained in solution in the form of its Me_2Im^{Me} adduct, possibly due to the more Lewis acidic boron atom resulting from the electron-withdrawing CF_3-substituent. This observation explains why an additional 0.5 equivalents of Me_2Im^{Me}·B_2pin_2 **20** are required for full conversion of **4-I** and **4-Br**. The ^{1}H NMR resonances of the *in situ* formed NHC adduct are in accordance with 4-F_3C-C_6H_4-Bpin·Me_2Im^{Me} **34** (see chapter 4.3).

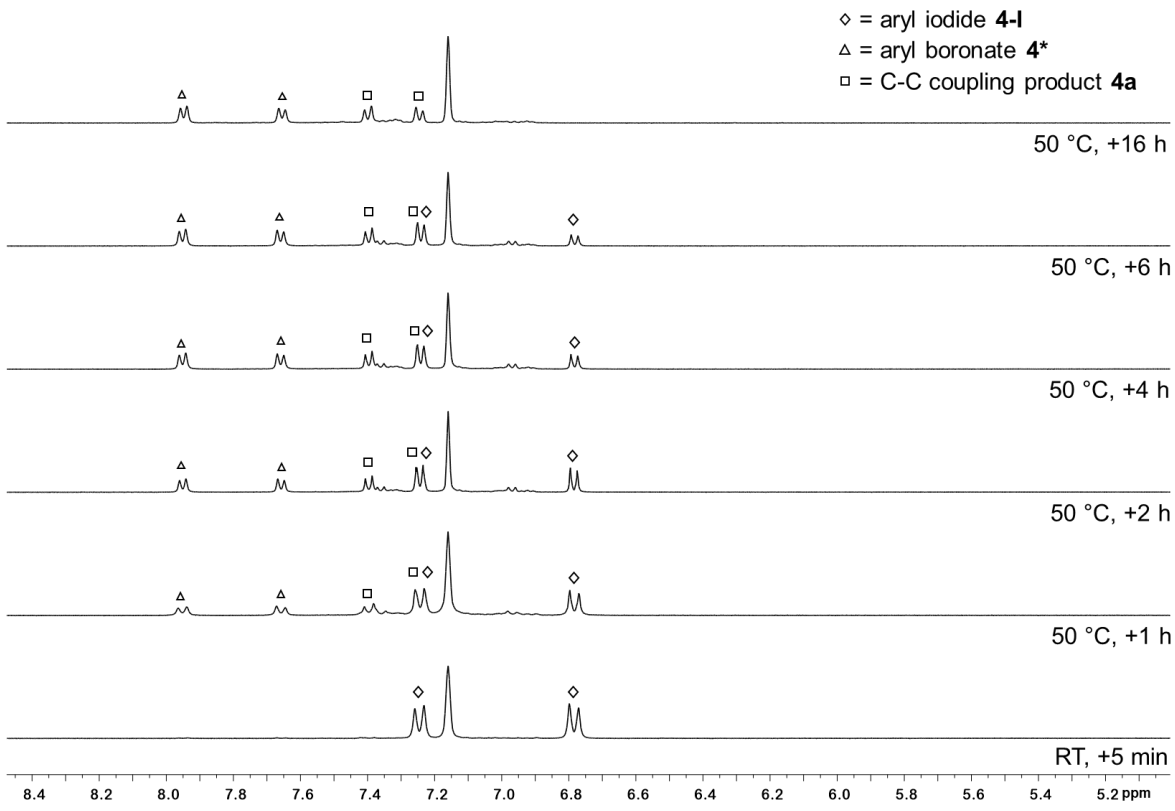

Figure 4.21 *In situ* ^{1}H NMR spectra (aromatic region) of the reaction of the mono-NHC adduct Me_2Im^{Me}·B_2pin_2 **20** and 4-iodo-benzotrifluoride **4-I** in C_6D_6 at 50 °C (400 MHz). Diamond: 4-iodobenzotrifluoride **4-I**. Triangle: aryl boronic ester **4** (* in solution the boron atom is coordinated by Me_2Im^{Me} forming the NHC adduct **34**). Square: C–C coupling product **4a**.

For substrate **4-I**, the reaction also proceeds slowly at room temperature, with 84% conversion after 1 week, and a **4**/**4a** ratio of 2:1. The absence of light did not have any impact on the reaction outcome. For aryl chlorides, no reaction occurred at temperatures of 50 °C. The reaction of the aryl chloride **5-Cl** led to traces of **5** at 80 °C, whereas for the more activated aryl chloride **4-Cl**, 20% of the aryl boronic ester **4** and 12% of the coupling product **4a** were observed at 80 °C (Table 4.2, entry 11-12). The aryl boronic esters were isolated and characterized by NMR spectroscopy, GC-MS, and HRMS.

Therefore, in contrast to most metal-catalyzed processes, this boryl transfer reaction is most effective when using electron-rich aryl halides, with a good leaving group (I > Br >> Cl), at reaction temperatures of 50 °C. Utilizing electron-poor aryl iodides and bromides at elevated reaction temperatures of 80 °C, results in the C–C coupling product of the aryl halide with the solvent being the major product. In general, higher reaction temperatures promote the formation of the C–C coupling product.

Table 4.2 Reaction of the mono-NHC adduct Me_2Im^{Me}·B_2pin_2 **20** with the aryl halides **4-I**-**6-I**, **4-Br**, **5-Br**, **4-Cl**, and **5-Cl** in C_6D_6.[a]

Entry	R	X	T [°C]	Borylation Product [%][b]	Side product **a** [%]
1	CF_3 **4-I**[c]	I	80	44[d]	56
2	CF_3 **4-I**[c]	I	50	55[d] (44)	45
3	CH_3 **5-I**	I	80	75	25
4	CH_3 **5-I**	I	50	93 (85)	7
5	OCH_3 **6-I**	I	80	80	20
6	OCH_3 **6-I**	I	50	91(82)	9
7	CF_3 **4-Br**[c]	Br	80	28[d]	72
8	CF_3 **4-Br**[c]	Br	50	70[d]	30
9	CH_3 **5-Br**	Br	80	73	27
10	CH_3 **5-Br**	Br	50	92	8
11	CF_3 **4-Cl**	Cl	80	20	12
12	CH_3 **5-Cl**	Cl	80	traces	traces

[a] Reaction conditions: 1.0 equivalent of the aryl halide, 2.5 equivalents of **20**, C_6D_6; [b] Yields are determined *via* quantitative ^{1}H NMR spectroscopy, as well as GC-MS yield with biphenyl as an internal standard. Isolated yields in parentheses; [c] 3.0 equivalents of **20**; [d] in solution, the boron atom is coordinated by Me_2Im^{Me} forming the NHC adduct **34**.

Attempts to suppress the C–C coupling side product by performing the reaction in MTBE instead of benzene, not providing any aromatic C–H bonds in the solvent, resulted in the formation of large quantities of a different side product, resulting from hydrodehalogenation of the aryl halide.

4.5 UNRAVELLING THE MECHANISM

Based on the successful boryl transfer reaction from the mono-NHC adduct Me_2Im^{Me}·B_2pin_2 **20** to aryl halides, it was of interest to gain more insight into how the reaction proceeds. The related bis-NHC adducts of diborane(4) compounds usually undergo spontaneous RER, for which the exact mechanism also remains unclear. As the RER is an intramolecular reaction with no further substrates involved, the mechanistic investigations began by examining this reaction in more detail, using the reaction of B_2neop_2 with two equivalents of Me_2Im^{Me} as an example (Scheme 4.19).

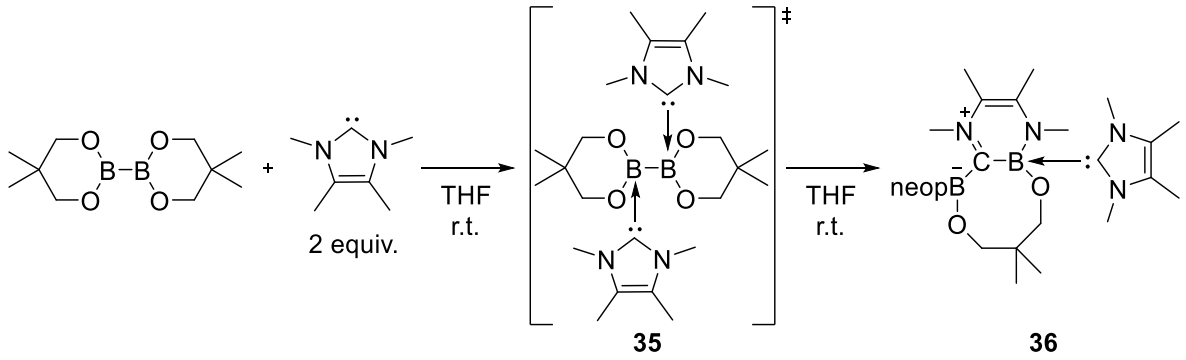

Scheme 4.19 Reaction of B_2neop_2 with two equivalents of Me_2Im^{Me} at room temperature forming the ring expanded product RER-B_2neop_2·$(Me_2Im^{Me})_2$ **36** with the bis-NHC adduct $(Me_2Im^{Me})_2$·B_2neop_2 **35** as an intermediate.

As the ring expansion reaction is very fast, and intermediates were not detected previously, the studies began by monitoring the RER of B_2neop_2 with two equivalents of Me_2Im^{Me} in THF by EPR spectroscopy (Figure 4.22). Starting at -80 °C, the temperature was slowly raised, as previous studies showed that, at room temperature, the ring-expanded product RER-$(Me_2Im^{Me})_2$·B_2neop_2 **36** is generated quantitatively within minutes.

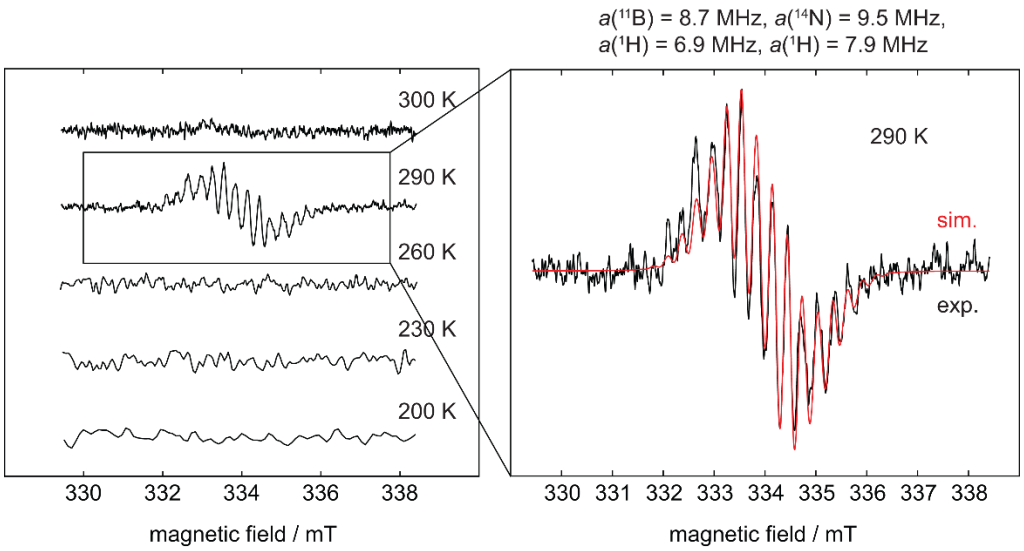

Figure 4.22 Simulated (red) and experimental (black) EPR spectrum of the RER of B_2neop_2 with two equivalents of Me_2Im^{Me} in THF.

At 290 K (16.9 °C) a weak EPR signal was detected with an isotropic *g*-value of 2.003, revealing hyperfine couplings to boron ($a(^{11}B)$ = 8.7 MHz), nitrogen ($a(^{14}N)$ = 9.5 MHz), and to the methyl protons of the NHC ($a(^{1}H)$ = 6.9 and 7.9 MHz). The simulated parameters (Figure 4.22, red) are consistent with a radical of the type NHC–$BR_2^{\bullet}$ (Me_2Im^{Me}–Bneop$^{\bullet}$) **35a**, presumably generated by homolytic cleavage of the B–B bond in B_2neop_2. Bis-NHC adducts such as $(Me_2Im^{Me})_2$·B_2neop_2 **35**, with both boron atoms coordinated by an NHC reveal an increased bond length and, therefore, a weakened boron-boron bond. The structure of the NHC–$BR_2^{\bullet}$ radical **35a** and its spin density distribution were computed by DFT calculations (DFT, def2-TZVP, M06-2x; see Figure 4.23). The NHC-boryl radical is nearly planar with the spin density delocalized between the boron atom and the NHC ring.

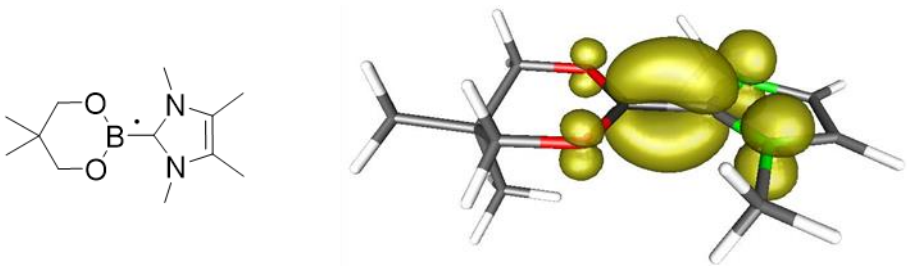

Figure 4.23 Schematic (left) and calculated (right) structures of the NHC**–**$BR_2^{\bullet}$ radical **35a** with an overlay of the computed spin density.

To verify that the detected EPR signal arose from a species proceeding the RER of **35**, the reaction process was monitored by VT ^{1}H and $^{11}B\{^{1}H\}$ NMR spectroscopy. While the ^{1}H NMR spectra showed broad signals as expected, the presence of the bis-NHC adduct $(Me_2Im^{Me})_2{\cdot}B_2neop_2$ **35** at low temperatures and the onset of the ring expansion reaction at 16 °C were easily followed by $^{11}B\{^{1}H\}$ NMR (Figure 4.24). Below 5 °C, no signal was detected, due to the poor solubility of the starting materials. Upon warming to 5 °C, a broad signal for the bis-NHC adduct **35** was detected at 5.12 ppm, which is significantly shifted from that of free B_2neop_2, as a result of the change in hybridization at boron.

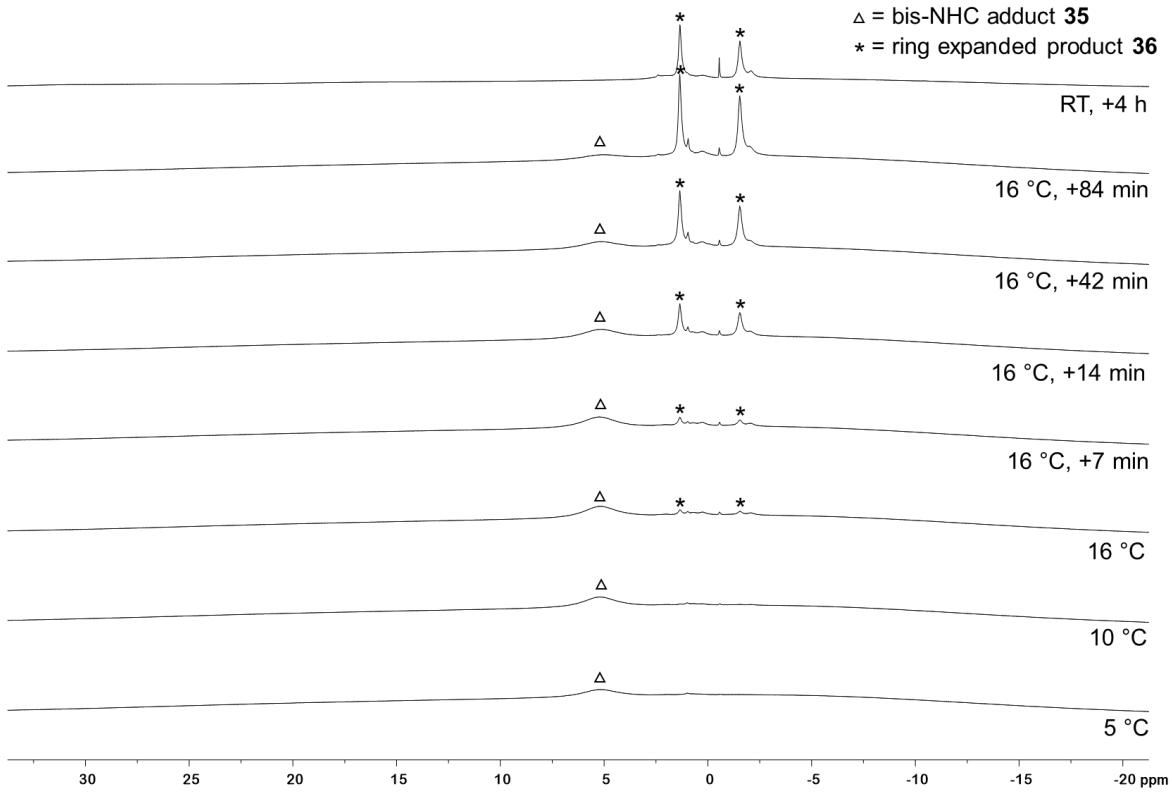

Figure 4.24 $^{11}B\{^{1}H\}$ VT-NMR spectra of the RER of B_2neop_2 with two equivalents Me_2Im^{Me} in d_8-THF (160 MHz). Triangle: bis-NHC adduct $(Me_2Im^{Me})_2{\cdot}B_2neop_2$ **35**. Asterisk: ring-expanded product RER-$(Me_2Im^{Me})_2{\cdot}B_2neop_2$ **36**.

At 16 °C, the signals for the ring-expanded product RER-$(Me_2Im^{Me})_2{\cdot}B_2neop_2$ **35** began to arise at 1.40 and -1.53 ppm. The reaction was complete within 90 min. This observation, i.e., that the RER began at the same temperature (16 °C) according to NMR spectroscopy as the EPR resonance was observed (16.9 °C), supports the assumption that the EPR signal detected derives from a species which proceeds the RER. Another NMR spectrum recorded after 4 h at room temperature revealed that **36** had already started to decompose, which is in accordance with previous

observations.[160] A first assumption was that the decomposition product might be the NHC adduct of DBneop, formed by the reaction of **35a** with the solvent d_8-THF *via* deuterium atom abstraction. However, the signal at -0.54 ppm in the $^{11}B\{^1H\}$ NMR spectrum differs with those observed for the analogous NHC adducts of pinacolborane **26**-**28** (ca. 2.50 ppm).

In addition, the intermediate bis-NHC adduct $(Me_2Im^{Me})_2{\cdot}B_2neop_2$ **35** was structurally characterized by X-ray diffraction of single crystals obtained from a saturated mixture of B_2neop_2 with two equivalents of Me_2Im^{Me} in toluene at -30 °C (Figure 4.25).[175] Both boron atoms are sp^3-hybridized and tetrahedrally coordinated, with a B–B bond distance of 1.770(2) Å, i.e., slightly elongated compared to that observed for B_2neop_2 (1.712(3) Å).[160]

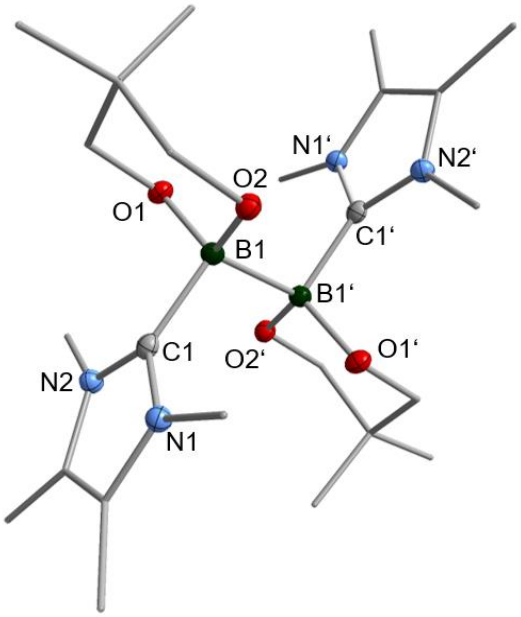

Figure 4.25 Molecular structure of $(Me_2Im^{Me})_2{\cdot}B_2neop_2$ **35**. Hydrogen atoms are omitted for clarity and the thermal ellipsoids are drawn at 50% probability. Selected bond lengths [Å] and angles [°]: B1−C1 1.662(2), B1−B1’ 1.770(2), B1−O1 1.482(1), B1−O2 1.486(1), C1-B1-O1 109.82(8), C1-B1-O2 110.13(8).

Following studies by Stephan *et al.* on the reactivity of a doubly base stabilized diborane(4) compound, which undergoes homolytic cleavage of the weakened B–B bond,[176] it was looked for further evidence for the *in situ* observed NHC–$BR_2^{\bullet}$ moiety **35a**. Therefore, it was tried to trap **35a** at temperatures below the onset of the RER as well as during the RER process with common radical scavengers including TEMPO, *N*-*tert*-butyl-α-phenylnitrone, diphenyl disulfide, and sulfur. However, these attempts

were unsuccessful, probably due to the extremely short lifetime of the radical **35a**, as the RER is an intramolecular reaction. Based on the work of Curran, Lacôte, and Lalevée with respect to radical polymerization reactions,[164-168] radical **35a** was then employed as an initiator for the polymerization of styrene.

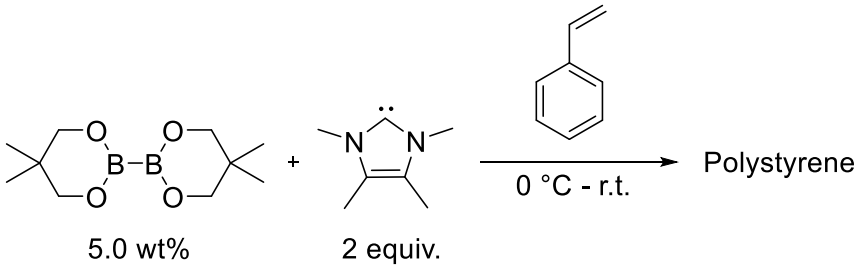

Scheme 4.20 Polymerization reaction of polystyrene initiated by radical **35a** formed from a mixture of B_2neop_2 and Me_2Im^{Me} in a 1:2 ratio.

Therefore, 5.0 wt% of the diborane(4) compound and two equivalents of the NHC were combined in precooled (0 °C) styrene, which was used as the solvent (Scheme 4.20). The reaction mixture was allowed to warm slowly to room temperature and was stirred for 16 h. Upon addition of an excess of methanol, a colorless precipitate formed, which was identified as polystyrene by gel permeation chromatography (GPC) analysis (Figure 4.26). The number-average molecular weight (M_n) of polystyrene was determined to 8540 Da, with a polydispersity index (PDI) of 1.74. The analogous reaction only using the diborane(4) compound (without the NHC) did not lead to the formation of polystyrene. Thus, the *in situ* observed radical **35a** was experimentally confirmed as it successfully initiated the radical polymerization reaction of styrene giving polystyrene with 90% conversion.

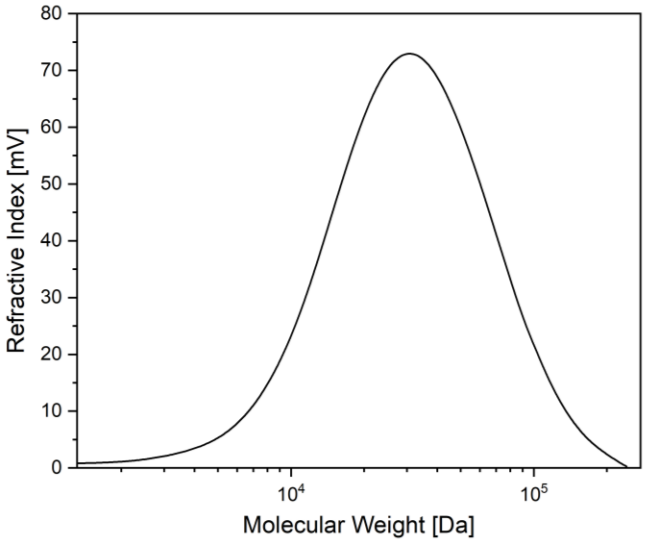

Figure 4.26 Gel permeation chromatography (GPC) analysis of polystyrene formed during the RER (detection of the polymer chains by refractive index detection).

Attempts to apply the boryl moiety **35a** in metal-free borylation reactions, suppressing the RER of **35** by providing appropriate substrates (e.g. aryl iodides), failed, and only the ring-expanded product **36** and the substrate employed were obtained.

As homolytic bond cleavage to yield the radical **35a** was observed for the bis-NHC adduct $(Me_2Im^{Me})_2{\cdot}B_2neop_2$ **35**, preliminary mechanistic investigations were initiated to determine how the observed boryl transfer from the mono-NHC adduct $Me_2Im^{Me}{\cdot}B_2pin_2$ **20** to the aryl halide proceeds, and whether boryl radicals might be involved. The C–C coupling with the solvent, as well as the observed hydrodehalogenation products were preliminary indications that the reaction might be radical in nature, including the generation of an aryl radical formed from the aryl halide.[177, 178]

Previous observations with 4-iodobenzotrifluoride **4-I** revealed that the boryl transfer proceeds slowly at room temperature (which is not the case for the other aryl iodides); thus, it was attempted to investigate this reaction by EPR spectroscopy. An EPR signal was detected; however, due to the very slow reaction progress at room temperature, with probably only a small number of radicals being present at any time, the signal was very weak and ill-defined. Thus, the determination of hyperfine couplings and, hence, insight into the nature of the radical was precluded. Nonetheless, the isotropic *g*-value of 2.006, together with the broad linewidth, suggest the presence of a boron-based radical (Figure 4.27).

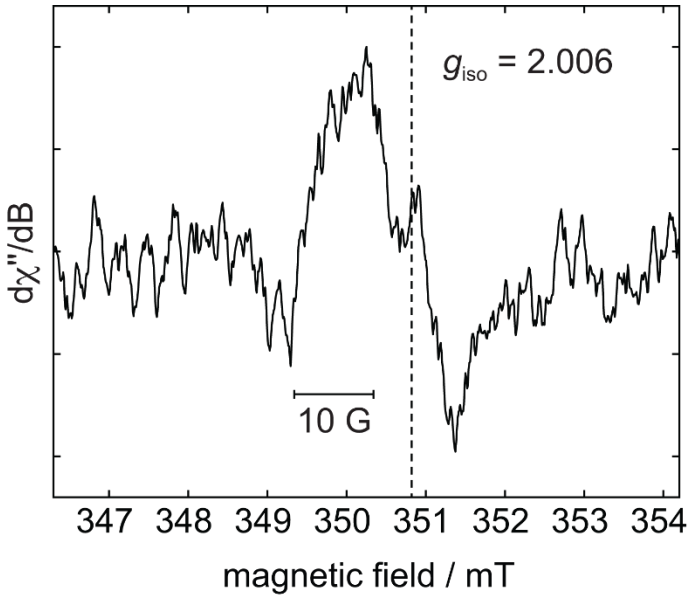

Figure 4.27 *In situ* EPR spectrum of the reaction of Me_2Im^{Me}·B_2pin_2 **20** with 4-iodobenzotrifluoride **4-I** in benzene at room temperature.

Furthermore, the standard boryl transfer reaction was performed in styrene (as the solvent) at 80 °C, to see whether the polymerization to polystyrene takes place, which would provide further experimental proof for the presence of radicals in the course of the reaction. GPC analysis (Figure 4.28) confirmed the formation of polystyrene; however, with a large number-average molecular weight (M_n) of 25870 Da and a PDI of 4.15, indicating very long and highly varying chain lengths, possibly due to a larger number of radicals formed in the reaction.

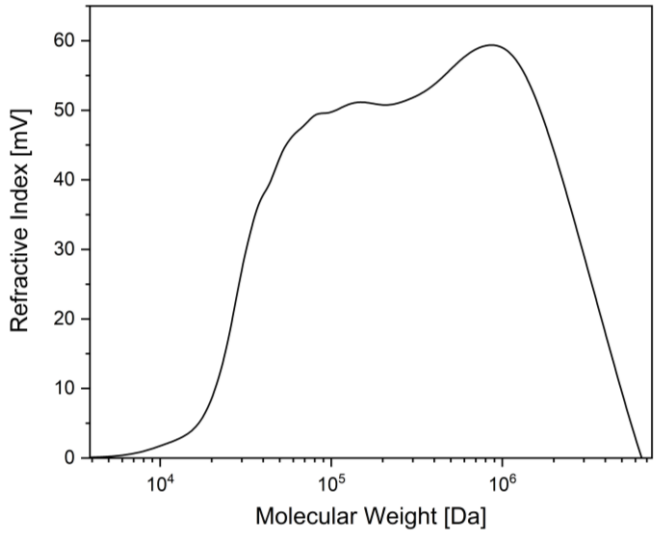

Figure 4.28 Gel permeation chromatography (GPC) analysis of polystyrene formed during the boryl transfer reaction using Me_2Im^{Me}·B_2pin_2 **20** and 4-iodobenzotrifluoride **4-I** (detection of the polymer chains by refractive index detection).

Next, the reaction mixture of the completed reaction of **20** with **4-I** as the aryl iodide, was analyzed by NMR and GC-MS. Besides the aryl boronic ester **4** and the C–C coupling product **4a**, of **4-I** with C_6D_6, residual free B_2pin_2 was detected in solution. The precipitate that was formed during the reaction was redissolved in chloroform and analyzed by GC-MS and NMR spectroscopy. While the GC-MS only showed traces of **4** and B_2pin_2, the ^1H NMR spectrum additionally revealed the formation of two other species (Figure 4.29), possibly of ionic nature, as they were not detectable by GC-MS.

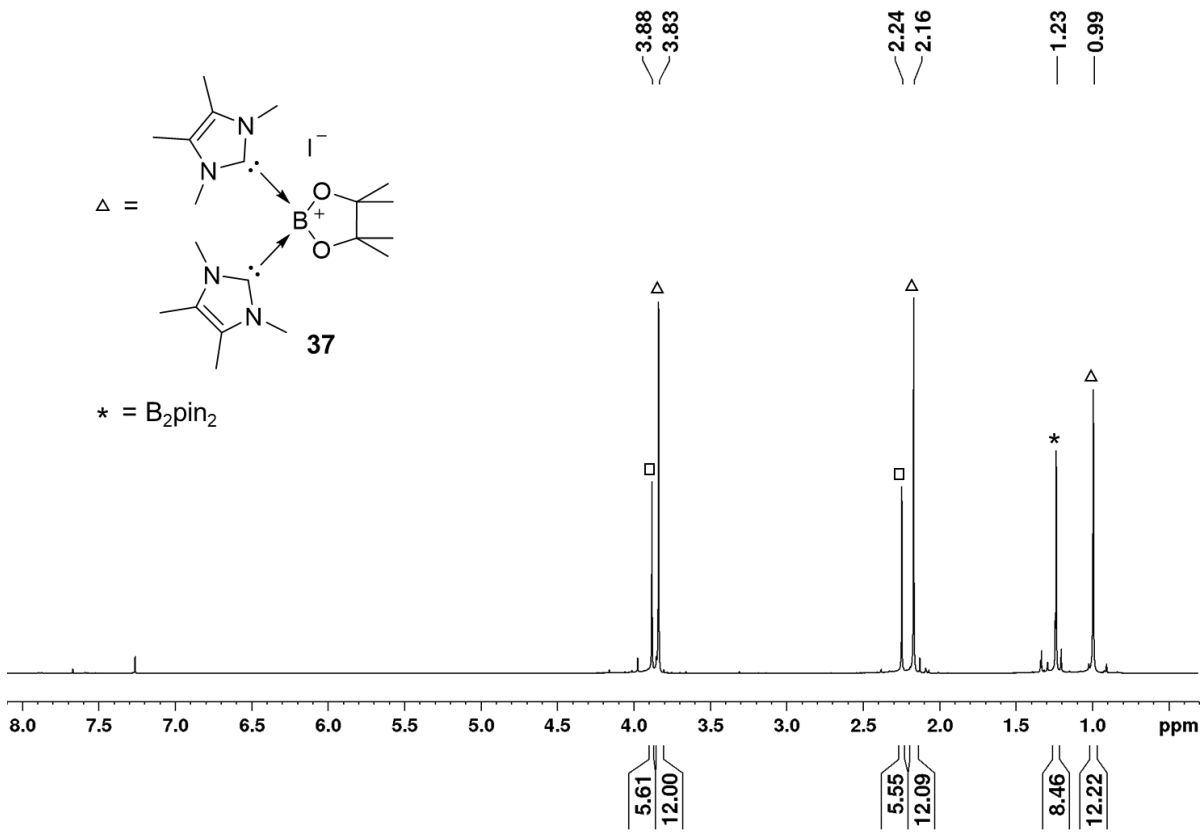

Figure 4.29 ^1H NMR spectrum (recorded in $CDCl_3$, 400 MHz) of the residue of the reaction mixture showing the boronium cation **37** (triangle), B_2pin_2 (asterisk), and an unknown species (square).

In the corresponding $^{11}B\{^1H\}$ NMR spectrum, besides B_2pin_2, only one significant signal was observed with a chemical shift of 1.77 ppm (Figure 4.30) which, together with HRMS, and X-ray diffraction analysis (Figure 4.31) was assigned to the boronium cation $[(Me_2Im^{Me})_2{\cdot}Bpin]^+$ **37** with iodide as the counterion. This compound might demonstrate the fate of the second boryl moiety in the boryl transfer reaction based on the mono-NHC adduct **20**. The amount of **37** formed is, according to the amount of isolated residue and estimation of the ratio (of **37** to the unknown species) in the ^1H

NMR spectrum, on an appropriate scale for being formed stoichiometrically during the generation of the borylated arene.

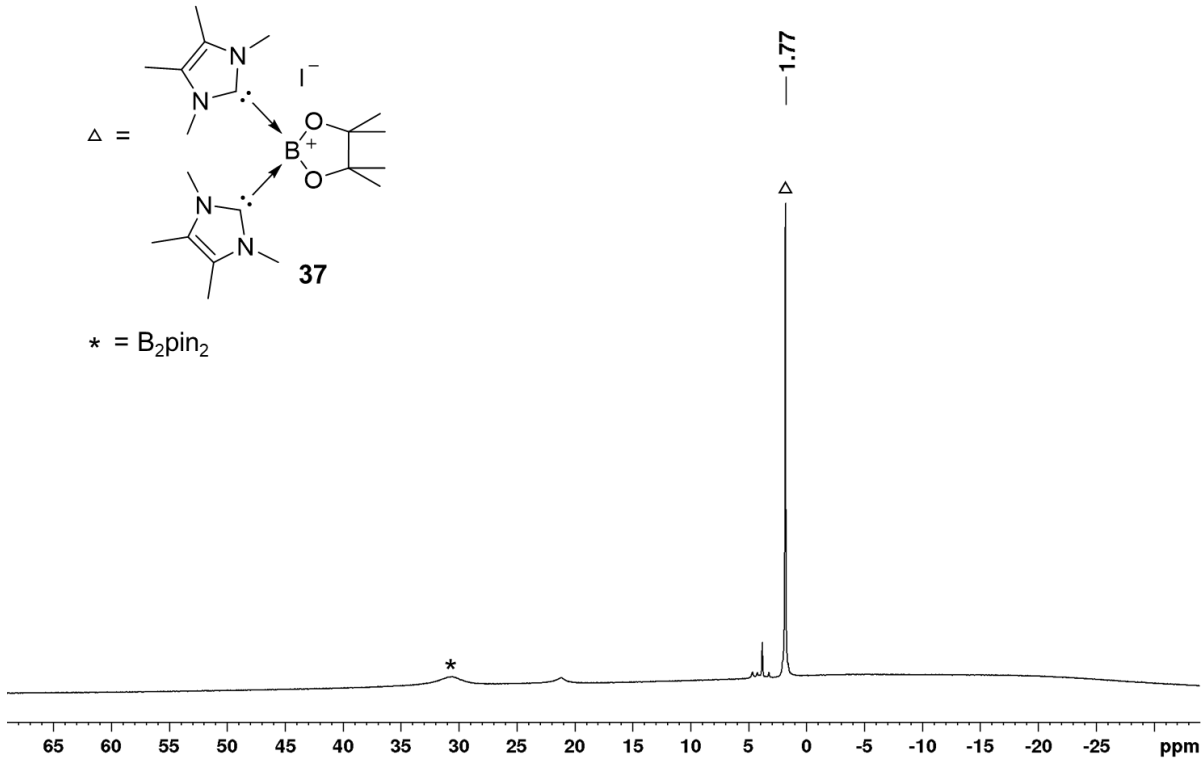

Figure 4.30 $^{11}B\{^{1}H\}$ NMR spectrum (recorded in $CDCl_3$, 128 MHz) of the residue of the reaction mixture showing the boronium cation **37** (triangle) and B_2pin_2 (asterisk).

The molecular structure of $[(Me_2Im^{Me})_2{\cdot}Bpin]^+I^-$ **37** is shown in Figure 4.31. The boron atom is four-coordinate bound to the pinacolato unit and the two NHCs as *σ*-donating ligands, with a B–C1 bond distance of 1.663(4) Å. The data obtained match those previously reported for boronium ions.[179-181]

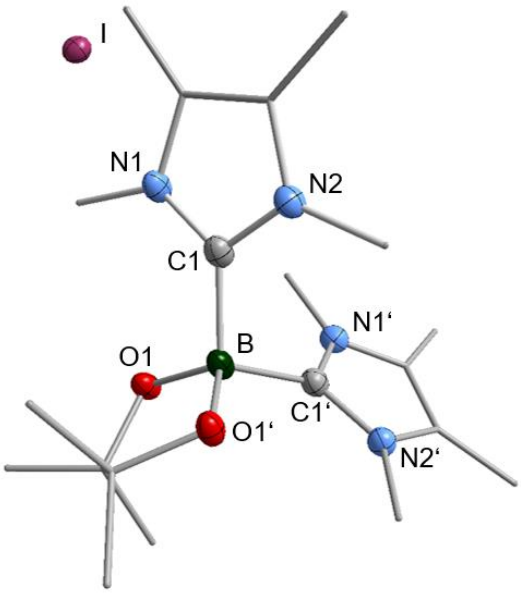

Figure 4.31 Molecular structure of $[(Me_2Im^{Me})_2{\cdot}Bpin]^+I^-$ **37**. Hydrogen atoms are omitted for clarity and the thermal ellipsoids are drawn at 50% probability. Selected bond lengths [Å] and angles [°]: B−C1 1.663(4), B−O1 1.471(3), C1-B-O1 110.80(12), C1-B-O1’ 111.23(12), C1-B1-C1’ 106.9(3).

Next, the role of the NHC was studied (Table 4.3) by running the reaction with only B_2pin_2 and 4-iodotoluene **5-I** (1:1 ratio) under the standard conditions. As expected, after 16 h at 80 °C, only starting material was detected, which excludes the possibility of radicals generated by the diborane(4) compound and traces of oxygen.[182]

Table 4.3 Influence of the amount of NHC (Me_2Im^{Me}) on the outcome of the borylation reaction of 4-iodotoluene **5-I** in C_6D_6 at 80 °C.

Amount of NHC	Amount of B_2pin_2	Conversion of **5-I**
-	1.0 equivalent	-
0.5 equivalent	1.0 equivalent	12%[a]
0.5 equivalent	2.5 equivalents	12%[a]
1.0 equivalent	2.5 equivalents	30%[a]
2.5 equivalents	2.5 equivalents	97% (**5**:**5a** = 75/22)

[a] Ratio **5**:**5a** could not be determined as the amount of formed **5a** was too small to be detected by ^{1}H NMR spectroscopy.

When 0.5 equivalents of NHC were added, ca. 12% conversion was obtained. Adding another 1.5 equivalents of B_2pin_2 to the reaction mixture to accommodate for the need of the 2.5 equivalents in the standard reaction, no reaction progress was observed. The subsequent addition of another 0.5 equivalents of NHC resulted in 30% conversion, revealing that the NHC does not serve as a catalyst and is required in stoichiometric amounts. The need for 2.5 equivalents of B_2pin_2 is also required, as with smaller amounts, more of the C–C coupling side product **5a** is generated. In general, the reaction also proceeds when B_2pin_2 and Me_2Im^{Me} are added separately to the reaction mixture, but shows slightly increased conversion when the pre-prepared mono-NHC adduct Me_2Im^{Me}·B_2pin_2 **20** is employed.

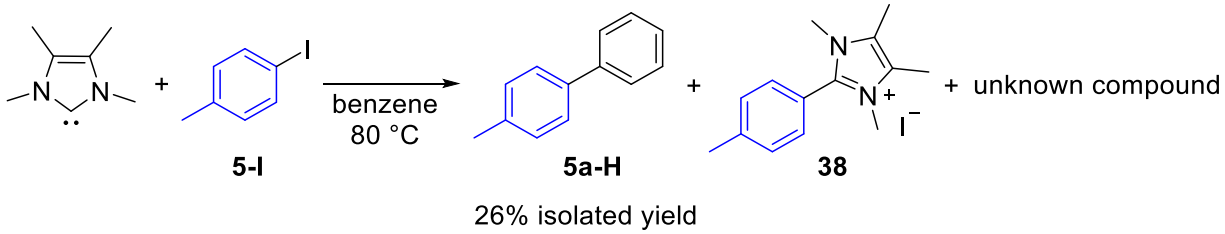

Scheme 4.21 Reaction of the free NHC Me_2Im^{Me} with 4-iodotoluene **5-I** in benzene at 80 °C forming the C–C coupling product with the solvent **5a-H**, the imidazolium salt [4-CH_3-C_6H_4-Me_2Im^{Me}]$^+I^-$ **38**, and an unknown comound.

Notably, the reaction of **5-I** with stoichiometric amounts of the free NHC in the absence of B_2pin_2 in benzene at 80 °C also generated the C–C coupling product **5a-H** in 26% isolated yield (Scheme 4.21). Figure 4.32 shows the *in situ* ^{1}H NMR spectra of the analogous reaction in C_6D_6 after 1 h at room temperature and after 2 h at 80 °C, revealing new signals arising from the C–C coupling product **5a** of the aryl iodide **5-I** with the solvent.

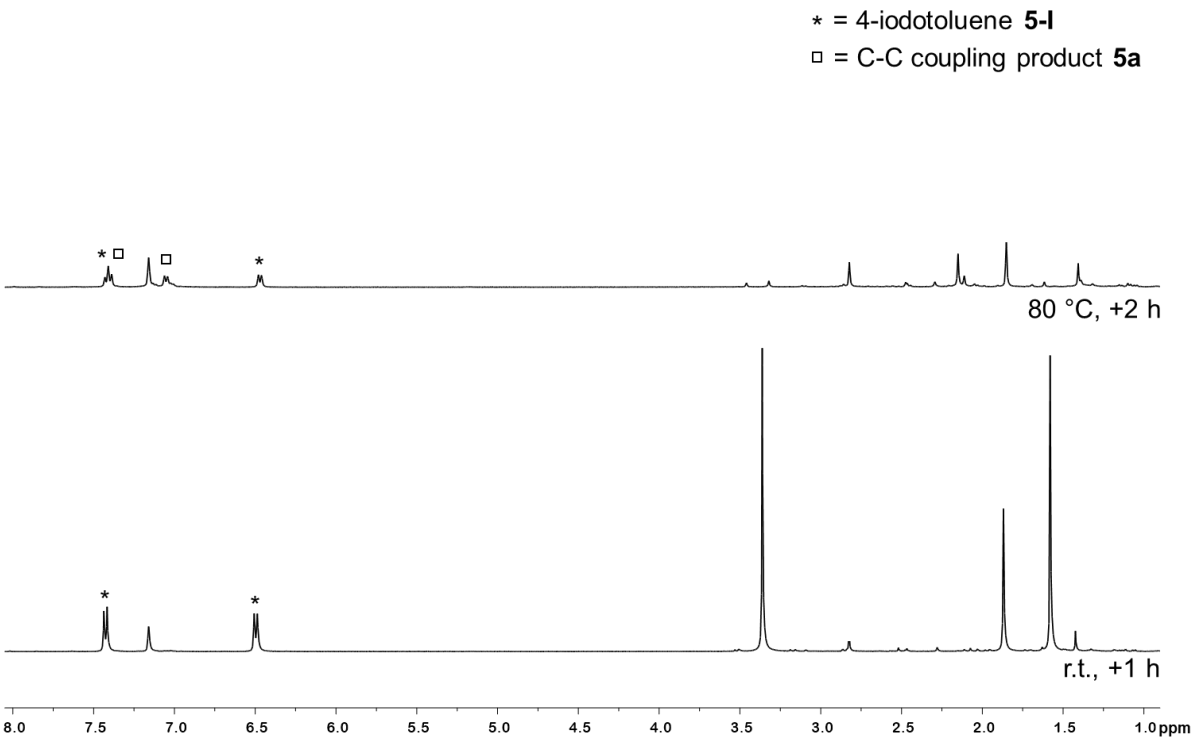

Figure 4.32 *In situ* ^{1}H NMR spectra (400 MHz) of the stoichiometric reaction of 4-iodotoluene **5-I** and Me_2Im^{Me} in C_6D_6 after 1 h at room temperature (bottom) and after 2 h at 80 °C (top). Asterisk: 4-iodotoluene **5-I**. Square: C–C coupling product **5a**.

The precipitate that was formed during the reaction, was re-dissolved in chloroform and is suggested to contain the imidazolium salt $[4\text{-}CH_3\text{-}C_6H_4\text{-}Me_2Im^{Me}]^+I^-$ **38**, indicated by GC-MS (detected as m/z = 200 $[M\text{-}CH_3I]^+$ after thermal decomposition in the injector), HRMS and NMR spectroscopy. Besides the imidazolium salt, another species is formed as a side product (Scheme 4.21). The ^{1}H NMR spectrum is shown in Figure 4.33. Compound **38** was not detected in the residue of the reaction mixture of the analogous reaction in the presence of B_2pin_2.

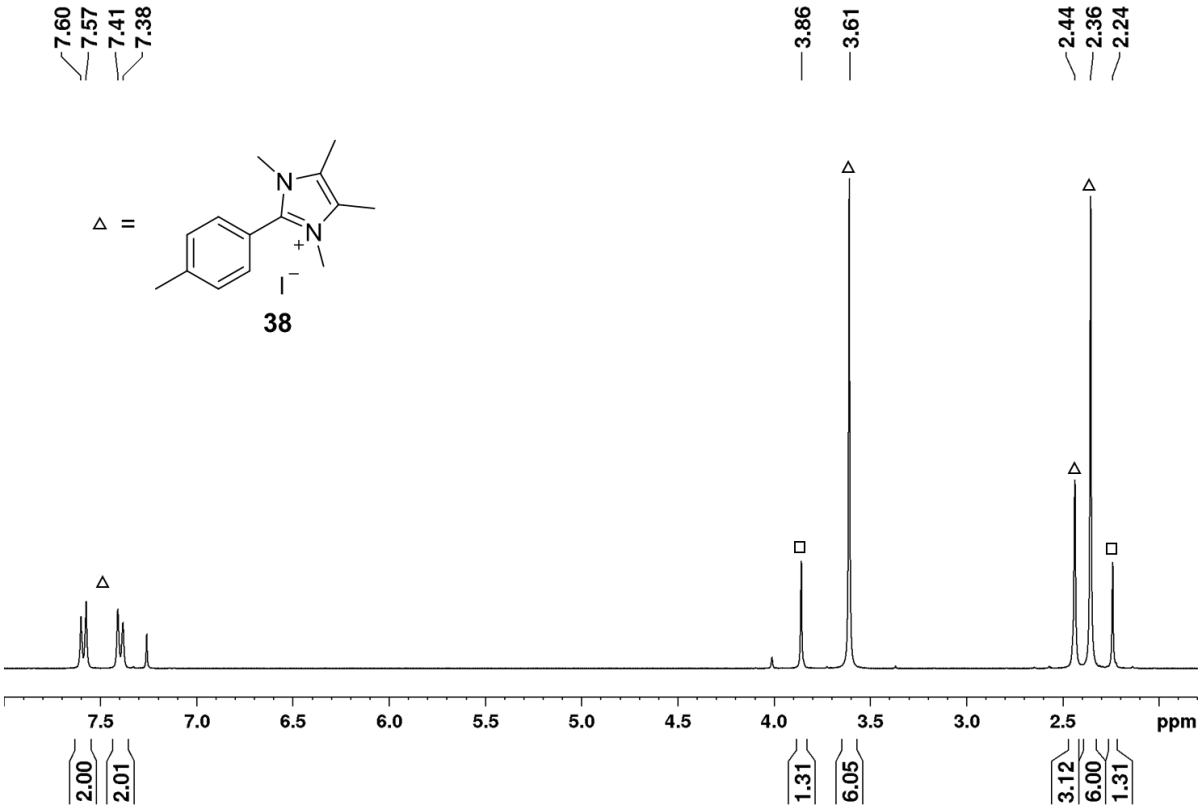

Figure 4.33 ^{1}H NMR spectrum (recorded in $CDCl_3$, 400 MHz) of the residue formed in the reaction of stoichiometric amounts of the free NHC with 4-iodotoluene **5-I** showing the imidazolium salt [4-CH_3-C_6H_4-Me_2Im^{Me}]$^{+}$I^{-} **38** and the unknown species (square).

The signals of the second species detected in the ^{1}H NMR spectrum at a chemical shift of 2.24 and 3.86 ppm (square), match those set of signals found in the ^{1}H NMR spectrum recorded of the residue formed during the boryl transfer reaction (2.24 and 3.88 ppm; cf. Figure 4.29). Thus, as this compound is also generated in the absence of boron and does not show any resonances in the aromatic region, it presumably must be formed from Me_2Im^{Me}. The most obvious presumption is the signals arising from the imdazolium salt [$Me_2Im^{Me}H$]$^{+}$I^{-}, generated from protonation of the free NHC during the coupling of **5-I** with benzene, as two singlets are detected in the expected region for the CH_3 protons of the backbone (2.24 ppm) and the NCH_3 protons (3.86 ppm) in a 1:1 ratio. However, no signal is detected for the C*H* proton at the former carbene carbon atom, and comparison of the signals with those of previously prepared [$Me_2Im^{Me}H$]$^{+}$I^{-} (recorded in $CDCl_3$) also disproves this assumption (2.20 and 3.81 ppm). The possibility of residual free NHC in the residue reacting with $CDCl_3$ forming the analogous imidazolium salt [$Me_2Im^{Me}D$]$^{+}$Cl^{-} was also excluded by a control experiment (2.14 and 3.78 ppm).

As in this test reaction with only the NHC employed, the C–C coupling of **5-I** with benzene was also observed, the NHC itself might initiate the formation of an aryl radical. A control experiment was performed by heating **5-I** in C_6D_6, which verified that only starting material is detectable after 16 h and no formation of the C–C coupling product **5a** was observed.

To gain insight into the redox properties of the reactants, cyclic voltammograms (CV) of 4-iodotoluene **5-I**, Me_2Im^{Me}, and $Me_2Im^{Me}{\cdot}B_2pin_2$ **20** were measured in THF. The redox potentials are given versus Ag/Ag^+ instead of Fc/Fc^+, as the free NHC reacts with Fc^+ and THF resulting in the corresponding imidazolium salt.[183] For **5-I**, an irreversible reduction was found at E_c = -2.63 V, showing a high electrochemical stability with respect to the acceptance of an electron (Figure 4.34). An irreversible oxidation for Me_2Im^{Me} was detected at E_a = -1.17 V and an irreversible reduction at E_c = -2.99 V. Thus, the formation of an aryl radical by reduction of the aryl iodide **5-I** by electron transfer from the free NHC can be excluded by comparing the respective potentials. The CV of the mono-NHC adduct **20** reveals an irreversible oxidation at E_a = -1.17 V, and a second one at E_a = -0.08 V. The former potential is identical with that observed for the free NHC. DFT calculations by the groups of Marder and Lin[146] showed that during the exchange of the NHC between the two boron atoms in a mono-NHC adduct, no transition state could be located for an intramolecular process. Instead, a dissociation-reassociation mechanism was suggested by their theoretical studies. Thus, it is suggested that some Me_2Im^{Me} dissociates from B_2pin_2 in **20**.

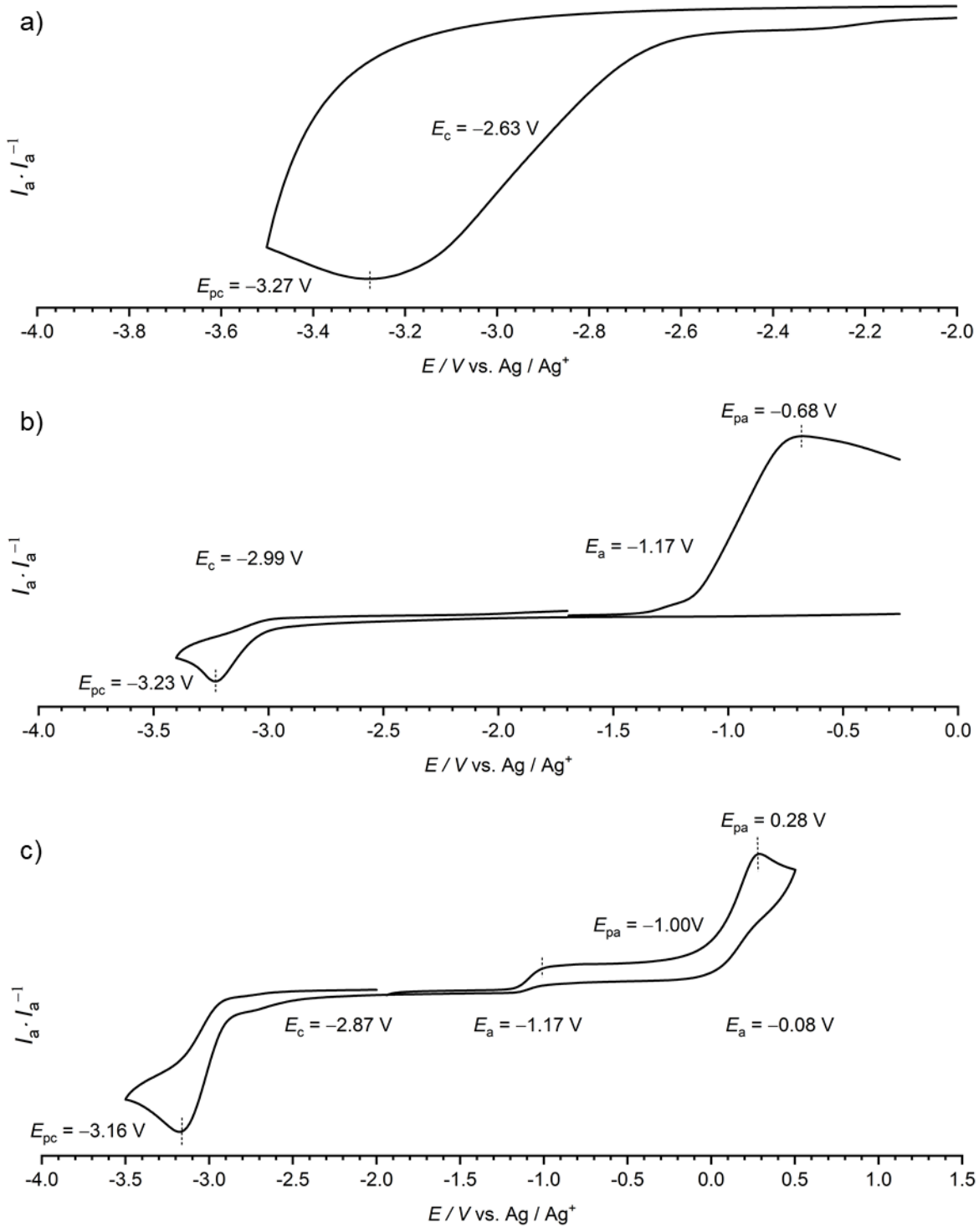

Figure 4.34 Cyclic voltammograms of a) 4-iodotoluene **5-I**, b) Me_2Im^{Me}, and c) $Me_2Im^{Me}{\cdot}B_2pin_2$ **20**.

Performing the reaction shown in Scheme 4.21 in the presence of stoichiometric amounts of the radical scavenger TEMPO, trace of amounts of the coupling product aryl–TEMPO were detected by GC-MS, which provides evidence for the existence of aryl radicals.

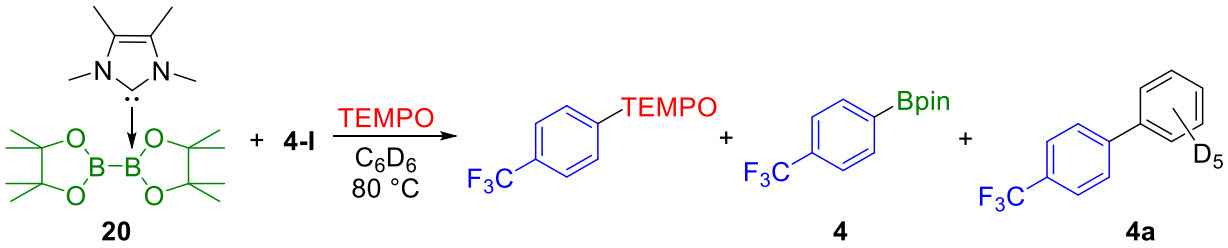

Scheme 4.22 Boryl transfer reaction, using **20** and 4-iodobenzotrifluoride **4-I**, in the presence of TEMPO in C_6D_6 at 80 °C.

The same coupling product between the aryl radical and TEMPO was observed in larger amounts by running the standard boryl transfer reaction using Me_2Im^{Me}·B_2pin_2 **20** and 4-iodobenzotrifluoride **4-I** in the presence of TEMPO (Scheme 4.22); however, there was no evidence for trapping of a boryl moiety. The GC-MS total ion chromatogram (TIC) of the reaction mixture and the mass spectrum of the coupling product aryl–TEMPO are shown in Figure 4.35.

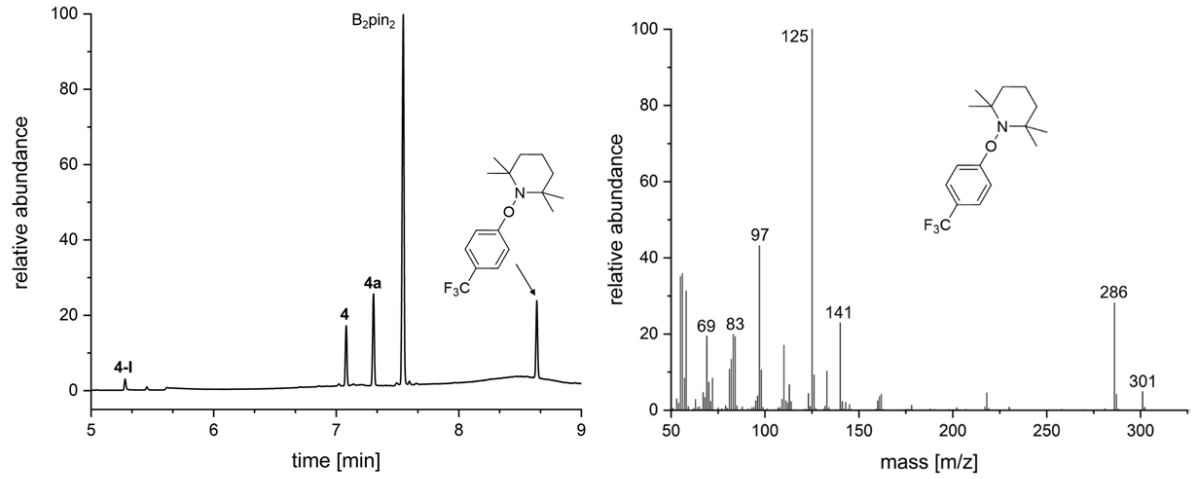

Figure 4.35 Left: GC-MS TIC of the reaction mixture of **20** and 4-iodobenzotrifluoride **4-I**, in the presence of TEMPO in C_6D_6 after 16 h at 80 °C. Right: Mass spectrum of the coupling product aryl–TEMPO.

Thus, for the bis-NHC adduct $(Me_2Im^{Me})_2$·B_2neop_2 **35**, in course of the RER, evidence for a boryl radical of the type NHC–Bneop$^{\bullet}$ **35a** was found, which suggests homolytic B–B bond cleavage as a key step in the RER. The established boryl transfer reaction based on the mono-NHC adduct Me_2Im^{Me}·B_2pin_2 **20** is also presumed to proceed *via* a radical pathway, which was experimentally proven by the radical polymerization of styrene, and the trapping of an aryl radical by TEMPO. However, the only indication

for boron-based radicals in this reaction is an ill-defined EPR signal, which cannot be assigned beyond doubt.

An increasing number of transition metal-free borylation reactions for diboration of unsaturated substrates reported in the literature,[29, 77, 147] proceed *via* a nucleophilic boryl moiety, which is generated when one of the boron atoms is coordinated to a strong Lewis base. Unlike this heterolysis, the homolytic cleavage of the B–B bond is more challenging, due to the relatively high bond dissociation energy of diborane(4) compounds. Recently, new borylation methodologies have been reported, wherein the boron reagent apparently participates in free radical coupling *via* the homolytic cleavage of the boron–boron bond.[77, 184-186] To date, there are mainly two ways to realize this homolytic cleavage, i.e., pyridine induced or by irradiation. Initially, the groups of Suginome and Ohmura, reported the transition metal-free diboration of 1,4-dihydropyrazine derivatives (Scheme 4.23) and 4,4'-bipyridine, respectively, with only B_2pin_2 at elevated temperatures.[187, 188]

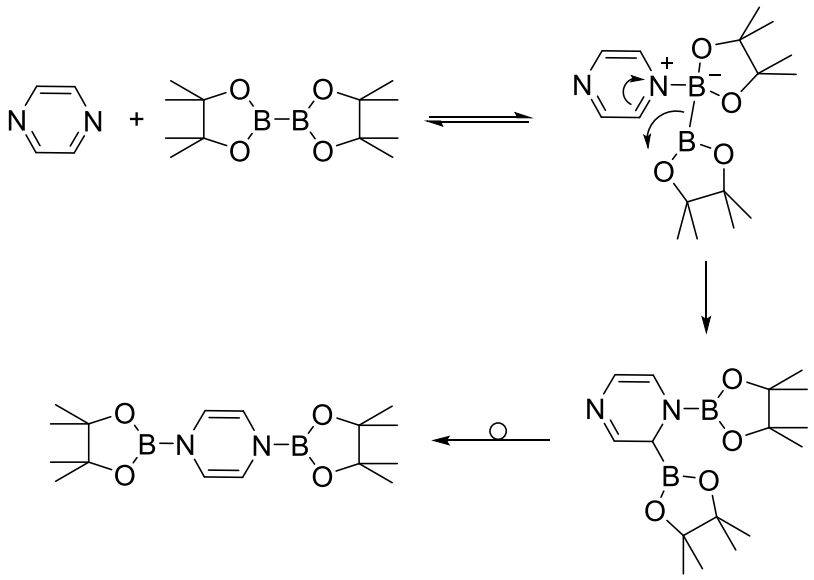

Scheme 4.23 A proposed mechanism for the metal-free borylation of pyrazine.[187]

The group proposed a mechanism proceeding *via* the initial coordination of pyrazine to one of the boron atoms in B_2pin_2 forming an intermediate with a four-coordinate boron atom, in which the second Bpin-moiety and the C2 carbon atom of the pyrazine become nucleophilic and electrophilic, respectively. *Via* an intramolecular nucleophilic attack of the Bpin moiety at the C2 carbon atom, the 1,2-borylated pyrazine is formed, followed by a rearrangement to the final product.[187] Even though they proposed that

the mechanism proceeded *via* a nucleophilic pathway, subsequent reports reveal that, a radical process with a homolytic cleavage of the B–B bond cannot be excluded in this case. In 2016, Li *et al.* reported the homolytic cleavage of the B–B bond of B_2pin_2 *via* the coordination of 4-cyanopyridine to both boron atoms, generating pyridine-stabilized boryl radicals (Scheme 4.24), which were employed for the synthesis of various organo boronates.[189-191] The group explained the stability of this boryl radical by the captodative effect, which implies that 4-cyanopyridine acts as both a *σ*-electron donor and *π*-acceptor.

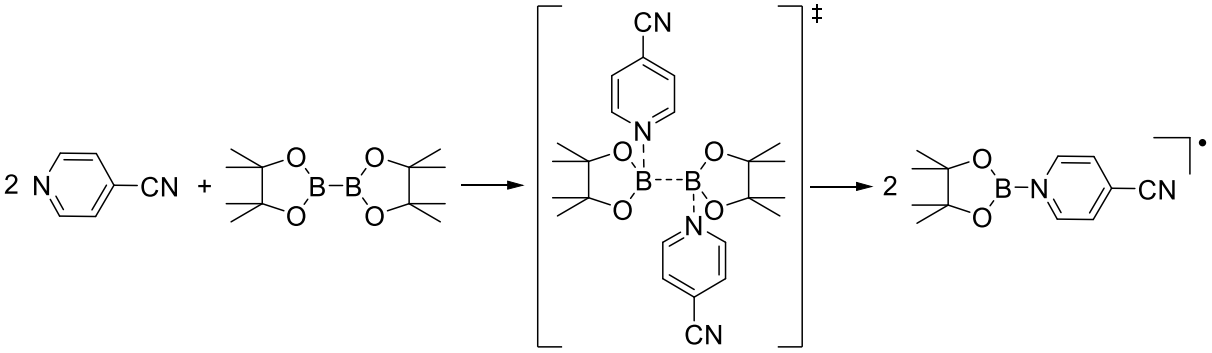

Scheme 4.24 Homolytic B**–**B bond cleavage in B_2pin_2 by 4-cyanopyridine forming a captodatively stabilized boryl radical.[189]

The hydroboration of alkenes using B_2pin_2 and catalytic amounts of 4-cyanopyridine was demonstrated by the group of Cai, who also proposed that the reaction proceeded *via* the formation of a pyridine-stabilized boryl radical.[192] Jiao *et al.* described the borylation of various aryl halides with B_2pin_2 using potassium methoxide in the presence of catalytic amounts of 4-phenylpyridine, proposing the *in situ* generation of super electron donors (SED) based on boryl-pyridine species (Scheme 4.25).[193, 194]

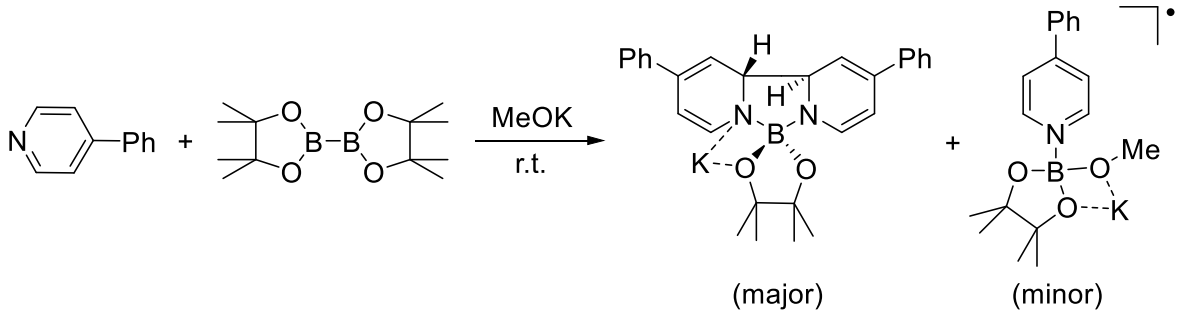

Scheme 4.25 Pyridine- and boron containing complexes as SEDs.[194]

Contrary to the initial assumption of a homolytic B–B bond cleavage,[193] DFT studies demonstrate that the SEDs are generated by heterolytic cleavage of the B–B bond in B_2pin_2 *via* coordination of the boron atoms by pyridine and methoxide.[194] The group proposed a mechanism for the radical borylation proceeding *via* the initial formation of the SEDs (Scheme 4.25), which generate an aryl radical by SET. The aryl radical further reacts with B_2pin_2 forming the aryl boronate (Scheme 4.26).

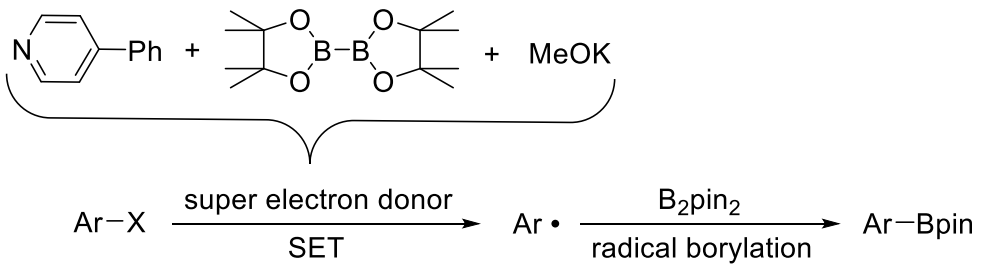

Scheme 4.26 Proposed mechanism for the borylation of aryl halides *via* the formation of SEDs.[194]

Later, the same group developed an efficient method for the borylation of unactivated aryl chlorides by photoactivation of the *in situ* generated SED.[195] In 2017, the groups of Pinet and Pucheault reported the stoichiometric borylation of various aryl iodides, mediated by an *in situ* formed fluoride sp^2-sp^3 diborane adduct **4.27-I** from B_2pin_2 and CsF.[196] The anionic adduct **4.27-I**, which is analogous to the structurally characterized $[B_2pin_2(F)][NMe_4]$,[29] is proposed to reduce the aryl iodide *via* an SET, forming FBpin and a boryl radical **4.27-II**, which is stabilized by pyridine, as well as the radical anion **4.27-III**, which further reacts to give an aryl radical. The desired aryl boronic ester is generated by reaction of the aryl radical with the pyridine-stabilized boryl radical **4.27-II**, or with B_2pin_2 along with the regeneration of the boryl radical **4.27-II**.

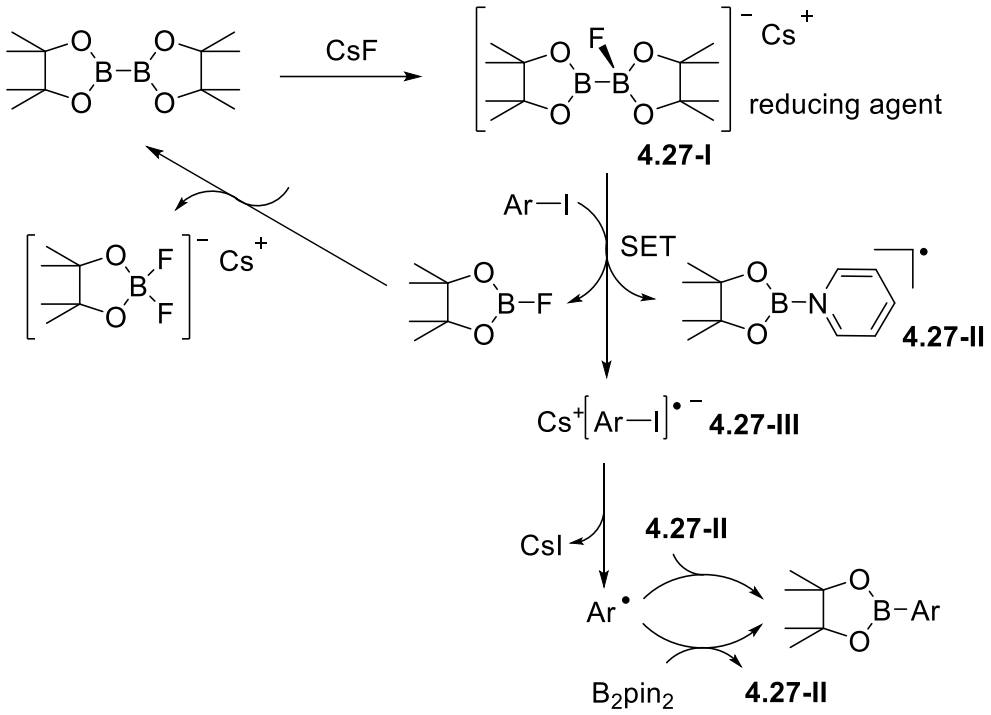

Scheme 4.27 Proposed mechanism for the borylation of aryl iodides mediated by an *in situ* formed anionic sp^2–sp^3 diborane from B_2pin_2 and CsF in the presence of pyridine.[196]

Furthermore, decarboxylative borylation of aryl and alkenyl carboxylic acids *via* a radical coupling mechanism was reported by Fu and co-workers.[197] An *in situ* formed three component bis adduct **4.28-I** between B_2pin_2, the carboxylic acid substrate, and a pyridine derivative is assumed to undergo homolytic B–B bond cleavage by an intramolecular SET, generating a carboxylate radical **4.28-II** and a pyridine-stabilized boryl radical **4.28-III.** The latter further reacts with an aryl radical formed from **4.28-II** after decarboxylation (Scheme 4.28).

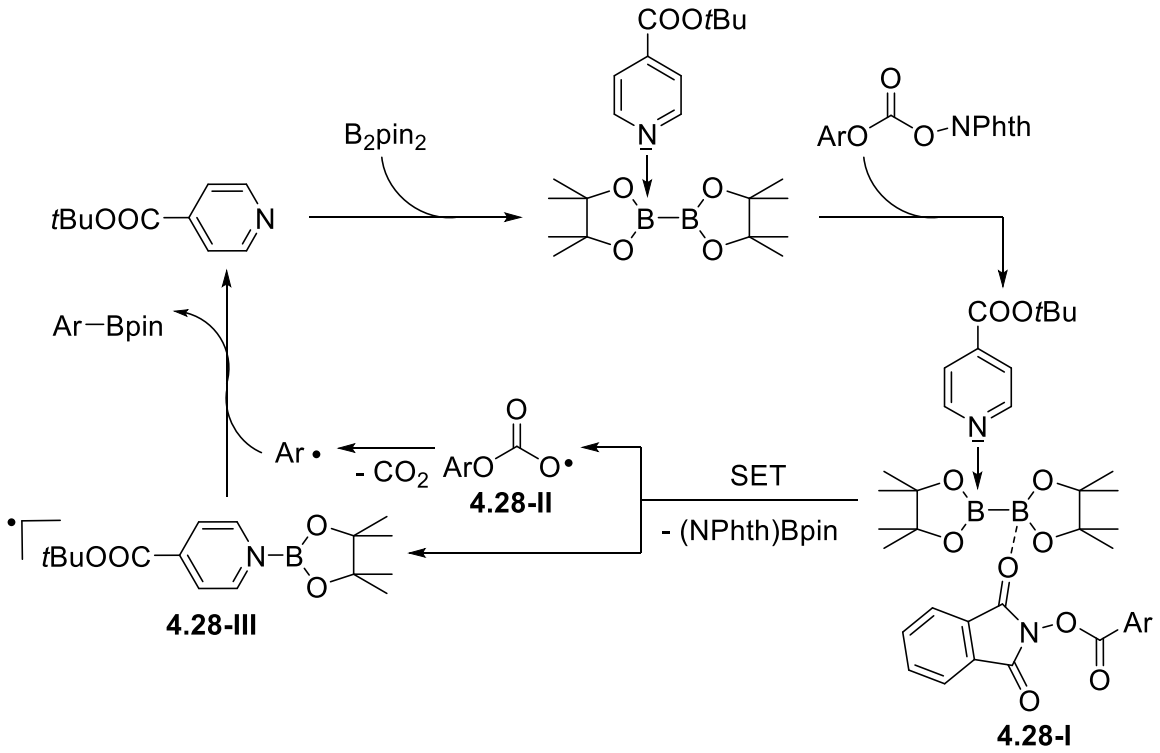

Scheme 4.28 Proposed mechanism for the decarboxylative borylation of aryl and alkenyl carboxylic acids.[197]

Ogawa *et al.* reported the transformation of terminal alkynes to 1,2-diborylalkenes with B_2pin_2 under irradiation by a high pressure mercury lamp in the presence of catalytic amounts of diphenyl disulfide and triphenylphosphine, respectively.[198, 199] The mechanism is not yet clear, but boron-centered radicals are proposed to be formed from B_2pin_2 and PPh_3 under irradiation.[199] In 2018, Studer and co-workers introduced a radical borylation of alkyl and aryl iodides initiated by a photoinduced C–I bond homolysis.[200] The alkyl/aryl radical formed presumably adds to B_2cat_2 and, along with coordinating DMF, the weakened B–B bond homolyzes giving the alkyl/aryl boronic ester and a DMF-stabilized boryl radical (Scheme 4.29).[200, 201]

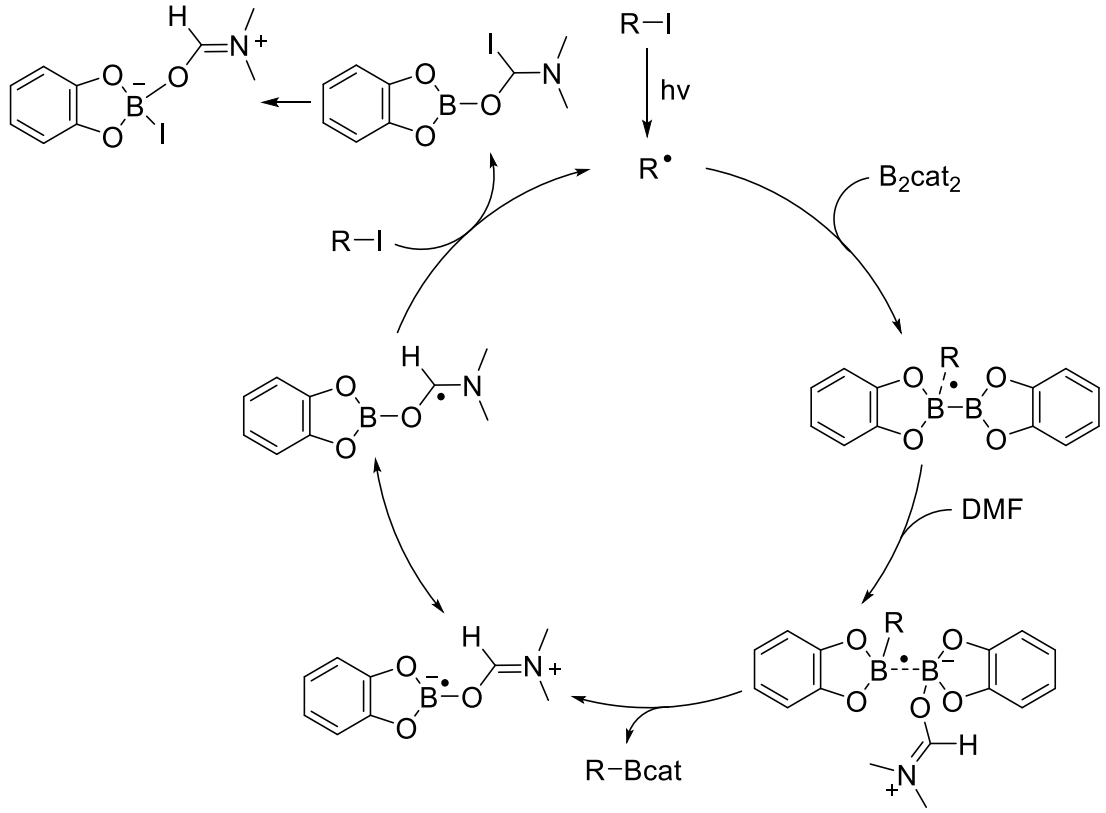

Scheme 4.29 Proposed mechanism for the photoinduced radical borylation of alkyl and aryl iodides *via* a DMF-stabilized boryl radical. [200]

Typical methods for stabilizing radical species involve delocalization of the unpaired electron and/or utilizing sterically hindered groups to prevent dimerization.[202] With respect to boron-centered radicals, the long known anionic species of the type $BR_3^{\bullet -}$ are generated by occupying the vacant p-orbital of an electron deficient borane with a single electron,[202-204] whereas the neutral analogue requires a Lewis base (L) coordinated to the boron center giving an $L–BR_2^{\bullet}$ adduct. In recent years, the electrophilicity of *N*-heterocyclic carbenes (NHCs) has been employed for stabilizing such boron centered radicals. Offering an empty p-orbital, the NHC is able to engage in π-backbonding interactions which delocalize electron density.[205, 206]

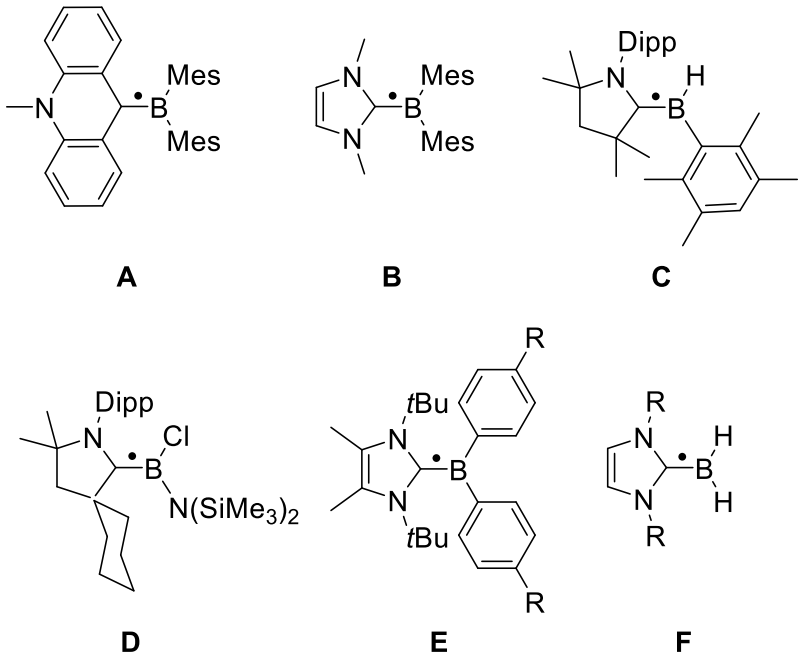

Figure 4.36 Selected neutral boryl radicals stabilized by carbenes.[162, 207-210]

The acridinyl radical **A**, reported by Gabbaï *et al.* in 2007, can be considered as the first structurally characterized carbene-stabilized neutral boryl radical (Figure 4.36).[207] However, in this example, the unpaired electron is largely delocalized over the acridinyl fragment with very little contribution from the boron atom, as indicated by EPR spectroscopy. The same group observed, but could not isolate, radical **B** by introducing an imidazolin-2-ylidene as a more nucleophilic NHC (Figure 4.36), *via* reversible reduction of an NHC-stabilized borenium cation.[208] Radical **B** reveals a higher boron radical character and significant localization of the unpaired electron in a $(B–C_{NHC})_{\pi}$-orbital. In 2014, Braunschweig and co-workers isolated the $cAAC^{Me}$-stabilized boryl radical **C** by reduction of the corresponding haloborane adduct.[209] EPR and DFT data indicate that the spin density is delocalized over the strong *π*-accepting cAAC ligand. In the same year, the similar $cAAC^{Cy}$-stabilized aminoboryl radical **D**, generated analogously by reduction of the corresponding adduct, was introduced by the groups of Bertrand and Stephan.[211] Recently, Tamm *et al.* reported the NHC-stabilized boryl radical **E**, by reduction of the corresponding borenium cation. Radical **E** was structurally confirmed and characterized by EPR spectroscopy, revealing that the unpaired electron is almost exclusively localized on the $B(Ar)_2$ moiety.[210] The generation of related radicals of the type $NHC–BH_2^{\bullet}$ **F**, formed from the borane adduct $NHC{\cdot}BH_3$ by homolytic B–H bond cleavage, is facilitated by the relatively small bond dissociation energy (80-88 kcal mol^{-1})[162, 163] in the precursor. This bond cleavage can

be realized by laser flash photolysis with UV irradiation as well as in the presence of radical initiators such as di-*tert*-butylperoxide (DTBP) or azobisisobutyronitrile (AIBN). However, these radicals are transient and cannot be isolated. EPR and corroborating theoretical studies reveal that radicals of the type **F** are planar, with the spin density delocalized over the NHC ligand and the boron center.[162] The groups of Curran, Lacôte, and Lalevée have extensively studied this class of compounds and applied them as efficient co-initiators in radical photopolymerization reactions as well as radical reductions of halides and xanthates.[164-168, 212-215] The same groups generated the corresponding aryl boron radicals by analogously abstracting hydrogen atoms from NHC·BH_2Ar compounds *via* homolytic B–H bond cleavage.[215] The groups of Curran, Taniguchi, and Wang achieved various borylative radical cyclization reactions[216-219] and borylation of polyfluoroarenes,[220] as well as radical hydroboration of alkenes,[221] also utilizing NHC·BH_3 with *in situ* formation of the NHC-boryl radical **F** by hydrogen atom abstraction using di-*tert*-butyl hyponitrile and AIBN, respectively.

Most of the transition metal-free borylation reactions which are proposed to proceed *via* a radical pathway, involve stabilization of the boryl radical by a pyridine ligand.[189-197] However, there are several examples of boryl radicals stabilized by NHCs,[162, 163, 208, 210] of which **E** was even isolable.[210] In particular, radicals of the type NHC–$BH_2^{\bullet}$ **F** reported by the groups of Curran, Lacôte, and Lalevée,[162, 163] are closely related to the observed radical Me_2Im^{Me}–Bneop$^{\bullet}$ **35a**. However, radicals of type **F** and **35a** are only transient, due to the lack of sufficient stabilization *via* delocalization of the unpaired electron by, for example, aromatic substituents in the molecule or by the strong *π*-accepting cAAC ligand, as it is the case for the boryl radicals **A**, **C**-**E** introduced above (Figure 4.36). Thus, for the established boryl transfer reaction to aryl halides based on Me_2Im^{Me}·B_2pin_2 **20**, a mechanism with the involvement of a transient NHC-stabilized boryl radical can be considered.

A preliminary proposed mechanism, for the boryl transfer reaction, is depicted in Scheme 4.30. Presumably, a very small amount of the bis-NHC adduct $(Me_2Im^{Me})_2$·B_2pin_2 **4.30-I** is formed in solution *via* a dismutation process of the mono-NHC adduct **20**, as observed for mpy·B_2cat_2[148, 149] and pyridine·B_2cat_2 **18** (cf. Scheme 4.1). However, attempts to isolate $(Me_2Im^{Me})_2$·B_2pin_2 **4.30-I** from the reaction of B_2pin_2 with two equivalents of Me_2Im^{Me} were unsuccessful and led to undefined decomposition (with no indications for a RER as observed for $(Me_2Im^{Me})_2$·B_2neop_2 **35**). This observation suggests this type of proposed bis-NHC adduct to be highly reactive,

offering a very activated B–B bond, and that it is crucial for a controlled reaction process that only very small amounts of **4.30-I** are formed in an equilibrium. Thus, the proposed radical pathway starts with the homolytic cleavage of the weakened B–B bond of intermediate **4.30-I** to give two NHC-stabilized radicals of the type NHC–Bpin• **4.30-II**. This proposed radical **4.30-II** is closely related to the observed radical **35a** and would be formed analogously. Furthermore, it is related to the NHC-stabilized borane radicals reported by Curran, Lacôte, and Lalevée.[162, 163] Next, one boryl radical moiety **4.30-II** (green) reacts with the aryl iodide to give intermediate **4.30-III** and free Me_2Im^{Me}. The aryl boronic ester is formed with recovery of aromaticity as a driving force. In the same step, an iodine radical is generated, which recombines with the second boryl radical moiety **4.30-III** (blue) forming an NHC-stabilized iodo-Bpin adduct intermediate **4.30-IV.** The latter is related to previously reported NHC adducts of FBpin,[30] which are also assumed to play a role as a side product in Ni-catalyzed defluoroborylation reactions of aryl fluorides.[20, 27] The Lewis acidic **4.30-IV** is further coordinated by a second NHC, generating the boronium salt **37**, which was spectroscopically and structurally characterized.

In a possible side reaction, a small amount of free Me_2Im^{Me} reacts with the aryl iodide to form the imidazolium salt $[R\text{-}C_6H_4\text{-}Me_2Im^{Me}]^+I^-$ **38**. Compound **38** was identified as a product of the test reaction of the aryl iodide and Me_2Im^{Me} in the absence of B_2pin_2 (cf. Scheme 4.21). The NHC-stabilized boryl radical **4.30-II** might serve as a reducing agent in this side reaction by donating an electron to the imidazolium salt $[R\text{-}C_6H_4\text{-}Me_2Im^{Me}]^+I^-$ **38**, with formation of the boronium salt **37** and the experimentally detected/trapped aryl radical. The latter can further undergo a radical C–C coupling with the solvent (benzene) forming the C–C coupling side product **a**.

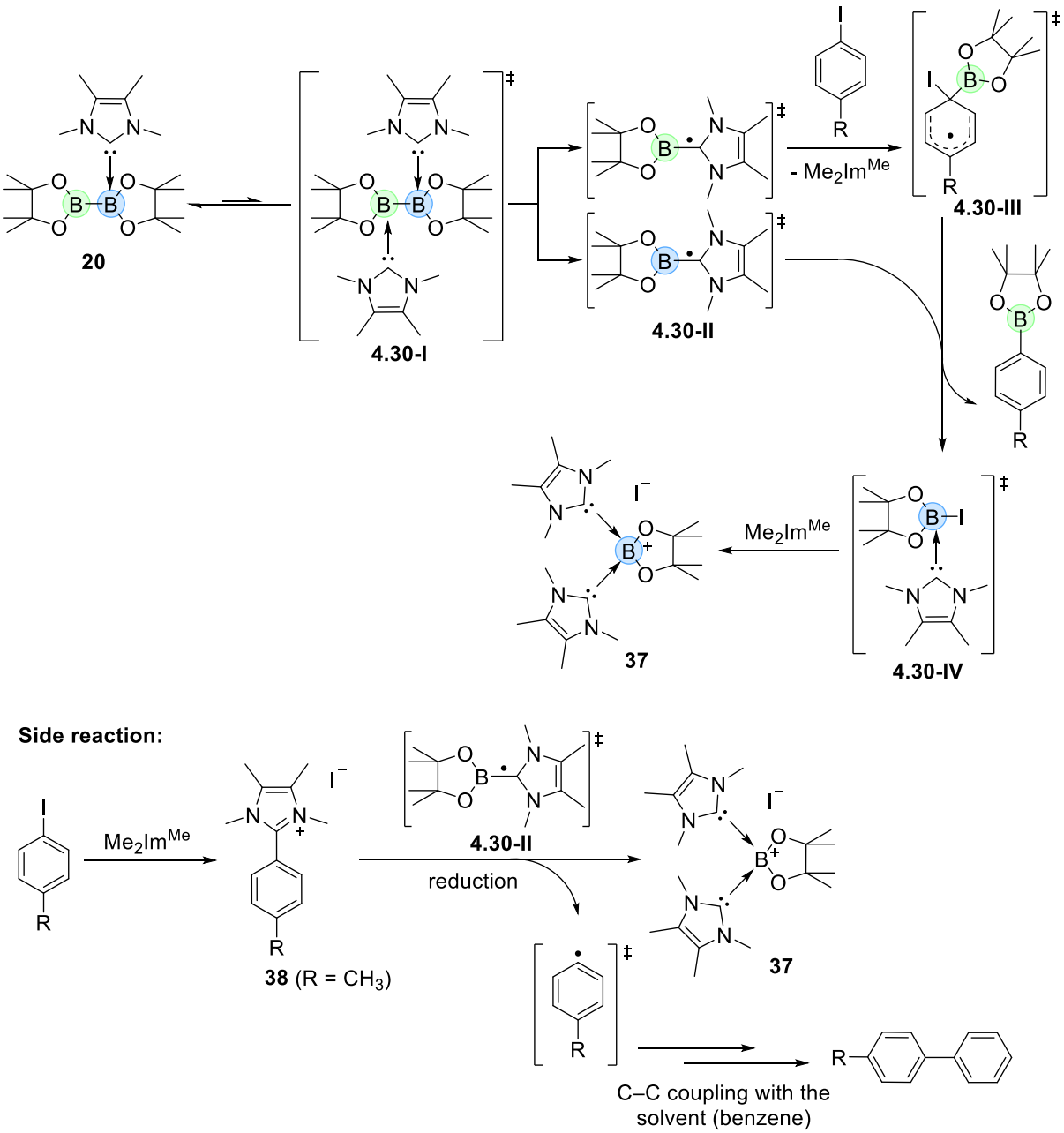

Scheme 4.30 Proposed mechanism for the boryl transfer reaction from the mono-NHC adduct $Me_2Im^{Me}{\cdot}B_2pin_2$ **20** to aryl iodides.

4.6 CONCLUSION

A variety of pyridine and NHC adducts of the type pyridine·B_2cat_2 **18**-**19**, NHC·$B_2(OR)_4$ **20-23**, $(NHC)_2$·B_2cat_2 **24**-**25**, as well as NHC adducts of pinacolborane **26**-**28** and aryl boronic esters **30**-**34** were synthesized and characterized. For the reaction of pinacolborane with $cAAC^{Me}$, instead of an adduct, the activation product **29** of HBpin, formed *via* the insertion of the $cAAC^{Me}$ carbene carbon atom into the B–H bond, was isolated and characterized. Furthermore, adducts of the type pyridine·B_2cat_2 **18**-**19** and NHC·$B_2(OR)_4$ **20**-**23** were examined for their ability to transfer a boryl moiety to an aryl iodide. The stoichiometric reaction of Me_2Im^{Me}·B_2pin_2 **20** with different substituted aryl iodides and bromides in benzene, at elevated temperatures, gave the desired aryl boronic esters in good yields. Interestingly, a C–C coupling product between the aryl halide and the solvent (benzene), depending on the reaction temperature, was detected as a side product which, together with observed hydrodehalogenation of the aryl halide, provide indications that the reaction might be radical in nature.

Previous studies by the groups of Marder and Radius have shown that bis-NHC adducts are thermally unstable, undergoing ring expansion reactions.[159, 160] When monitoring such an RER by EPR spectroscopy, using the reaction of B_2neop_2 with two equivalents of Me_2Im^{Me} as an example, evidence was found for the RER starting at 16 °C *via* the formation of a boryl radical of the type NHC–BR_2˙ **35a**, presumably formed by homolytic B–B bond cleavage. When monitoring the boryl transfer reaction based on Me_2Im^{Me}·B_2pin_2 **20** by EPR spectroscopy, a signal (though very weak and ill-defined) was detected, which could also be suggestive of a mechanism involving a boron-based radical.

5 EXPERIMENTAL SECTION

5.1 GENERAL PROCEDURES

All reactions and subsequent manipulations were performed under an argon atmosphere using standard Schlenk techniques or in a glovebox (Innovative Technology Inc. and Braun Uni Lab). All reactions were carried out in oven-dried glassware. Solvents were purified by distillation from an appropriate drying agent (toluene, benzene, and ethers from sodium/potassium alloy with benzophenone as indicator). Halocarbons, *n*-hexane and acetonitrile were dried and deoxygenated using an Innovative Technology Inc. Pure-Solv 400 Solvent Purification System, and further deoxygenated by using the freeze-pump-thaw method. C_6D_6 was dried over potassium or sodium and was freshly distilled before usage.

5.1.1 Analytical Methods

Elemental analysis

Elemental analyses (C, H, N, S) were measured with a ‘vario Micro cube’ from Elementar for combustion analysis.

High-Resolution Mass Spectrometry (HRMS)

High-resolution mass spectra were obtained using a Thermo Scientific Exactive Plus spectrometer equipped with an Orbitrap Mass Analyzer. Measurements were accomplished using an ASAP/APCI source with a corona needle, and carrier-gas (N_2) temperature of 400 °C, 350 °C or 250 °C, respectively. Ionizations were accomplished in Liquid Injection Field Desorption Ionization mode using a LIFDI 700 from Linden CMS with 10 kV at the emitter and an accelerating voltage of 5 V. ESI mass spectrometry was performed using a HESI source with an auxiliary gas temperature of 50 °C.

Cyclic Voltammetry (CV)

CV experiments were performed under an argon atmosphere with a Metrohm PGSTAT30 potentiostat (Metrohm Autolab B.V., Netherlands) and a Microcell HC set-up with a Eurotherm temperature controller (rhd instruments, Germany) at 20 °C with a scan rate of 50 $mV \cdot s^{-1}$ and an Ag/Ag^+ micro reference electrode with THF as solvent

from rhd instruments. A 0.1 mL Pt-cell TSC-70-closed from rhd instruments served as counter electrode and was equipped with a glassy carbon working electrode (surface area: $3.14 \cdot 10^{-2}$ cm^2).

Flash chromatography

Flash chromatography was performed using a Biotage® Isolera Four equipped with HP-Sil or KP-Sil cartridges and a diode array UV detector.

Gel permeation chromatography (GPC)

The device consists of a Viscotek SECmax system with a refractive index (RI) detector (Viscotek VE3580), both from Malvern. The column was a 30 cm long, linear (2) Phenogel 5 µm with a width of 7.8 mm, heated up to 35 °C in a column oven. The column material was porous polystyrene (PS) with a pore diameter of 13 µm. $CHCl_3$, including 0.5-1.0% EtOH, was used as solvent with a flow rate of 1.0 mL min^{-1}. For calibration, PS standards were utilized.

Gas Chromatography (GC)

GC-MS analyses were performed using a Thermo Fisher Scientific Trace 1310 gas chromatograph (column: TG-SQC 5% phenyl methyl siloxane, 15 m, ø 0.25 mm, film 0.25 µm; injector: 250 °C; oven: 40 °C (2 min), 40 °C to 280 °C; carrier gas: He (1.2 mL min^{-1}).

Quantitation and determination of the response factors

This method requires the determination of the compound-specific response factors (RF) against an internal standard. This means a prepared mixture with compound A and B with the ratio 1:1 can show an integration area ratio of 1:5, for example. The relative ratios depend on the (unknown) concentration of the compounds in the reaction mixture, whereas the concentration of the internal standard has to be known and constant. This enables the calibration for a specific range of concentrations. The concentration of the reaction mixtures to be analyzed has to be in the range of the concentration of the calibration run, otherwise the error would increase if the concentration is out of range (too high or too low). The quantitation was performed using the internal standard method, and the compounds of interest were calibrated against biphenyl as an inert internal standard.

The compound-specific response factors (RF), for each stock solution concentration (0.1 mg·mL^{-1}, 0.5 mg·mL^{-1}, 1.0 mg·mL^{-1}) of the calibration runs, were calculated according to the following equation:

$$\mathrm{RF}_{specific\ compound} = \frac{\mathrm{area}_{internal\ standard} \cdot \mathrm{amount}_{specific\ compound}}{\mathrm{amount}_{internal\ standard} \cdot \mathrm{area}_{specific\ compound}}$$

The calibration always was carried out directly before a batch of samples was measured. With the average value of the compound-specific response factor, the amount of a specific compound of an analyte was calculated according to the following equation:

$$\mathrm{amount}_{specific\ compound} = \frac{\mathrm{amount}_{internal\ standard} \cdot \mathrm{area}_{specific\ compound} \cdot \mathrm{RF}_{specific\ compound}}{\mathrm{area}_{internal\ standard}}$$

5.1.2 Spectroscopic Methods

IR Spectroscopy

All IR spectra were recorded on a NICOLET 380 FT-IR or a Bruker Alpha FT-IR spectrometer using ATR. Dependent on the intensity of the vibration bands, the intensity was assigned to the following abbreviations: very strong (vs), strong (s), middle (m), weak (w) and very weak (vw).

NMR Spectroscopy

All NMR spectra were recorded on Bruker Avance 200 (^{1}H, 199.9 MHz; ^{13}C, 50.3 MHz, ^{11}B, 64.1 MHz; ^{19}F, 188.1 MHz), Avance 400 (^{1}H, 400.4 MHz; ^{13}C, 100.7 MHz, ^{11}B, 128.5 MHz; ^{19}F, 376 MHz), DRX-300 (^{1}H, 300.2 MHz; ^{13}C, 75.5 MHz, ^{11}B, 96.31 MHz;) or Avance 500 (^{1}H, 500.1 MHz; ^{13}C, 125.8 MHz, ^{11}B, 160.46 MHz; ^{19}F, 470.6 MHz) spectrometers and were measured at 296 K. ^{1}H NMR chemical shifts are expressed in parts per million (ppm) and are referenced *via* residual proton resonances of the corresponding deuterated solvent C_6D_5H (^{1}H: δ = 7.16 ppm, C_6D_6), C_7D_7H (^{1}H: δ = 2.08, 6.97, 7.01, 7.09 ppm, d_8-toluene), $CDHCl_2$ (^{1}H: δ = 5.32 ppm, CD_2Cl_2), $CHCl_3$ (^{1}H: δ = 7.26 ppm, $CDCl_3$), HDO (^{1}H: δ = 4.79 ppm, D_2O). ^{13}C NMR spectra are reported relative to TMS using the carbon resonances of the deuterated solvent C_6D_6 (^{13}C: δ = 128.06 ppm), d_8-toluene (^{13}C: δ = 20.43, 125.13, 127.96, 128.87, 137.48 ppm), CD_2Cl_2 (^{13}C: δ = 53.84 ppm), $CDCl_3$ (^{13}C: δ = 77.16 ppm). All ^{13}C NMR spectra are ^{1}H broadband decoupled. ^{11}B NMR chemical shifts are reported relative to

$BF_3 \cdot Et_2O$ and ^{19}F NMR chemical shifts relative to external $CFCl_3$ as external standard. The coupling constants (*J*) are given in Hertz (Hz) without consideration of the sign. For multiplicities, the following abbreviations are used: s = singlet, d = doublet, t = triplet, q = quartet, sept = septet, m = multiplet, br = broad.

NMR Spectroscopy in the solid state

The solid-state magic-angle spinning (MAS) NMR spectra were recorded using a Bruker DSX-400 spectrometer (^{11}B, 128.38 MHz; ^{13}C, 100.61 MHz; ^{15}N, 40.56 MHz, ZrO_2 rotor 4 mm OD.

EPR Spectroscopy

EPR measurements at X-band (9.4 GHz) were carried out using a BRUKER ELEXSYS E580 CW EPR spectrometer equipped with an Oxford Instruments helium cryostat (ESR900) and a MercuryiTC temperature controller. The spectral simulations were performed using MATLAB 9.6 (R2019a) and the EasySpin 5.2.25 toolbox.[222]

UV/VIS Spectroscopy

All photophysical measurements were carried out under an argon atmosphere. All solution state measurements were performed in standard quartz cuvettes (1 cm x 1 cm cross section). UV/Vis absorption spectra were recorded using an Agilent 1100 diode array UV/Vis spectrophotometer.

5.1.3 Computational Details

Calculations were carried out using the TURBOMOLE V7.2 2017 program suite, a development of the University of Karlsruhe and the Forschungszentrum Karlsruhe GmbH, 1989-2007, TURBOMOLE GmbH, since 2007; available from http://www.turbomole.com.[223, 224] Geometry optimizations were performed using (RI-)DFT calculations[225-229] on a m4 grid employing the M06-2x[230] functional and a def2-TZVP basis set for boron and def2-SVP basis sets for C, H and O atoms.[231-236] Vibrational frequencies were calculated at the same level with the AOFORCE[237] module and all structures represented true minima without imaginary frequencies. Energies were calculated on single point calculations of the def2-TZVP/def2-SVP optimized structures using the M06-2X functional and a def2-TZVPP basis set for boron and def2-TZVP basis sets for C, H and O.

5.2 STARTING MATERIALS

$[Ni(\eta^4\text{-}COD)_2]$,[238] $[Ni(Cy_2Im)_2(Br)_2]$,[239] $[Ni(Mes_2Im)_2]$,[240] $[Ni_2(iPr_2Im)_4(\mu\text{-}(\eta^2\text{:}\eta^2)\text{-}COD)]$,[105] $[(Me_2Im)_2Ni(CO)_2]$,[241] $[Cu(Dipp_2Im)(Cl)]$,[242] $[Cu(Mes_2Im)(Cl)]$,[242] $[Cu(CaaC^{Me})(Cl)]$,[243] $[(PCy_3)Cu(\mu\text{-}I_2)Cu(PCy_3)]$,[244] [Cu(Xantphos)(Cl)],[245] iPr_2Im,[246-248] cAAC,[209, 249] B_2cat_2,[250, 251] B_2eg_2,[252] $B_2(OMe)_4$,[253] $Cy_2Im{\cdot}B_2pin_2$,[146] $Me_2Im^{Me}{\cdot}B_2cat_2$,[159] and $(Me_2Im^{Me})_2{\cdot}B_2cat_2$[159] were prepared according to published procedures. The diborane(4) reagents B_2pin_2 and B_2neop_2 were a generous gift from AllyChem Co. Ltd. Anhydrous NMe_4F is commercially available; for this work, however, it was synthesized according to a literature procedure.[254] All other reagents were purchased from Aldrich or ABCR and were checked for purity.

Synthesis of 1,3-dicyclohexylimidazolin-2-ylidene Cy_2Im[255]

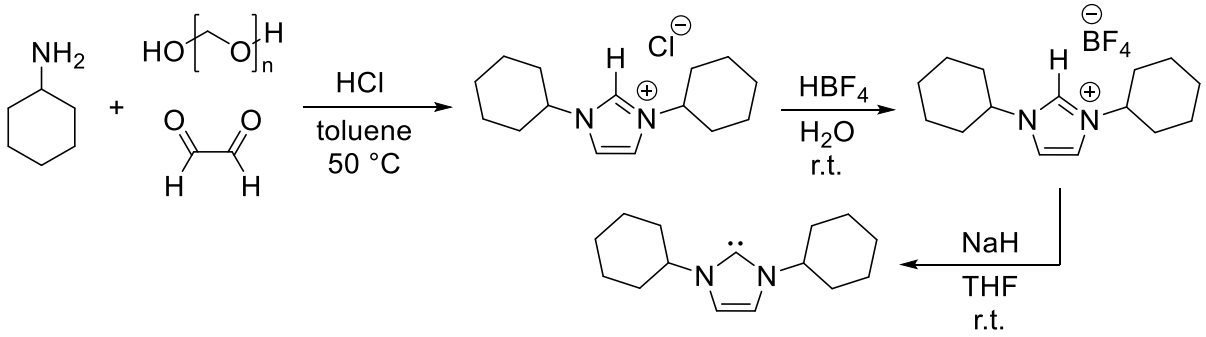

Synthesis of 1,3-dicyclohexylimidazolium chloride

Cyclohexylamine (9.92 g, 11.5 mL, 100 mmol, 1.0 equiv.) was dissolved in toluene (100 mL), and paraformaldehyde (3.00 g, 100 mmol, 1.0 equiv.) was added under intense stirring. After 30 min at room temperature, the reaction mixture was cooled to 0 °C and another equivalent of cyclohexylamine (9.92 g, 11.5 mL, 100 mmol, 1.0 equiv.) was added. After 10 min at 0 °C, 3.3 M aqueous HCl (30 mL, 100 mmol, 1.0 equiv.) was added dropwise. The reaction mixture was allowed to warm to room temperature and 40% aqueous glyoxal (14.5 mL, 100 mmol, 1.0 equiv.) was added slowly. The reaction mixture was stirred overnight at 50 °C. After the mixture had cooled to room temperature, diethylether (100 mL) and a saturated Na_2CO_3 solution (50 mL) were added, and the layers separated. The aqueous layer was washed with diethylether (3x 100 mL). All volatiles were removed *in vacuo*, the residue was

extracted with CH_2Cl_2 (150 mL) and dried over $MgSO_4$. After removal of the solvent under reduced pressure, the residue was dried *in vacuo*.

Yield: 19.1 g (71.1 mmol, 71%) of a hygroscopic, colorless solid.

^{1}H NMR (300 MHz, 25 °C, D_2O): δ = 1.28-2.18 (m, 20H, C*H*$_2$), 3.67 (m, 2H, N-C*H*), 7.54 (s, 2H, C*H*C*H*), 8.79 (s, 1H, NC*H*N) ppm.

Synthesis of 1,3-dicyclohexylimidazolium tetrafluoroborate

1,3-Dicyclohexylimidazolium chloride (18.5 g, 68.9 mmol, 1.0 equiv.) was dissolved in the minimum amount of water (500 mL) and, with vigorous stirring, 50 wt% aqueous tetrafluoroboronic acid (9.44 mL, 75.8 mmol, 1.1 equiv.) was added slowly. The white precipitate, which formed immediately, was collected by filtration, washed three times with 25 mL water, and dried *in vacuo*.

Yield: 19.4 g (60.6 mmol, 88%) of a colorless powder.

^{1}H NMR (400 MHz, 25 °C, $CDCl_3$): δ = 1.20-2.20 (m, 20H, C*H*$_2$), 4.32 (m, 2H, N-C*H*), 7.37 (s, 2H, NC*H*C*H*N), 8.97 (s, 1H, NC*H*N) ppm.

^{13}C{^{1}H} NMR (75 MHz, 25 °C, $CDCl_3$): δ = 24.7 (*C*H$_2$), 25.0 (*C*H$_2$), 33.1 (*C*H$_2$), 60.2 (N-*C*H), 120.3 (N*CC*N), 133.6 (N*C*HN) ppm.

^{11}B{^{1}H} NMR (128 MHz, 25 °C, $CDCl_3$): δ = -0.90 ppm.

^{19}F{^{1}H} NMR (376 MHz, 25 °C, $CDCl_3$): δ = -151.5 ppm.

Synthesis of 1,3-dicyclohexylimidazolin-2-ylidene

1,3-Dicyclohexylimidazolium tetrafluoroborate (8.14 g, 25.4 mmol, 1.0 equiv.) was suspended in THF (130 mL) and a mixture of sodium hydride (671 mg, 28.0 mmol, 1.1. equiv.) and KO*t*Bu (280 mg, 2.54 mmol, 0.1 equiv.) was added in small portions. After stirring the reaction mixture overnight at room temperature, the solvent was removed under reduced pressure. *Via* condensation, under reduced pressure at 140 °C (oil bath), the desired compound was transferred into a cooling trap charged with liquid nitrogen.

Yield: 5.70 g (24.5 mmol, 97%) of a colorless solid.

^{1}H NMR (400 MHz, 25 °C, C_6D_6): δ = 1.02-2.09 (m, 20H, C*H*$_2$), 4.11 (m, 2H, N-C*H*), 6.61 (s, 2H, NC*H*C*H*N) ppm.

^{13}C{^{1}H} NMR (100 MHz, 25 °C, C_6D_6): δ = 25.9 (*C*H$_2$), 26.0 (*C*H$_2$), 35.3 (*C*H$_2$), 60.0 (N-*C*H), 115.9 (N*CC*N), 212.7 (N*C*N) ppm.

Synthesis of 1,3,4,5-tetramethylimidazolin-2-ylidene Me$_2$Im$^{Me[246-248]}$

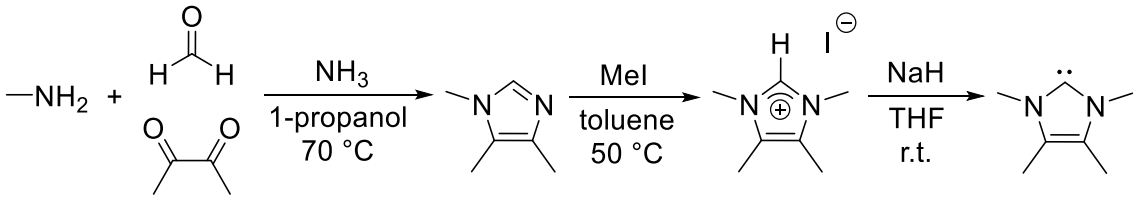

Synthesis of 1,4,5-trimethylimidazole

In a three-necked-flask, 1-propanol (100 mL) was heated to 70 °C. *Via* two dropping funnels two different solutions (dropping funnel 1: diacetyl (101 g, 102 mL, 1.16 mol, 1.16 equiv.), 40% aqueous formaldehyde (75.2 g, 68.6 mL, 1.00 mol, 1.0 equiv.), 1-propanol (50 mL); dropping funnel 2: 20% aqueous methylamine (80.4 g, 89.2 mL, 1.04 mol, 1.04 equiv.), 25% aqueous ammonia (154 g, 170 mL, 2.28 mol, 2.28 equiv.)) were added simultaneously dropwise within 1.5 h. Afterwards the reaction mixture was stirred for another 2 h at 70 °C and overnight at room temperature. The reaction mixture was concentrated to 150-200 mL and the residue was fractionally distilled (125 °C oil bath). Initially, *via* a rough distillation at 10 mbar residual water was removed. Then the desired compound was distilled: fraction 1: 7 mbar and 90 °C; fraction 2: 13 mbar and 100-105 °C.

Yield: 58.4 g (0.53 mol, 53%) of a pale yellow liquid.

^{1}H NMR (300 MHz, 25 °C, C_6D_6): δ = 1.59 (s, 3H, NC(C*H*$_3$)), 2.26 (s, 3H, NC(C*H*$_3$)), 2.46 (s, 3H, NC*H*$_3$), 6.98 (s, 1H, NC*H*N) ppm.

^{13}C{^{1}H} NMR (75 MHz, 25 °C, C_6D_6): δ = 8.1 (NC(*C*H$_3$)), 12.5 (NC(*C*H$_3$)), 31.3 (N*C*H$_3$), 122.1 (N*C*CN), 133.7 (NC*C*N), 135.1 (N*C*HN) ppm.

Synthesis of 1,3,4,5-tetramethylimidazolium iodide

The compound 1,4,5-trimethylimidazole (33.3 g, 302 mmol, 1.0 equiv.) was dissolved in toluene (300 mL) and methyl iodide (18.8 mL, 42.9 g, 302 mmol, 1.0 equiv.) was added and the reaction mixture was stirred overnight at 50 °C. The precipitate which formed was collected by filtration, washed with toluene (100 mL) and *n*-hexane (100 mL), and dried *in vacuo*.

Yield: 68.0 g (270 mmol, 89%) of a hygroscopic, colorless solid.

^{1}H NMR (400 MHz, 25 °C, D_2O): δ = 2.23 (s, 6H, NC(C*H*$_3$)), 3.72 (s, 6H, NC*H*$_3$), 8.46 (s, 1H, NC*H*N) ppm.

^{13}C{^{1}H} NMR (100 MHz, 25 °C, D_2O): δ = 9.1 (NC(*C*H$_3$)), 31.3 (N*C*H$_3$), 122.8 (N*CC*N), 138.7 (N*C*HN) ppm.

Synthesis of 1,3,4,5-tetramethylimidazolin-2-ylidene

The compound 1,3,4,5-tetramethylimidazolium iodide (68.0 g, 270 mmol, 1.0 equiv.) was suspended in THF (450 mL) and a mixture of sodium hydride (7.40 g, 308 mmol, 1.14 equiv.) and KO*t*Bu (3.00 g, 27.0 mmol, 0.1 equiv.) was added in small portions. After stirring the reaction mixture overnight at room temperature, the solvent was removed under reduced pressure. The residue was transferred into a small flask (very important!). *Via* condensation, under reduced pressure at 160-170 °C (oil bath), the desired compound was transferred into a cooling trap charged with liquid nitrogen. Yield (crude product): 17.1 g (138 mmol, 51%).

The crude product was dissolved in THF (20 mL) and stored at -30 °C for 3 days. The formed crystalline precipitate was separated from the solvent *via* syringe, and dried *in vacuo*.

Yield: 13.4 g (108 mmol, 40%)

^{1}H NMR (400 MHz, 25 °C, C_6D_6): δ = 1.59 (s, 6H, NC(C*H*$_3$)), 3.37 (s, 6H, NC*H*$_3$) ppm.

^{13}C{^{1}H} NMR (100 MHz, 25 °C, C_6D_6): δ = 8.83 (NC(*C*H$_3$)), 35.2 (N*C*H$_3$), 122.6 (N*CC*N), 213.0 (N*C*N) ppm.

5.3 SYNTHETIC PROCEDURES FOR CHAPTER 2

[Ni$_2$(Cy$_2$Im)$_4$(μ-(η^2:η^2)-COD)] 1

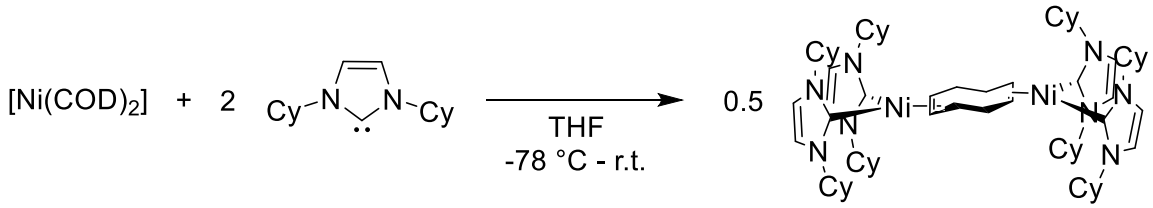

[Ni(η^4-COD)$_2$] (406 mg, 1.48 mmol, 1.0 equiv.) was dissolved in THF (80 mL) and cooled to -78 °C. A solution of 1,3-dicyclohexylimidazolin-2-ylidene Cy$_2$Im (686 mg, 2.95 mmol, 2.0 equiv.) in THF (20 mL) was added slowly. The yellow solution was allowed to warm to room temperature and stirred overnight. All volatiles were removed under reduced pressure and the residue was suspended in *n*-hexane (20 mL). The product was collected by filtration, washed with *n*-hexane (10 mL) and dried *in vacuo*.

Yield: 697 mg (1.33 mmol, 90%) of a bright yellow solid.

Elemental Analysis for $C_{68}H_{108}N_8Ni_2$ [1155.05 g/mol]: calculated (found): C 70.71 (70.30), H 9.43 (9.73), N 9.70 (9.44). In the course of the synthesis of **1**, varying amounts of the mononuclear compound [Ni(Cy$_2$Im)$_2$(η^4-COD)] **1a** were detected as a side product.

^{1}H NMR (400 MHz, 25 °C, C_6D_6): δ = 1.04-2.18 (m, 84H, Cy-C*H*$_2$, COD-C*H*$_2$), 2.54 (m, 4H, COD-C*H*$_2$), 2.87 (m, 4H, COD-C*H*), 5.10 (m, 4H, N-C*H*), 6.61 (s, 4H, NC*H*C*H*N) ppm.

^{13}C{^{1}H} NMR (100 MHz, 25 °C, C_6D_6): δ = 25.8-35.1 (Cy-*C*H$_2$), 38.6 (COD-*C*H$_2$), 54.7 (COD-*C*H), 57.6 (N-*C*H), 114.8 (N*CC*N), 205.3 (N*C*N) ppm.

HRMS-LIFDI (m/z): calculated (found) for $C_{30}H_{48}N_4Ni$ [Ni(Cy$_2$Im)$_2$]$^+$ 522.3227 (522.3226).

IR (ATR [cm^{-1}]): $\tilde{\nu}$ = 506 (vw), 543 (w), 558 (w), 668 (s), 687 (w), 760 (vw), 793 (w), 818 (w), 892 (w), 928 (vw), 974 (w), 988 (m), 1022 (vw), 1082 (w), 1134 (w), 1215 (vs), 1269 (m), 1370 (vw), 1387 (w), 1406 (w), 1447 (vw), 2852 (w), 2923 (m).

[Ni(Cy$_2$Im)$_2$(η^2-C$_2$H$_4$)] 2

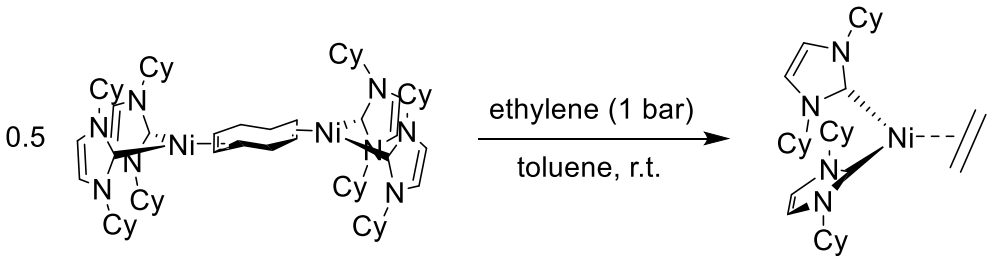

Ethylene was passed through a solution of complex **1** (300 mg, 260 µmol) in toluene (30 mL) at room temperature. All volatiles were removed under reduced pressure and the residue was suspended in cooled *n*-hexane (20 mL). The product was collected by filtration, washed with *n*-hexane (5 mL) and dried *in vacuo*.

Yield: 191 mg (346 µmol, 67%) of a yellow solid.

Elemental Analysis for $C_{32}H_{52}N_4Ni$ [551.49 g/mol]: calculated (found): C 69.69 (69.55), H 9.50 (9.30), N 10.16 (9.88).

^{1}H NMR (400 MHz, 25 °C, C_6D_6): δ = 1.00-2.13 (m, 40H, Cy-C*H*$_2$), 1.92 (s, 4H, η^2-C$_2$*H*$_4$), 5.09 (m, 4H, N-C*H*), 6.59 (s, 4H, NC*H*C*H*N) ppm.

^{13}C{^{1}H} NMR (100 MHz, 25 °C, C_6D_6): δ = 25.9 (Cy-*C*H$_2$), 34.6 (Cy-*C*H$_2$), 26.6 (η^2-*C*$_2$H$_4$), 58.2 (N-*C*H), 115.1 (N*CC*N), 204.1 (N*C*N) ppm.

HRMS-LIFDI (m/z): calculated (found) for $C_{30}H_{48}N_4Ni$ [M-C_2H_4]$^+$ 522.3227 (522.3220).

[Ni(Cy$_2$Im)$_2$(η^2-COE)] 3

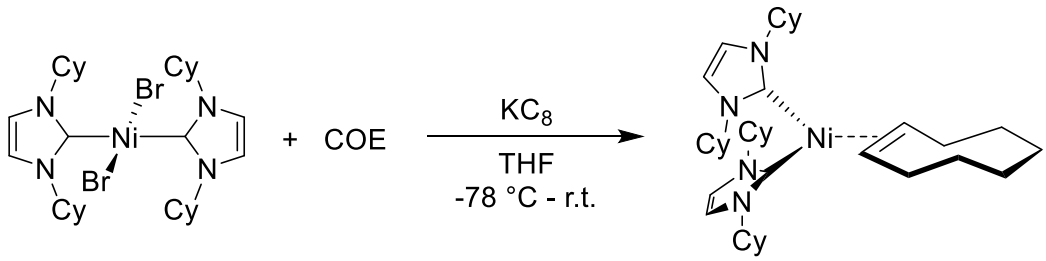

[Ni(Cy$_2$Im)$_2$(Br)$_2$] (160 mg, 23.0 µmol, 1.0 equiv.) was dissolved in THF (7 mL). Under rapid stirring, cyclooctene (COE) (37.5 µL, 28.1 µmol, 1.2 equiv.) and KC_8 (101 mg, 74.0 µmol, 3.2 equiv.) were added at -78 °C. The reaction mixture was allowed to warm to room temperature and stirred overnight. The dark suspension was filtered through a pad of Celite and washed with THF (12 mL). All volatiles were removed under

reduced pressure, the crude product was redissolved in toluene (10 mL) and filtered again through a pad of Celite. The solvent was removed under reduced pressure, the residue washed with *n*-hexane (2 mL) and dried *in vacuo*.

Yield: 74.0 mg (12.0 µmol, 52%) of a yellow solid.

For X-Ray diffraction: A saturated solution of [Ni(Cy$_2$Im)$_2$(η^2-COE)] in *n*-hexane was cooled to -30 °C to obtain single-crystals suitable for X-ray diffraction.

Elemental Analysis for $C_{38}H_{62}N_4Ni$ [633.54 g/mol]: calculated (found): C 72.03 (71.62), H 9.86 (9.78), N 8.84 (8.78).

^{1}H NMR (400 MHz, 25 °C, C_6D_6): δ = 1.45-2.17 (m, 52H, Cy/COE-C*H*$_2$), 2.44 (m, 2H, COE-C*H*), 5.04 (m, 4H, N-C*H*), 6.61 (s, 4H, NC*H*C*H*N) ppm.

^{13}C{^{1}H} NMR (100 MHz, 25 °C, C_6D_6): δ = 26.0-35.0 (Cy/COE-*C*H$_2$), 48.9 (COE-*C*H), 57.8 (N-*C*H), 115.1 (N*C*CN), 204.9 (N*C*N) ppm.

HRMS-LIFDI (m/z): calculated (found) for $C_{30}H_{48}N_4Ni$ [M-COE]$^+$ 522.3227 (522.3216).

IR (ATR [cm^{-1}]): $\tilde{\nu}$ = 444 (w), 505 (w), 538 (w), 556 (m), 670 (vs), 689 (m), 730 (vw), 761 (vw), 815 (m), 863 (vw), 892 (m), 974 (w), 989 (m), 1021 (w), 1084 (w), 1136 (vw), 1215 (vs), 1266 (m), 1347 (vw), 1367 (vw), 1385 (w), 1407 (w), 1449 (w), 2825 (vw), 2853 (m), 2922 (m).

General Procedures for the Synthesis of Organoboronic Esters

Method A

A mixture of [Ni$_2$(Cy$_2$Im)$_4$(μ-(η^2:η^2)-COD)] **1** (2.5 mol%), NaOAc (1.5 equiv.) and B_2pin_2 (1.5 equiv.) was dissolved in methylcyclohexane (5 mL) in a Schlenk tube equipped with a magnetic stirring bar. The aryl chloride (1.0 equiv.) was then added to the solution. The reaction mixture was heated at 100 °C for 24 h. Afterwards, the products and yields were determined by GC-MS with biphenyl as an internal standard.

Method B

This method was performed on a preparative scale. A mixture of [Ni$_2$(Cy$_2$Im)$_4$(μ-(η^2:η^2)-COD)] **1** (2.5 mol%), NaOAc (1.5 equiv.) and B_2pin_2 (1.5 equiv.) was dissolved in

methylcyclohexane (50 mL) in a Schlenk tube equipped with a magnetic stirring bar. The aryl chloride (1.0 equiv.) was then added to the solution. The reaction mixture was heated at 100 °C for 24 h and was then filtered and the remaining solid was washed with diethyl ether (10 mL Et_2O). The filtrate was concentrated *in vacuo*, purified by silica-gel column chromatography with *n*-hexane and then an *n*-hexane and ethyl acetate mixture (*n*-hexane/EtOAc =100/1) as eluent. The solvent of the product-containing fraction of the eluent was evaporated *in vacuo.*

2-(4-Trifluoromethyl-phenyl)-4,4,5,5-tetramethyl-[1,3,2]dioxaborolane 4

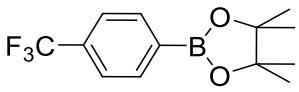

Method A was employed for the preparation of **4**, using 4-chlorobenzotrifluoride **4-Cl** (49.2 µL, 368 µmol) as the aryl chloride. The yield was determined by GC-MS with biphenyl as an internal standard (>99%).

The reaction was also performed on a preparative scale using method B with 4-chlorobenzotrifluoride **4-Cl** (3.68 mmol), which afforded 851 mg (85%) of **4** as a pale yellow solid after workup.

^{1}H NMR (400 MHz, 25 °C, CD_2Cl_2): 1.35 (s, 12H, CH_3), 7.63 (d, 2H, $^{3}J_{HH}$ = 7.6 Hz, aryl-CH_m), 7.90 (d, 2H, $^{3}J_{HH}$ = 7.6 Hz, aryl-CH_o) ppm.

^{13}C{^{1}H} NMR (100 MHz, 25 °C, CD_2Cl_2): 25.1 (*C*H_3), 84.7 (pin-C_q), 124.7 ($^{1}J_{CF}$ = 272 Hz, *C*F_3), 124.7 ($^{3}J_{CF}$ = 3.8 Hz, aryl-*C*H_m), 132.9 ($^{2}J_{CF}$ = 32 Hz, aryl-$C_q$$CF_3$), 135.4 (aryl-*C*$H_o$) ppm.

^{11}B{^{1}H} NMR (128 MHz, 25 °C, CD_2Cl_2): 30.5 ppm.

^{19}F{^{1}H} NMR (376 MHz, 25 °C, CD_2Cl_2): -63.4(s) ppm.

GC-MS: Ret.: 7.27 min; m/z: 272 $[M]^+$, 257 $[M\text{-}CH_3]^+$, 186 $[M\text{-}C_5H_{10}O]^+$, 173 $[M\text{-}C_6H_{11}O]^+$.

HRMS-ASAP (m/z): Calculated (found) for $C_{13}H_{17}BF_3O_2$ $[M+H]^+$ 273.1268 (273.1255).

The spectroscopic data for **4** match those reported in the literature.[34, 256]

2-(4-Methyl-phenyl)-4,4,5,5-tetramethyl-[1,3,2]dioxaborolane 5

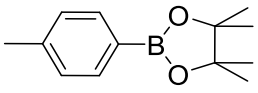

Method A was employed for the preparation of **5**, using 4-chlorotoluene **5-Cl** (54.3 µL, 459 µmol) as the aryl chloride. The yield was determined by GC-MS with biphenyl as an internal standard (80% yield).

The reaction was also performed on a preparative scale using method B with 4-chlorotoluene **5-Cl** (4.59 mmol), which afforded 611 mg (61%) of **5** as a colorless solid after workup.

^{1}H NMR (400 MHz, 25 °C, CD_2Cl_2): 1.33 (s, 12H, pin-C*H*$_3$), 2.36 (s, 3H, tolyl-C*H*$_3$), 7.19 (d, 2H, $^{3}J_{HH}$ = 7.7 Hz, aryl-C*H*$_m$), 7.65 (d, 2H, $^{3}J_{HH}$ = 7.7 Hz, aryl-C*H*$_o$) ppm.

^{13}C{^{1}H} NMR (100 MHz, 25 °C, CD_2Cl_2): 21.8 (tolyl-*C*H$_3$), 25.1 (pin-*C*H$_3$), 84.0 (pin-*C*$_q$), 128.9 (aryl-*C*H$_m$), 135.1 (aryl-*C*H$_o$) 141.9 (aryl-*C*$_q$tolyl) ppm.

^{11}B{^{1}H} NMR (128 MHz, 25 °C, CD_2Cl_2): 30.9 ppm.

GC-MS: Ret.: 8.06 min; m/z: 218 $[M]^+$, 203 $[M\text{-}CH_3]^+$, 132 $[M\text{-}C_5H_{10}O]^+$, 119 $[M\text{-}C_6H_{11}O]^+$.

HRMS-ASAP (m/z): Calculated (found) for $C_{13}H_{20}BO_2$ $[M+H]^+$ 219.1551 (219.1548).

The spectroscopic data for **5** match those reported in the literature.[118, 122]

2-(4-Methoxy-phenyl)-4,4,5,5-tetramethyl-[1,3,2]dioxaborolane 6

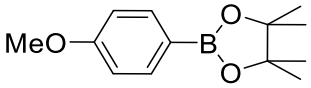

Method A was employed for the preparation of **6**, using 4-chloroanisole **6-Cl** (52.1µL, 427 µmol) as the aryl chloride. The yield was determined by GC-MS with biphenyl as an internal standard (>99% yield).

The reaction was also performed on a preparative scale using method B with 4-chloroanisole **6-Cl** (4.27 mmol), which afforded 880 mg (88%) of **6** as a pale yellow solid after workup.

^{1}H NMR (400 MHz, 25 °C, CD_2Cl_2): 1.32 (s, 12H, pin-C*H*$_3$), 3,82 (s, 3H, OC*H*$_3$), 6.90 (m, 2H, $^{3}J_{HH}$ = 8.7 Hz, aryl-C*H*$_m$), 7.70 (m, 2H, $^{3}J_{HH}$ = 8.7 Hz, aryl-C*H*$_o$) ppm.

^{13}C{^{1}H} NMR (100 MHz, 25 °C, CD_2Cl_2): 25.1 (pin-*C*H$_3$), 55.4 (O*C*H$_3$), 83.9 (*C*$_q$-pin), 113.7 (aryl-*C*H$_m$), 136.8 (aryl-*C*H$_o$) 162.6 (aryl-*C*$_q$OMe) ppm.

^{11}B{^{1}H} NMR (128 MHz, 25 °C, CD_2Cl_2): 30.7 ppm.

GC-MS: Ret.: 9.01 min; m/z: 234 $[M]^+$, 219 $[M\text{-}CH_3]^+$, 148 $[M\text{-}C_5H_{10}O]^+$, 134 $[M\text{-}C_6H_{11}O]^+$.

HRMS-ASAP (m/z): Calculated (found) for $C_{13}H_{20}BO_3$ $[M+H]^+$ 235.1500 (235.1489).

The spectroscopic data for **6** match those reported in the literature.[118]

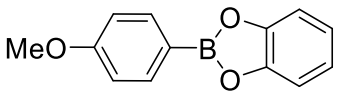

Method A was employed for the preparation of **6-cat**, using 4-chloroanisole **6-Cl** (54.3 µL, 442 µmol) as the aryl chloride. Only traces of the product were observed by GC-MS using biphenyl as an internal standard.

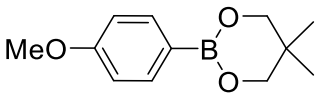

Method A was employed for the preparation of **6-neop**, using 4-chloroanisole **6-Cl** (55.5 µL, 452 µmol) as the aryl chloride. The product yield was determined by GC-MS using biphenyl as an internal standard (76% yield).

The reaction was also performed on a preparative scale using method B with 4-chloroanisole **6-Cl** (4.52 mmol), which afforded 587 mg (59%) of **6-neop** as a pale yellow solid after workup.

^{1}H NMR (400 MHz, 25 °C, CD_2Cl_2): 1.01 (s, 6H, C*H*$_3$-neop), 3.75 (s, 4H C*H*$_2$), 3,81 (s, 3H, OC*H*$_3$), 6.87 (d, 2H, $^{3}J_{HH}$ = 8.7 Hz, aryl-C*H*$_m$), 7.71 (d, 2H, $^{3}J_{HH}$ = 8.7 Hz, aryl-C*H*$_o$) ppm.

^{13}C{^{1}H} NMR (100 MHz, 25 °C, CD_2Cl_2): 22.0 (neop-*C*H$_3$), 32.2 (neop-C$_q$), 55.4 (O*C*H$_3$), 72.6 (*C*H$_2$), 113.5 (aryl-*C*H$_m$), 135.8 (aryl-*C*H$_o$) 162.2 (aryl-*C*$_i$OCH$_3$) ppm.

$^{11}B\{^1H\}$ NMR (128 MHz, 25 °C, CD_2Cl_2): 26.7 ppm.

GC-MS: Ret.: 9.43 min; m/z: 220 $[M]^+$, 205 $[M\text{-}CH_3]^+$, 189 $[M\text{-}CH_3O]^+$, 177 $[M\text{-}C_2H_3O]^+$, 162 $[M\text{-}C_3H_6O]^+$, 149 $[M\text{-}C_4H_7O]^+$, 134 $[M\text{-}C_5H_{10}O]^+$.

HRMS-ASAP (m/z): Calculated (found) for $C_{12}H_{18}BO_3$ $[M+H]^+$ 221.1311 (221.1312).

The spectroscopic data for **6-neop** match those reported in the literature.[3]

2-(Phenyl)-4,4,5,5-tetramethyl-[1,3,2]dioxaborolane 7

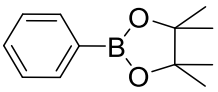

Method A was employed for the preparation of **7**, using chlorobenzene **7-Cl** (49.7 µL, 490 µmol) as the aryl chloride. The yield was determined by GC-MS using biphenyl as an internal standard (97% yield.)

The reaction was also performed on a preparative scale using method B with 4-chlorobenzene **7-Cl** (4.90 mmol), which afforded 792 mg (79%) of **7** as a colorless oil after workup.

^1H NMR (400 MHz, 25 °C, CD_2Cl_2): 1.36 (s, 12H, CH_3), 7.39 (m, 2H, aryl-CH_m), 7.48 (m, 1H, aryl-CH_p), 7.79 (m, 2H, aryl-CH_o) ppm.

$^{13}C\{^1H\}$ NMR (100 MHz, 25 °C, CD_2Cl_2): 25.1 (CH_3), 84.2 (C_q-Bpin), 128.1 (aryl-CH_m), 131.6 (aryl-CH_p), 135.0 (aryl-CH_o) ppm.

$^{11}B\{^1H\}$ NMR (128 MHz, 25 °C, CD_2Cl_2): 30.9 ppm.

GC-MS: Ret.: 7.32 min; m/z: 204 $[M]^+$, 189 $[M\text{-}CH_3]^+$, 118 $[M\text{-}C_5H_{10}O]^+$, 105 $[M\text{-}C_6H_{11}O]^+$.

HRMS-ASAP (m/z): Calculated (found) for $C_{12}H_{18}BO_2$ $[M+H]^+$ 205.1394 (205.1386).

The spectroscopic data for **7** match those reported in the literature.[87]

2-(3,5-Difluorophenyl)-4,4,5,5-tetramethyl-[1,3,2]dioxaborolane 8

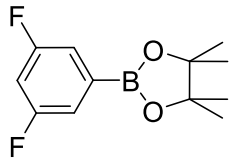

Method A was employed for the preparation of **8**, using 3,5-difluorochlorobenzene **8-Cl** (46.5 µL, 417 µmol) as the aryl chloride. The yield was determined by GC-MS with biphenyl as an internal standard (72% yield).

The reaction was also performed using method B on a preparative scale using 3,5-difluorochlorobenzene **8-Cl** (4.17 mmol), which afforded 631 mg (63 %) of **8** as a colorless solid after workup.

^{1}H NMR (400 MHz, 25 °C, CD_2Cl_2): 1.33 (s, 12H, C*H*$_3$), 6.91 (tt, 1H, $^{4}J_{HH}$ = 2.4 Hz, aryl-C*H*$_p$), 7.27 (m, 2H, $^{4}J_{HH}$ = 2.4 Hz, aryl-C*H*$_o$) ppm.

^{13}C{^{1}H} NMR (100 MHz, 25 °C, CD_2Cl_2): 25.1 (*C*H$_3$), 84.9 (*C*$_q$-Bpin), 106.7 (t, $^{2}J_{CF}$ = 25 Hz, aryl-*C*H$_p$), 117.1 (m, aryl-*C*H$_o$), 163.2 (dd, $^{1}J_{CF}$ = 249 Hz, $^{3}J_{CF}$ = 11 Hz, aryl-*C*F) ppm.

^{11}B{^{1}H} NMR (128 MHz, 25 °C, CD_2Cl_2): 30.1 ppm.

^{19}F{^{1}H} NMR (376 MHz, 25 °C, CD_2Cl_2): -111.5 (s) ppm.

GC-MS: Ret.: 7.02 min; m/z: 240 $[M]^+$, 225 $[M\text{-}CH_3]^+$, 154 $[M\text{-}C_5H_{10}O]^+$, 141 $[M\text{-}C_6H_{11}O]^+$.

HRMS-ASAP (m/z): Calculated (found) for $C_{12}H_{16}BF_2O_2$ $[M+H]^+$ 241.1206 (241.1203).

The spectroscopic data for **8** match those reported in the literature.[20]

2-(4-Fluorophenyl)-4,4,5,5-tetramethyl-[1,3,2]-dioxaborolane 9

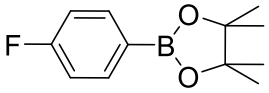

Method A was employed for the preparation of **9**, using 4-fluorochlorobenzene **9-Cl** (47.9 µL, 450 µmol) as the aryl chloride. The yield was determined by GC-MS using biphenyl as an internal standard (90% yield).

The reaction was also performed using method B on a preparative scale using 4-fluorochlorobenzene **9-Cl** (4.50 mmol), which afforded 769 mg (77 %) of **9** as a colorless solid after workup.

^{1}H NMR (400 MHz, 25 °C, $CDCl_3$): 1.34 (s, 12H, C*H*$_3$), 7.05 (m, 2H, aryl-C*H*$_m$), 7.81 (m, 2H, aryl-C*H*$_o$) ppm.

^{13}C{^{1}H} NMR (100 MHz, 25 °C, $CDCl_3$): 25.0 (*C*H_3), 84.0 (*C*$_q$-Bpin), 115.0 (d, $^{2}J_{CF}$ = 20 Hz, aryl-*C*H$_m$), 137.2 (d, $^{3}J_{CF}$ = 7.8 Hz aryl-*C*H$_o$), 165.2 (d, $^{1}J_{CF}$ = 250 Hz, aryl-*C*F) ppm.

^{11}B{^{1}H} NMR (128 MHz, 25 °C, $CDCl_3$): 30.6 ppm.

^{19}F{^{1}H} NMR (376 MHz, 25 °C, $CDCl_3$): -108.4 (s) ppm.

GC-MS: Ret.: 7.02 min; m/z: 222 $[M]^+$, 207 $[M\text{-}CH_3]^+$, 136 $[M\text{-}C_5H_{10}O]^+$, 123 $[M\text{-}C_6H_{11}O]^+$.

HRMS-ASAP (m/z): Calculated (found) for $C_{12}H_{17}BF_1O_2$ $[M+H]^+$ 223.1300 (223.1298).

The spectroscopic data for **9** match those reported in the literature.[257]

2-(Pyridin-3-yl)-4,4,5,5-tetramethyl-[1,3,2]-dioxaborolane 10

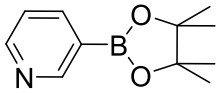

Method A was employed for the preparation of **10**, using 3-chloropyridine **10-Cl** (46.0 µL, 488 µmol) as the aryl chloride. The yield was determined by GC-MS using biphenyl as an internal standard (>99% yield).

GC-MS: Ret.:7.84 min; m/z: 205 $[M]^+$, 190 $[M\text{-}CH_3]^+$, 148, 120, 106.

***trans*-[Ni(Cy$_2$Im)$_2$(Cl)(4-(F$_3$C)C$_6$H$_4$)] 11**

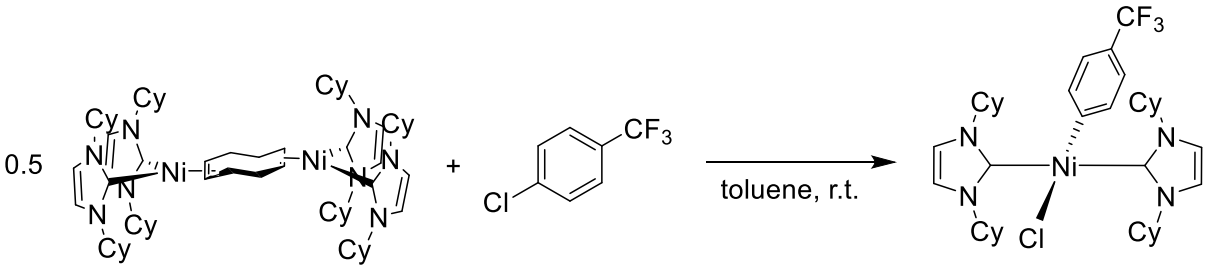

In a Schlenk tube, [Ni$_2$(Cy$_2$Im)$_4$(μ-(η^2:η^2)-COD)] **1** (100 mg, 86.6 µmol, 1.0 equiv.) was dissolved in toluene (7 mL) and 4-chlorobenzotrifluoride **4** (25.6 µL, 191 µmol, 2.2 equiv.) was added at room temperature and the reaction was stirred overnight. All volatiles were removed under reduced pressure and the residue was suspended in *n*-hexane (3 mL). The product was collected by filtration, washed with *n*-hexane (2 mL) and dried *in vacuo*.

Yield: 94.3 mg (134 µmol, 71%) of a pale yellow solid.

Elemental analysis for $C_{37}H_{52}ClF_3N_4Ni$ [704.00 g/mol]: calculated (found): C 63.13 (63.19), H 7.45 (7.60), N 7.96 (7.81).

^{1}H NMR (400 MHz, 25 °C, C_6D_6): 1.06-2.85 (m, 40H, C*H*$_2$), 6.18 (m, 4H, N-C*H*), 6.29 (s, 4H, NC*H*C*H*N), 7.08 (d, 2H, $^3J_{HH}$ = 7.8 Hz, aryl-C*H*$_o$), 7.71 (d, 2H, $^3J_{HH}$ = 7.8 Hz, aryl-C*H*$_m$) ppm.

^{13}C{^{1}H} NMR (125 MHz, 25 °C, CD_2Cl_2): 25.9-34.8 (*C*H$_2$), 60.1 (N-*C*H), 117.0 (N*CC*N), 121.2 ($^3J_{CF}$ = 4.4 Hz, aryl-*C*H$_m$), 122.6 ($^2J_{CF}$ = 31 Hz, aryl-*C*$_q$CF$_3$), 125.9 ($^1J_{CF}$ = 271 Hz, *C*F$_3$), 137.1 (aryl-*C*H$_o$), 167.9 (aryl-*C*$_i$), 181.9 (NCN) ppm.

^{19}F{^{1}H} NMR (376 MHz, 25 °C, C_6D_6): -61.2 (s) ppm.

HRMS-LIFDI (m/z): calculated (found) for $C_{37}H_{52}F_3N_4Ni$ [M-Cl]$^+$ 667.3492 (667.3484).

IR (ATR [cm^{-1}]): $\tilde{\nu}$ = 565 (vw), 598 (vw), 696 (vs), 734 (vw), 756 (vw), 813 (s), 897 (w), 998 (w), 1009 (m), 1030 (vw), 1069 (s), 1106 (s), 1153 (m), 1191 (w), 1234 (m), 1274 (w), 1290 (s), 1318 (s), 1348 (vw), 1381 (w), 1403 (w), 1423 (w), 1445 (w), 1463 (vw), 1582 (w), 2845 (w), 2917 (w), 2936 (w).

***trans*-[Ni(Cy$_2$Im)$_2$(Cl)(4-MeOC$_6$H$_4$)] 12**

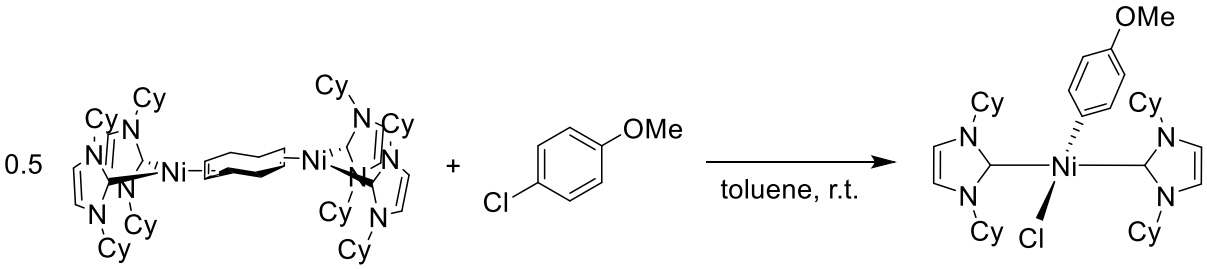

In a Schlenk tube, [Ni$_2$(Cy$_2$Im)$_4$(μ-(η^2:η^2)-COD)] **1** (90.0 mg, 77.9 µmol, 1.0 equiv.) was dissolved in toluene (7 mL) and 4-chloroanisole **6** (20.8 µL, 171 µmol, 2.2 equiv.) was added at room temperature and the reaction was stirred overnight. All volatiles were removed under reduced pressure and the residue was suspended in *n*-hexane (3 mL). The product was collected by filtration, washed with *n*-hexane (2 mL) and dried *in vacuo*.

Yield: 61.9 mg (92.9 µmol, 54%) of a pale yellow solid.

Elemental analysis for $C_{37}H_{55}ClN_4NiO$ [666.02 g/mol]: calculated (found): C 66.73 (66.42), H 8.32 (8.32), N 8.41 (8.41).

^{1}H NMR (400 MHz, 25 °C, C_6D_6): 1.08-2.90 (m, 40H, C*H*$_2$), 3.30 (s, 3H, OC*H*$_3$), 6.31 (m, 4H, N-C*H*), 6.36 (s, 4H, NC*H*C*H*N), 6.65 (d, 2H, $^3J_{HH}$ = 8.6 Hz, aryl-C*H*$_o$), 7.41 (d, 2H, $^3J_{HH}$ = 8.6 Hz, aryl-C*H*$_m$) ppm.

^{13}C{^{1}H} NMR (100 MHz, 25 °C, C_6D_6): 26.0-34.7 (*C*H$_2$), 54.5 (O*C*H$_3$), 59.8 (N-*C*H), 112.5 (aryl-*C*H$_m$), 116.3 (N*CC*N), 137.9 (aryl-*C*H$_o$), 143.5 (aryl-*C*$_q$OCH$_3$), 155.8 (aryl-*C*$_i$), 185.2 (N*C*N) ppm.

HRMS-LIFDI (m/z): calculated (found) for $C_{37}H_{55}N_4NiO$ [M-Cl]$^+$ 629.3724 (629.3717).

IR (ATR [cm^{-1}]): $\tilde{\nu}$ = 510 (vw), 565 (vw), 579 (vs), 690 (vs), 758 (vw), 799 (m), 813 (w), 897 (w), 986 (vw), 998 (vw), 1026 (w), 1091 (vw), 1170 (w), 1197 (w), 1223 (m), 1234 (w), 1258 (ww), 1289 (vw), 1381 (w), 1403 (w), 1403 (w), 1423 (w), 1446 (w), 1464 (w), 1476 (w), 1574 (vw), 2847 (w), 2920 (m).

***trans*-[Ni(Cy$_2$Im)$_2$(Cl)(C$_6$H$_5$)] 13**

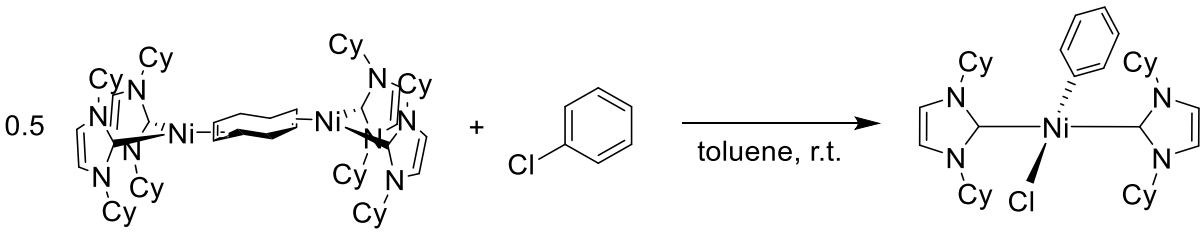

In a Schlenk tube, [Ni$_2$(Cy$_2$Im)$_4$(μ-(η^2:η^2)-COD)] **1** (100 mg, 86.6 µmol, 1.0 equiv.) was dissolved in toluene (7 mL) and chlorobenzene **7** (19.3 µL, 190 µmol, 2.2 equiv.) was added at room temperature and the reaction was stirred overnight. All volatiles were removed under reduced pressure and the residue was suspended in *n*-hexane (3 mL). The product was collected by filtration, washed with *n*-hexane (2 mL) and dried *in vacuo*.

Yield: 76.3 mg (120 µmol, 63%) of a colorless solid.

Elemental analysis for C$_{36}$H$_{53}$ClN$_4$Ni [635.99 g/mol]: calculated (found): C 67.99 (67.60), H 8.40 (8.73), N 8.81 (8.59).

^{1}H NMR (400 MHz, 25 °C, CD$_2$Cl$_2$): 1.30-2.52 (m, 40H, C*H*$_2$), 6.05 (m, 4H, N-C*H*), 6.49 (m, 1H, aryl-C*H*$_p$), 6.68 (m, 2H, aryl-C*H*$_m$), 6.78 (s, 4H, NC*H*C*H*N), 7.37 (m, 2H, aryl-C*H*$_o$) ppm.

^{13}C{^{1}H} NMR (100 MHz, 25 °C, CD$_2$Cl$_2$): 25.9-34.9 (*C*H$_2$), 59.9 (N-*C*H), 116.7 (N*CC*N), 120.4 (aryl-*C*H$_p$), 125.7 (aryl-*C*H$_o$), 137.3 (aryl-*C*H$_m$), 157.5 (aryl-*C*$_i$), 183.6 (N*C*N) ppm.

HRMS-LIFDI (m/z): calculated (found) for C$_{36}$H$_{53}$N$_4$Ni [M-Cl]$^+$ 599.3618 (599.3611).

IR (ATR [cm^{-1}]): $\tilde{\nu}$ = 490 (vw), 567 (vw), 692 (vs), 735 (m), 758 (vw), 819 (vw), 894 (w), 983 (vw), 997 (vw), 1019 (vw), 1055 (vw), 1194 (w), 1234 (w), 1262 (vw), 1290 (vw), 1382 (vw), 1423 (w), 1446 (w), 1563 (vw), 2853 (w), 2924 (w).

***trans*-[Ni(Cy$_2$Im)$_2$(Cl)(3,5-F$_2$C$_6$H$_3$)] 14**

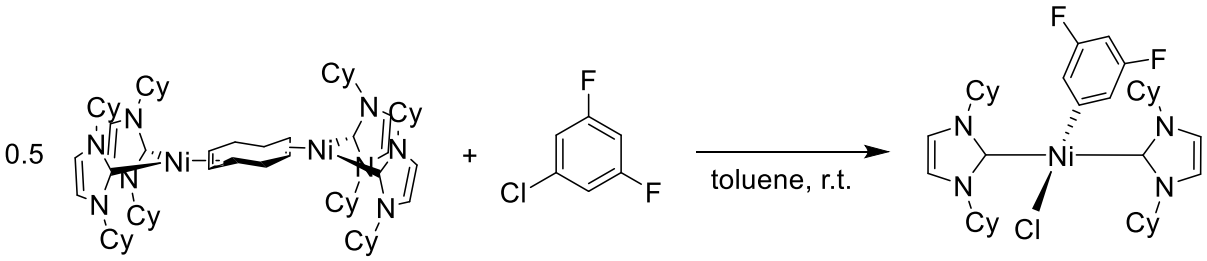

In a Schlenk tube, [Ni$_2$(Cy$_2$Im)$_4$(μ-(η^2:η^2)-COD)] **1** (91 mg, 78.8 µmol, 1.0 equiv.) was dissolved in toluene (7 mL) and 3,5-difluorochlorobenzene **8** (19.3 µL, 173 µmol, 2.2 equiv.) was added at room temperature and the reaction was stirred overnight. All volatiles were removed under reduced pressure and the residue was suspended in *n*-hexane (3 mL). The product was collected by filtration, washed with *n*-hexane (2 mL) and dried *in vacuo*.

Yield: 76.0 mg (113 µmol, 65%) of a colorless solid.

For X-Ray diffraction: Single-crystals suitable for X-ray diffraction were obtained by slow evaporation of the solvent of a saturated solution of [Ni(Cy$_2$Im)$_2$(Cl)(3,5-F$_2$C$_6$H$_3$)] in benzene.

Elemental analysis for C$_{36}$H$_{51}$ClF$_2$N$_4$Ni [671.97 g/mol]: calculated (found): C 64.35 (64.62), H 7.65 (7.91), N 8.34 (8.48).

^{1}H NMR (400 MHz, 25 °C, C$_6$D$_6$): 1.04-2.81 (m, 40H, C*H*$_2$), 6.22 (m, 1H, aryl-C*H*$_p$), 6.22 (m, 4H, N-C*H*), 6.29 (s, 4H, NC*H*C*H*N), 7.29 (m, 2H, aryl-C*H*$_o$) ppm.

^{13}C{^{1}H} NMR (100 MHz, 25 °C, C$_6$D$_6$): 26.5-34.6 (*C*H$_2$), 60.0 (N-*C*H), 95.9 (t, $^2J_{CF}$ = 25 Hz, aryl-*C*H$_p$), 116.6 (N*C*CN), 118.9 (m, $^2J_{CF}$ = 14 Hz, $^4J_{CF}$ = 3.4 Hz, aryl-*C*H$_o$), 160.6 (dd, $^1J_{CF}$ = 250 Hz, $^3J_{CF}$ = 11 Hz, aryl-*C*F), 165.8 (Ni-*C*$_i$), 182.4 (N*C*N) ppm.

^{19}F{^{1}H} NMR (376 MHz, 25 °C, C$_6$D$_6$): -115.9 (s) ppm.

IR (ATR [cm^{-1}]): $\tilde{\nu}$ = 512 (vw), 525 (vw), 568 (vw), 694 (vs), 758 (vw), 805 (w), 820 (w), 849 (w), 895 (w), 964 (w), 985 (vw), 996 (vw), 1029 (vw), 1107 (w), 1194 (m), 1235 (w), 1269 (vw), 1292 (vw), 1347 (vw), 1397 (w), 1424 (w), 1441 (w), 1464 (w), 1564 (w), 1587 (m), 2853 (w), 2925 (m). 3044 (vw).

Investigations Concerning the Reaction Mechanism

Reaction of B_2pin_2, NaOAc and 4-chlorobenzotrifluoride 4 with catalytic amounts of $[Ni(Cy_2Im)_2(Cl)(4\text{-}(F_3C)C_6H_4)]$ **11**

In a Schlenk tube, $[Ni(Cy_2Im)_2(Cl)(4\text{-}(F_3C)C_6H_4)]$ **11** (4.3 mg ,6.13 µmol, 5.0 mol%), B_2pin_2 (46.7 mg, 184 µmol, 1.5 equiv.), NaOAc (15.1 mg, 184 µmol, 1.5 equiv.) were dissolved in methylcyclohexane (1.5 mL) and 4-chlorobenzotrifluoride **4** (16.4 µL, 123 µmol, 1.0 equiv.) was added at room temperature and stirred overnight at 100 °C. Analyzing the reaction mixture by GC-MS indicated the formation of the borylated chloroarene **4a** in 88% yield (estimated by ^{19}F NMR spectroscopy) and residual B_2pin_2.

Stoichiometric reaction of $[Ni_2(Cy_2Im)_4(\mu\text{-}(\eta^2{:}\eta^2)\text{-COD})]$ **1** with B_2pin_2

In a Young's tap NMR tube, B_2pin_2 (11.0 mg, 43.3 µmol, 1.0 equiv.) and $[Ni_2(Cy_2Im)_4(\mu\text{-}(\eta^2{:}\eta^2)\text{-COD})]$ **1** (25.0 mg, 21.6 µmol, 0.5 equiv.) were added to methylcyclohexane (0.7 mL). Investigating the reaction mixture by $^{11}B\{^1H\}$ NMR spectroscopy revealed, in addition to the signal for B_2pin_2 at 30.8 ppm, a second signal at 44.5 ppm (Figure 2.3). Figure 2.4 shows the ^1H NMR spectrum of the isolated nickel-boryl complex also indicating free B_2pin_2. High resolution mass spectra indicated the formation of a $[Ni(Cy_2Im)_2(Bpin)_2]$ species. However, the reaction does not proceed to completion, as it appears to be an equilibrium process, so there is always free B_2pin_2 observed in the NMR spectra. The proposed nickel-boryl complex also has limited stability in common deuterated-solvents such as C_6D_6, d_8-THF and d_8-toluene, making further characterization extremely difficult.

HRMS-LIFDI (m/z): Calculated (found) for $C_{42}H_{72}B_2N_4NiO_4$ $[M]^+$ 776.5088 (776.5074).

5.4 SYNTHETIC PROCEDURES FOR CHAPTER 3

[Cu(*i*Pr$_2$Im)(Cl)] 15 [139, 258]

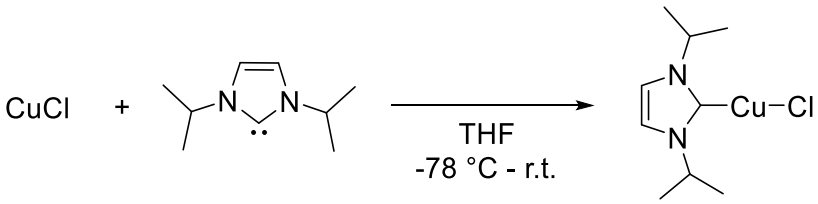

Copper(I) chloride (2.00 g, 20.2 mmol, 1.0 equiv.) in THF (15 mL) was cooled to -78 °C and *i*Pr$_2$Im (3.08 g, 20.2 mmol, 3.08 mL, 1.0 equiv.) was added dropwise. The mixture was allowed to warm slowly to room temperature and stirred overnight. All volatiles were removed under reduced pressure. The crude product was suspended in *n*-hexane (20 mL), collected by filtration and dried *in vacuo*.

Yield: 4.54 g (18.1 mmol, 90%) of a colorless solid.

Elemental analysis for $C_9H_{16}ClCuN_2$ [251.24 g/mol]: Calculated (found) C 43.03 (42.99), H 6.42 (6.45), N 11.15 (11.04).

^{1}H NMR (400 MHz, 25 °C, C_6D_6): δ = 0.93 (d, 12H, $^3J_{HH}$ = 7.3 Hz, CHC*H*$_3$), 4.34 (sept, 2H, $^3J_{HH}$ = 7.3 Hz, C*H*CH$_3$), 6.25 (s, 2H, NC*H*C*H*N) ppm.

^{13}C{^{1}H} NMR (100 MHz, 25 °C, C_6D_6): δ = 23.5 (CH*C*H$_3$), 53.6 (*C*HCH$_3$), 117.0 (N*CC*N), 174.5 (N*C*N) ppm.

HRMS-ASAP (m/z): calculated (found) for $C_{18}H_{32}Cl_2Cu_2N_4$ [2 M]$^+$ 502.0572 (502.0554).

[Cu(Me$_2$Im^{Me})(Cl)] 16 [139]

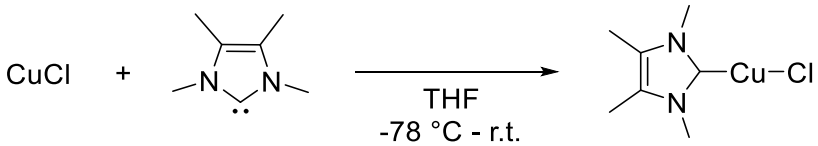

Copper(I) chloride (198 mg, 2.00 mmol, 1.0 equiv.) and Me$_2$Im^{Me} (248 mg, 2.00 mmol, 1.0 equiv.) were cooled to -110 °C. THF (5 mL) was added slowly down the inside of the cooled Schlenk tube. The mixture was allowed to warm slowly to room temperature and stirred overnight. The solvent was removed under reduced pressure. The crude

product was suspended in *n*-hexane (10 mL), collected by filtration and dried *in vacuo*. **Yield:** 295 mg (1.32 mmol, 66%) of an off-white solid.

Elemental analysis for $C_7H_{12}ClCuN_2$ [223.18 g/mol]: Calculated (found) C 37.67 (38.04), H 5.42 (5.47), N 12.55 (12.70).

^{1}H NMR (400 MHz, 25 °C, C_6D_6): δ = 1.19 (s, 6H, NC(C*H*$_3$)), 2.88 (s, 6H, NC*H*$_3$) ppm.

^{13}C{^{1}H} NMR (125 MHz, 25 °C, $CDCl_3$): δ = 9.1 (NC(*C*H$_3$)), 35.8 (N*C*H$_3$), 125.2 (N*CC*N), 174.4 (N*C*N) ppm.

HRMS-ASAP (m/z): calculated (found) for $C_7H_{12}CuN_2$ [M-Cl]$^+$ 187.0291 (187.0285).

[Cu(Cy$_2$Im)(Cl)] 17 [140]

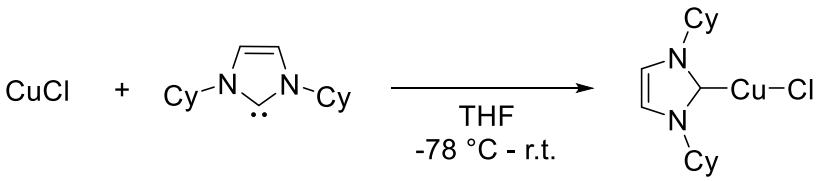

Copper(I) chloride (2.00 g, 20.2 mmol, 1.0 equiv.) in THF (15 mL) was cooled to -78 °C and Cy$_2$Im (4.69 g, 20.2 mmol, 1.0 equiv.) was added in small portions. The mixture was allowed to warm slowly to room temperature and stirred overnight. The solvent was removed under reduced pressure. The crude product was suspended in *n*-hexane (20 mL), collected by filtration and dried *in vacuo*.

Yield: 5.37 g (16.2 mmol, 80%) of a colorless solid.

Elemental analysis for $C_{15}H_{24}N_2CuCl$ [331.37 g/mol]: Calculated (found) C 54.37 (54.28), H 7.30 (7.48), N 8.45 (8.33).

^{1}H NMR (400 MHz, 25 °C, $CDCl_3$): δ = 1.22-2.07 (m, 20H, Cy-C*H*$_2$), 4.27 (m, 2H, N-C*H*), 6.91 (s, 2H, NC*H*C*H*N) ppm.

^{13}C{^{1}H} NMR (100 MHz, 25 °C, $CDCl_3$): δ = 25.2 (Cy-*C*H$_2$), 25.5 (Cy-*C*H$_2$), 34.8 (Cy-*C*H$_2$), 61.3 (N-*C*H) 117.5 (N*CC*N), 173.7 (N*C*N) ppm.

HRMS-ASAP (m/z): calculated (found) for $C_{15}H_{24}N_2CuCl$ [M]$^+$ 330.0919 (330.0911).

General Procedure for Catalyst Screening

[Cu] (10 mol%) and the solvent were added to a Schlenk tube equipped with a magnetic stirring bar. The base, the boron reagent, and the aryl chloride were added. The reaction mixture was stirred at 90 °C for the indicated time, then diluted with Et_2O (2 mL) and filtered through a pad of Celite (Ø 3 mm × 8 mm). Biphenyl was added as an internal standard and the crude reaction mixture was analyzed by GC-MS.

General Procedures for the Synthesis of Organoboronic Esters

[Cu(Cy_2Im)(Cl)] **17** (10 mol%) and methylcyclohexane (3 mL) were added to a Schlenk tube equipped with a magnetic stirring bar. The base (750 µmol, 1.5 equiv.), the boron reagent (750 µmol, 1.5 equiv.) and the aryl chloride (500 µmol, 1.0 equiv.) were added. The reaction mixture was stirred at 90 °C for 42 h and then filtered and the remaining solid was washed with Et_2O (10 mL). The filrate was concentrated *in vacuo*, purified by silica-gel column chromatography with *n*-hexane and then an *n*-hexane and ethyl acetate mixture (*n*-hexane/EtOAc =100/1) as eluent. The solvent of the product-containing fraction of the eluent was evaporated *in vacuo*. The gram scale reaction utilizing **4-Cl** was performed on a 6.00 mmol scale in 36 mL of methylcyclohexane giving a 70% yield of **4**.

For the analytic data of the borylation products **4**-**9** see chapter 5.3.

5.5 SYNTHETIC PROCEDURES FOR CHAPTER 4

Synthesis of Pyridine Adducts of B_2cat_2

Pyridine·B_2cat_2 18

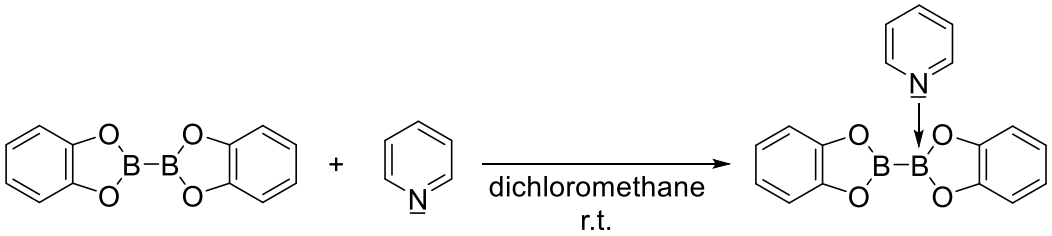

Pyridine (40.5 µL, 39.6 mg, 500 µmol, 1.0 equiv.) was added to a solution of B_2cat_2 (119 mg, 500 µmol, 1.0 equiv.) in dichloromethane (5 mL). After stirring the reaction mixture for 30 min at room temperature, the desired compound was precipitated by the addition of *n*-hexane (13 mL). The precipitate was collected by filtration and dried *in vacuo*.

Yield: 110 mg (348 µmol, 70%) of a pale yellow solid.

For X-ray diffraction: A saturated solution of B_2cat_2·pyridine in *n*-hexane/dichloromethane (3:1) was cooled to -30 °C to obtain single-crystals suitable for X-ray diffraction.

Elemental analysis for $C_{17}H_{13}B_2NO_4$ [316.91 g/mol]: calculated (found) C 64.43 (65.34), H 4.13 (4.79), N 4.42 (4.75).

^{1}H NMR (400 MHz, 25 °C, CD_2Cl_2): δ = 6.72-7.00 (m, 8H, cat-C*H*), 7.40 (m, 2H, pyridine-CH_m), 7.82 (m, 1H, pyridine-CH_p), 8.52 (m, 2H, pyridine-CH_o) ppm.

^{13}C{^{1}H} NMR (100 MHz, 25 °C, CD_2Cl_2): δ = 111.6 (cat-*C*H), 119.3 (cat-*C*H), 119.8 (cat-*C*H), 121.2 (cat-*C*H), 125.6 (pyridine-*C*H_m), 139.9 (pyridine-*C*H_p), 145.0 (pyridine-*C*H_o), 148.1 (cat-*C*$_q$), 150.1 (cat-*C*$_q$) ppm.

^{11}B{^{1}H} NMR (128 MHz, 25 °C, CD_2Cl_2): δ = 6.60 (sp^3-B atom, bis-pyridine adduct), 22.2 (br, B–B atom) ppm.

HRMS-ASAP (m/z): calculated (found) for $C_{17}H_{13}B_2NO_4$ $[M]^+$ 317.1025 (317.1023).

DMAP·B_2cat_2 19

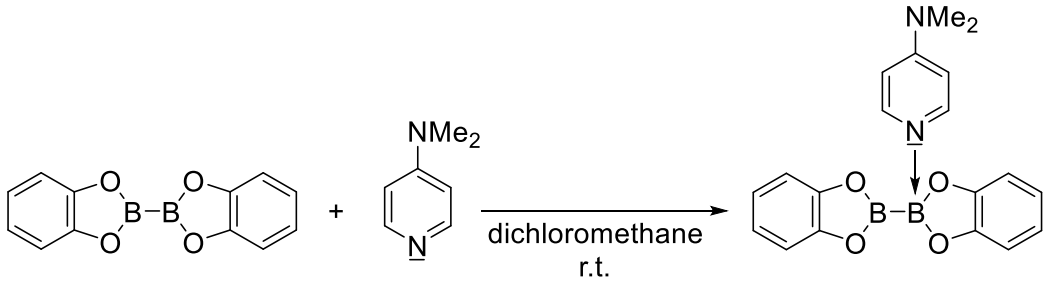

N,*N*-Dimethyl-4-aminopyridine (DMAP) (79.1 mg, 648 µmol, 1.0 equiv.) was added to a solution of B_2cat_2 (154 mg, 648 µmol, 1.0 equiv.) in dichloromethane (2 mL). After stirring the reaction mixture for 2 h at room temperature, the desired compound was precipitated by the addition of *n*-hexane (12 mL). The precipitate was collected by filtration and dried *in vacuo*.

Yield: 215 mg (597 µmol, 92%) of a colorless solid.

Elemental analysis for $C_{19}H_{18}B_2N_2O_4$ [359.98 g/mol]: calculated (found) C 63.39 (63.95), H 5.04 (5.58), N 7.78 (7.52).

^{1}H NMR (400 MHz, 25 °C, CD_2Cl_2): δ = 3.02 (s, 6H, N(CH_3)$_2$), 6.57 (m, 2H, pyridine-CH_m), 6.85 (m, 4H, cat-C*H*), 7.00 (m, 4H, cat-C*H*), 8.25 (m, 2H, pyridine-CH_o) ppm.

^{13}C{^{1}H} NMR (100 MHz, 25 °C, CD_2Cl_2): δ = 39.8 (N(*C*H$_3$)$_2$), 107.0 (pyridine-*C*H$_m$), 111.4 (cat-*C*H), 121.0 (cat-*C*H), 142.2 (pyridine-*C*H$_o$), 150.3 (cat-*C*$_q$), 156.6 (pyridine-*C*$_q$) ppm.

^{11}B{^{1}H} NMR (128 MHz, 25 °C, CD_2Cl_2): δ = 21.7 (br, B–B atom) ppm.

HRMS-ASAP (m/z): calculated (found) for $C_{19}H_{19}B_2N_2O_4$ $[M+H]^+$ 361.1525 (361.1524).

Synthesis of NHC Adducts of Diborane(4) Compounds

Me_2Im^{Me}·B_2pin_2 20

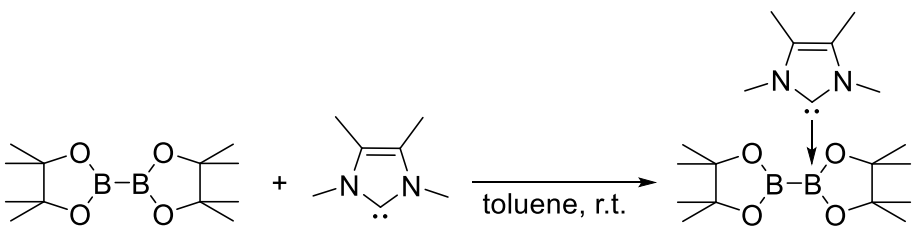

B_2pin_2 (2.54 g, 10.0 mmol, 1.0 equiv.) and Me_2Im^{Me} (1.24 g, 10.0 mmol, 1.0 equiv.) were dissolved in toluene (50 mL). After stirring the reaction mixture overnight at room temperature, the solvent was removed under reduced pressure. The residue was suspended in *n*-pentane (20 mL), collected by filtration and dried *in vacuo*.

Yield: 2.75 g (7.27 mmol, 73%) of a colorless solid.

Elemental analysis for $C_{19}H_{36}B_2N_2O_4$ [378.13 g/mol]: calculated (found) C 60.35 (60.34), H 9.60 (9.78), N 7.41 (7.60).

^{1}H NMR (400 MHz, 25 °C, C_6D_6): δ = 1.19 (s, 6H, NC(C*H*$_3$)), 1.29 (s, 24H, pin-C*H*$_3$), 3.67 (s, 6H, NC*H*$_3$) ppm.

^{13}C{^{1}H} NMR (100 MHz, 25 °C, C_6D_6): δ = 7.6 (NC(*C*H$_3$)), 25.6 (pin-C*H*$_3$), 32.4 (N*C*H$_3$), 79.9 (pin-*C*$_q$), 123.1 (N*CC*N), 168.1 (N*C*N) ppm.

^{11}B NMR (160 MHz, 25 °C, d_8-toluene): δ = 19.3 (br, B–B atom) ppm.

^{11}B NMR (160 MHz, 0 °C, d_8-toluene): δ = 2.94 (sp^3-B atom), 36.5 (sp^2-B atom) ppm.

HRMS-ASAP (m/z): calculated (found) for $C_{19}H_{37}B_2N_2O_4$ $[M+H]^+$ 379.2934 (379.2930).

*i*Pr$_2$Im^{Me}·B$_2$pin$_2$ 21

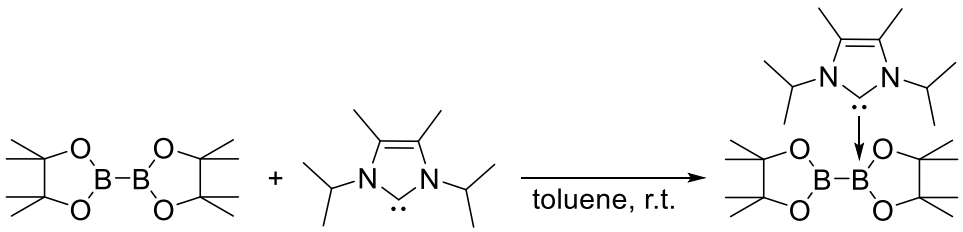

B_2pin_2 (1.00 g, 3.94 mmol, 1.0 equiv.) and *i*Pr_2Im^{Me} (710 mg, 3.94 mmol, 1.0 equiv.) were dissolved in toluene (20 mL). After stirring the reaction mixture overnight at room temperature, the solvent was removed under reduced pressure. The residue was suspended in *n*-hexane (10 mL), collected by filtration and dried *in vacuo*.

Yield: 1.56 g (3.59 mmol, 91%) of a colorless solid.

Elemental analysis for $C_{23}H_{44}B_2N_2O_4$ [434.24 g/mol]: calculated (found) C 63.62 (63.68), H 10.21 (10.28), N 6.45 (6.18).

^{1}H NMR (400 MHz, 25 °C, C_6D_6): δ = 1.25 (s, 24H, pin-C*H*$_3$), 1.31 (d, $^{3}J_{HH}$ = 7 Hz, 12H, *i*Pr-C*H*$_3$), 1.60 (s, 6H, NC(C*H*$_3$)), 6.23 (br, 2H, *i*Pr-C*H*) ppm.

^{13}C{^{1}H} NMR (100 MHz, 25 °C, C_6D_6): δ = 10.1 (NC(*C*H$_3$)), 21.9 (*i*Pr-*C*H$_3$), 25.7 (pin-C*H*$_3$), 48.5 (*i*Pr-*C*H), 79.8 (pin-*C*$_q$), 123.7 (N*CC*N), 169.8 (N*C*N) ppm.

^{11}B{^{1}H} NMR (128 MHz, 25 °C, C_6D_6): δ = 21.3 (br, B–B atom) ppm.

^{11}B NMR (160 MHz, 0 °C, d_8-toluene): δ = 2.91 (sp^3-B atom), 36.9 (sp^2-B atom) ppm.

HRMS-ASAP (m/z): calculated (found) for $C_{23}H_{45}B_2N_2O_4$ $[M+H]^+$ 435.3560 (435.3556).

*i*Pr$_2$Im^{Me}·B$_2$(OMe)$_4$ 22

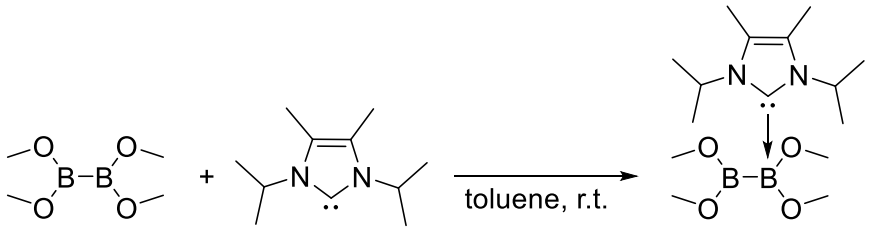

$B_2(OMe)_4$ (124 µL, 110 mg, 755 µmol, 1.1 equiv.) was added to a solution of *i*Pr$_2$Im^{Me} (123.7 mg, 686 µmol, 1.0 equiv.) in toluene (5 mL). After stirring the reaction mixture for 2 h at room temperature, all volatiles were removed under reduced pressure. The residue was suspended in *n*-hexane (3 mL), collected by filtration and dried *in vacuo*.

Yield: 96.2 mg (340 µmol, 45%) of a colorless solid.

For X-ray diffraction: Single-crystals suitable for X-ray diffraction were obtained by slow evaporation of the solvent of a saturated solution of *i*Pr$_2$Im^{Me}·B$_2$(OMe)$_4$ in benzene.

Elemental analysis for $C_{15}H_{32}B_2N_2O_4$ [326.05 g/mol]: calculated (found) C 55.26 (55.30), H 9.89 (9.89), N 8.59 (8.40).

^{1}H NMR (500 MHz, 25 °C, C_6D_6): δ = 1.30 (d, $^{3}J_{HH}$ = 6.3 Hz, 12H, *i*Pr-C*H*$_3$), 1.65 (s, 6H, NC(C*H*$_3$)), 3.75 (br, 12H, OC*H*$_3$), 6.22 (br, 2H, *i*Pr-C*H*) ppm.

^{13}C{^{1}H} NMR (125 MHz, 25 °C, C_6D_6): δ = 10.1 (NC(*C*H$_3$)), 22.3 (*i*Pr-*C*H$_3$), 48.2 (*i*Pr-*C*H), 51.3 (O*C*H$_3$), 123.7 (N*CC*N), 166.2 (N*C*N) ppm.

^{11}B{^{1}H} NMR (160 MHz, 25 °C, C_6D_6): δ = 4.05 (sp^3-B atom), 35.0 (sp^2-B atom) ppm.

$Cy_2Im{\cdot}B_2(OMe)_4$ 23

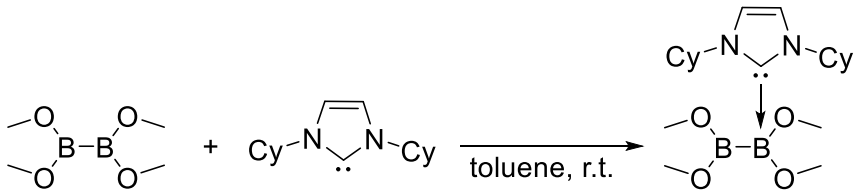

$B_2(OMe)_4$ (90.8 µL, 80.8 mg, 554 µmol, 1.1 equiv.) was added to a solution of Cy_2Im (117 mg, 504 µmol, 1.0 equiv.) in toluene (4 mL). After stirring the reaction mixture for 2 h at room temperature, all volatiles were removed under reduced pressure. The residue was suspended in *n*-hexane (5 mL), collected by filtration and dried *in vacuo*.

Yield: 93.4 mg (247 µmol, 49%) of a white solid.

Elemental analysis for $C_{19}H_{36}B_2N_2O_4$ [378.13 g/mol]: calculated (found) C 60.35 (60.68), H 9.60 (9.61), N 7.41 (7.48).

^{1}H NMR (400 MHz, 25 °C, C_6D_6): δ = 0.94-2.05 (m, 20H, Cy-CH_2), 3.78 (br, 12H, OCH_3), 5.81 (br, 2H, N-C*H*), 6.37 (s, 2H, NC*H*C*H*N) ppm.

^{13}C{^{1}H} NMR (125 MHz, 25 °C, C_6D_6): δ = 25.8 (Cy-*C*H_2), 26.0 (Cy-*C*H_2), 34.5 (Cy-*C*H_2), 51.3 (O*C*H_3), 56.1 (N-*C*H), 116.0 (N*CC*N), 167.3 (N*C*N) ppm.

^{11}B{^{1}H} NMR (128 MHz, 25 °C, C_6D_6): δ = 4.34 (sp^3-B atom), 36.4 (sp^2-B atom) ppm.

HRMS-ASAP (m/z): calculated (found) for $C_{19}H_{35}B_2N_2O_4$ $[M-H]^+$ 377.2777 (377.2772).

$(Cy_2Im)_2{\cdot}B_2cat_2$ 24

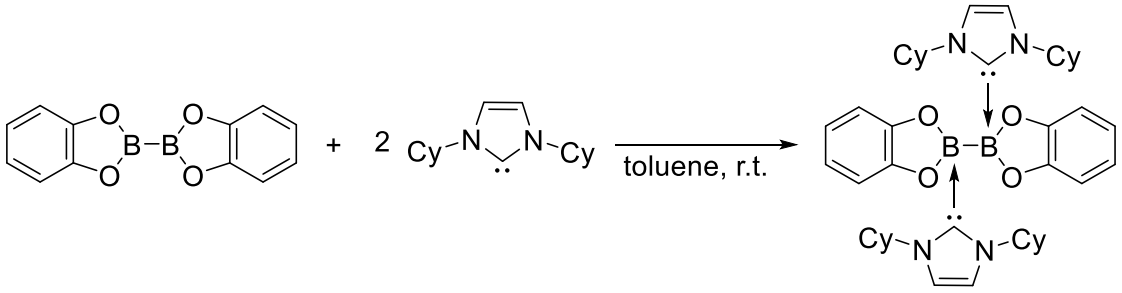

B_2cat_2 (150 mg, 631 µmol, 1.0 equiv.) and Cy_2Im (293 mg, 1.26 mmol, 2.0 equiv.) were dissolved in toluene (15 mL) and stirred overnight at room temperature. The solid that precipitated was collected by filtration and washed with toluene (5 mL) and *n*-hexane (5 mL).

Yield: 328 mg (467 mmol, 74%) of a colorless solid.

Elemental analysis for $C_{42}H_{56}B_2N_4O_4$ [702.55 g/mol]: calculated (found) C 71.80 (72.01), H 8.03 (8.29), N 7.97 (8.04).

^{13}C CP/MAS NMR (100 MHz, 25 °C): δ = 26.0 (Cy-*C*H$_2$), 27.7(Cy-*C*H$_2$), 34.4 (Cy-*C*H$_2$), 57.7 (N-*C*H), 108.2 (cat-*C*H), 108.7 (cat-*C*H), 115.7 (cat-*C*H), 116.8 (cat-*C*H), 118.4 (N*C*CN), 156.6 (cat-*C*$_q$), 157.2 (cat-*C*$_q$), 164.5 (br, N*C*N) ppm.

^{11}B RSHE/MAS NMR (128 MHz, 25 °C): δ_{iso} = 12.4 ± 0.1 ppm, CQ_{quad} = 2253 ± 10 kHz, η_{quad} = 0.42.

^{15}N CP/MAS NMR (40 MHz, 25 °C): δ = -182.1 ppm.

HRMS-ASAP (m/z): calculated (found) for $C_{42}H_{57}B_2N_4O_4$ $[M+H]^+$ 703.4560 (703.4544).

(*i*Pr$_2$Im^{Me})$_2$·B$_2$cat$_2$ 25

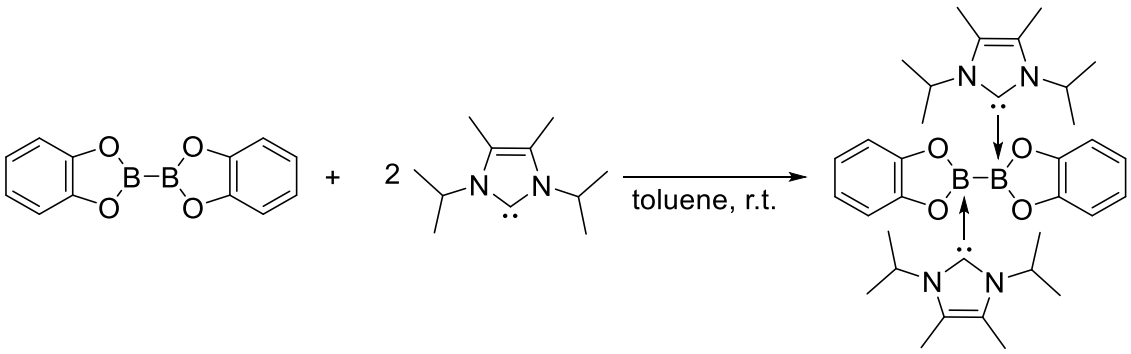

B$_2$cat$_2$ (150 mg, 631 µmol, 1.0 equiv.) and *i*Pr$_2$Im^{Me} (227 mg, 1.26 mmol, 2.0 equiv.) were dissolved in toluene (15 mL) and stirred overnight at room temperature. The white solid that precipitated was collected by filtration and washed with toluene (3 mL) and *n*-hexane (6 mL).

Yield: 317 mg (530 mmol, 84%) of a colorless solid.

For X-ray diffraction: Single-crystals suitable for X-ray diffraction were obtained by slow evaporation of the solvent of a saturated solution of (*i*Pr$_2$Im^{Me})$_2$·B$_2$cat$_2$ in benzene.

Elemental analysis for $C_{34}H_{48}B_2N_4O_4$ [598.40 g/mol]: calculated (found) C 68.24 (70.98), H 8.09 (8.23), N 9.36 (7.99). Although this elemental analysis results are outside the range viewed as established for analyzed purity, they are provided to illustrate the best values obtained to date. Notably, a significant amount of toluene still

remains in the final product (not removable under reduced pressure or by washing with *n*-hexane). Taking the amount of one solvent molecule of toluene into account (determined by the integration of the ^{1}H NMR spectrum), the elemental analysis results match the calculation; for $C_{34}H_{48}B_2N_4O_4$ + (toluene) C_7H_8: calculated (found) C 71.31 (70.98), H 8.17 (8.23), N 8.11 (7.99).

^{1}H NMR (300 MHz, 25 °C, C_6D_6): δ = 1.35 (d, $^{3}J_{HH}$ = 7.2 Hz, 24H, *i*Pr-C*H*$_3$), 1.48 (s, 12H, NC(C*H*$_3$)), 6.27 (sept, $^{3}J_{HH}$ = 7.2 Hz, 4H, *i*Pr-C*H*), 6.78 (m, 4H, cat-C*H*), 6.90 (m, 4H, cat-C*H*) ppm.

^{13}C{^{1}H} NMR (75 MHz, 25 °C, C_6D_6): δ = 10.2 (NC(*C*H$_3$)), 22.1 (*i*Pr-*C*H$_3$), 49.9 (*i*Pr-*C*H), 108.6 (cat-*C*H), 117.8 (cat-*C*H), 124.2 (N*C*CN), 156.2 (cat-*C*$_q$), 166.5 (N*C*N, assigned by increasing the line broadening parameter (lb 10)) ppm.

^{11}B{^{1}H} NMR (128 MHz, 25 °C, CD_2Cl_2): δ = 11.5 (sp^3-B) ppm.

HRMS-ASAP (m/z): calculated (found) for $C_{34}H_{49}B_2N_4O_4$ $[M+H]^+$ 599.3934 (599.3922).

Synthesis of NHC adducts of pinacolborane

Cy$_2$Im·HBpin 26

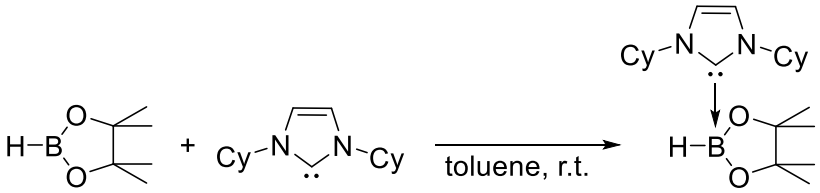

HBpin (227 µL, 200 mg, 1.56 mmol, 1.0 equiv.) was added to a solution of Cy$_2$Im (362 mg, 1.56 mmol, 1.0 equiv.) in toluene (7 mL). After stirring the reaction mixture for 2 h at room temperature, all volatiles were removed under reduced pressure. The residue was suspended in *n*-hexane (5 mL), collected by filtration and dried *in vacuo*.

Yield: 363 mg (1.01 mmol, 64%) of a colorless solid.

Elemental analysis for $C_{21}H_{37}BN_2O_2$ [360.35 g/mol]: calculated (found) C 70.00 (69.64), H 10.35 (10.42), N 7.77 (7.75).

^{1}H NMR (400 MHz, 25 °C, C_6D_6): δ = 0.88-2.03 (m, 20H, Cy-C*H*$_2$), 1.29 (s, 6H, pin-C*H*$_3$), 1.56 (s, 6H, pin-C*H*$_3$), 4.56 (q, $^{1}J_{BH}$ = 109 Hz, 1H, B*H*), 5.77 (m, 2H, N-C*H*), 6.31 (s, 2H, NC*H*C*H*N) ppm.

$^{13}C\{^{1}H\}$ NMR (100 MHz, 25 °C, C_6D_6): δ = 25.6 (pin-*C*H_3), 25.9 (Cy-*C*H_2), 25.9 (pin-*C*H_3), 31.5 (pin-C*H*$_3$), 34.1 (Cy-*C*H_2), 55.7 (N-*C*H), 78.2 (pin-*C*$_q$), 115.7 (N*CC*N), 166.8 (N*C*N) ppm.

^{11}B NMR (128 MHz, 25 °C, C_6D_6): δ = 2.50 (d, $^{1}J_{BH}$ = 109 Hz, sp_3-B atom, *B*H) ppm.

HRMS-ASAP (m/z): calculated (found) for $C_{21}H_{38}BN_2O_2$ $[M+H]^+$ 361.3021 (361.3014).

iPr$_2$Im^{Me}·HBpin 27

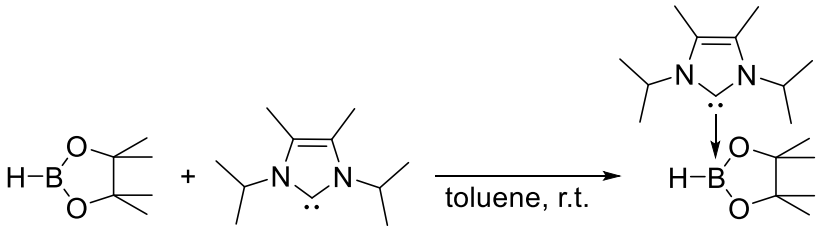

HBpin (227 µL, 200 mg, 1.56 mmol, 1.0 equiv.) was added to a solution of iPr$_2$Im^{Me} (281 mg, 1.56 mmol, 1.0 equiv.) in toluene (7 mL). After stirring the reaction mixture for 2 h at room temperature, all volatiles were removed under reduced pressure. The residue was suspended in *n*-hexane (5 mL), collected by filtration and dried *in vacuo*.

Yield: 226 mg (733 µmol, 47%) of a colorless solid.

Elemental analysis for $C_{17}H_{33}BN_2O_2$ [308.27 g/mol]: calculated (found) C 66.24 (66.00), H 10.79 (10.77), N 9.09 (8.72).

^{1}H NMR (500 MHz, 25 °C, C_6D_6): δ = 1.17 (d, $^{3}J_{HH}$ = 7.2 Hz, 12H, *i*Pr-C*H*$_3$), 1.36 (br, 6H, pin-C*H*$_3$), 1.57 (s, 6H, NC(C*H*$_3$)), 4.54 (q, $^{1}J_{BH}$ = 109 Hz, 1H, B*H*), 6.45 (br, 2H, *i*Pr-C*H*) ppm.

$^{13}C\{^{1}H\}$ NMR (125 MHz, 25 °C, C_6D_6): δ = 10.0 (NC(*C*H_3)), 21.5 (*i*Pr-*C*H_3), 25.5 (pin-C*H*$_3$), 26.1(pin-C*H*$_3$), 48.5 (*i*Pr-*C*H), 78.2 (pin-*C*$_q$), 123.9 (N*CC*N), 166.6 (N*C*N) ppm.

^{11}B NMR (160 MHz, 25 °C, C_6D_6): δ = 2.65 (d, $^{1}J_{BH}$ = 109 Hz, sp_3-B atom, *B*H) ppm.

HRMS-ASAP (m/z): calculated (found) for $C_{17}H_{34}BN_2O_2$ $[M+H]^+$ 309.2708 (309.2703).

Me_2Im^{Me}·HBpin 28

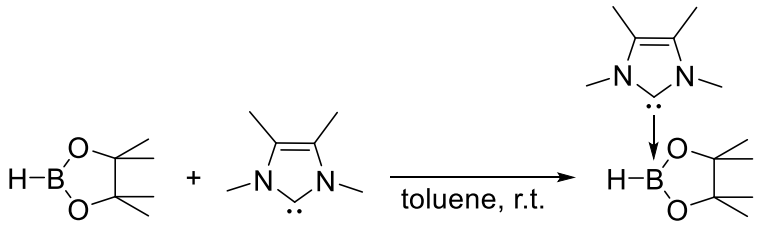

HBpin (227 µL, 200 mg, 1.56 mmol, 1.0 equiv.) was added to a solution of Me_2Im^{Me} (194 mg, 1.56 mmol, 1.0 equiv.) in toluene (7 mL). After stirring the reaction mixture for 2 h at room temperature, all volatiles were removed under reduced pressure. The residue was suspended in *n*-hexane (5 mL), collected by filtration and dried *in vacuo*.

Yield: 178 mg (706 µmol, 45%) of a pale yellow solid.

Elemental analysis for $C_{13}H_{25}BN_2O_2$ [252.17 g/mol]: calculated (found) C 61.92 (61.60), H 9.99 (9.80), N 11.11 (10.98).

^{1}H NMR (500 MHz, 25 °C, C_6D_6): δ = 1.15 (s, 6H, NC(C*H*$_3$)), 1.37 (s, 6H, pin-C*H*$_3$), 1.64 (s, 6H, pin-C*H*$_3$), 3.50 (s, 6H, NC*H*$_3$), 4.51 (q, $^1J_{BH}$ = 109 Hz, 1H, B*H*) ppm.

^{13}C{^{1}H} NMR (125 MHz, 25 °C, C_6D_6): δ = 7.5 (NC(*C*H$_3$)), 25.6 (pin-C*H*$_3$), 25.8 (pin-C*H*$_3$), 31.9 (NC*H*$_3$), 78.3 (pin-*C*$_q$), 123.1 (N*CC*N), 165.8 (N*C*N) ppm.

^{11}B NMR (160 MHz, 25 °C, C_6D_6): δ = 2.50 (d, $^1J_{BH}$ = 109 Hz, sp$_3$-B atom, *B*H) ppm.

HRMS-ASAP (m/z): calculated (found) for $C_{13}H_{26}BN_2O_2$ $[M+H]^+$ 253.2082 (253.2077).

$cAAC^{Me}$(H)Bpin 29

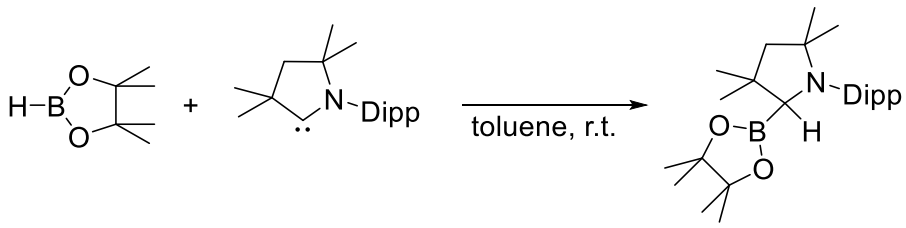

HBpin (102 µmol, 89.7 mg, 701 µmol, 1.0 equiv.) was added to a solution of $cAAC^{Me}$ (200 mg, 701 µmol, 1.0 equiv.) in toluene (10 mL). After stirring the reaction mixture for 2 h at room temperature, all volatiles were removed under reduced pressure. The residue was suspended in *n*-hexane (2 mL), collected by filtration and dried *in vacuo*.

Yield: 210 mg (508 µmol, 72%) of a colorless solid.

For X-ray diffraction: Single-crystals suitable for X-ray diffraction were obtained by slow evaporation of the solvent of a saturated solution of cAAC^{Me}(H)Bpin in benzene.

Elemental analysis for $C_{26}H_{44}BNO_2$ [413.45 g/mol]: calculated (found) C 75.53 (75.31), H 10.73 (10.54), N 3.39 (3.25).

^{1}H NMR (400 MHz, 25 °C, C_6D_6): δ = 0.75 (s, 6H, pin-C*H*$_3$), 0.89 (s, 6H, pin-C*H*$_3$), 1.17 (s, 3H, C*H*$_3$), 1.26 (d, $^3J_{HH}$ = 7.1 Hz, 3H, *i*Pr-C*H*$_3$), 1.30 (s, 3H, C*H*$_3$), 1.32 (s, 3H, C*H*$_3$), 1.39 (d, $^3J_{HH}$ = 7.1 Hz, 3H, *i*Pr-C*H*$_3$), 1.41 (d, $^3J_{HH}$ = 7.1 Hz, 3H, *i*Pr-C*H*$_3$), 1.43 (s, 3H, C*H*$_3$), 1.54 (d, $^3J_{HH}$ = 7.1 Hz, 3H, *i*Pr-C*H*$_3$), 1.79 (s, 2H, C*H*$_2$), 3.54 (sept, $^3J_{HH}$ = 7.1 Hz, 1H, *i*Pr-C*H*), 3.73 (s, 1H, C-*H*), 4.21 (sept, $^3J_{HH}$ = 7 Hz, 1H, *i*Pr-C*H*), 7.07-7.11 (m, 1H, aryl-C*H*), 7.17 (m, 1H, aryl-C*H*), 7.20-7.25(m, 1H, aryl-C*H*) ppm.

^{13}C{^{1}H} NMR (100 MHz, 25 °C, C_6D_6): δ = 24.0 (pin-*C*H$_3$), 25.2 (*i*Pr-*C*H$_3$), 25.4 (pin-*C*H$_3$), 25.5 (*i*Pr-*C*H$_3$), 25.7 (*i*Pr-*C*H$_3$), 25.8 (*i*Pr-*C*H$_3$), 27.2 (*C*H$_3$), 27.9 (*i*Pr-*C*H), 28.9 (*C*H$_3$), 29.2 (*C*H$_3$), 29.5 (*i*Pr-*C*H), 30.5 (*C*H$_3$), 40.4 (*C*$_q$(CH$_3$)$_2$), 59.0 (CH$_2$), 62.9 (br, *C*-Bpin), 63.4 (*C*$_q$(CH$_3$)$_2$), 82.8 (pin-*C*$_q$), 124.6 (aryl-*C*H), 124.7 (aryl-*C*H), 126.4 (aryl-*C*H), 140.7 (aryl-*C*$_q$), 150.7 (aryl-*C*$_q$), 153.1 (aryl-*C*$_q$) ppm.

^{11}B{^{1}H} NMR (128 MHz, 25 °C, C_6D_6): δ = 32.3 ppm.

HRMS-LIFDI (m/z): calculated (found) for $C_{26}H_{44}BNO_2$ $[M]^+$ 413.3460 (413.3456).

Synthesis of NHC Adducts of Aryl Boronic Esters

3,5-F$_2$C$_6$H$_3$Bpin·Cy$_2$Im 30

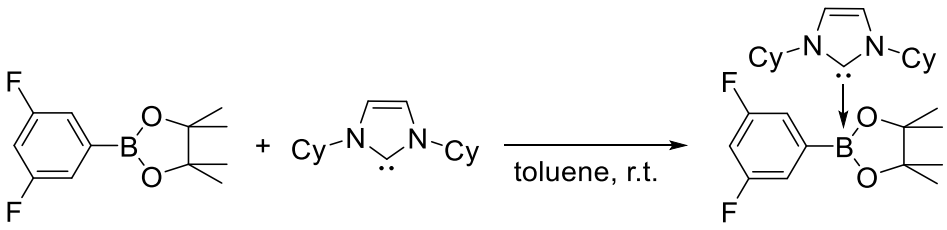

3,5-$F_2C_6H_3$Bpin (67.2 mg, 280 µmol, 1.0 equiv.) and Cy_2Im (65.1 mg, 280 µmol, 1.0 equiv.) were dissolved in toluene (2 mL). After stirring the reaction mixture overnight at room temperature, the solvent was removed under reduced pressure. The residue was suspended in *n*-hexane (5 mL), collected by filtration and dried *in vacuo*.

Yield: 56.0 mg (119 mmol, 42%) of a pale yellow solid.

Elemental analysis for $C_{27}H_{39}BF_2N_2O_2$ [472.43 g/mol]: calculated (found) C 68.64 (68.74), H 8.32 (8.37), N 5.93 (5.99).

^{1}H NMR (500 MHz, 25 °C, C_6D_6): δ = 0.85-1.77 (m, 20H, Cy-CH_2), 1.16 (s, 6H, pin-CH_3), 1.32 (s, 6H, pin-CH_3), 5.74 (m, 2H, N-CH), 6.16 (s, 2H, NCHCHN), 6.61 (m, 1H, aryl-CH_p), 7.49 (m, 2H, aryl-CH_o) ppm.

^{13}C{^{1}H} NMR (125 MHz, 25 °C, C_6D_6): δ = 25.5 (Cy-CH$_2$), 25.5 (Cy-CH$_2$), 25.8 (pin-CH$_3$), 26.4 (pin-CH$_3$), 34.2 (Cy-CH$_2$), 56.1 (N-CH), 79.3 (pin-C_q), 100.3 (t, $^2J_{CF}$ = 26 Hz, aryl-CH$_p$), 113.4 (dd, $^2J_{CF}$ = 16 Hz, $^4J_{CF}$ = 3 Hz, aryl-CH$_o$), 116.3 (NCCN), 161.7 (br, C_qB), 163.5 (dd, $^1J_{CF}$ = 248 Hz, $^3J_{CF}$ = 10 Hz, aryl-CF), 165.7 (NCN) ppm.

^{11}B{^{1}H} NMR (160 MHz, 25 °C, C_6D_6): δ = 4.02 ppm.

^{19}F{^{1}H} NMR (471 MHz, 25 °C, C_6D_6): δ = -112.9 ppm.

HRMS-ASAP (m/z): calculated (found) for $C_{27}H_{39}BF_2N_2O_2$ $[M]^+$ 472.3067 (472.3072).

4-CH_3-C_6H_4Bpin·Cy_2Im 31

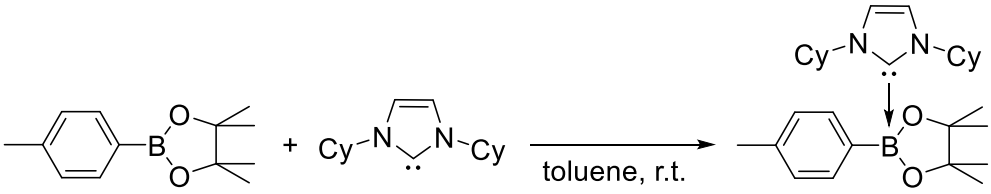

4-CH_3-C_6H_4Bpin (65.7 mg, 301 µmol, 1.0 equiv.) and Cy_2Im (70.0 mg, 301 µmol, 1.0 equiv.) were dissolved in toluene (2 mL). After stirring the reaction mixture for 1 h at room temperature, the solvent was removed under reduced pressure. The residue was suspended in *n*-hexane (5 mL), collected by filtration and dried *in vacuo*.

Yield: 68.9 mg (153 µmol, 51%) of a colorless solid.

Elemental analysis for $C_{28}H_{43}BN_2O_2$ [450.47 g/mol]: calculated (found) C 74.66 (74.63), H 9.62 (9.77), N 6.22 (6.24).

^{1}H NMR (500 MHz, 25 °C, C_6D_6): δ = 0.89-1.89 (m, 20H, Cy-CH_2), 1.31 (br, 12H, pin-CH_3), 2.27 (s, 3H, tolyl-CH_3), 5.90 (br, 2H, N-CH), 6.22 (s, 2H, NCHCHN), 7.25 (m, 2H, aryl-CH_m), 7.87 (m, 2H, aryl-CH_o) ppm.

$^{13}C\{^1H\}$ NMR (125 MHz, 25 °C, C_6D_6): δ = 21.6 (tolyl-*C*H_3), 25.6 (Cy-*C*H_2), 26.2 (pin-*C*H_3), 26.4 (pin-*C*H_3), 34.2 (Cy-*C*H_2), 55.9 (N-*C*H), 79.0 (pin-*C*$_q$), 116.0 (N*CC*N), 128.4 (aryl-*C*H_m), 132.1 (aryl-*C*H_o), 134.1 (br, aryl-*C*$_q$tolyl), 152.0 (br, *C*$_q$B), 168.3 (N*C*N) ppm.

$^{11}B\{^1H\}$ NMR (160 MHz, 25 °C, C_6D_6): δ = 4.88 ppm.

HRMS-ASAP (m/z): calculated (found) for $C_{28}H_{43}BN_2O_2$ $[M]^+$ 450.3412 (450.3413).

C_6H_5Bneop·Cy_2Im 32

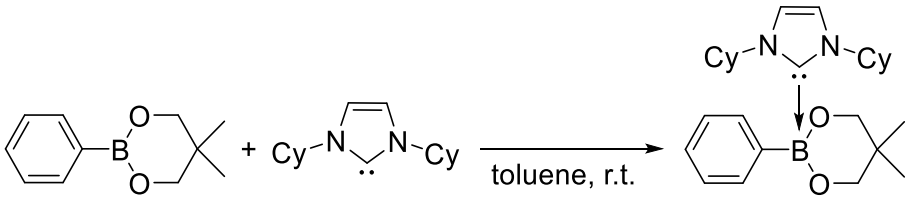

C_6H_5Bneop (65.0 mg, 342 µmol, 1.0 equiv.) and Cy_2Im (79.5 mg, 342 µmol, 1.0 equiv.) were dissolved in toluene (3 mL). After stirring the reaction mixture for 2 h at room temperature, the solvent was removed under reduced pressure. The residue was suspended in *n*-hexane (5 mL), collected by filtration and dried *in vacuo*.

Yield: 68.3 mg (162 µmol, 47%) of a colorless solid.

Elemental analysis for $C_{26}H_{39}BN_2O_4$ [422.42 g/mol]: calculated (found) C 73.93 (73.64), H 9.31 (9.33), N 6.63 (6.68).

^1H NMR (500 MHz, 25 °C, C_6D_6): δ = 0.90-1.88 (m, 20H, Cy-C*H*$_2$), 1.10 (s, 6H, neop-C*H*$_3$), 3.71 (s, 4H, neop-C*H*$_2$), 5.97 (m, 2H, N-C*H*), 6.32 (s, 2H, NC*H*C*H*N), 7.23 (m, 1H, aryl-C*H*$_p$), 7.40 (m, 2H, aryl-C*H*$_m$), 7.95 (m, 2H, aryl-C*H*$_o$) ppm.

$^{13}C\{^1H\}$ NMR (125 MHz, 25 °C, C_6D_6): δ = 23.4 (neop-*C*H_3), 25.6 (Cy-*C*H_2), 25.8 (Cy-*C*H_2), 33.2 (neop-*C*$_q$), 34.7 (Cy-*C*H_2), 56.0 (N-*C*H), 73.7 (neop-*C*H_2), 117.0 (N*CC*N), 126.0 (aryl-*C*H_p), 127.4 (aryl-*C*H_m), 132.6 (aryl-*C*H_o), 152.5 (br, aryl-*C*$_q$B), 165.8 (N*C*N) ppm.

$^{11}B\{^1H\}$ NMR (160 MHz, 25 °C, C_6D_6): δ = 2.94 ppm.

HRMS-ASAP (m/z): calculated (found) for $C_{26}H_{40}BN_2O_2$ $[M+H]^+$ 423.3177 (423.3164).

Biphenyl-Bneop·Cy$_2$Im 33

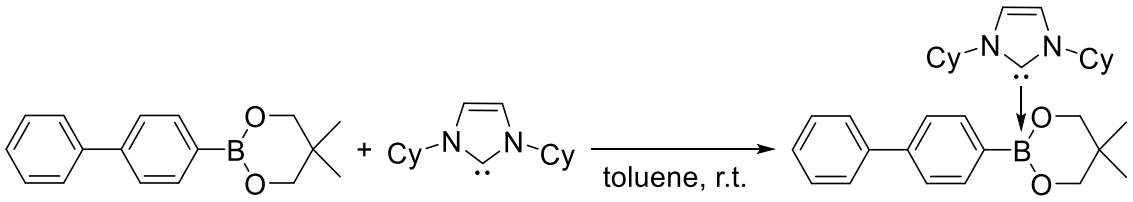

BiphenylBneop (70.0 mg, 263 µmol, 1.0 equiv.) and Cy$_2$Im (61.1 mg, 263 µmol, 1.0 equiv.) were dissolved in toluene (3 mL). After stirring the reaction mixture for 2 h at room temperature, the solvent was removed under reduced pressure. The residue was suspended in *n*-hexane (5 mL), collected by filtration and dried *in vacuo*.

Yield: 58.5 mg (117 µmol, 45%) of a colorless solid.

Elemental analysis for $C_{32}H_{43}BN_2O_4$ [498.52 g/mol]: calculated (found) C 77.10 (76.09), H 8.69 (8.92), N 5.62 (4.91). Although this elemental analysis results are outside the range viewed as established for analyzed purity, they are provided to illustrate the best values obtained to date.

^{1}H NMR (400 MHz, 25 °C, C_6D_6): δ = 0.90-1.92 (m, 20H, Cy-C*H*$_2$), 1.11 (s, 6H, neop-C*H*$_3$), 3.74 (s, 4H, neop-C*H*$_2$), 6.03 (m, 2H, N-C*H*), 6.35 (s, 2H, NC*H*C*H*N), 7.10 (m, 1H, aryl-C*H*$_p$), 7.20 (m, 2H, aryl-C*H*), 7.59 (m, 2H, aryl-C*H*), 7.68 (m, 2H, aryl-C*H*), 8.02 (m, 2H, aryl-C*H*) ppm.

^{13}C{^{1}H} NMR (100 MHz, 25 °C, C_6D_6): δ = 23.4 (neop-*C*H$_3$), 25.6 (Cy-*C*H$_2$), 25.8 (Cy-*C*H$_2$), 33.2 (neop-*C*$_q$), 34.8 (Cy-*C*H$_2$), 56.1 (N-*C*H), 73.7 (neop-*C*H$_2$), 117.1 (N*CC*N), 126.2 (aryl-*C*H), 126.6 (aryl-*C*H), 127.4 (aryl-*C*H), 128.9 (aryl-*C*H), 133.1 (aryl-*C*H), 138.8 (aryl-*C*$_q$), 142.9 (aryl-*C*$_q$), 151.7 (br, aryl-*C*$_q$B), 165.6 (N*C*N) ppm.

^{11}B{^{1}H} NMR (128 MHz, 25 °C, C_6D_6): δ = 3.29 ppm.

HRMS-ASAP (m/z): calculated (found) for $C_{32}H_{44}BN_2O_2$ $[M+H]^+$ 499.3490 (499.3481).

4-CF_3-C_6H_4Bpin·Me_2Im^{Me} 34

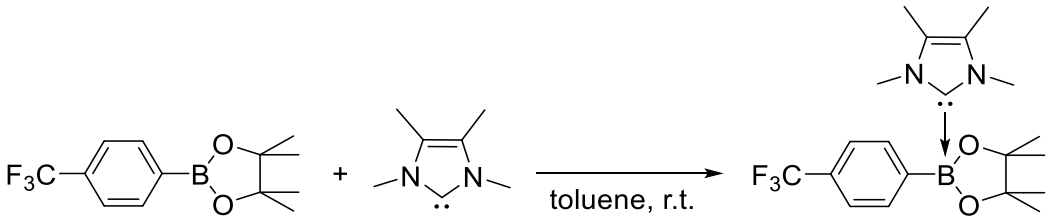

4-CF_3-C_6H_4Bpin (219 mg, 805 µmol, 1.0 equiv.) and Me_2Im^{Me} (100 mg, 805 µmol, 1.0 equiv.) were dissolved in toluene (5 mL). After stirring the reaction mixture overnight at room temperature, the solvent was removed under reduced pressure. The residue was suspended in *n*-hexane (8 mL), collected by filtration and dried *in vacuo*.

Yield: 218 mg (550 µmol, 68%) of a colorless solid.

Elemental analysis for $C_{20}H_{28}BF_3N_2O_2$ [396.22 g/mol]: calculated (found) C 60.62 (60.87), H 7.12 (7.23), N 7.07 (7.04).

^{1}H NMR (400 MHz, 25 °C, C_6D_6): δ = 1.12 (s, 6H, NC(C*H*)$_3$), 1.25 (s, 6H, pin-C*H*$_3$), 1.39 (s, 6H, pin-C*H*$_3$), 3.50 (s, 6H, NC*H*$_3$), 7.68 (m, 2H, aryl-C*H*$_m$), 7.96 (s, 2H, aryl-C*H*$_o$) ppm.

^{13}C{^{1}H} NMR (125 MHz, 25 °C, C_6D_6): δ = 7.6 (NC(*C*H$_3$)), 25.5 (pin-*C*H$_3$), 26.5 (pin-*C*H$_3$), 32.3 (N*C*H$_3$), 79.4 (pin-*C*$_q$), 123.7 (N*CC*N), 123.9 ($^3J_{CF}$ = 3.3 MHz, aryl-*C*H$_m$), 126.2 ($^1J_{CF}$ = 271 MHz, *C*F$_3$), 127.6 ($^2J_{CF}$ = 31 MHz, *C*$_q$CF$_3$), 132.1 (aryl-*C*H$_o$), 160.8 (br, *C*$_q$B), 165.7 (N*C*N) ppm.

^{11}B{^{1}H} NMR (128 MHz, 25 °C, C_6D_6): δ = 4.13 ppm.

^{19}F{^{1}H} NMR (376 MHz, 25 °C, C_6D_6): δ = -61.4 ppm.

HRMS-ASAP (m/z): calculated (found) for $C_{20}H_{28}BF_3N_2O_2$ $[M]^+$ 396.2190 (396.2189).

General Procedures for the Reaction of 20 with Aryl Halides

Method A

In a Young's tap NMR tube $Me_2Im^{Me}{\cdot}B_2pin_2$ **20** (70.8 mg, 187 µmol, 2.5 equiv.; 3.0 equiv. when using **4-I**/**4-Br** as the aryl halide) was dissolved in C_6D_6 (0.7 mL) and the aryl halide (62.4 µmol, 1.0 equiv.) was added at room temperature. The reaction mixture was stirred for 16 h at 50 °C or 80 °C. Afterwards, the products and yields were determined by ^{1}H NMR spectroscopy and GC-MS with biphenyl as an internal standard.

Method B

This method was performed on a preparative scale: $Me_2Im^{Me}{\cdot}B_2pin_2$ **20** (531 mg, 1.40 mmol, 2.5 equiv.; 3.0 equiv. when using **4-I** as the aryl iodide) was dissolved in benzene (7 mL) and the aryl iodide (467 µmol, 1.0 equiv.) was added at room temperature. The reaction mixture was stirred for 16 h at 50 °C and was then filtered, and the remaining solid was washed with diethyl ether (10 mL). The filtrate was concentrated *in vacuo*, purified by silica-gel column chromatography with *n*-hexane and then an *n*-hexane and ethyl acetate mixture (*n*-hexane/EtOAc =100/1) as eluent. The solvent of the product-containing fraction of the eluent was evaporated *in vacuo.*

For reasons of comparability the NMR data of the borylation products **4**-**6** are again shown recorded in C_6D_6 (for NMR of **4**-**6** recorded in CD_2Cl_2 see chapter 5.3)

2-(4-Trifluoromethyl-phenyl)-4,4,5,5-tetramethyl-[1,3,2]dioxaborolane 4

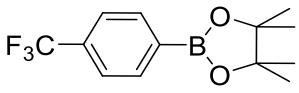

The reaction was performed on a preparative scale using method B with 4-iodobenzotrifluoride **4-I** (127 mg, 467 µmol), which afforded 55.9 mg (205 µmol, 44%) of **4** as a pale yellow solid after workup.

^{1}H NMR (400 MHz, 25 °C, C_6D_6): 1.08 (s, 12H, C*H*$_3$), 7.37 (d, 2H, $^3J_{HH}$ = 7.6 Hz, aryl-C*H*$_m$), 7.95 (d, 2H, $^3J_{HH}$ = 7.6 Hz, aryl-C*H*$_o$) ppm.

$^{13}C\{^{1}H\}$ NMR (100 MHz, 25 °C, C_6D_6): 24.9 (*C*H_3), 84.2 (pin-*C*$_q$), 124.7 ($^{1}J_{CF}$ = 272 Hz, *C*F_3), 124.7 ($^{3}J_{CF}$ = 3.8 Hz, aryl-*C*H_m), 133.2 ($^{2}J_{CF}$ = 32 Hz, aryl-*C*$_q$$CF_3$), 135.6 (aryl-*C*$H_o$) ppm.

$^{11}B\{^{1}H\}$ NMR (128 MHz, 25 °C, C_6D_6): 30.7 ppm.

$^{19}F\{^{1}H\}$ NMR (376 MHz, 25 °C, C_6D_6): -62.7(s) ppm.

GC-MS: Ret.: 7.27 min; m/z: 272 $[M]^+$, 257 $[M\text{-}CH_3]^+$, 186 $[M\text{-}C_5H_{10}O]^+$, 173 $[M\text{-}C_6H_{11}O]^+$.

HRMS-ASAP (m/z): Calculated (found) for $C_{13}H_{17}BF_3O_2$ $[M+H]^+$ 273.1268 (273.1255).

The spectroscopic data for **4** match those reported in the literature.[34, 256]

2-(4-Methyl-phenyl)-4,4,5,5-tetramethyl-[1,3,2]dioxaborolane 5

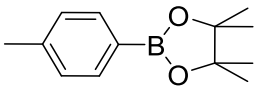

The reaction was performed on a preparative scale using method B with 4-iodotoluene **5-I** (102 mg, 467 µmol), which afforded 86.6 mg (397 µmol, 85%) of **5** as a colorless solid after workup.

^{1}H NMR (400 MHz, 25 °C, C_6D_6): 1.13 (s, 12H, pin-C*H*$_3$), 2.07 (s, 3H, tolyl-C*H*$_3$), 7.05 (d, 2H, $^{3}J_{HH}$ = 7.7 Hz, aryl-C*H*$_m$), 8.11 (d, 2H, $^{3}J_{HH}$ = 7.7 Hz, aryl-C*H*$_o$) ppm.

$^{13}C\{^{1}H\}$ NMR (100 MHz, 25 °C, C_6D_6): 21.7 (tolyl-*C*H_3), 25.0 (pin-*C*H_3), 83.6 (pin-*C*$_q$), 129.0 (aryl-*C*H_m), 135.6 (aryl-*C*H_o) 141.5 (aryl-*C*$_q$tolyl) ppm.

$^{11}B\{^{1}H\}$ NMR (128 MHz, 25 °C, C_6D_6): 31.2 ppm.

GC-MS: Ret.: 8.06 min; m/z: 218 $[M]^+$, 203 $[M\text{-}CH_3]^+$, 132 $[M\text{-}C_5H_{10}O]^+$, 119 $[M\text{-}C_6H_{11}O]^+$.

HRMS-ASAP (m/z): Calculated (found) for $C_{13}H_{20}BO_2$ $[M+H]^+$ 219.1551 (219.1548).

The spectroscopic data for **5** match those reported in the literature.[118, 122]

4-Methyl-1,1'-bipehnyl 5a-H

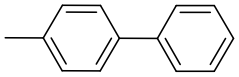

^{1}H NMR (400 MHz, 25 °C, $CDCl_3$): δ = 2.40 (s, 3H, C*H*$_3$), 7.26 (m, 2H, aryl-C*H*), 7.33 (m, 1H, aryl-C*H*), 7.43 (m, 2H, aryl-C*H*), 7.50 (m, 2H, aryl-C*H*), 7.59 (m, 2H, aryl-C*H*) ppm.

^{13}C{^{1}H} NMR (100 MHz, 25 °C, $CDCl_3$): δ = 21.2 (*C*H$_3$), 127.1 (aryl-*C*H), 127.1 (aryl-*C*H), 128.8 (aryl-*CH*), 129.6 (aryl-*C*H), 137.2 (aryl-*C*$_q$), 138.5 (aryl-*C*$_q$), 141.3 (aryl-*C*$_q$) ppm.

HRMS-ASAP (m/z): calculated (found) for $C_{13}H_{13}$ $[M+H]^+$ 169.1012 (169.1008).

The spectroscopic data for **5a-H** match those reported in the literature.[259]

4'-Methyl-1,1'-biphenyl-2,3,4,5,6-d$_5$ 5a

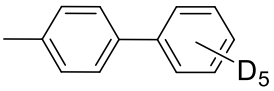

^{1}H NMR (500 MHz, 25 °C, CD_2Cl_2): δ = 2.39 (s, 3H, C*H*$_3$), 7.26 (m, 2H, aryl-C*H*), 7.51 (m, 2H, aryl-C*H*) ppm.

^{13}C{^{1}H} NMR (100 MHz, 25 °C, CD_2Cl_2): δ = 21.2 (*C*H$_3$), 126.6 (aryl-*C*D), 126.9 (aryl-*C*D), 127.2 (aryl-*CH*), 128.6 (aryl-*C*D), 129.9 (aryl-*C*H), 137.6 (aryl-*C*$_q$), 138.5 (aryl-*C*$_q$), 141.2 (aryl-*C*$_q$) ppm.

HRMS-ASAP (m/z): calculated (found) for $C_{13}H_8D_5$ $[M+H]^+$ 174.1326 (174.1320).

The spectroscopic data for **5a** match those reported in the literature.[260]

2-(4-Methoxy-phenyl)-4,4,5,5-tetramethyl-[1,3,2]dioxaborolane 6

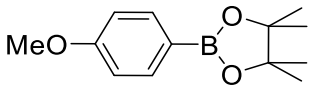

The reaction was performed on a preparative scale using method B with 4-iodoanisole **6-I** (109 mg, 467 µmol), which afforded 89.6 mg (383 µmol, 82%) of **6** as a pale yellow solid after workup.

^{1}H NMR (400 MHz, 25 °C, C_6D_6): 1.14 (s, 12H, pin-C*H*$_3$), 3,24 (s, 3H, OC*H*$_3$), 6.83 (m, 2H, $^{3}J_{HH}$ = 8.7 Hz, aryl-C*H*$_m$), 8.12 (m, 2H, $^{3}J_{HH}$ = 8.7 Hz, aryl-C*H*$_o$) ppm.

^{13}C{^{1}H} NMR (100 MHz, 25 °C, C_6D_6): 25.0 (pin-*C*H$_3$), 54.6 (O*C*H$_3$), 83.5 (*C*$_q$-pin), 113.8 (aryl-*C*H$_m$), 137.2 (aryl-*C*H$_o$) 162.9 (aryl-*C*$_q$OCH$_3$) ppm.

^{11}B{^{1}H} NMR (128 MHz, 25 °C, C_6D_6): 31.1 ppm.

GC-MS: Ret.: 9.01 min; m/z: 234 $[M]^+$, 219 $[M\text{-}CH_3]^+$, 148 $[M\text{-}C_5H_{10}O]^+$, 134 $[M\text{-}C_6H_{11}O]^+$.

HRMS-ASAP (m/z): Calculated (found) for $C_{13}H_{20}BO_3$ $[M+H]^+$ 235.1500 (235.1489).

The spectroscopic data for **6** match those reported in the literature.[118]

5.6 MECHANISTIC INVESTIGATIONS FOR CHAPTER 4

Monitoring the RER by EPR spectroscopy

Via a standard solution, B_2neop_2 (115 µg, 1.00 µmol, 1.0 equiv.) and Me_2Im^{Me} (125 µg, 0.50 µmol, 2.0 equiv.) were dissolved in THF (160 µL) and immediately cooled to -196 °C (liquid N_2). The EPR monitoring was started at -80 °C, and the temperature was slowly raised. A signal was detected at 16.9 °C (see Figure 4.22, main text, chapter 4.5).

RER in styrene to initiate radical polymerization reaction

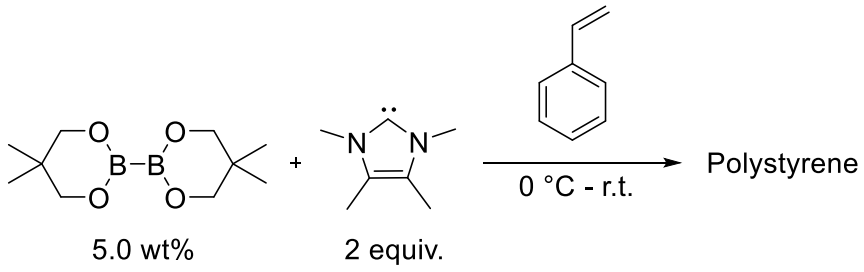

In a Schlenk tube, B_2neop_2 (62.5 mg, 277 µmol, 5.0 wt%, based on styrene) and Me_2Im^{Me} (62.5 mg, 554 µmol, 2.0 equiv., based on B_2neop_2) was combined in precooled (0 °C) styrene. (1.25 g, 1.40mL, 12.0 mmol) The reaction mixture was allowed to slowly warm to room temperature and was stirred for 16 h. All volatiles were removed under reduced pressure, the residue was dissolved in THF and poured in 50 mL of methanol. The colorless precipitate was analyzed by GPC (see Figure 4.26, main text, chapter 4.5)

Monitoring the boryl transfer reaction by EPR spectroscopy

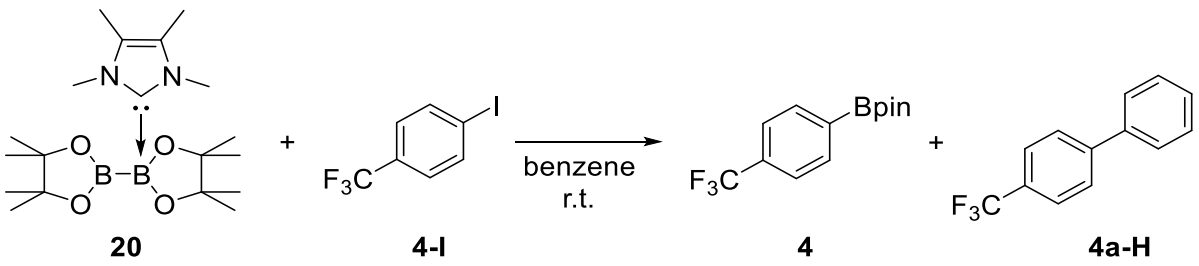

Via a standard solution, $Me_2Im^{Me}{\cdot}B_2pin_2$ **20** (1.70 mg, 4.50 µmol, 3.0 equiv.) and 4-iodobenzotrifluoride **4-I** (408 µg, 1.50 µmol, 1.0 equiv.) were dissolved in benzene (160 µL) at room temperature. The reaction mixture was immediately monitored by EPR spectroscopy at room temperature (see Figure 4.27, main text, chapter 4.5).

Boryl transfer reaction in styrene to initiate radical polymerization reaction

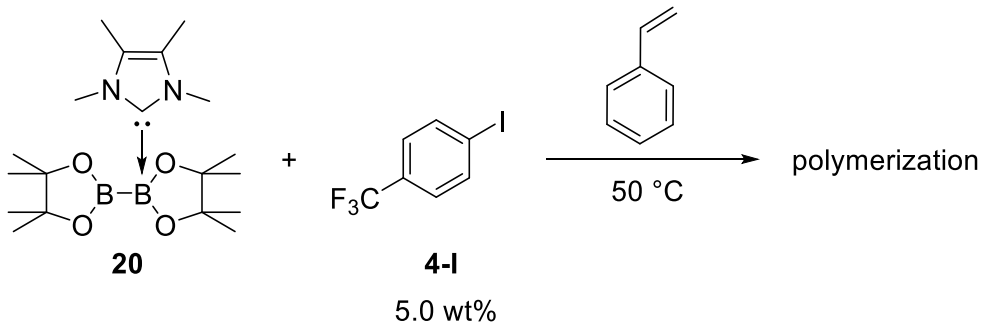

20 **4-I**

5.0 wt%

In a Schlenk tube, $Me_2Im^{Me}{\cdot}B_2pin_2$ **20** (261 mg, 690 µmol, 3.0 equiv., based on **4-I**) was dissolved in styrene (1.25 g, 1.40mL, 12.0 mmol) and 4-iodobenzotrifluoride **4-I** (62.5 mg, 33.8 µL, 230 µmol, 5.0 wt%., based on styrene) was added at room temperature. The reaction mixture was stirred for 16 h at 50 °C. All volatiles were removed under reduced pressure, the residue was dissolved in THF and poured in 50 mL of methanol. The colorless precipitate was analyzed by GPC (see Figure 4.28, main text, chapter 4.5)

Analyzing the precipitate formed during the boryl transfer reaction

$Me_2Im^{Me}{\cdot}B_2pin_2$ **20** (150 mg, 397 µmol, 3.0 equiv.) was dissolved in C_6D_6 (2 mL) and 4-iodobenzotrifluoride **4-I** (36.0 mg, 132 µmol, 1.0 equiv.) was added at room temperature and the reaction mixture was stirred for 16 h at 50 °C. The precipitate formed during the reaction was collected by filtration and dried *in vacuo* (45.9 mg). It was dissolved in chloroform/$CDCl_3$ and analyzed by GC-MS and NMR spectroscopy. While the GC-MS only showed traces of the aryl boronate **4** and B_2pin_2, the ^1H NMR spectrum additionally revealed the formation of two other species (Figure 4.29). In the corresponding ^{11}B NMR spectrum only one significant signal was observed with a chemical shift of 1.77 ppm which, together with HRMS and X-ray analysis, was assigned to the boronium cation $[(Me_2Im^{Me})_2{\cdot}Bpin]^+ I^-$ **37**.

[(Me$_2$Im^{Me})$_2$·Bpin]$^+$ I$^-$ 37

^{1}H NMR (400 MHz, 25 °C, $CDCl_3$): 0.99 (s, 12H, pin-C*H*$_3$), 2,16 (s, 12H, NC(C*H*)$_3$), 3.83 (s, 12H, NC*H*$_3$) ppm.

^{11}B{^{1}H} NMR (128 MHz, 25 °C, $CDCl_3$): 1.77 ppm.

HRMS-ESI pos (m/z): Calculated (found) for $C_{20}H_{36}BN_4O_2$ $[M]^+$ 375.2926 (375.2919). **HRMS-ESI neg** (m/z): Calculated (found) for I $[M]^-$ 126.9050 (126.9038).

Reaction of Me$_2$Im^{Me} with 4-iodotoluene **5-I**

Me$_2$Im^{Me} (41.7 mg, 33.6 µmol, 1.0 equiv.) and 4-iodotoluene **5-I** (73.2 mg, 33.6 µmol, 1.0 equiv.) were dissolved in benzene (2 mL). and stirred for 16 h at 80 °C. The precipitate that formed during the reaction was collected by filtration, and the filtrate was concentrated *in vacuo*, and purified by silica-gel column chromatography with *n*-hexane as eluent. The solvent of the product-containing fraction of the eluent was evaporated *in vacuo.* The product was identified as the C–C coupling product with the solvent **5a-H** in an isolated yield of 26%.

The precipitate that formed during the reaction was washed with benzene (5 mL) and dried *in vacuo*. NMR analysis revealed the formation of the imidazolium salt [4-CH_3-C_6H_4-Me$_2$Im^{Me}]$^+$I$^-$ **38**, which was confirmed by HRMS.

[4-CH_3-C_6H_4-Me$_2$Im^{Me}]$^+$I$^-$ 38

^{1}H NMR (400 MHz, 25 °C, $CDCl_3$): δ = 2.24 (s, 6H, NC(C*H*$_3$)), 2.44 (s, 24H, tolyl-C*H*$_3$), 3.61 (s, 6H, NC*H*$_3$), 7.40 (d, 2H, $^3J_{HH}$ = 7.9 Hz, aryl-C*H*$_m$), 7.59 (d, 2H, $^3J_{HH}$ = 7.9 Hz, aryl-C*H*$_o$) ppm.

^{13}C{^{1}H} NMR (100 MHz, 25 °C, $CDCl_3$): δ = 9.7 (NC(*C*H$_3$)), 21.7 (tolyl-*C*H$_3$), 33.9 (N*C*H$_3$), 118.7 (aryl-*C*$_i$), 127.1 (N*CC*N), 130.6 (aryl-*C*H$_m$), 130.9 (aryl-*C*H$_o$), 143.3. (aryl-*C*$_q$tolyl), 143.6 (N*C*N) ppm.

HRMS-ESI pos (m/z): Calculated (found) for $C_{14}H_{19}N_2$ $[M]^+$ 215.1543 (215.1537). **HRMS-ESI neg** (m/z): Calculated (found) for I $[M]^-$ 126.9050 (126.9038).

Stoichiometric reaction of Me_2Im^{Me} with 4-iodobenzotrifluoride **4-I** in the presence of TEMPO

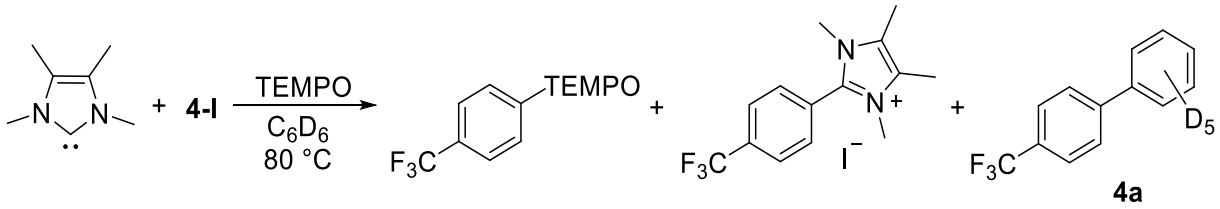

In a Young's tap NMR tube Me_2Im^{Me} (6.3 mg, 51.1 µmol, 1.0 equiv.) and TEMPO (8.0 mg, 51.1 µmol, 1.0 equiv.) were dissolved in C_6D_6 (0.7 mL) and 4-iodobenzotrifluoride **4-I** (13.9 mg, 7.5 µL, 51.1 µmol, 1.0 equiv.) was added at room temperature. The reaction mixture was stirred for 16 h at 80 °C. Besides the imidazolium salt [4-CF_3-C_6H_4-Me_2Im^{Me}]$^+I^-$, and traces of the C–C coupling product **4a**, GC-MS analysis indicated the formation of trace amounts of the coupling product aryl–TEMPO.

Boryl transfer reaction in the presence of TEMPO

In a Young's tap NMR tube Me_2Im^{Me}·B_2pin_2 **20** (50.0 mg, 132 µmol, 3.0 equiv.) and TEMPO (6.9 mg, 44.1 µmol, 1.0 equiv.) were dissolved in C_6D_6 (0.7 mL) and 4-iodobenzotrifluoride **4-I** (12.0 mg, 6.5 µL, 44.1 µmol, 1.0 equiv.) was added at room temperature. The reaction mixture was stirred for 16 h at 80 °C. Besides residual starting material **4-I**, aryl boronate **4** and the C–C coupling product **4a**, GC-MS analysis indicated the formation of the coupling product aryl–TEMPO (see Figure 4.35, main text, chapter 4.5).

6 CRYSTALLOGRAPHIC DATA

6.1 CRYSTALLOGRAPHIC DATA COLLECTION PARAMETERS

Crystals were immersed in a film of perfluoropolyether oil on a glass fiber and transferred to a Bruker X8 Apex-2 diffractometer, with CCD area detector and mirror-monochromated Mo-Kα radiation, equipped with an Oxford Cryosystems low-temperature device, or a XtaLAB Synergy diffractometer, with CCD area detector and Cu-Kα radiation from Rigaku. Data were collected at 100 K. The images were processed with the Bruker software packages and equivalent reflections were merged. Corrections for Lorentz-polarization effects and absorption were performed if necessary and the structures were solved by direct methods. Subsequent difference Fourier syntheses revealed the positions of all other non-hydrogen atoms, and hydrogen atoms were included in calculated positions and refined using a riding model. Extinction corrections were applied as required. Crystallographic calculations were performed using the SHELXTL software package.[261] All non-hydrogen atoms were refined anisotropically. Hydrogen atoms were assigned to idealized positions and were included in structure factors calculations. Unless specified, all non-hydrogen atoms were refined with anisotropic displacement parameters and hydrogen atoms were included in calculated positions and refined using a riding model. Refinement, analysis of the structures and the preparation of graphics were performed using SHELXTL,[262] ORTEP 3,[263] DIAMOND,[264] WinGX,[265] PLATON.[266]

6.2 CCDC-NUMBERS OF PUBLISHED COMPOUNDS

The crystallographic data (cif-files) of the published compounds were uploaded to the CAMBRIDGE CRYSTALLOGRAPHIC DATA CENTRE (CCDC) and can be downloaded *via* *http://www.ccdc.cam.ac.uk*. Table 6.1 lists the corresponding CCDC-numbers.

Table 6.1 CCDC-numbers of published compounds.

Compound	CCDC-number
[Ni(Cy_2Im)$_2$(η^2-COE)] **3**	1897241
trans-[Ni(Cy_2Im)$_2$(Cl)(3,5-$F_2C_6H_3$)] **14**	1897242

6.3 CRYSTALLOGRAPHIC DATA OF SYNTHESIZED COMPOUNDS

Table 6.2 Crystallographic data collection parameters for adduct Pyridine·B_2cat_2 **18**.

Pyridine·B_2cat_2 **18**	
Empirical formula	$C_{17}H_{13}B_2NO_4$
Formula weight [g/mol]	316.90
Temperature [K]	100
Wavelength [Å]	0.71073
Crystal system	Triclinic
Space group	$P\bar{1}$
Unit cell dimensions	a = 8.5052(7) Å
	b = 9.5253(8) Å
	c = 12.8948(11) Å
	α = 80.489(3)°
	β = 76.583(3)°
	γ = 64.391(3)°
Volume [A^3]	913.82(14)
Z	2
Density (calculated) [g/cm^3]	1.152
Absorption coefficient [mm^{-1}]	0.080
F(000)	328
No. of reflections collected	15257
No. of unique reflections	3936 [R_{int} = 0.0205]
Observed reflections [I>2σ(I)]	3462
Data / restraints / parameters	3936 / 0 / 218
GooF	1.035
Final R indices [I>2σ (I)]	R_1 = 0.0359, wR_2 = 0.0896
R indices (all data)	R_1 = 0.0410, wR_2 = 0.0930
Largest diff. peak and hole [e A^3]	0.350 and -0.198
Diffractometer	Bruker Smart Apex 2

Table 6.3 Crystallographic data collection parameters for adduct *i*Pr$_2$Im^{Me}·B$_2$(OMe)$_4$ **22**.

*i*Pr$_2$Im^{Me}·B$_2$(OMe)$_4$ **22**	
Empirical formula	$C_{15}H_{32}B_2N_2O_4$
Formula weight [g/mol]	326.05
Temperature [K]	100
Wavelength [Å]	1.54184
Crystal system	Monoclinic
Space group	$P2_1/c$
Unit cell dimensions	a = 15.2801(2) Å
	b = 15.4420(2) Å
	c = 17.3918(3) Å
	α = 90°
	β = 112.928(2)°
	γ = 90°
Volume [A^3]	3779.47(11)
Z	4
Density (calculated) [g/cm^3]	1.146
Absorption coefficient [mm^{-1}]	0.638
F(000)	1424
No. of reflections collected	39777
No. of unique reflections	7866 [R_{int} = 0.0405]
Observed reflections [I>2σ(I)]	6795
Data / restraints / parameters	7866 / 0 / 468
GooF	1.045
Final R indices [I>2σ (I)]	R_1 = 0.0437, wR_2 = 0.1090
R indices (all data)	R_1 = 0.0517, wR_2 = 0.1135
Largest diff. peak and hole [e A^3]	0.373 and -0.224
Diffractometer	XtaLAB Synergy

Table 6.4 Crystallographic data collection parameters for adduct (iPr$_2$Im^{Me})$_2$·B$_2$cat$_2$ **25**.

(iPr$_2$Im^{Me})$_2$·B$_2$cat$_2$ **25**	
Empirical formula	$C_{34}H_{48}B_2N_4O_4$·2(C_6H_6)
Formula weight [g/mol]	754.60
Temperature [K]	100
Wavelength [Å]	1.54184
Crystal system	Triclinic
Space group	$P\bar{1}$
Unit cell dimensions	a = 11.5699(2) Å
	b = 11.5794(3) Å
	c = 16.3012(3) Å
	α = 90.095(2)°
	β = 90.074(2)°
	γ = 101.071(2)°
Volume [A^3]	2143.26(8)
Z	2
Density (calculated) [g/cm^3]	1.169
Absorption coefficient [mm^{-1}]	0.575
F(000)	812
No. of reflections collected	42040
No. of unique reflections	8434 [R_{int} = 0.0262]
Observed reflections [I>2σ(I)]	7742
Data / restraints / parameters	8434 / 648 / 717
GooF	1.052
Final R indices [I>2σ (I)]	R_1 = 0.0500, wR_2 = 0.1249
R indices (all data)	R_1 = 0.0532, wR_2 = 0.1276
Largest diff. peak and hole [e A^3]	0.390 and -0.280
Diffractometer	XtaLAB Synergy

Table 6.5 Crystallographic data collection parameters for cAAC^{Me}(H)Bpin **29**.

cAAC^{Me}(H)Bpin **29**	
Empirical formula	$C_{26}H_{44}BNO_2$
Formula weight [g/mol]	413.19
Temperature [K]	100
Wavelength [Å]	1.54184
Crystal system	Monoclinic
Space group	$P2_1/c$
Unit cell dimensions	a = 17.1256(4) Å
	b = 12.4195(3) Å
	c = 12.0659(2) Å
	α = 90°
	β = 94.304(2)°
	γ = 90°
Volume [A^3]	2559.08(10)
Z	4
Density (calculated) [g/cm^3]	1.072
Absorption coefficient [mm^{-1}]	0.498
F(000)	911
No. of reflections collected	22643
No. of unique reflections	5347 [R_{int} = 0.0379]
Observed reflections [I>2σ(I)]	4686
Data / restraints / parameters	5347 / 289 / 400
GooF	1.057
Final R indices [I>2σ (I)]	R_1 = 0.0502, wR_2 = 0.1275
R indices (all data)	R_1 = 0.0562, wR_2 = 0.1320
Largest diff. peak and hole [e A^3]	0.344 and -0.217
Diffractometer	XtaLAB Synergy

Table 6.6 Crystallographic data collection parameters for $[(Me_2Im^{Me})_2{\cdot}Bpin]^+I^-$ **37**.

$[(Me_2Im^{Me})_2{\cdot}Bpin]^+I^-$ **37**

Empirical formula	$C_{20}H_{36}BIN_4O_2$
Formula weight [g/mol]	502.24
Temperature [K]	100
Wavelength [Å]	1.54184
Crystal system	Monoclinic
Space group	P2/*c*
Unit cell dimensions	a = 13.3858(2) Å
	b = 14.2988(2) Å
	c = 13.1709(2) Å
	90°
	β = 109.650(2)°
	90°
Volume [A^3]	2374.11(7)
Z	4
Density (calculated) [g/cm^3]	1.405
Absorption coefficient [mm^{-1}]	10.760
F(000)	1032
Θ range [°]	3.1360 - 76.4690
No. of reflections collected	26822
No. of unique reflections	5002 [R_{int} = 0.0845]
Observed reflections [I>2σ(I)]	4539
Data / restraints / parameters	5002 / 78 / 297
GooF	1.090
Final R indices [I>2σ (I)]	R_1 = 0.0367, wR_2 = 0.0946
R indices (all data)	R_1 = 0.0422, wR_2 = 0.1018
Largest diff. peak and hole [e A^3]	0.889 and -1.368
Diffractometer	XtaLAB Synergy

7 SUMMARY

The present work focusses on the borylation of aryl halides. The first chapter presents a detailed review about previously reported nickel-catalyzed borylation reactions. The second and third chapters deal with the borylation of aryl chlorides mediated by catalysts based on the Earth-abundant metals nickel and copper, respectively, and chapter 4 focusses on the development of a transition metal-free alternative for the borylation of aryl halides.

The second chapter of the thesis describes, for the first time, the borylation reaction of C–Cl bonds in aryl chlorides mediated by an NHC-stabilized nickel catalyst. The cyclohexyl substituted NHC Cy_2Im was used to synthesize novel Cy_2Im-stabilized nickel complexes $[Ni_2(Cy_2Im)_4(\mu\text{-}(\eta^2\text{:}\eta^2)\text{-COD})]$ **1**, $[Ni(Cy_2Im)_2(\eta^2\text{-}C_2H_4)]$ **2**, and $[Ni(Cy_2Im)_2(\eta^2\text{-COE})]$ **3**, which were further investigated for their ability to catalyze the C–Cl bond borylation of aryl chlorides. The reaction of $[Ni(\eta^4\text{-COD})_2]$ with two equivalents of free Cy_2Im in THF afforded the dinuclear, COD-bridged complex $[Ni_2(Cy_2Im)_4(\mu\text{-}(\eta^2\text{:}\eta^2)\text{-COD})]$ **1**, which can be easily converted to the ethylene complex $[Ni(Cy_2Im)_2(\eta^2\text{-}C_2H_4)]$ **2** (Scheme 7.1). In addition, complex $[Ni(Cy_2Im)_2(\eta^2\text{-COE})]$ **3** was prepared by the reaction of $[Ni(Cy_2Im)_2(Br)_2]$ with COE under reductive conditions (Figure 7.1).

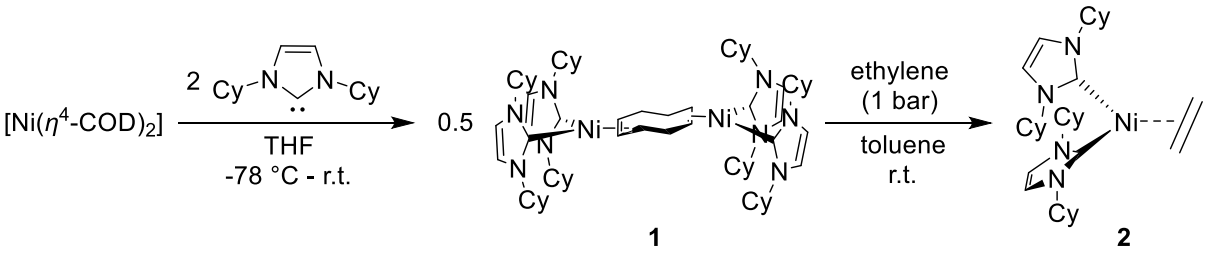

Scheme 7.1 Synthesis of the dinuclear, COD-bridged complex $[Ni_2(Cy_2Im)_4(\mu\text{-}(\eta^2\text{:}\eta^2)\text{-COD})]$ **1**, which was further reacted with ethylene forming $[Ni(Cy_2Im)_2(\eta^2\text{-}C_2H_4)]$ **2**.

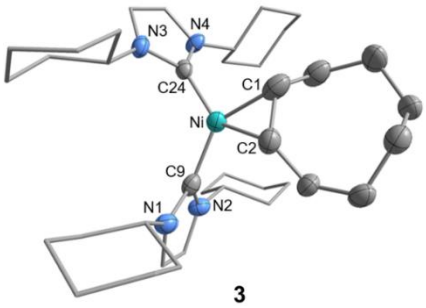

Figure 7.1 Molecular structure of $[Ni(Cy_2Im)_2(\eta^2\text{-COE})]$ **3**.

The catalytic activity of the NHC-nickel complexes **1**-**3** for the C–Cl borylation of aryl chlorides was investigated. An optimized procedure was developed using 5 mol% of the Ni-catalyst, 1.5 equivalents of the boron reagent B_2pin_2, and 1.5 equivalents of NaOAc as the base in methylcyclohexane at 100 °C. This system compares well with other Ni-catalyzed

borylation reactions, with the advantages of NaOAc being used as a very mild and inexpensive base and that no further ligand or additive is required. With these optimized conditions, it was shown that a variety of aryl chlorides, containing either electron-withdrawing or -donating groups, were converted to the corresponding aryl boronic esters in yields up to 99% (88% isolated) yield (Scheme 7.2). The use of B_2neop_2 instead of B_2pin_2 as the boron source, also yielded the corresponding aryl boronic ester in 76% (59% isolated) yield.

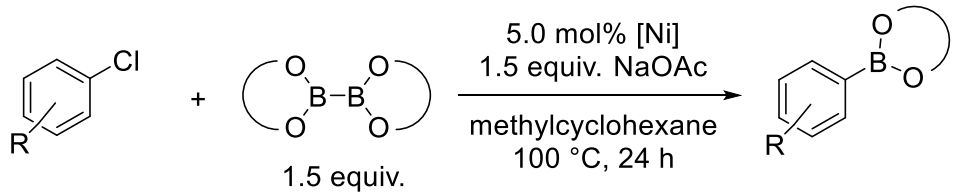

Scheme 7.2 Borylation reaction of aryl chloride C–Cl bonds mediated by Cy_2Im-stabilized nickel catalysts ([Ni] = $[Ni_2(Cy_2Im)_4(\mu\text{-}(\eta^2{:}\eta^2)\text{-COD})]$ **1**, $[Ni(Cy_2Im)_2(\eta^2\text{-}C_2H_4)]$ **2**, $[Ni(Cy_2Im)_2(\eta^2\text{-COE})]$ **3**).

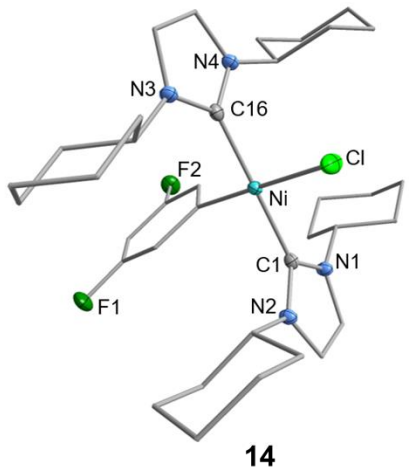

14

Figure 7.2 Molecular structure of the oxidative addition product *trans*-$[Ni(Cy_2Im)_2(Cl)(3,5\text{-}F_2C_6H_3)]$ **14**.

Mechanistic investigations revealed that the C–Cl oxidative addition product $[Ni(Cy_2Im)_2(Cl)(4\text{-}F_3C\text{-}C_6H_4)]$ **11**, which has been synthesized and isolated separately, also catalyzes the reaction. Thus, rapid oxidative addition of the C–Cl bond of the aryl chloride to $[Ni_2(Cy_2Im)_4(\mu\text{-}(\eta^2{:}\eta^2)\text{-COD})]$ **1** to yield *trans*-$[Ni(Cy_2Im)_2(Cl)(Ar)]$ represents the first step in the catalytic cycle. Interestingly, the reaction of $[Ni_2(Cy_2Im)_4(\mu\text{-}(\eta^2{:}\eta^2)\text{-COD})]$ **1** with stoichiometric amounts of B_2pin_2 at room temperature indicated the formation of a nickel-bisboryl complex of the type $[Ni(Cy_2Im)_2(Bpin)_2]$, which seems to be in an equilibrium with B_2pin_2 and $[Ni(Cy_2Im)_2]$. Further characterization of the observed nickel-boryl species was not possible, as it proved to be highly reactive and only showed limited stability in common deuterated-solvents.

Notably, the formation of the nickel-boryl species does not compete effectively with the oxidative addition of the C–Cl bond to $[Ni_2(Cy_2Im)_4(\mu\text{-}(\eta^2{:}\eta^2)\text{-COD})]$ **1**, as the latter shows a much higher reaction rate. The rate limiting step in this catalytic cycle is the transmetalation of boron to nickel forming *trans*-$[Ni(Cy_2Im)_2(Bpin)(Ar)]$, which was not possible to isolate. The boryl transfer reagent is assumed to be the anionic adduct

Na[$B_2pin_2(OAc)$]. A final reductive elimination step gives the desired borylated product Ar–Bpin and regenerates [Ni($Cy_2Im)_2$].

As Marder, Lin and co-workers introduced a room temperature Cu-catalyzed borylation of aryl iodides and bromides using a CuI/P*n*Bu_3 catalyst in 2009,[85] the first effective C–Cl bond borylation of aryl chlorides using NHC-stabilized Cu(I)-complexes of the type [Cu(NHC)(Cl)] was developed in the next chapter of the thesis. Initial investigations demonstrated that phosphine-stabilized Cu(I) complexes were ineffective for the borylation of aryl chlorides. The known complexes [Cu(*i*Pr_2Im)(Cl)] **15**,[139] [Cu(Me_2Im^{Me})(Cl)] **16**,[139] and [Cu(Cy_2Im)(Cl)] **17**,[140] bearing the small alkyl substituted NHCs, were synthesized in good yields by the reaction of copper(I) chloride with the corresponding free NHC at low temperature (-78 °C) in THF (Scheme 7.3).

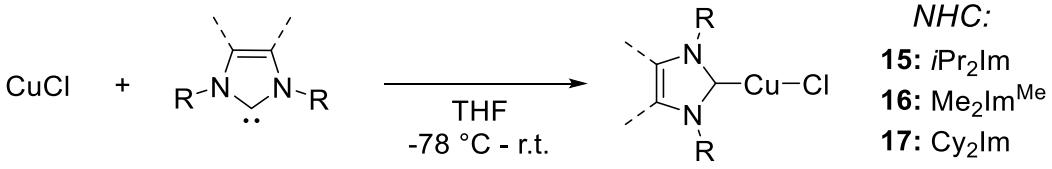

Scheme 7.3 Reaction of CuCl with the corresponding free NHCs forming complexes of the type [Cu(NHC)(Cl)] **15**-**17**.

A range of catalysts, bases, solvents, and boron sources were screened to determine the scope and limitations of this reaction. Complex [Cu(Cy_2Im)(Cl)] **17** revealed a significantly higher catalytic activity than [Cu(*i*Pr_2Im)(Cl)] **15**. KO*t*Bu turned out to be the only efficient base for this borylation reaction. Besides methylcyclohexane, toluene was the only solvent that gave the borylated product in moderate yields of 53%. The optimized conditions are depicted in Scheme 7.4.

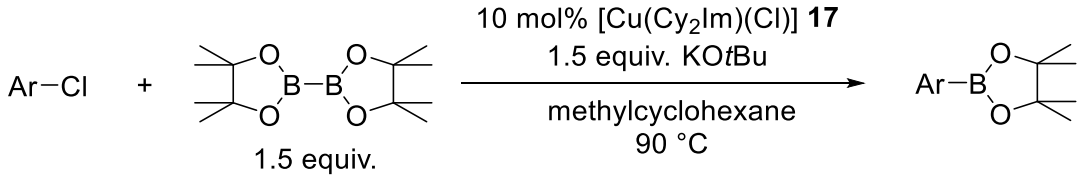

Scheme 7.4 Borylation of C–Cl bonds in aryl chlorides mediated by [Cu(Cy_2Im)(Cl)] **17**.

It was shown that a variety of electron-rich and electron-poor aryl chlorides can be converted to the corresponding aryl boronic esters in isolated yields of up to 80% using these optimized conditions. The use of B_2neop_2 as the boron reagent gave yields slightly lower than those observed for B_2pin_2, whereas B_2cat_2, B_2eg_2, and diboronic acid were unreactive under the standard conditions.

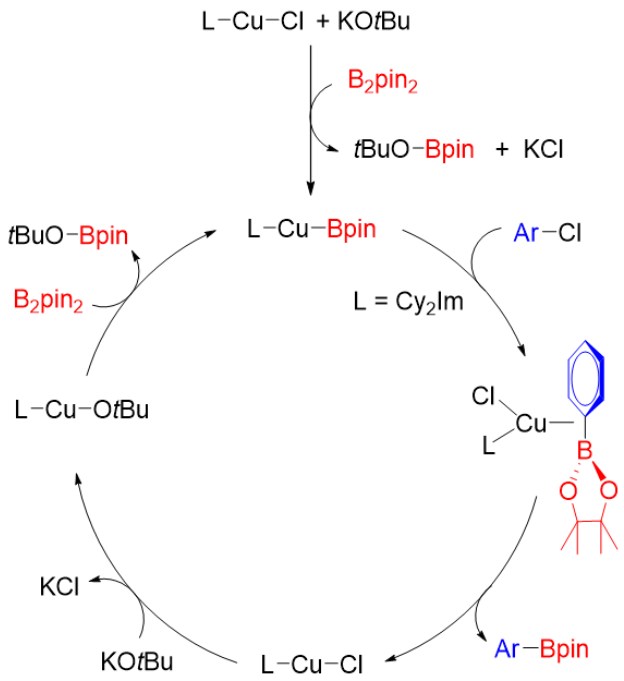

Scheme 7.5 Proposed mechanism for the NHC-copper-catalyzed borylation of aryl chlorides.

A mechanism was proposed, in which a Cu-boryl complex [Cu(L)(Bpin)] is formed in the initial step (Scheme 7.5). This is followed by C–B bond formation *via* σ-bond metathesis with the aryl chloride forming the aryl boronic ester and [Cu(L)(Cl)]. [Cu(L)(Cl)] reacts with KO*t*Bu to give [Cu(L)(O*t*Bu)], which subsequently regenerates the copper boryl complex by reaction with B_2pin_2.

Chapter 4 describes studies directed towards the transition metal-free borylation of aryl halides using Lewis base adducts of diborane(4) compounds. A variety of novel pyridine and NHC adducts of boron compounds were synthesized. The reaction of pyridine and DMAP with B_2cat_2 led to the formation of pyridine·B_2cat_2 **18** and DMAP·B_2cat_2 **19**, respectively. Reaction of one equivalent of free Me_2Im^{Me} or iPr_2Im^{Me} with B_2pin_2 gave the corresponding mono-NHC adducts of the type NHC·B_2pin_2 **20**-**21**. For the related diborane(4) compound $B_2(OMe)_4$, mono-NHC adducts were only isolable if the small alkyl substituted NHCs iPr_2Im^{Me} and Cy_2Im were used, leading to iPr_2Im^{Me}·$B_2(OMe)_4$ **22** and Cy_2Im·$B_2(OMe)_4$ **23**. The reaction of the free NHCs Cy_2Im and iPr_2Im^{Me} with B_2cat_2 in a 2:1 ratio led to the formation of the bis-NHC adducts $(Cy_2Im)_2$·B_2cat_2 **24** and $(iPr_2Im^{Me})_2$·B_2cat_2 **25**, respectively. In addition, Cy_2Im·HBpin **26,** iPr_2Im^{Me}·HBpin **27**, and Me_2Im^{Me}·HBpin **28** were synthesized by the reaction of one equivalent of the corresponding free NHC with pinacolborane.

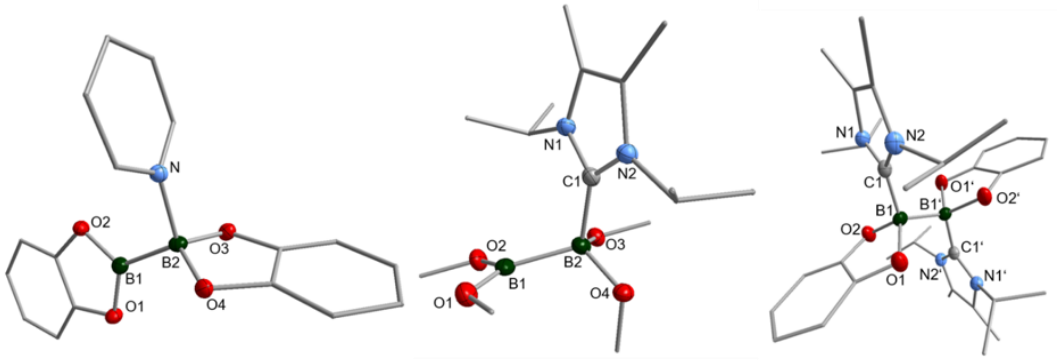

18 **22** **25**

Figure 7.3 Molecular structures of the adducts pyridine·B_2cat_2 **18**, *i*Pr_2Im^{Me}·$B_2(OMe)_4$ **22**, and (*i*Pr_2Im^{Me})$_2$·B_2cat_2 **25**.

The reaction of pinacolborane with $cAAC^{Me}$ led to the isolation of the B–H activation product, $cAAC^{Me}$(H)Bpin **29** (Figure 7.4) instead of an adduct, which was formed *via* the insertion of the $cAAC^{Me}$ carbene carbon atom into the B–H bond. NHC adducts of aryl boronic esters were generated by the reaction of the corresponding aryl boronic ester with one equivalent of the free NHC, yielding 3,5-$F_2C_6H_3$Bpin·Cy_2Im **30**, 4-CH_3-C_6H_4Bpin·Cy_2Im **31**, C_6H_5Bneop·Cy_2Im **32**, BiphenylBneop·Cy_2Im **33**, and 4-F_3C-C_6H_4Bpin·Me_2Im^{Me} **34**.

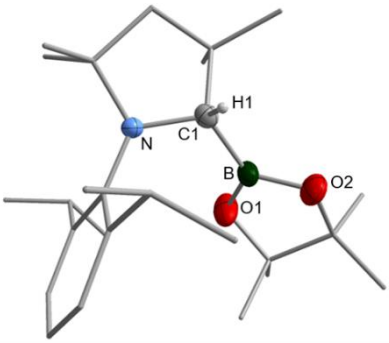

29

Figure 7.4 Molecular structure of (S)-$cAAC^{Me}$(H)Bpin **29**.

Adducts of the type pyridine·B_2cat_2 **18**-**19** and NHC·$B_2(OR)_4$ **20**-**23** were examined for their ability to transfer a boryl moiety to an aryl iodide. However, only Me_2Im^{Me}·B_2pin_2 **20** was found to be effective. The stoichiometric reaction of **20** with different substituted aryl iodides and bromides in benzene, at elevated temperatures, gave the desired aryl boronic esters in good yields (Scheme 7.6). An electron-poor aryl chloride was also borylated, but in a low yield of 20%.

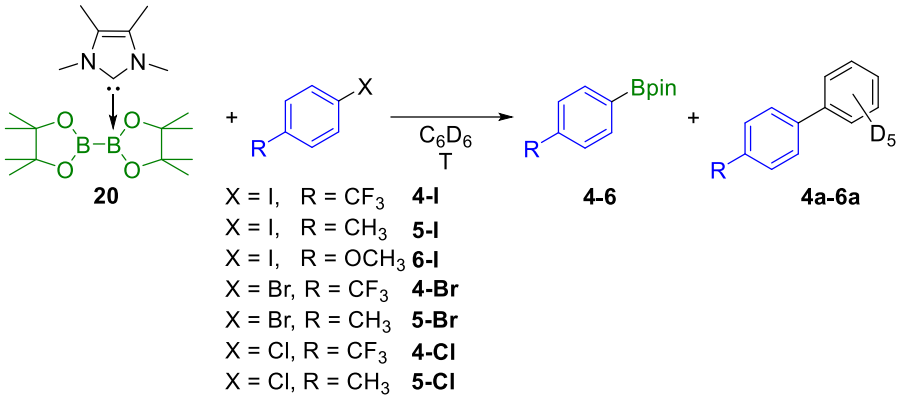

Scheme 7.6 Reaction of the mono-NHC adduct Me_2Im^{Me}·B_2pin_2 **20** with aryl halides (X = I, Br, Cl) forming the corresponding borylation products **4**-**6** and the C–C coupling products **4a**-**6a** arising from C–C coupling between the substrate and the solvent C_6D_6.

Interestingly, depending on the reaction temperature, C–C coupling between the aryl halide and the solvent (benzene), was detected leading to a side product which, together with observed hydrodehalogenation of the aryl halide, provided indications that the reaction might be radical in nature.

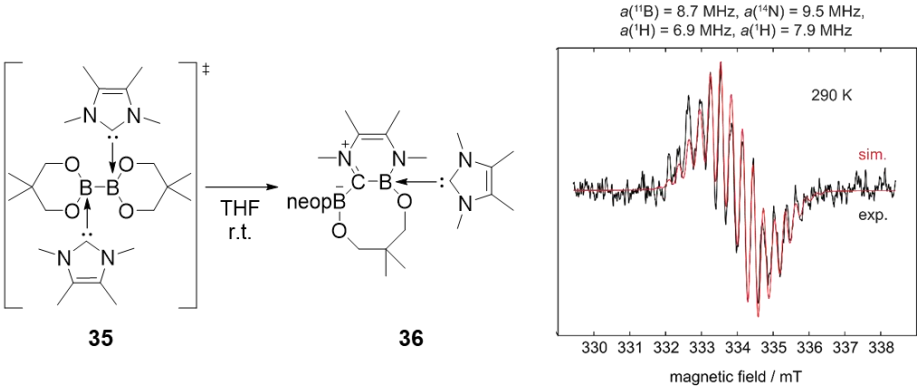

Scheme 7.7 (Left) Reaction of B_2neop_2 with two equivalents of Me_2Im^{Me} at room temperature forming the ring expanded product RER-B_2neop_2·$(Me_2Im^{Me})_2$ **36** with the bis-NHC adduct $(Me_2Im^{Me})_2$·B_2neop_2 **35** as an intermediate. (Right) Simulated (red) and experimental (black) EPR spectrum of the RER.

Previous studies have shown that bis-NHC adducts are thermally unstable, undergoing ring expansion reactions. Monitoring the reaction of B_2neop_2 with two equivalents of Me_2Im^{Me} by EPR spectroscopy (Scheme 7.7), provided evidence that the RER proceeds *via* the formation of a boryl radical NHC–BR_2˙ **35a**, presumably formed by homolytic B–B bond cleavage (Figure 7.5). Radical **35a** was successfully employed as an initiator for the polymerization of styrene (Figure 7.6).

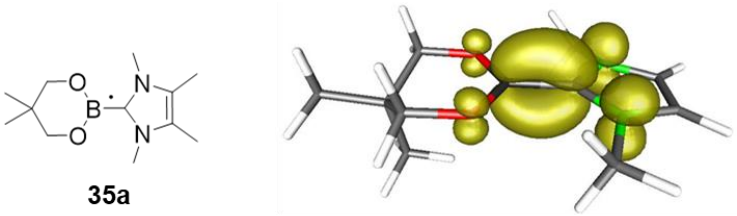

Figure 7.5 Schematic (left) and calculated (right) structure of the NHC–$BR_2^{\bullet}$ radical **35a** with an overlay of the computed spin density.

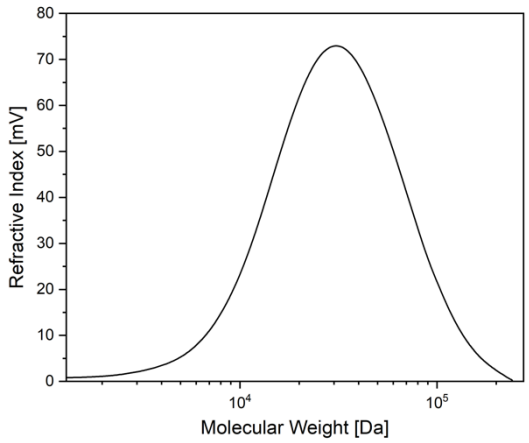

Figure 7.6 GPC analysis of polystyrene formed during the RER.

Furthermore, when the boryl transfer reaction based on Me_2Im^{Me}·B_2pin_2 **20** was followed by EPR spectroscopy, a signal (though very weak and ill-defined) was detected, which is suggestive of a mechanism involving a boron-based radical. Further studies gave experimental proof for the presence of radicals in the course of the reaction, as an aryl radical was trapped by TEMPO, and running the boryl transfer reaction in styrene also led to its polymerization. In addition, the boronium cation $[(Me_2Im^{Me})_2$·Bpin$]^+$ **37** (Figure 7.7) with iodide as the counterion was isolated from the reaction residue, indicating the fate of the second boryl moiety.

Further studies concerning the mechanism showed that the reaction of the aryl iodide with the free NHC Me_2Im^{Me} in the absence of B_2pin_2 also led, besides the formation of the imidazolium salt [4-CH_3-C_6H_4-$Me_2Im^{Me}]^+I^-$ **38**, to the C–C coupling product of the aryl iodide with the solvent. A preliminary mechanism (Scheme 7.8) for the boryl transfer from Me_2Im^{Me}·B_2pin_2 **20** to aryl iodides was proposed, which involves an NHC–Bpin$^{\bullet}$ radical, closely related to the observed radical **35a**, as the key intermediate. Me_2Im^{Me}–Bpin$^{\bullet}$ is formed by homolytic B–B bond cleavage of the bis-NHC adduct $(Me_2Im^{Me})_2$·B_2pin_2, which is formed *in situ* in small amounts under the reaction conditions. Me_2Im^{Me}–Bpin$^{\bullet}$ reacts with the aryl iodide to give the aryl boronic ester with

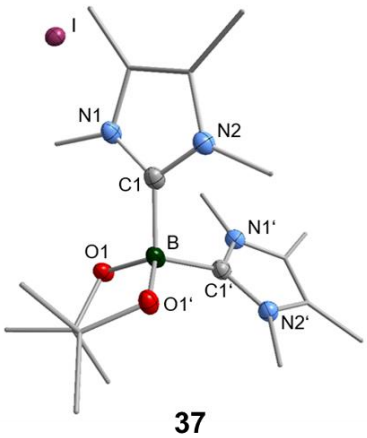

37

Figure 7.7 Molecular structure of $[(Me_2Im^{Me})_2$·Bpin$]^+I^-$ **37**.

recovery of aromaticity. In the same step, from the second equivalent of NHC–Bpin•, an NHC-stabilized iodo-Bpin adduct is formed as an intermediate, which is further coordinated by another NHC, yielding the spectroscopically and structurally characterized boronium salt $[(Me_2Im^{Me})_2{\cdot}Bpin]^+I^-$ **37**.

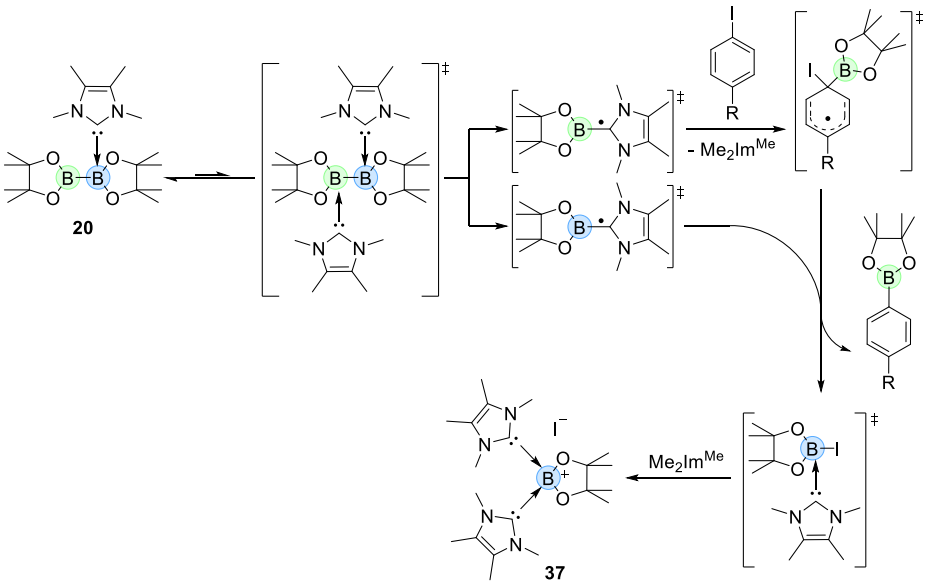

Scheme 7.8 Proposed mechanism for the boryl transfer reaction from the mono-NHC adduct $Me_2Im^{Me}{\cdot}B_2pin_2$ **20** to aryl iodides.

In a possible side reaction, the boryl radical NHC–Bpin• might serve as a reducing agent by donating an electron to the imidazolium salt $[R\text{-}C_6H_4\text{-}Me_2Im^{Me}]^+I^-$ **38** (R = CH_3), which was formed in small amounts by a side reaction of the free NHC with the aryl iodide. This step again forms **37** and an aryl radical. The latter further undergoes a radical C–C coupling pathway, which explains the formation of the coupling product between the aryl iodide and the solvent (benzene).

8 ZUSAMMENFASSUNG

Die vorliegende Arbeit befasst sich mit Borylierungsreaktionen von Arylhalogeniden. Das erste Kapitel gibt zunächst einen detaillierten Überblick über die Nickel-katalysierte Borylierung. In den beiden darauffolgenden Kapiteln liegt der Fokus auf der Borylierung von Arylchloriden mit den leicht verfügbaren Übergangsmetallen Nickel und Kupfer. Das letzte Kapitel der Arbeit setzt sich mit der Entwicklung einer übergangsmetallfreien Alternative für die Borylierung von Arylhalogeniden auseinander.

Das zweite Kapitel dieser Arbeit beschreibt die Borylierung von Arylchloriden mithilfe NHC-stabilisierter Nickelkatalysatoren. Dafür wurden zunächst die neuen Nickelkomplexe [$Ni_2(Cy_2Im)_4(\mu\text{-}(\eta^2\text{:}\eta^2)\text{-COD})$] **1**, [$Ni(Cy_2Im)_2(\eta^2\text{-}C_2H_4)$] **2** und [$Ni(Cy_2Im)_2(\eta^2\text{-COE})$] **3** dargestellt, welche anschließend auf ihre katalytische Fähigkeit zur C–Cl-Borylierung von Arylchloriden untersucht wurden. Durch die Reaktion von [$Ni(\eta^4\text{-COD})_2$] mit zwei Äquivalenten Cy_2Im wurde der dinukleare, COD-verbrückte Komplex [$Ni_2(Cy_2Im)_4(\mu\text{-}(\eta^2\text{:}\eta^2)\text{-COD})$] **1** erhalten, welcher sich unter Ethenatmosphäre quantitativ in den mononuklearen Komplex [$Ni(Cy_2Im)_2(\eta^2\text{-}C_2H_4)$] **2** überführt ließ (Schema 8.1).

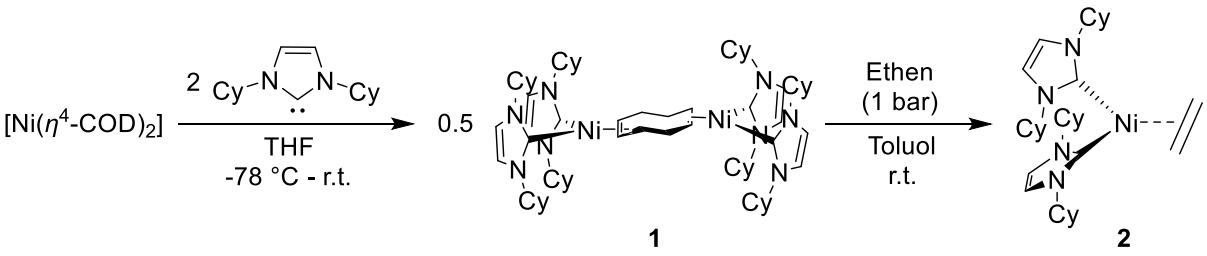

Schema 8.1 Synthese des dinuklearen, COD-verbrückten Komplexes [$Ni_2(Cy_2Im)_4(\mu\text{-}(\eta^2\text{:}\eta^2)\text{-COD})$] **1**, welcher durch Reaktion mit Ethen in [$Ni(Cy_2Im)_2(\eta^2\text{-}C_2H_4)$] **2** überführt werden konnte.

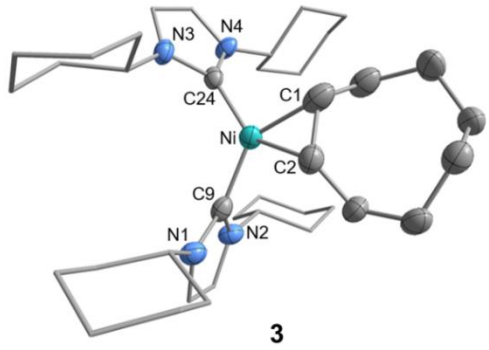

Abbildung 8.1 Molekülstruktur von [$Ni(Cy_2Im)_2(\eta^2\text{-COE})$] **3**.

Die Synthese von [$Ni(Cy_2Im)_2(\eta^2\text{-COE})$] **3** erfolgte hingegen durch Umsetzung von [$Ni(Cy_2Im)_2(Br)_2$] mit COE unter reduktiven Bedingungen (Abbildung 8.1). Des Weiteren wurde die katalytische Aktivität der NHC-stabilisierten Nickelkomplexe **1**-**3** bezüglich der C–Cl-Borylierung von Arylchloriden untersucht. Als optimale Bedingungen für die Borylierung

haben sich 5 Mol-% des Ni-Katalysators, 1.5 Äquivalente des Borylierungsreagenzes B_2pin_2 und 1.5 Äquivalente NaOAc als Base in Methylcyclohexan bei 100 °C erwiesen (Schema 8.2).

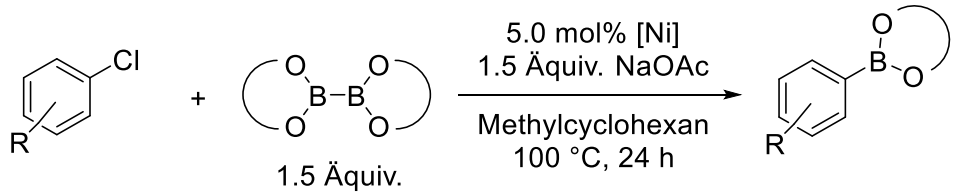

Schema 8.2 C–Cl-Borylierung von Arylchloriden mithilfe von Cy_2Im-stabilisierten Nickelkomplexen ([Ni] = $[Ni_2(Cy_2Im)_4(\mu\text{-}(\eta^2\text{:}\eta^2)\text{-COD})]$ **1**, $[Ni(Cy_2Im)_2(\eta^2\text{-}C_2H_4)]$ **2**, $[Ni(Cy_2Im)_2(\eta^2\text{-COE})]$ **3**).

Dieses System zeigt im Vergleich mit bereits literaturbekannten Ni-katalysierten Borylierungsreaktionen ähnliche bis bessere Aktivität, wobei im Gegensatz zu anderen Systemen keine Zugabe eines weiteren Liganden oder Additivs erforderlich ist und die Verwendung der sehr milden und kostengünstigen Base NaOAc von Vorteil ist. Unter diesen optimierten Bedingungen lassen sich eine Vielzahl unterschiedlicher Arylchloride in die jeweiligen Arylboronsäureester in Ausbeuten von bis zu 99% (88% für die isolierte Verbindung) überführen (Schema 8.2). Die Verwendung von B_2neop_2 als Borquelle führte ebenfalls zur Bildung des entsprechenden Arylboronsäureesters in Ausbeuten von 76% (59% für die isolierte Verbindung).

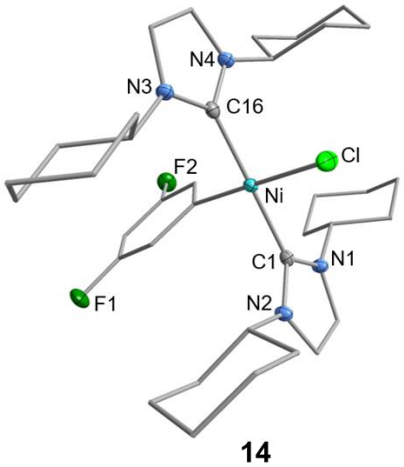

Abbildung 8.2 Molekülstruktur des oxidativen Additionsprodukts *trans*-$[Ni(Cy_2Im)_2(Cl)(3,5\text{-}F_2C_6H_3)]$ **14**.

Der Komplex $[Ni(Cy_2Im)_2(Cl)(4\text{-}F_3C\text{-}C_6H_4)]$ **11**, das Produkt der oxidativen Addition von 4-F_3C-C_6H_4-Cl an $[Ni_2(Cy_2Im)_4(\mu\text{-}(\eta^2\text{:}\eta^2)\text{-COD})]$ **1**, katalysiert ebenfalls die Reaktion. Mechanistischen Untersuchungen zufolge, stellt die rasche oxidative Addition der C–Cl-Bindung des Arylchlorids an $[Ni_2(Cy_2Im)_4(\mu\text{-}(\eta^2\text{:}\eta^2)\text{-COD})]$ **1** unter der Ausbildung von *trans*-$[Ni(Cy_2Im)_2(Cl)(Ar)]$, den ersten Schritt des Katalysezykluses dar. Interessanterweise führte die stöchiometrische Umsetzung von $[Ni_2(Cy_2Im)_4(\mu\text{-}(\eta^2\text{:}\eta^2)\text{-COD})]$ **1** mit B_2pin_2 bei Raumtemperatur zur Bildung eines Nickel-Bisboryl-Komplexes des Typs $[Ni(Cy_2Im)_2(Bpin)_2]$, welcher mit B_2pin_2 und $[Ni(Cy_2Im)_2]$ im Gleichgewicht zu sein scheint. Eine weitere Charakterisierung der beobachteten Nickel-Boryl-Spezies war nicht möglich, da sich diese als hochreaktiv erwies und nur eine begrenzte Stabilität in

gängigen deuterierten Lösungsmitteln zeigte. Die Bildung des Nickel-Boryl-Komplexes konkurriert nicht mit der oxidativen Addition der C–Cl-Bindung an [$Ni_2(Cy_2Im)_4$(μ-(η^2:η^2)-COD)] **1**, da letztere eine viel höhere Reaktionsgeschwindigkeit aufweist. Der geschwindigkeitsbestimmende Schritt in diesem Katalysezyklus ist die Transmetallierung von Bor zu Nickel unter Bildung von *trans*-[$Ni(Cy_2Im)_2$(Bpin)(Ar)], welches nicht isoliert werden konnte. Es wird angenommen, dass es sich bei dem Boryltransferreagenz um das anionische Addukt Na[B_2pin_2(OAc)] handelt. Ein letzter reduktiver Eliminierungsschritt ergibt das gewünschte borylierte Produkt Ar–Bpin unter Rückgewinnung von [$Ni(Cy_2Im)_2$].

Im nächsten Kapitel der Arbeit wurde basierend auf der im Jahr 2009 von Marder, Lin *et al.* gezeigten CuI/P*n*Bu_3-katalysierten Borylierung von Aryliodiden und -bromiden,[85] die erste effiziente C–Cl-Borylierung von Arylchloriden entwickelt. Ersten Untersuchungen zufolge sind Phosphan-stabilisierte Cu(I)-Komplexe für die Borylierung von Arylchloriden ungeeignet, während sich die Katalyse gut mit NHC-stabilisierten Cu(I)-Komplexen des Typs [Cu(NHC)(Cl)] durchführen lässt. Die literaturbekannten NHC-stabilisierten Komplexe [Cu(*i*Pr_2Im)(Cl)] **15**,[139] [Cu(Me_2Im^{Me})(Cl)] **16**[139] und [Cu(Cy_2Im)(Cl)] **17**,[140] welche kleine Alkyl-substituierte NHCs als Liganden tragen, wurden in guten Ausbeuten durch stöchiometrische Umsetzung von Kupfer(I)chlorid mit dem jeweiligen NHC bei tiefen Temperaturen (-78 °C) in THF dargestellt (Schema 8.3).

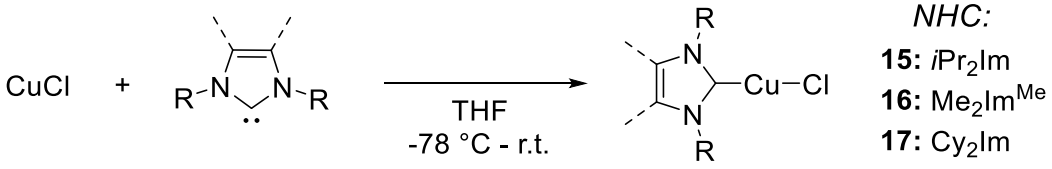

Schema 8.3 Synthese der Komplexe des Typs [Cu(NHC)(Cl)] **15**-**17** durch stöchiometrische Umsetzung von CuCl mit dem jeweiligen NHC.

Eine Reihe verschiedener Katalysatoren, Basen, Lösungsmitteln und Borylierungsreagenzien wurden untersucht, um die Anwendungsmöglichkeiten und Grenzen dieser Reaktion zu bestimmen. Der Komplex [Cu(Cy_2Im)(Cl)] **17** zeigte dabei eine signifikant höhere katalytische Aktivität als [Cu(*i*Pr_2Im)(Cl)] **15**. Des Weiteren erwies sich KO*t*Bu als einzige geeignete Base für diese Reaktion und Methylcyclohexan stellte sich als optimales Lösungsmittel heraus. Einzig Toluol bietet eine Alternative, wobei das borylierte Produkt dann nur in mäßigen Ausbeuten von 53% generiert wurde. Die optimierten Bedingungen sind in Schema 8.4 dargestellt.

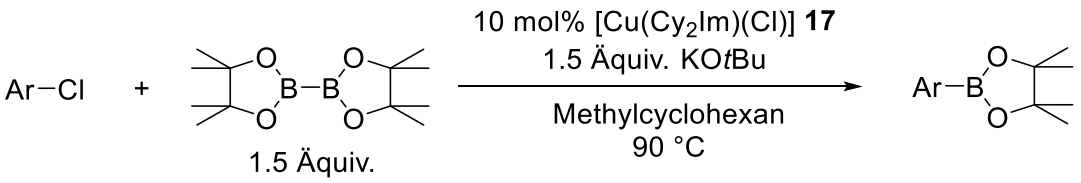

Schema 8.4 C–Cl-Borylierung von Arylchloriden mithilfe von [Cu(Cy$_2$Im)(Cl)] **17**.

Unter diesen optimierten Bedingungen lassen sich eine Vielzahl, sowohl elektronenreicher als auch elektronenarmer Arylchloride in die entsprechenden Arylboronsäureester in Ausbeuten von bis zu 80% überführen. Die Verwendung von B$_2$neop$_2$ anstelle von B$_2$pin$_2$ als Borylierungsreagenz führte zu geringfügig niedrigeren Ausbeuten, während B$_2$cat$_2$, B$_2$eg$_2$ und Diboronsäure unter den Standardbedingungen unreaktiv waren.

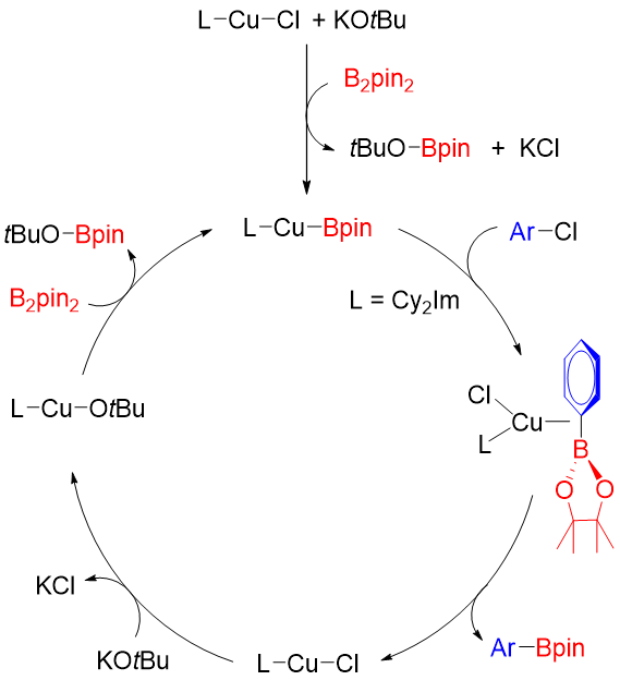

Schema 8.5 Postulierter Mechanismus für die NHC-Kupfer katalysierte Borylierung von Arylchloriden.

Ein Mechanismus der Reaktion wurde postuliert, wonach zunächst ein Kupfer-Boryl-Komplex [Cu(L)(Bpin)] gebildet wird (Schema 8.5). Darauf folgt die Knüpfung einer C–B-Bindung durch eine σ-Bindungsmetathese mit dem Arylchlorid, wobei der gewünschte Aryl-boronsäureester und [Cu(L)(Cl)] gebildet wird. Im Folgenden reagiert [Cu(L)(Cl)] mit KO*t*Bu zu [Cu(L)(O*t*Bu)], wodurch im nächsten Schritt durch Reaktion mit B$_2$pin$_2$ der Kupfer-Boryl-Komplex regeneriert wird.

Kapitel 4 beschreibt Untersuchungen zur übergangsmetallfreien Borylierung von Arylhalogeniden unter Verwendung von Lewis-Basen-Addukten von Diboran(4)-Verbindungen. Zunächst wurden verschiedene, neuartige Lewis-Basen-Addukte synthetisiert. Die Reaktion von Pyridin und DMAP mit B$_2$cat$_2$ führte zur Bildung von Pyridin·B$_2$cat$_2$ **18** bzw. DMAP·B$_2$cat$_2$ **19**. Die stöchiometrische Umsetzung von Me$_2$Im^{Me} bzw. *i*Pr$_2$Im^{Me} mit B$_2$pin$_2$ ergab die entsprechenden Mono-NHC-Addukte des Typs NHC·B$_2$pin$_2$ **20**-**21**. Für die verwandte Diboran(4)-Verbindung B$_2$(OMe)$_4$ waren Mono-NHC-Addukte nur unter Verwendung der kleinen Alkyl-substituierten NHCs

*i*Pr$_2$Im^{Me} und Cy$_2$Im zugänglich, wodurch die Verbindungen *i*Pr$_2$Im^{Me}·B$_2$(OMe)$_4$ **22** und Cy$_2$Im·B$_2$(OMe)$_4$ **23** erhalten wurden. Die Reaktion der freien NHCs Cy$_2$Im und *i*Pr$_2$Im^{Me} mit B$_2$cat$_2$ im Verhältnis 2:1 führte zur Bildung der Bis-NHC-Addukte (Cy$_2$Im)$_2$·B$_2$cat$_2$ **24** bzw. (*i*Pr$_2$Im^{Me})$_2$·B$_2$cat$_2$ **25**. Des Weiteren wurden Cy$_2$Im·HBpin **26**, *i*Pr$_2$Im^{Me}·HBpin **27** sowie Me$_2$Im^{Me}·HBpin **28** durch Umsetzung eines Äquivalents des entsprechenden NHCs mit Pinakolboran synthetisiert.

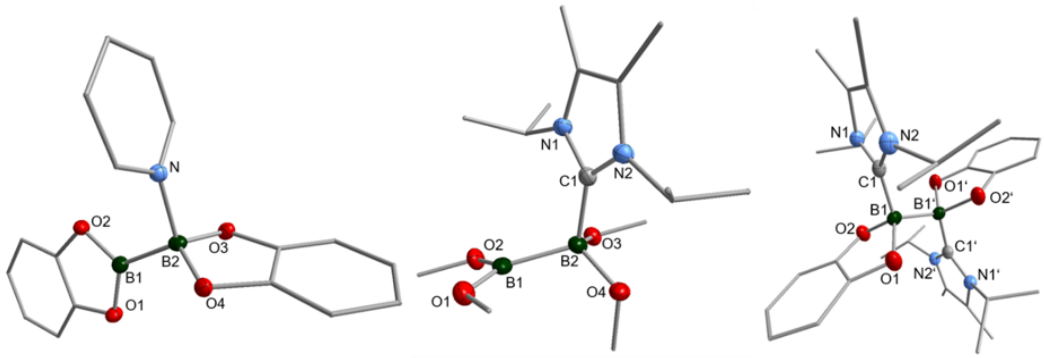

Abbildung 8.3 Molekülstrukturen der Addukte Pyridin·B$_2$cat$_2$ **18**, *i*Pr$_2$Im^{Me}·B$_2$(OMe)$_4$ **22** und (*i*Pr$_2$Im^{Me})$_2$·B$_2$cat$_2$ **25**.

Die Reaktion von Pinakolboran mit cAAC^{Me} führte unter Insertion des cAAC^{Me}-Carben-Kohlenstoffatoms in die B–H-Bindung, zur Ausbildung des B–H-Aktivierungsprodukts cAAC^{Me}(H)Bpin **29** (Abbildung 8.4). Die NHC-Addukte der Arylboronsäureester wurden durch Umsetzung der entsprechenden Arylboronsäureester mit einem Äquivalent des NHCs dargestellt, wobei die Addukte 3,5-F$_2$C$_6$H$_3$Bpin·Cy$_2$Im **30**, 4-CH$_3$-C$_6$H$_4$Bpin·Cy$_2$Im **31**, C$_6$H$_5$Bneop·Cy$_2$Im **32**, BiphenylBneop·Cy$_2$Im **33** und 4-F$_3$C-C$_6$H$_4$Bpin·Me$_2$Im^{Me} **34** erhalten wurden.

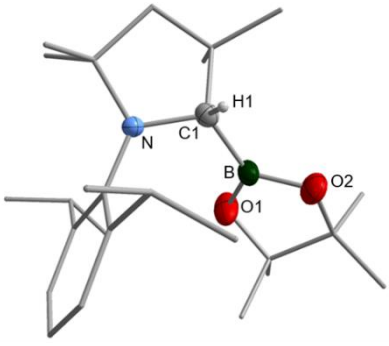

Abbildung 8.4 Molekülstruktur von (S)-cAAC^{Me}(H)Bpin **29**.

Die Addukte des Typs Pyridin·B$_2$cat$_2$ **18**-**19** und NHC·B$_2$(OR)$_4$ **20**-**23** wurden weiter auf ihre Fähigkeiten hin untersucht, eine Boryleinheit auf ein Aryliodid zu übertragen. Ausschließlich Me$_2$Im^{Me}·B$_2$pin$_2$ **20** stellte sich hierbei als wirksam heraus. Die stöchiometrische Reaktion von **20** mit verschiedenartig substituierten Aryliodiden und -bromiden in Benzol bei erhöhten Temperaturen lieferte die gewünschten Arylboronsäureester in guten Ausbeuten (Schema 8.6). Ein elektronenarmes Arylchlorid konnte ebenfalls boryliert werden, jedoch in einer geringen Ausbeute von 20%.

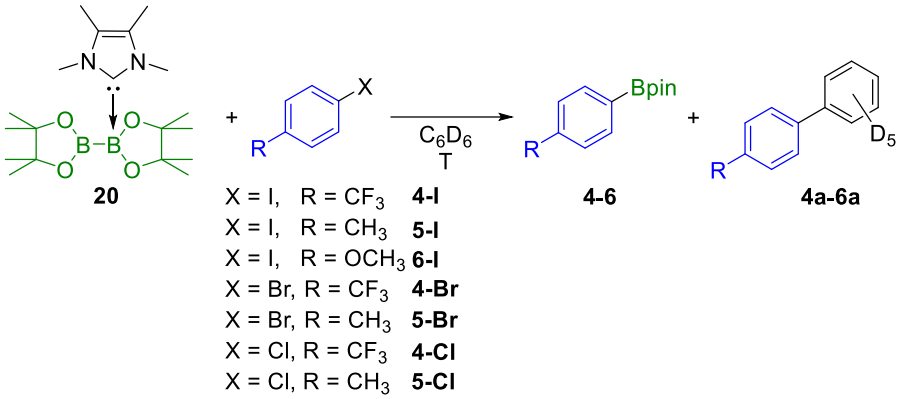

Schema 8.6 Reaktion des Mono-NHC-Addukts Me_2Im^{Me}·B_2pin_2 **20** mit Arylhalogeniden (X = I, Br, Cl) unter Bildung der entsprechenden Borylierungsprodukte **4**-**6** sowie der C–C-Kupplungsprodukte **4a**-**6a**.

Interessanterweise wurde als Nebenreaktion eine von der Reaktionstemperatur abhängige C–C-Kupplung zwischen dem Arylhalogenid und dem Lösungsmittel (Benzol) beobachtet. Sowohl das C–C-Kupplungsnebenprodukt, als auch eine beobachtete Hydrodehalogenierung des Arylhalogenids deuten darauf hin, dass die Reaktion von radikalischer Natur sein könnte.

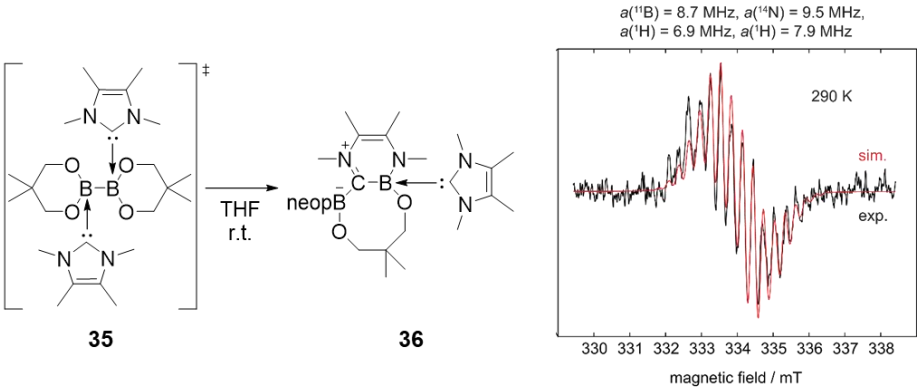

Schema 8.7 (Links) Reaktion von B_2neop_2 mit zwei Äquivalenten Me_2Im^{Me} bei Raumtemperatur unter Bildung des Ringerweiterungsprodukts RER-B_2neop_2·$(Me_2Im^{Me})_2$ **36** mit dem Bis-NHC-Addukt $(Me_2Im^{Me})_2$·B_2neop_2 **35** als Intermediat. (Rechts) Simuliertes (rot) und experimentelles (schwarz) ESR Spektrum der RER.

Frühere Untersuchungen haben gezeigt, dass Bis-NHC-Addukte thermisch instabil sind und Ringerweiterungsreaktionen eingehen. Die Verfolgung der Reaktion von B_2neop_2 mit zwei Äquivalenten Me_2Im^{Me} mittels ESR-Spektroskopie (Schema 8.7) zeigte, dass die RER über die Bildung eines Borylradikals des Typs NHC–$BR_2^{\bullet}$ **35a** verläuft, welches vermutlich durch homolytische Spaltung der B–B-Bindung gebildet wird (Abbildung 8.5).

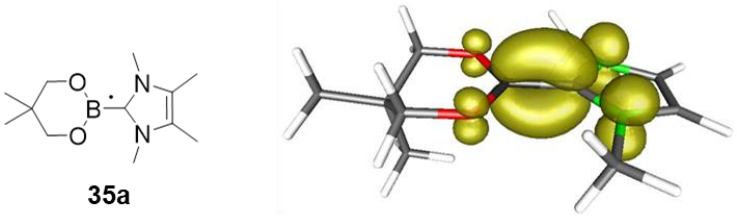

Abbildung 8.5 Schematische (links) und gerechnete (rechts) Struktur des NHC–BR_2•-Radikals **35a** mit Überlagerung der berechneten Spindichte.

Das Radikal **35a** konnte erfolgreich als Initiator für die Polymerisation von Styrol eingesetzt werden (Abbildung 8.6).

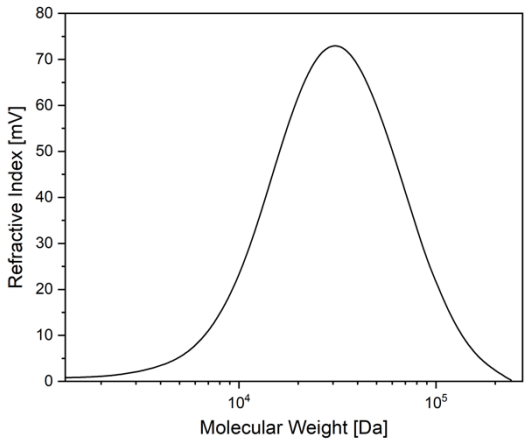

Abbildung 8.6 GPC Analyse des während der RER gebildeten Polystyrols.

Die Verfolgung der von Me_2Im^{Me}•B_2pin_2 **20** ausgehenden Boryltransferreaktion mittels ESR-Spektroskopie zeigte ein Signal (jedoch sehr schwach und schlecht definiert), was auf einen Mechanismus mit Beteiligung eines Borradikals hinweist. Weitere Untersuchungen ergaben experimentelle Beweise für die Anwesenheit von Radikalen im Verlauf der Reaktion. So konnte ein Arylradikal durch TEMPO abgefangen werden und die Durchführung der Boryltransferreaktion in Styrol führte ebenfalls zu dessen Polymerisation. Des Weiteren wurde das Boroniumkation $[(Me_2Im^{Me})_2$•$Bpin]^+$ **37** (Abbildung 8.7) mit Iodid als Gegenion aus dem Reaktionsrückstand isoliert, was den Verbleib der zweiten Boryleinheit erklärt.

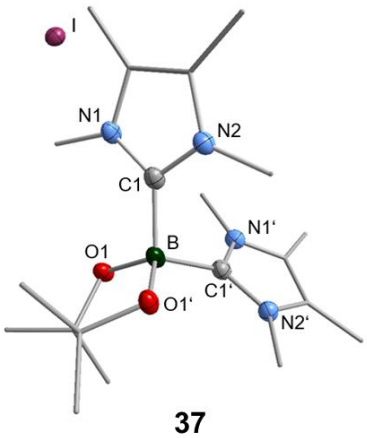

37

Abbildung 8.7 Molekülstruktur von $[(Me_2Im^{Me})_2$•$Bpin]^+I^-$ **37**.

Weitere Untersuchungen belegten, dass es bei der Reaktion des Aryliodids mit dem freien NHC Me_2Im^{Me} in Abwesenheit von B_2pin_2 neben der Ausbildung des Imidazoliumsalzes $[4\text{-}CH_3\text{-}C_6H_4\text{-}Me_2Im^{Me}]^+I^-$ **38** auch zur C–C-Kupplung zwischen dem Aryliodid und dem Lösungsmittel kommt. Ein vorläufiger Mechanismus (Schema 8.8) für den Boryltransfer von Me_2Im^{Me}•B_2pin_2 **20** auf Aryliodide wurde vorgeschlagen, wobei ein NHC–Bpin•-Radikal, welches eng mit dem beobachteten Radikal **35a** verwandt ist, als Schlüsselintermediat fungiert. Me_2Im^{Me}–Bpin• wird durch

homolytische Spaltung der B–B-Bindung des Bis-NHC-Addukts (Me_2Im^{Me})$_2$·B_2pin_2 gebildet, welches unter den gegebenen Reaktionsbedingungen in geringen Mengen *in situ* gebildet wird. Me_2Im^{Me}–Bpin· reagiert mit dem Aryliodid unter Rückgewinnung der Aromatizität zum gewünschten Arylboronsäureester. Im gleichen Schritt wird aus dem zweiten Äquivalent NHC–Bpin· ein NHC-stabilisiertes Iod-Bpin-Addukt als Zwischenprodukt gebildet. Dieses wird von einem weiteren NHC, unter Bildung des spektroskopisch und strukturell charakterisierten Boroniumsalzes [(Me_2Im^{Me})$_2$·Bpin]$^+$I$^-$ **37** koordiniert.

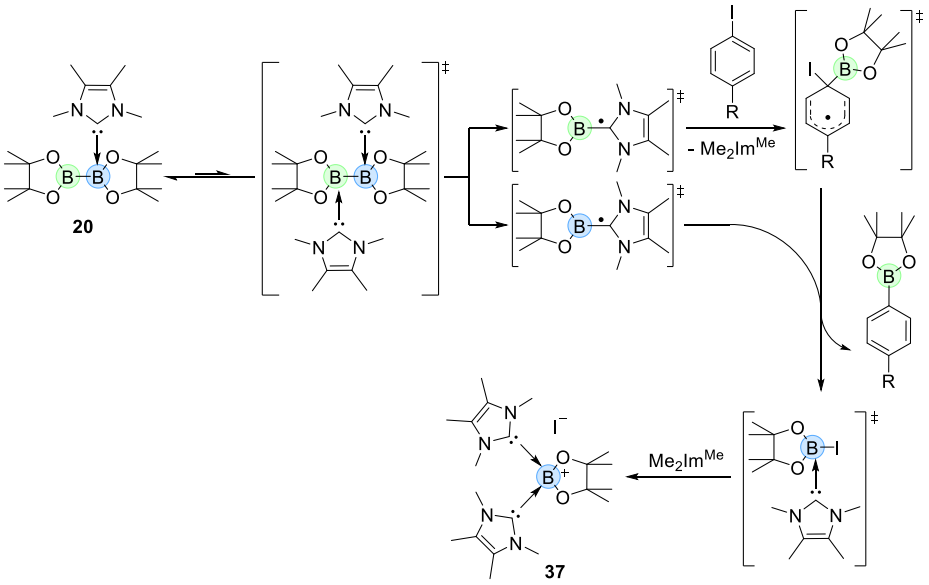

Schema 8.8 Postulierter Mechanismus für die Boryltransferreaktion vom Mono-NHC-Addukt Me_2Im^{Me}·B_2pin_2 **20** auf Aryliodide.

In einer möglichen Nebenreaktion könnte das Borylradikal NHC–Bpin· als Reduktionsmittel dienen, indem es ein Elektron an das Imidazoliumsalz [R-C_6H_4-Me_2Im^{Me}]$^+$I$^-$ **38** (R = CH_3) überträgt, welches in geringen Mengen in einer Nebenreaktion des freien NHCs mit dem Aryliodid gebildet wird. Dieser Schritt führt ebenfalls zur Bildung von **37** sowie einem Arylradikal. Letzteres kann eine radikalische C–C-Kupplungsreaktion eingehen, was die Bildung des Kupplungsprodukts zwischen dem Aryliodid und dem Lösungsmittel (Benzol) erklärt.

9 APPENDIX

9.1 ABBREVIATIONS

CARBENE LIGANDS

Me_2Im	1,3-dimethylimidazolin-2-ylidene
iPr_2Im	1,3-di-*iso*-propylimidazolin-2-ylidene
Cy_2Im	1,3-dicyclohexylimidazolin-2-ylidene
$Dipp_2Im$	1,3-(2,6-di-*iso*-propylphenyl)imidazolin-2-ylidene
$Dipp_2SIm$	1,3-(2,6-di-*iso*-propylphenyl)imidazolidine-2-ylidene
Mes_2Im	1,3-dimesitylimidazolin-2-ylidene
iPr_2Im^{Me}	1,3-di-*iso*-propyl-4,5-dimethylimidazolin-2-ylidene
Me_2Im^{Me}	1,3,4,5-tetramethylimidazolin-2-ylidene
$cAAC^{Me}$	1-(2,6-di-*iso*-propylphenyl)-3,3,5,5-tetramethylpyrrolidin-2-ylidene

BORON COMPOUNDS

B_2pin_2	bis(pinacolato)diborane(4)
B_2cat_2	bis(catecholato)diborane(4)
B_2neop_2	bis(neopentylglycolato)diborane(4)
B_2eg_2	bis(ethyleneglycolato)diborane(4)
$B_2(OH)_4$	(tetrahydroxy)diborane(4)
$B_2(OMe)_4$	(tetramethoxy)diborane(4)
HBpin	pinacolborane
HBcat	catecholborane

GENERAL

acac	acetylacetonato
AIBN	azobisisobutyronitrile
Ar	aryl
BDE	bond dissociation energy
BINAP	2,2'-bis(diphenylphosphino)-1,1'-binaphthyl
Bn	benzylic
BOC	tert-butyloxycarbonyl
cat	catecholato
cAAC	cyclic alkyl amino carbene
C_6D_6	deuterated benzene
COD	1,5-cyclooctadiene
COE	cyclooctene
COSY	correlation spectroscopy
CSD	Cambridge Structural Database
CV	Cyclic Voltammetry
Cy	cyclohexyl
Cyp	cyclopentyl
DBN	1,5-diazabicyclo[4.3.0]non-5-ene
DFT	Density Functional Theory
DIBAH	di-*iso*-butylaluminium hydride
diglyme	2-methoxyethyl ether
Dipp	2,6-di-*iso*-propylphenyl
DMAP	4-dimethylaminopyridine
DME	dimethoxyethane

DMF	dimethylformamide
DMS	dimethylsulfide
dppe	1,2-bis(diphenylphosphino)ethane
dppf	1,1’-bis(diphenylphosphino)ferrocene
dppp	1,3-bis(diphenylphosphino)propane
DTBP	di-*tert*-butylperoxide
dtbpy	4,4’-di-*tert*-butyl-2,2’-bipyridine
eg	ethylene glycolato
EPR	electron paramagnetic resonance
equiv.	equivalents
ESR	Elektronenspinresonanz
Et	ethyl
Et_2O	diethylether
EWG	electron withdrawing group
GC	gas chromatography
GPC	gel permeation chromatography
h	hour
HRMS	high-resolution mass spectrometry
*i*Pr	*iso*-propyl
ISC	intersystem-crossing
J	coupling constant in NMR spectroscopy, Hz
M	molar concentration, 1 M = 1 mol L^{-1}
M^+	molecular ion peak in MS
MAS	magic-angle spinning
Me	methyl

MeCN	acetonitrile
Me-Cy	methylcyclohexane
MeO	methoxy
MeOH	methanol
Mes	mesityl
MHz	megahertz
min	minute
mol%	percentage by amount
mpy	4-methyl-pyridine
MS	mass spectrometry
MTBE	methyl *tert*-butyl ether
m/z	mass-to-charge ratio in MS
*n*Bu	*n*-butyl
neop	neopentylglycolato
*n*Pr	*n*-propyl
NHC	*N*-heterocyclic carbene
NMR	nuclear magnetic resonance
OD	outer diameter
PDI	polydispersity index
PDIPA	pinacolato di-*iso*-propanol-aminato
Ph	phenyl
pin	pinacolato
piv	pivalyl
PNP	*N*-{2-P(*i*Pr$_2$)$_2$-4-methylphenyl}$_2$
ppm	parts per million

PyO	2-pyridyloxy
RER	ring expansion reaction
RF	response factor
r.t.	room temperature
SED	single electron donor
SET	single electron transfer
SOMO	single occupied molecular orbital
TCNE	tetracyanoethene
TCNQ	7,7,8,8-tetracyano-*p*-quinodimethane
TEMPO	(2,2,6,6-tetramethylpiperidin-1-yl)oxyl
TET	triplet energy transfer
THF	tetrahydrofuran
TIC	total ion current
TMS	trimethylsilyl
*t*Bu	*tert*-butyl
*t*BuO	*tert*-butoxy
VCB	vinylcyclobutane
VCP	vinylcyclopropane
wt%	percent by weight
XantPhos	4,5-bis(diphenylphosphino)-9,9-dimethylxanthene

9.2 LIST OF COMPOUNDS

1 [$Ni_2(Cy_2Im)_4(\mu\text{-}(\eta^2\text{:}\eta^2)\text{-}COD)$]

2 [$Ni(Cy_2Im)_2(\eta^2\text{-}C_2H_4)$]

3 [$Ni(Cy_2Im)_2(\eta^2\text{-}COE)$]

4 4-F_3C-C_6H_4Bpin

5 4-CH_3-C_6H_4Bpin

6 4-MeO-C_6H_4Bpin

7 C_6H_5Bpin

8 3,5-$F_2C_6H_3$Bpin

9 4-FC_6H_4Bpin

10 3-PyridineBpin

11 *trans*-[$Ni(Cy_2Im)_2(Cl)(4\text{-}F_3C\text{-}C_6H_4)$]

12 *trans*-[$Ni(Cy_2Im)_2(Cl)(4\text{-MeO-}C_6H_4)$]

13 *trans*-[$Ni(Cy_2Im)_2(Cl)(C_6H_5)$]

14 *trans*-[$Ni(Cy_2Im)_2(Cl)(3,5\text{-}F_2C_6H_3)$]

15 [$Cu(i\text{Pr}_2Im)(Cl)$]

16 [$Cu(Me_2Im^{Me})(Cl)$]

17 [$Cu(Cy_2Im)(Cl)$]

18 Pyridine·B_2cat_2

19 DMAP·B_2cat_2

20 Me_2Im^{Me}·B_2pin_2

21 $i\text{Pr}_2Im^{Me}$·B_2pin_2

22 $i\text{Pr}_2Im^{Me}$·$B_2(OMe)_4$

23 Cy_2Im·$B_2(OMe)_4$

24 $(Cy_2Im)_2$·B_2cat_2

25 (iPr$_2$Im^{Me})$_2$·B$_2$cat$_2$

26 Cy$_2$Im·HBpin

27 iPr$_2$Im^{Me}·HBpin

28 Me$_2$Im^{Me}·HBpin

29 cAAC^{Me}(H)Bpin

30 3,5-F$_2$C$_6$H$_3$Bpin·Cy$_2$Im

31 4-CH$_3$-C$_6$H$_4$Bpin·Cy$_2$Im

32 C$_6$H$_5$Bneop·Cy$_2$Im

33 BiphenylBneop·Cy$_2$Im

34 4-F$_3$C-C$_6$H$_4$Bpin·Me$_2$Im^{Me}

35 (Me$_2$Im^{Me})$_2$·B$_2$neop$_2$

35a Me$_2$Im^{Me}–Bneop$^{\cdot}$

36 RER-(Me$_2$Im^{Me})$_2$·B$_2$neop$_2$

37 [(Me$_2$Im^{Me})$_2$·Bpin]$^+$I$^-$

38 [4-CH$_3$-C$_6$H$_4$-Me$_2$Im^{Me}]$^+$I$^-$

9.3 ADDITIONAL NMR DATA OF UNPUBLISHED COMPOUNDS

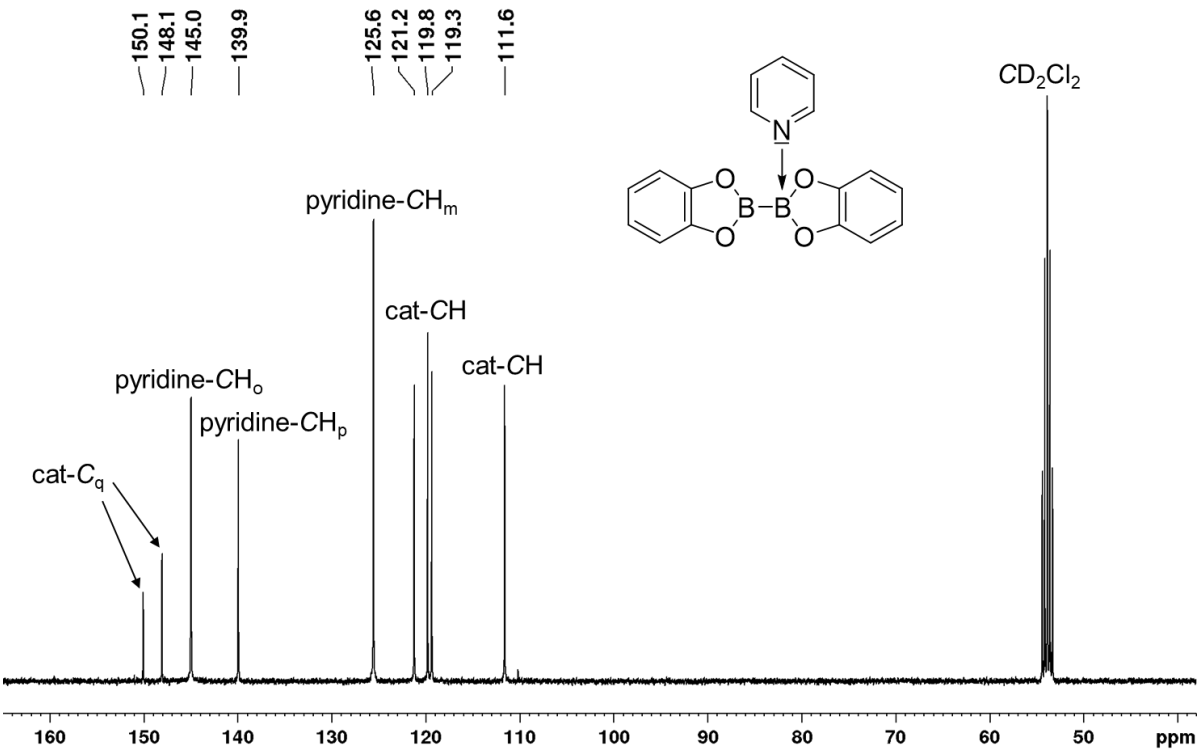

Figure 9.1 $^{13}C\{^{1}H\}$ NMR spectrum of pyridine·B_2cat_2 **18** recorded in CD_2Cl_2 (400 MHz).

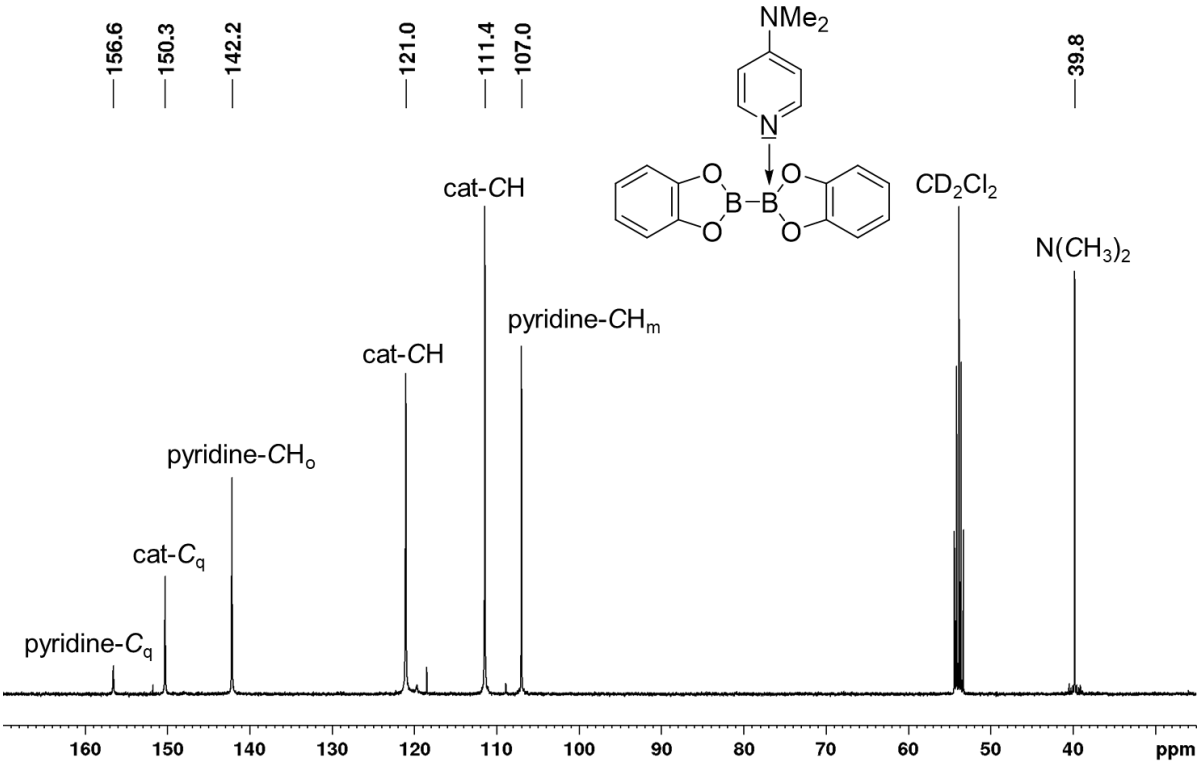

Figure 9.2 $^{13}C\{^{1}H\}$ NMR spectrum of DMAP·B_2cat_2 **19** recorded in CD_2Cl_2 (100 MHz).

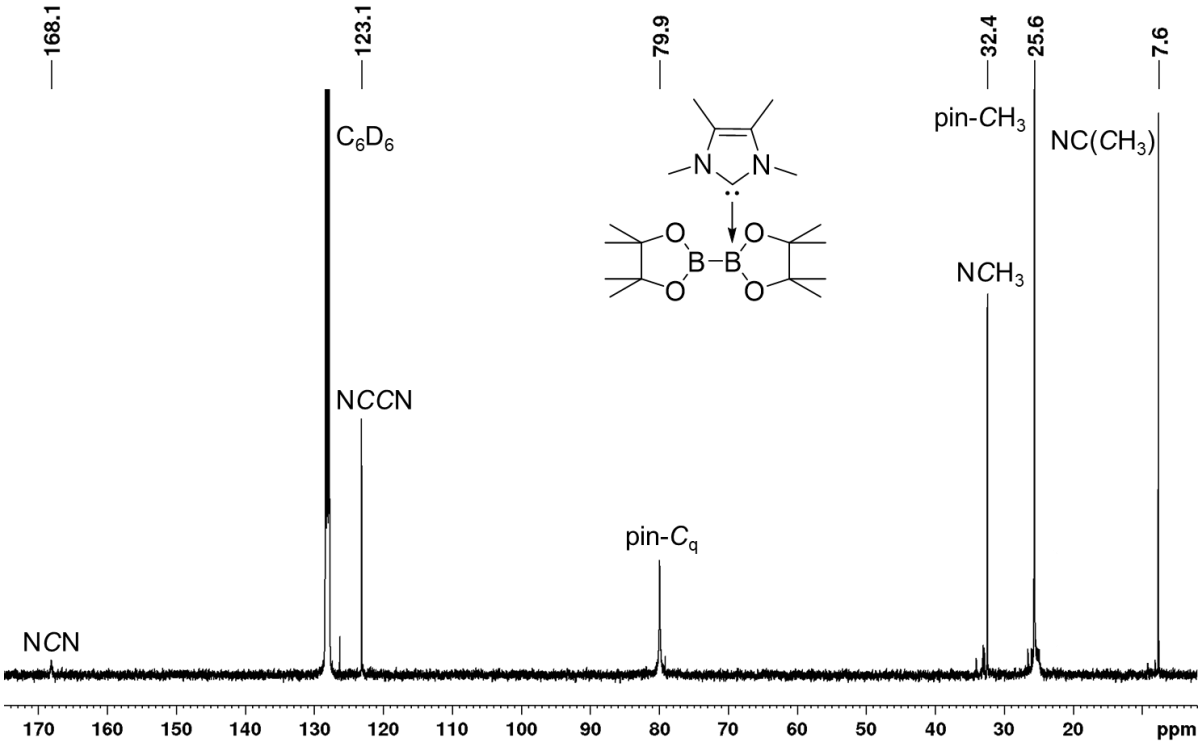

Figure 9.3 $^{13}C\{^{1}H\}$ NMR spectrum of $Me_2Im^{Me}{\cdot}B_2pin_2$ **20** recorded in C_6D_6 (100 MHz).

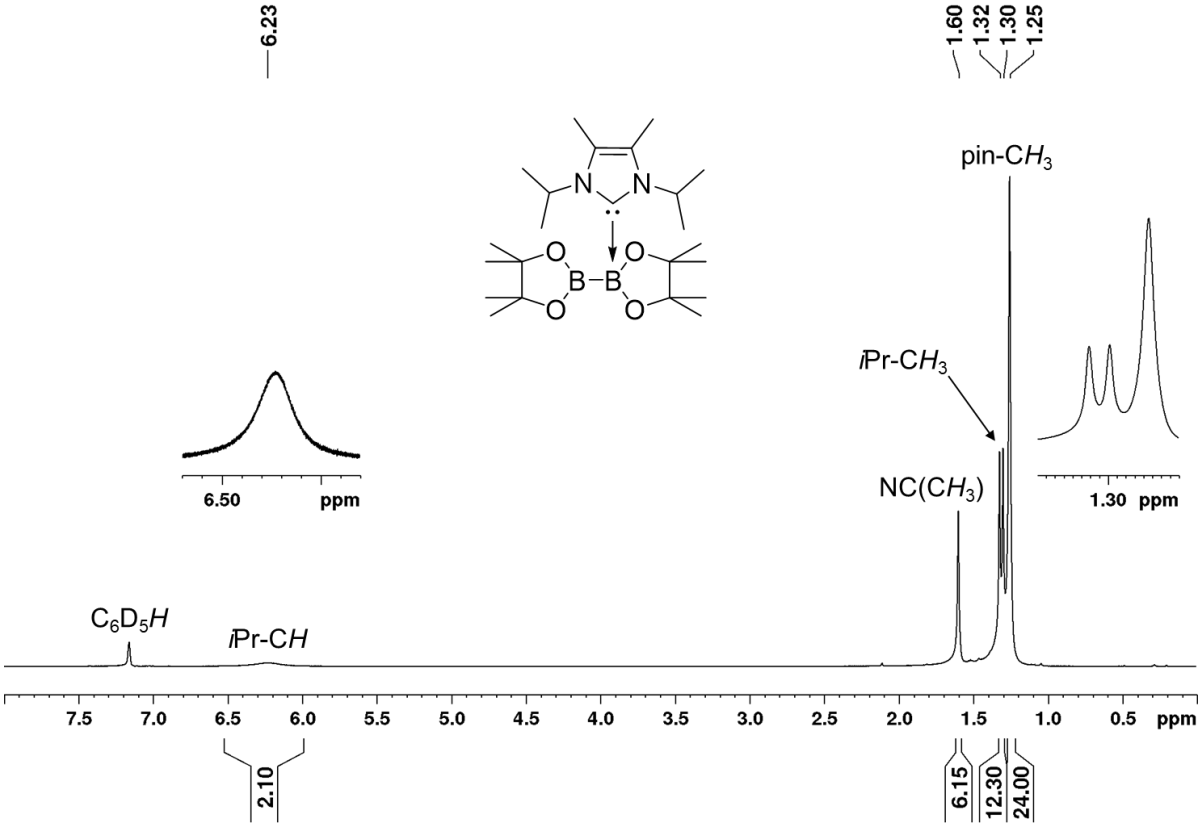

Figure 9.4 ^{1}H NMR spectrum of $iPr_2Im^{Me}{\cdot}B_2pin_2$ **21** recorded in C_6D_6 (400 MHz).

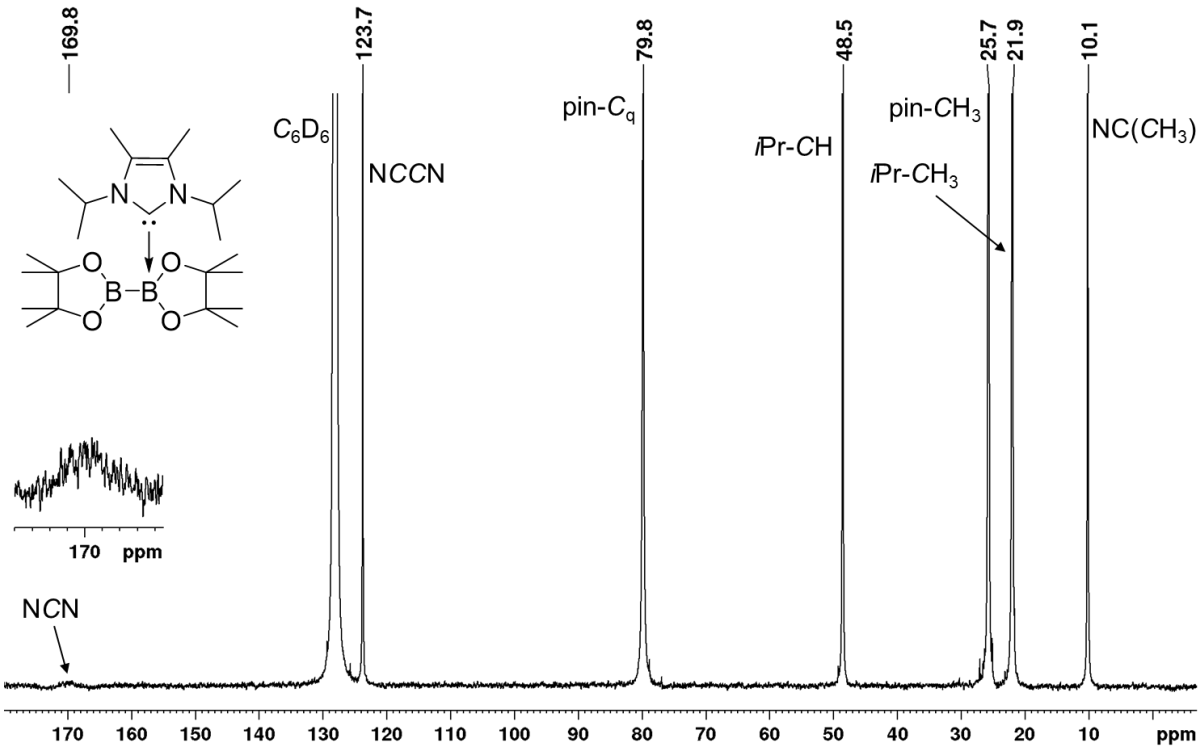

Figure 9.5 $^{13}C\{^1H\}$ NMR spectrum of *i*Pr_2Im^{Me}·B_2pin_2 **21** recorded in C_6D_6 (100 MHz).

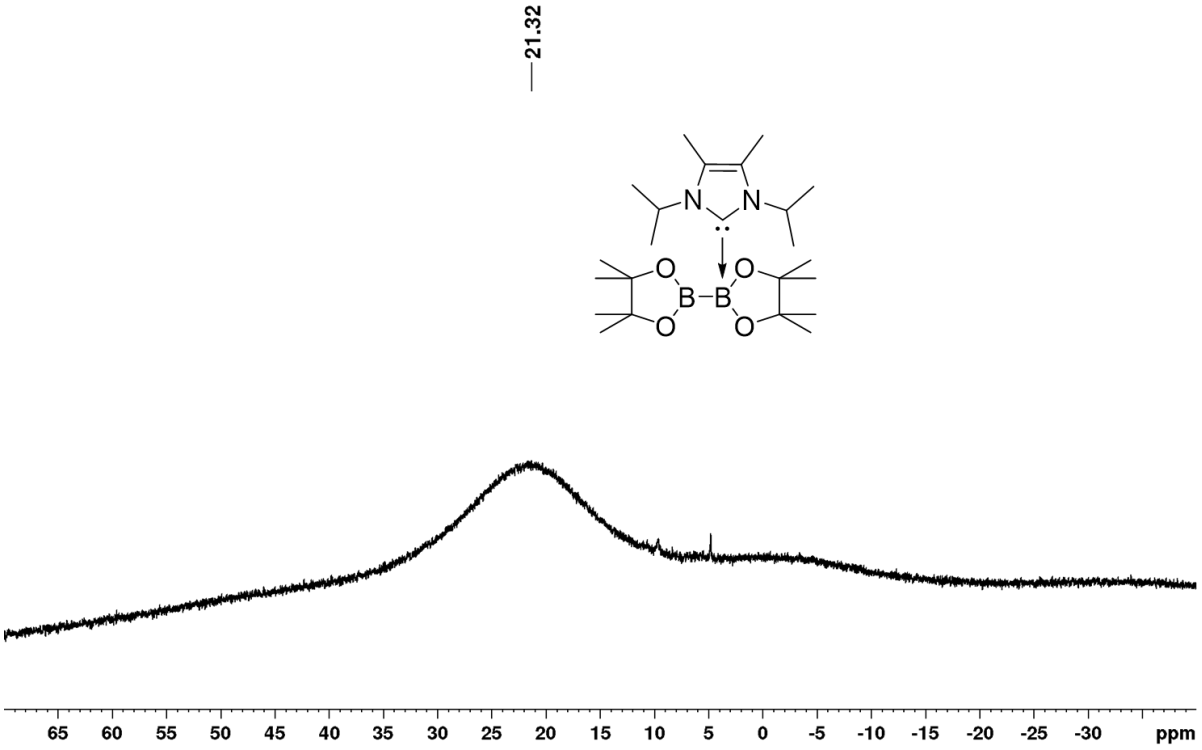

Figure 9.6 $^{11}B\{^1H\}$ NMR spectrum of *i*Pr_2Im^{Me}·B_2pin_2 **21** recorded in C_6D_6 at 25 °C (128 MHz).

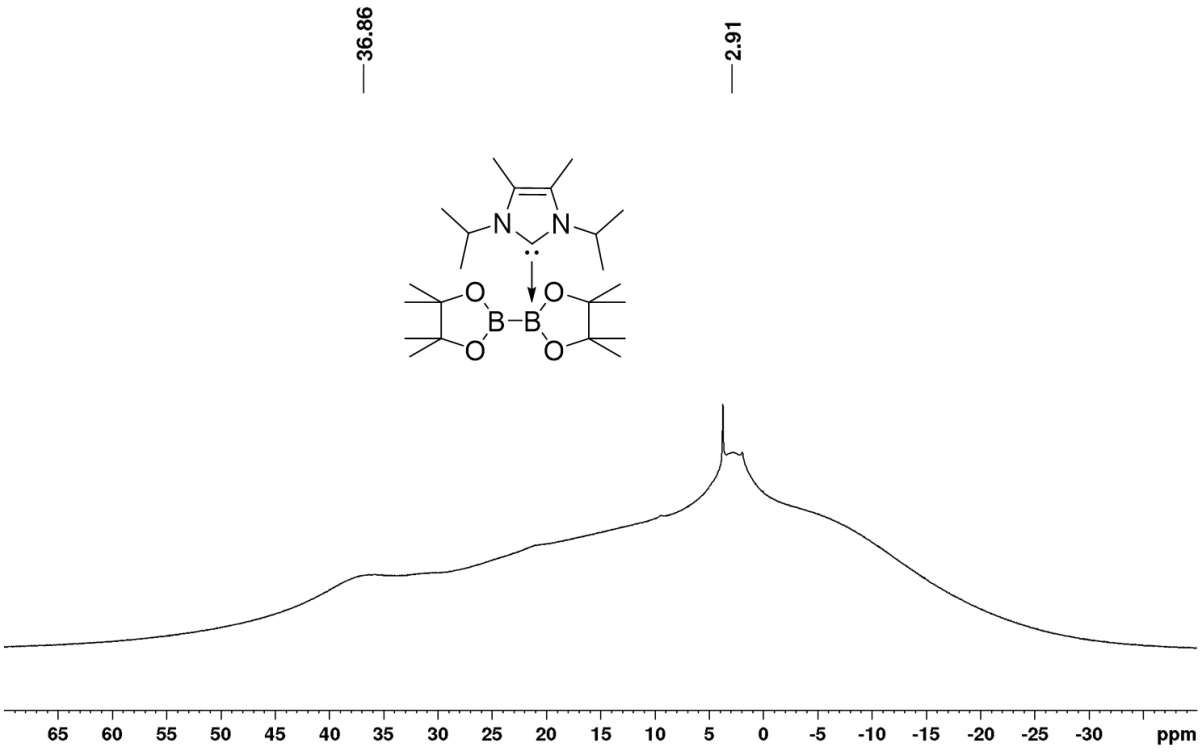

Figure 9.7 ^{11}B NMR spectrum of *i*Pr$_2$Im^{Me}·B$_2$pin$_2$ **21** recorded in C_6D_6 at 0 °C (160 MHz).

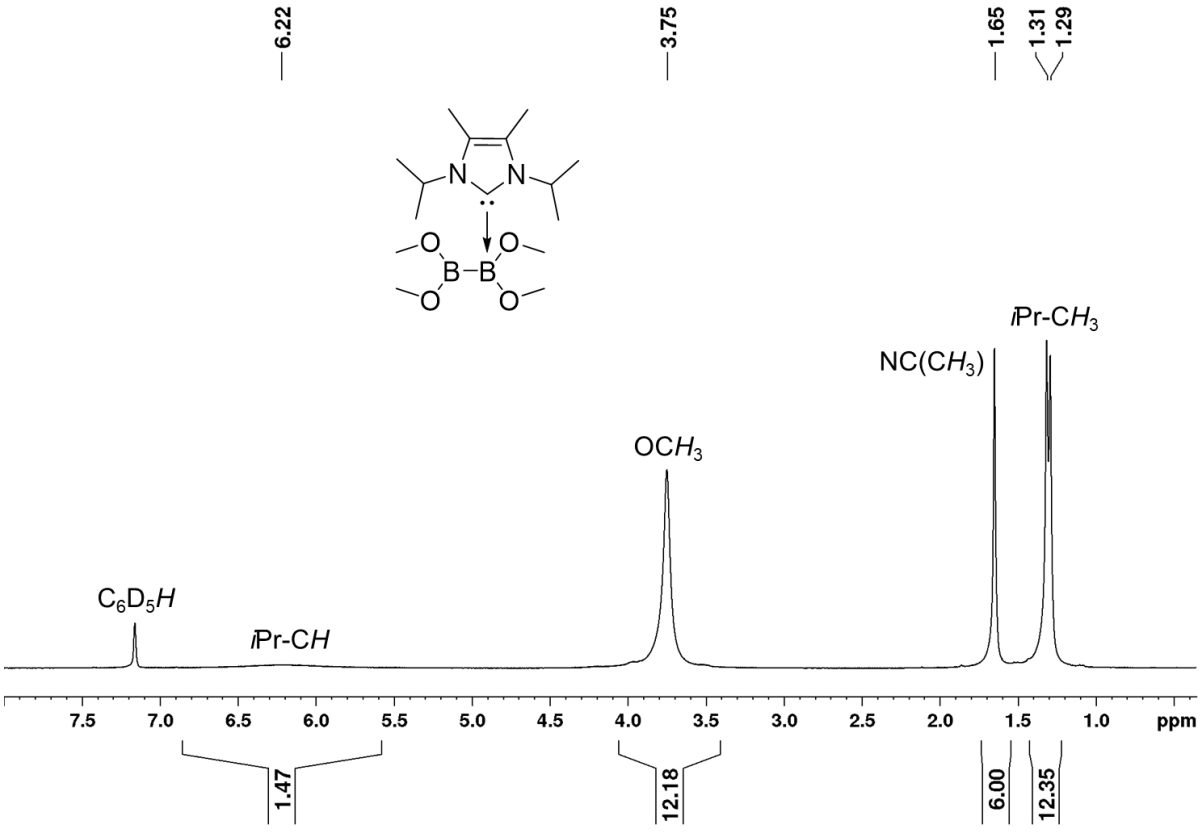

Figure 9.8 ^{1}H NMR spectrum of *i*Pr$_2$Im^{Me}·B$_2$(OMe)$_4$ **22** recorded in C_6D_6 (500 MHz).

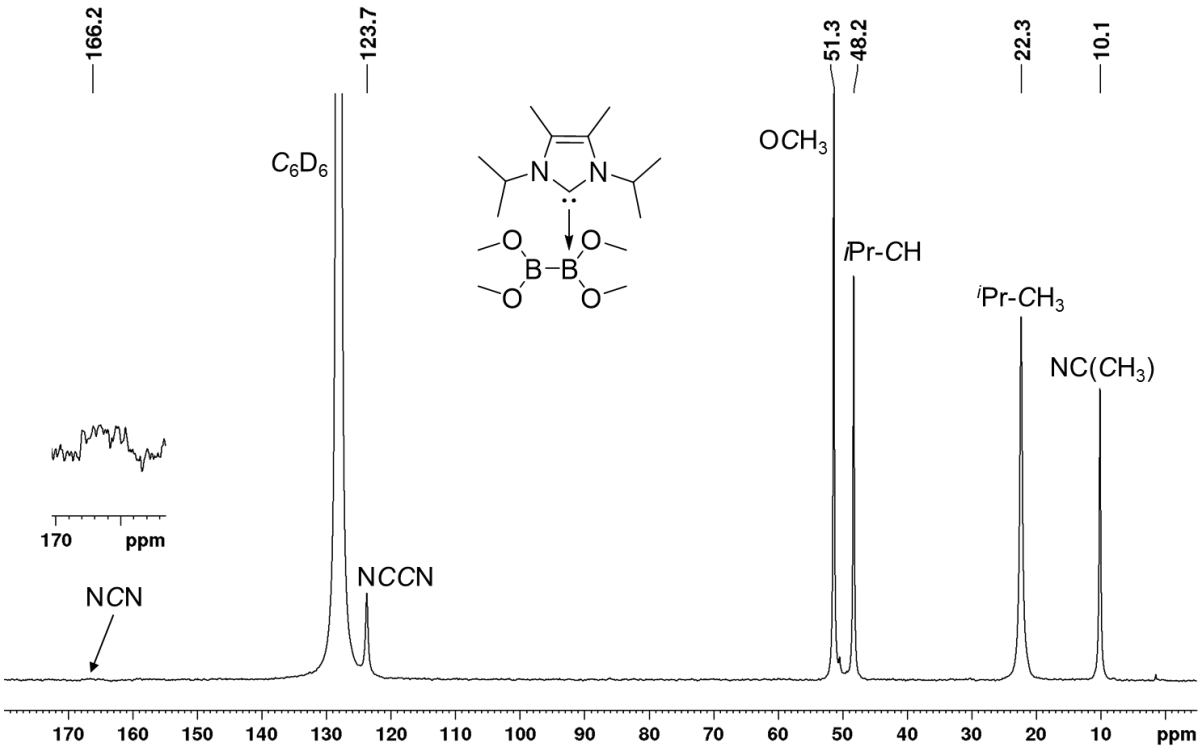

Figure 9.9 $^{13}C\{^{1}H\}$ NMR spectrum of *i*Pr_2Im^{Me}·$B_2(OMe)_4$ **22** recorded in C_6D_6 (125 MHz).

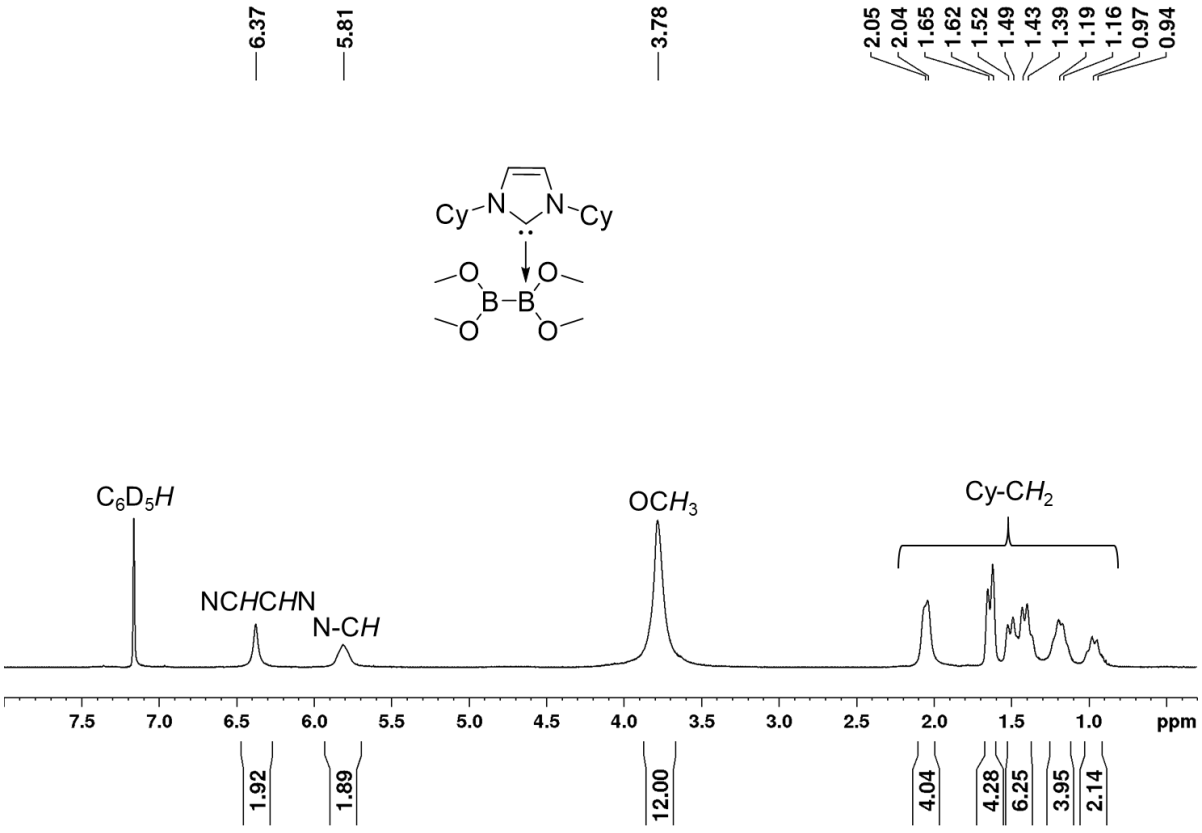

Figure 9.10 ^{1}H NMR spectrum of Cy_2Im·$B_2(OMe)_4$ **23** recorded in C_6D_6 (400 MHz).

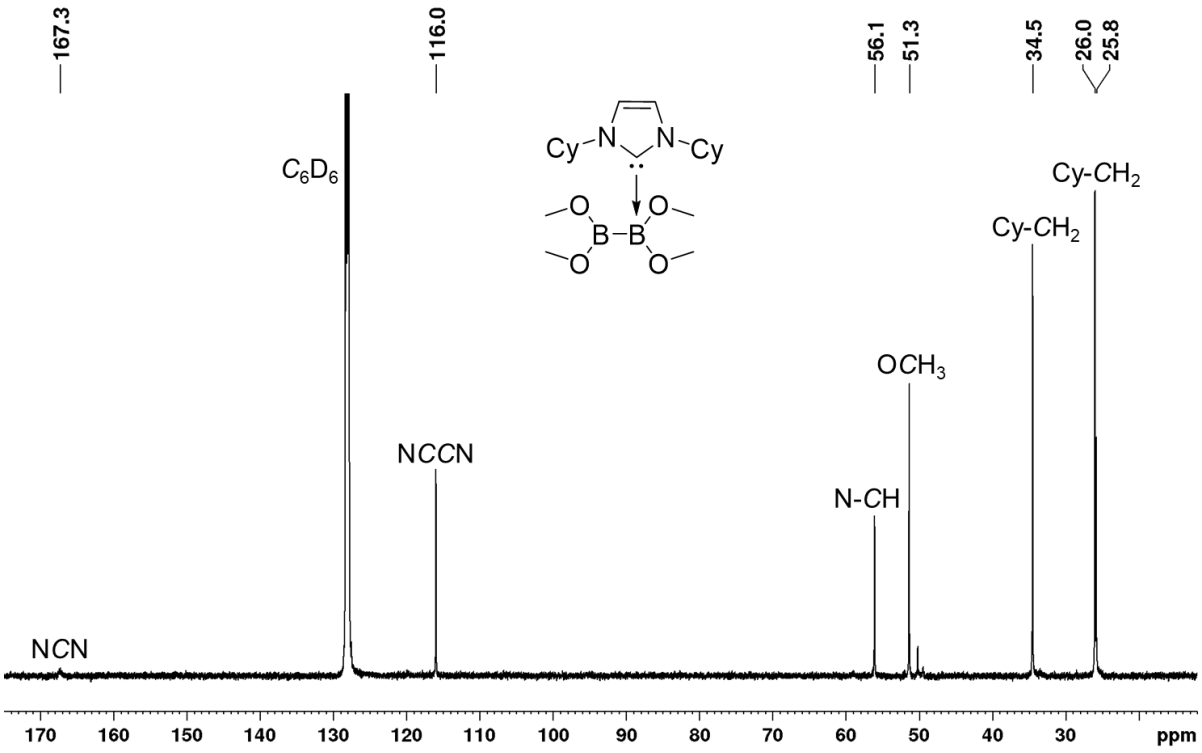

Figure 9.11 $^{13}C\{^{1}H\}$ NMR spectrum of $Cy_2Im{\cdot}B_2(OMe)_4$ **23** recorded in C_6D_6 (125 MHz).

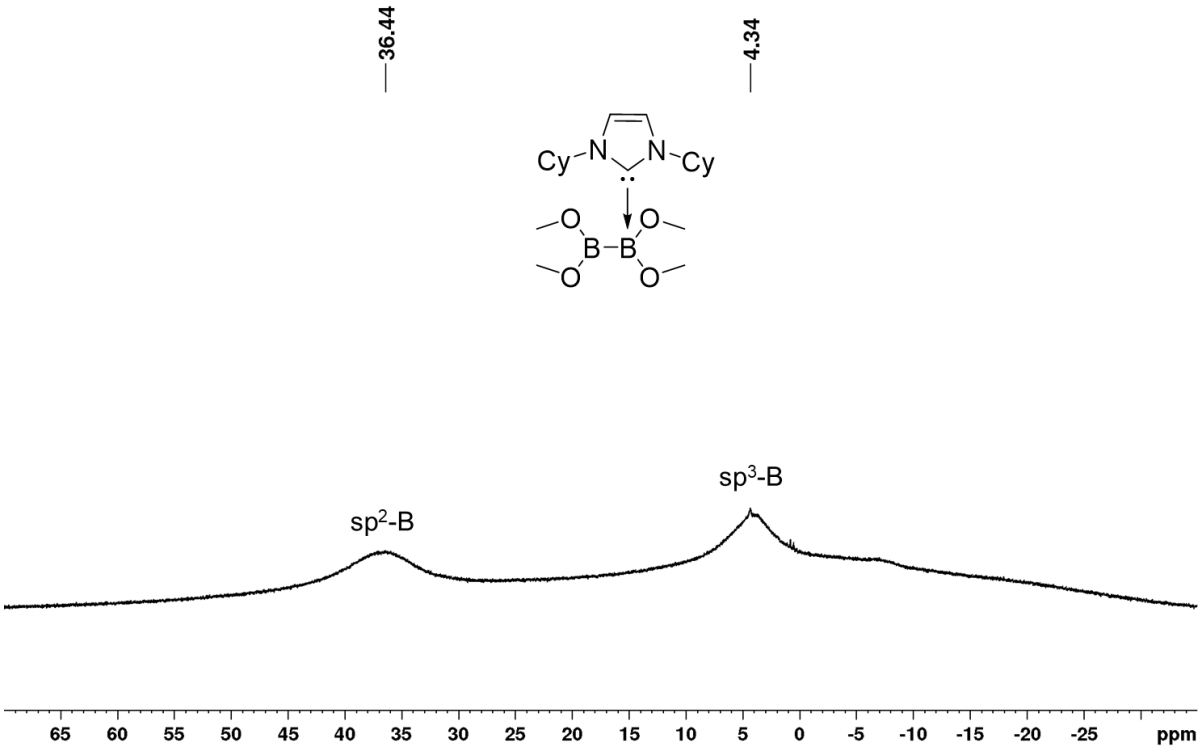

Figure 9.12 $^{11}B\{^{1}H\}$ NMR spectrum of $Cy_2Im{\cdot}B_2(OMe)_4$ **23** recorded in C_6D_6 (128 MHz).

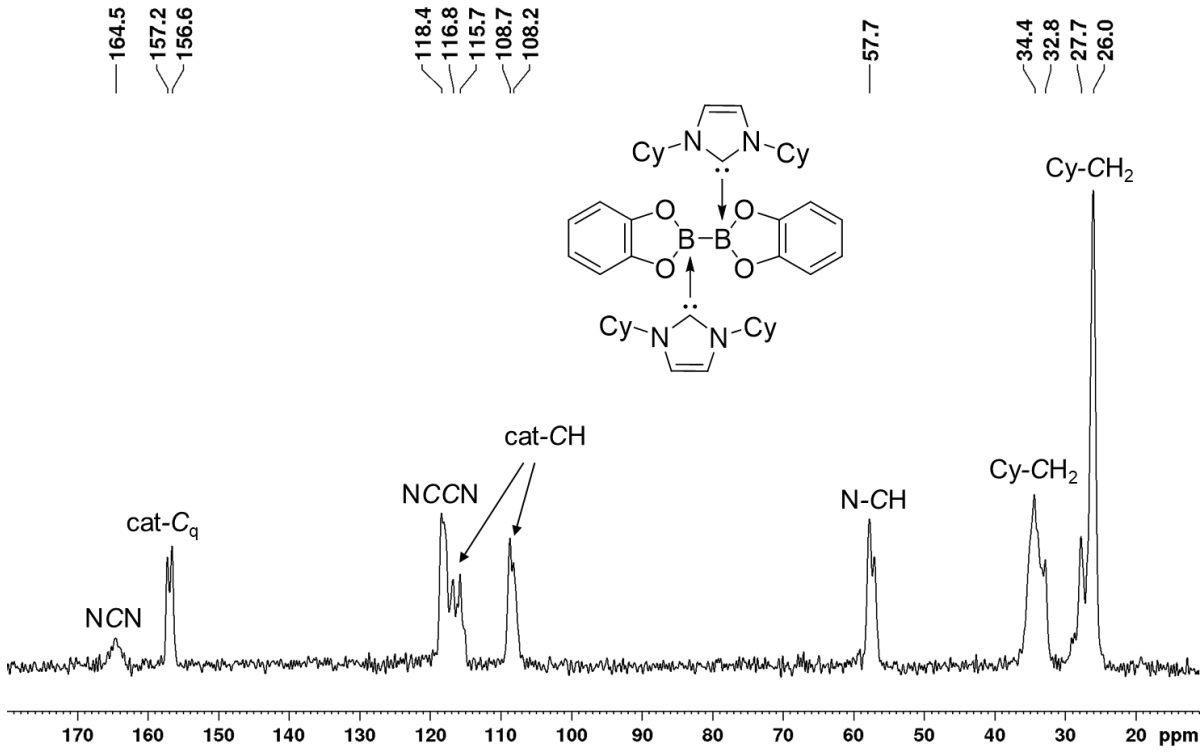

Figure 9.13 ^{13}C CP/MAS NMR spectrum of $(Cy_2Im)_2 \cdot B_2cat_2$ **24** (100 MHz, 25 °C, *v* rot = 9000 Hz**)**.

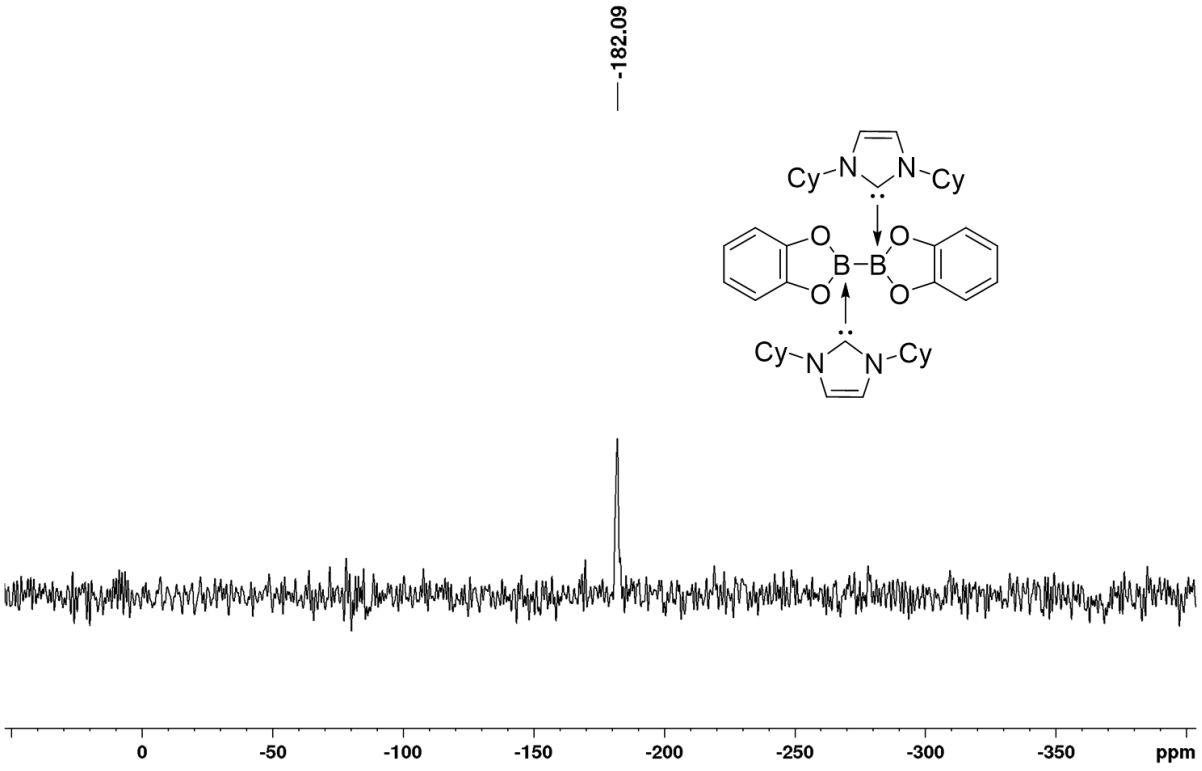

Figure 9.14 ^{15}N CP/MAS NMR spectrum of $(Cy_2Im)_2 \cdot B_2cat_2$ **24 (**40 MHz, 25 °C, *v* rot = 8000 Hz**)**.

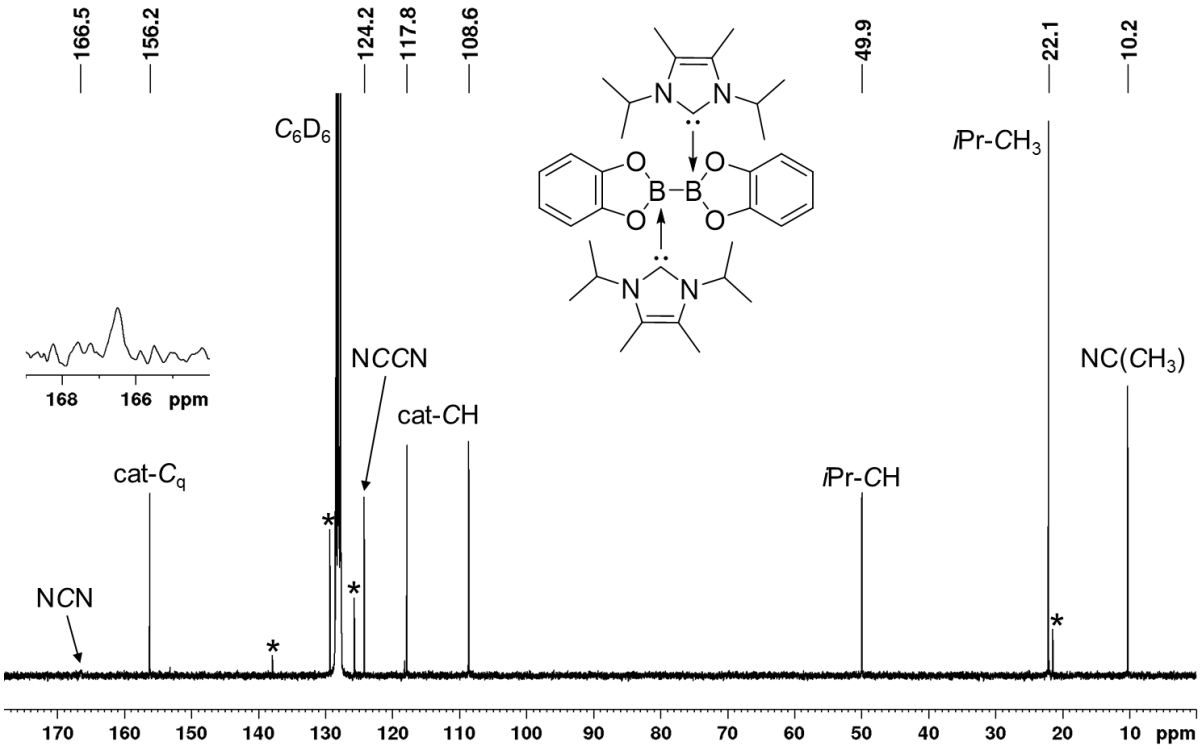

Figure 9.15 $^{13}C\{^{1}H\}$ NMR spectrum of $(i\text{Pr}_2\text{Im}^{Me})_2\cdot B_2\text{cat}_2$ **25** recorded in C_6D_6 (75 MHz; asterisk: toluene in a 1:1 ratio (**25**:toluene)).

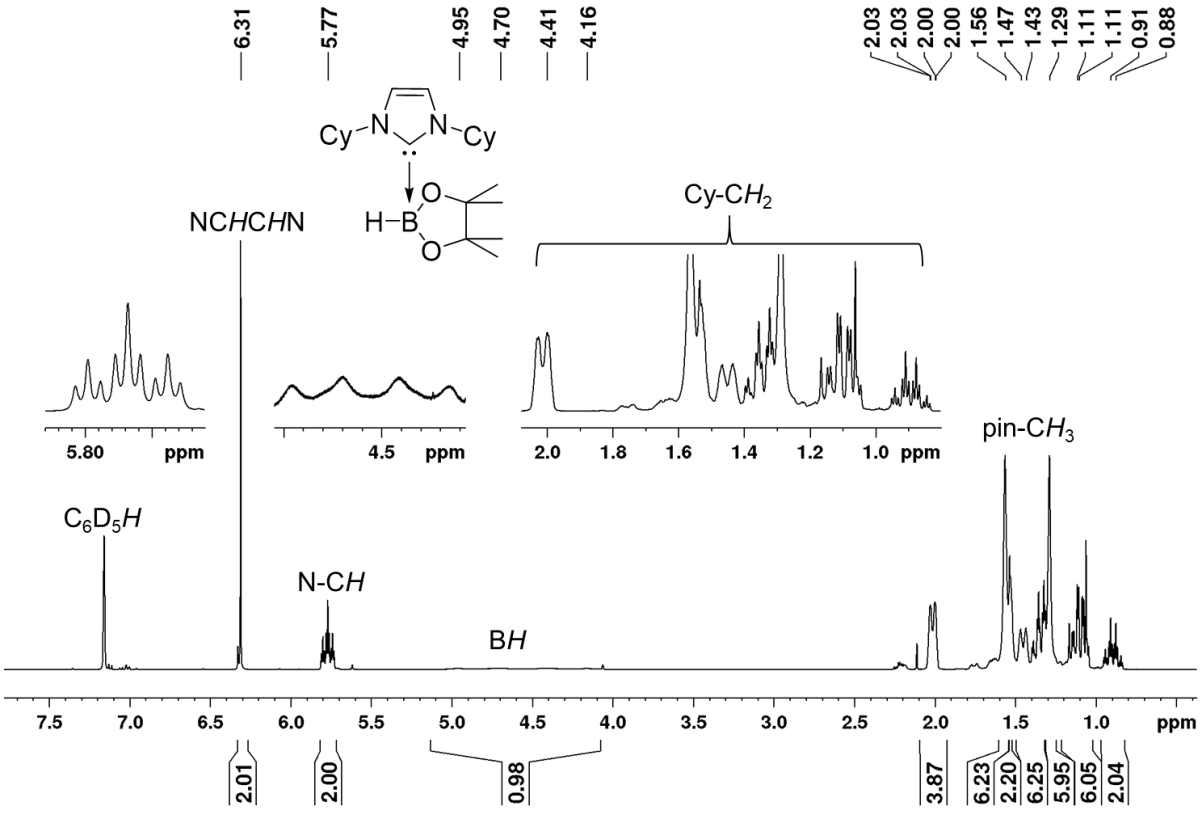

Figure 9.16 ^{1}H NMR spectrum of $Cy_2\text{Im}\cdot\text{HBpin}$ **26** recorded in C_6D_6 (400 MHz).

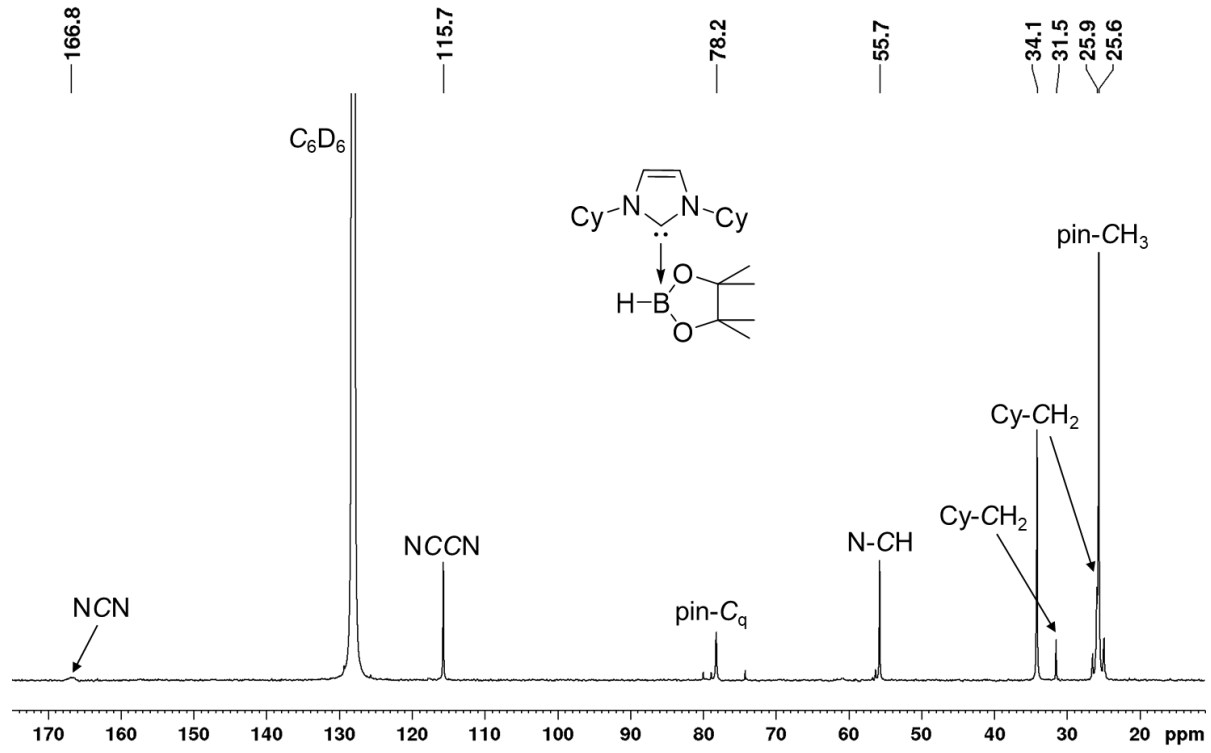

Figure 9.17 $^{13}C\{^{1}H\}$ NMR spectrum of $Cy_2Im{\cdot}HBpin$ **26** recorded in C_6D_6 (100 MHz).

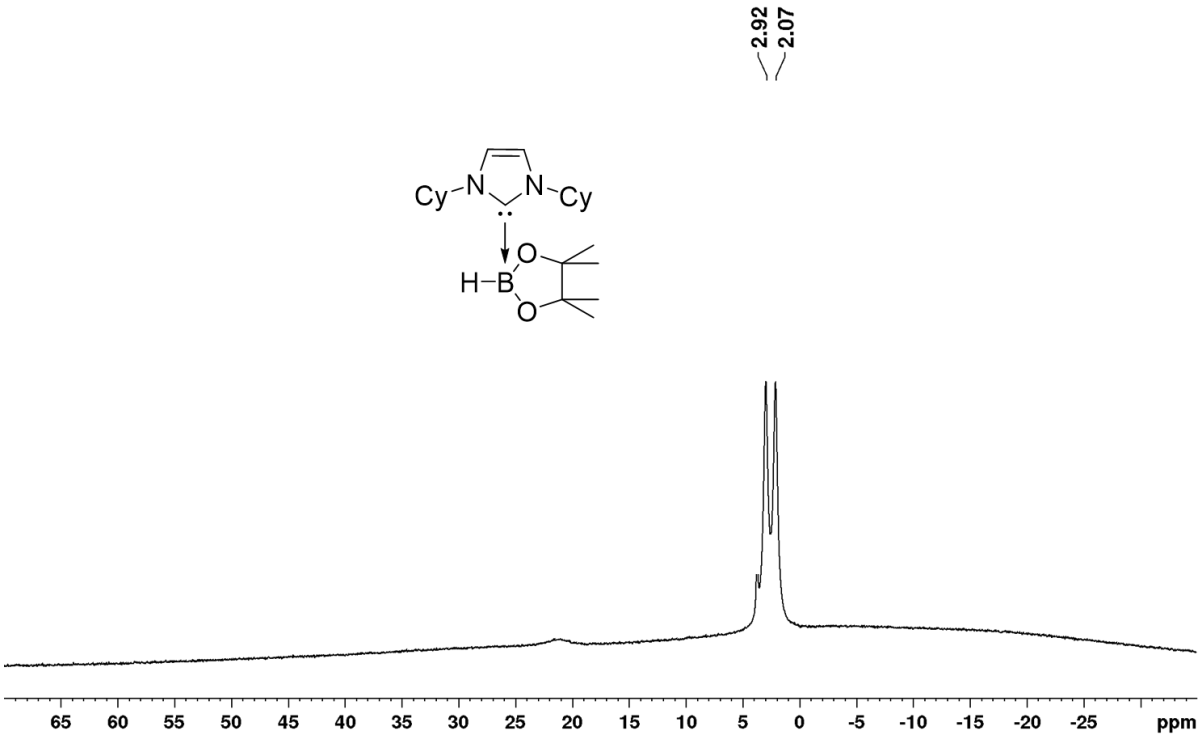

Figure 9.18 ^{11}B NMR spectrum of $Cy_2Im{\cdot}HBpin$ **26** recorded in C_6D_6 (128 MHz).

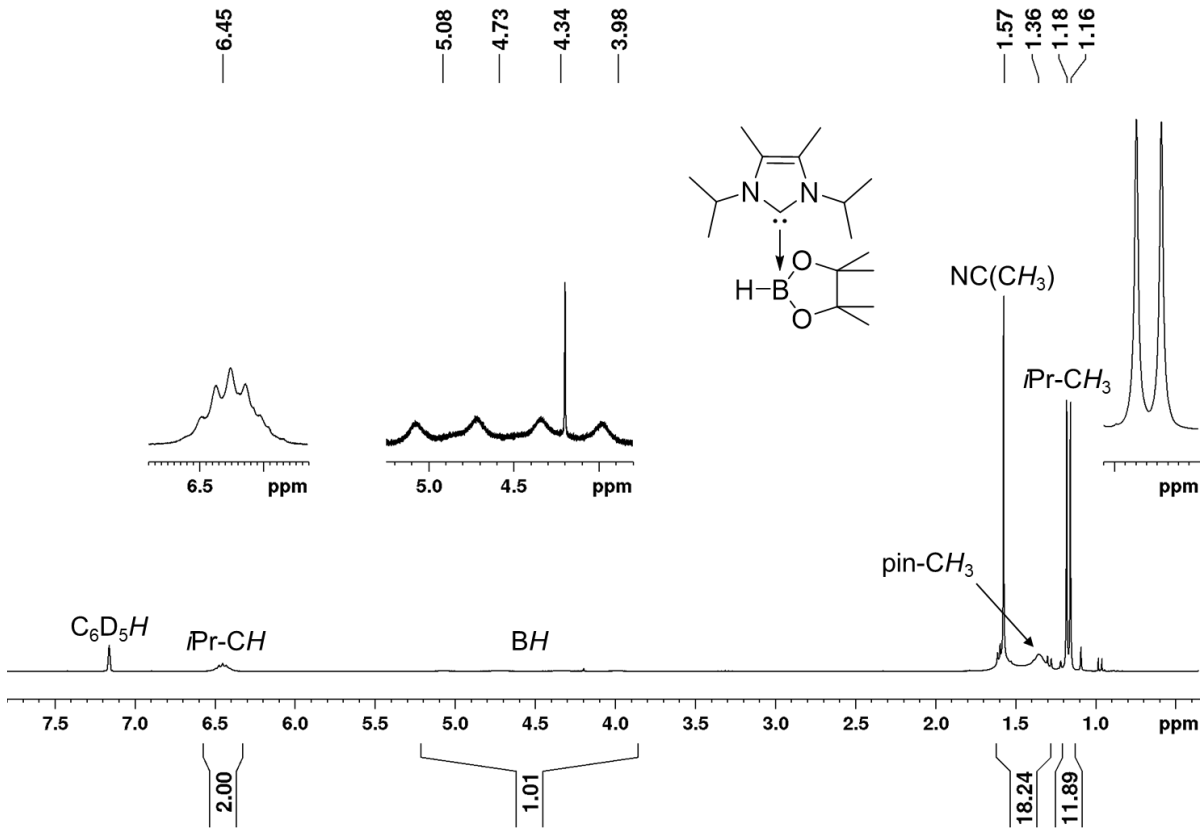

Figure 9.19 ^{1}H NMR spectrum of *i*Pr$_2$Im^{Me}·HBpin **27** recorded in C_6D_6 (500 MHz).

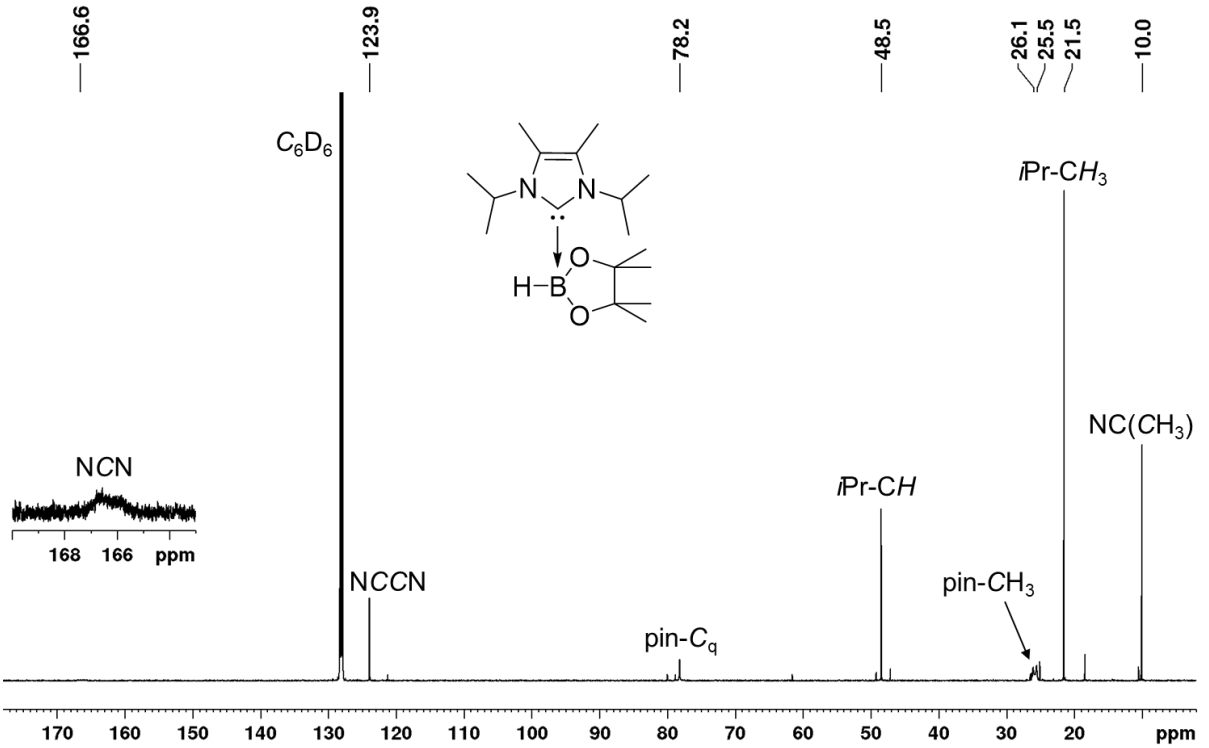

Figure 9.20 ^{13}C{^{1}H} NMR spectrum of *i*Pr$_2$Im^{Me}·HBpin **27** recorded in C_6D_6 (125 MHz).

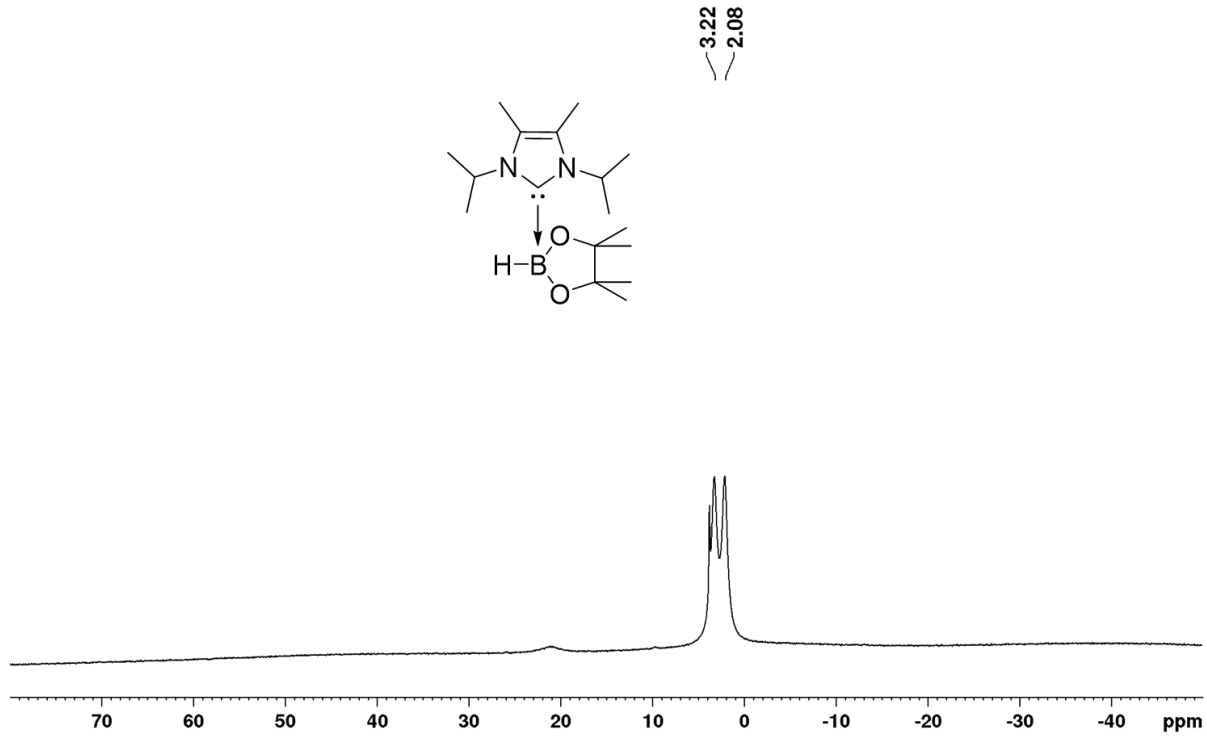

Figure 9.21 ^{11}B NMR spectrum of *i*Pr$_2$Im^{Me}·HBpin **27** recorded in C_6D_6 (160 MHz).

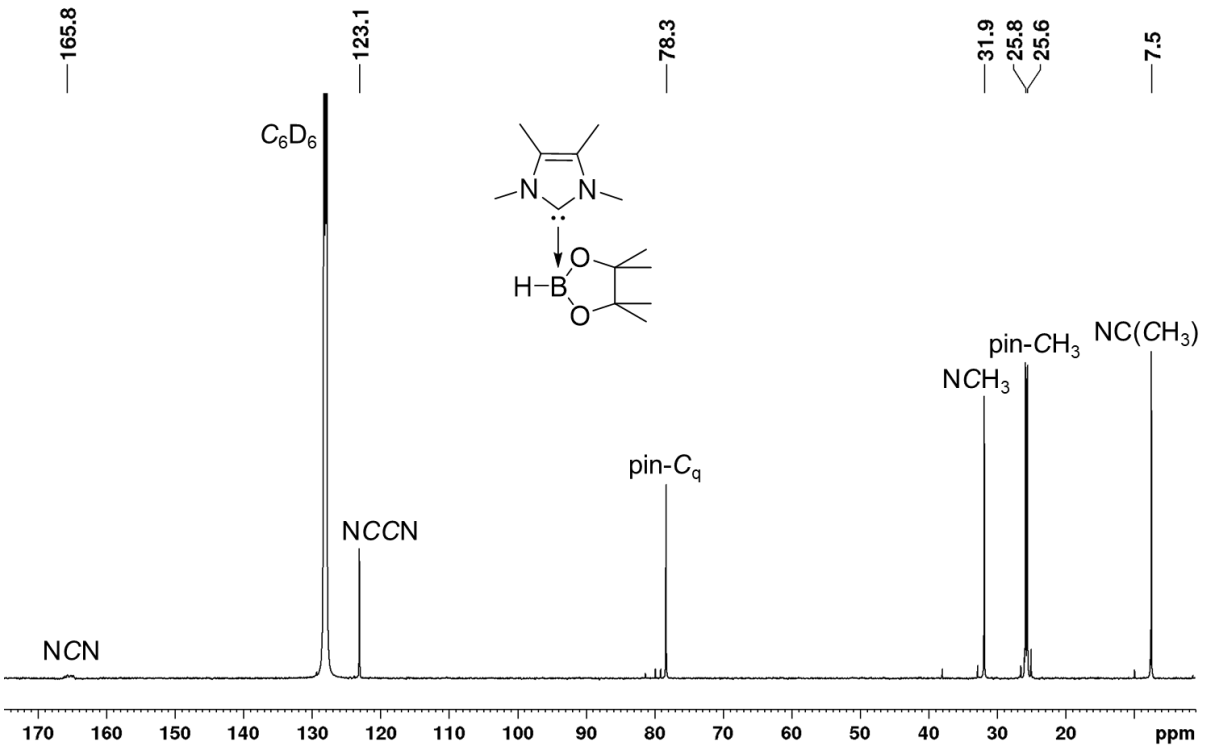

Figure 9.22 ^{13}C{^{1}H} NMR spectrum of Me$_2$Im^{Me}·HBpin **28** recorded in C_6D_6 (125 MHz).

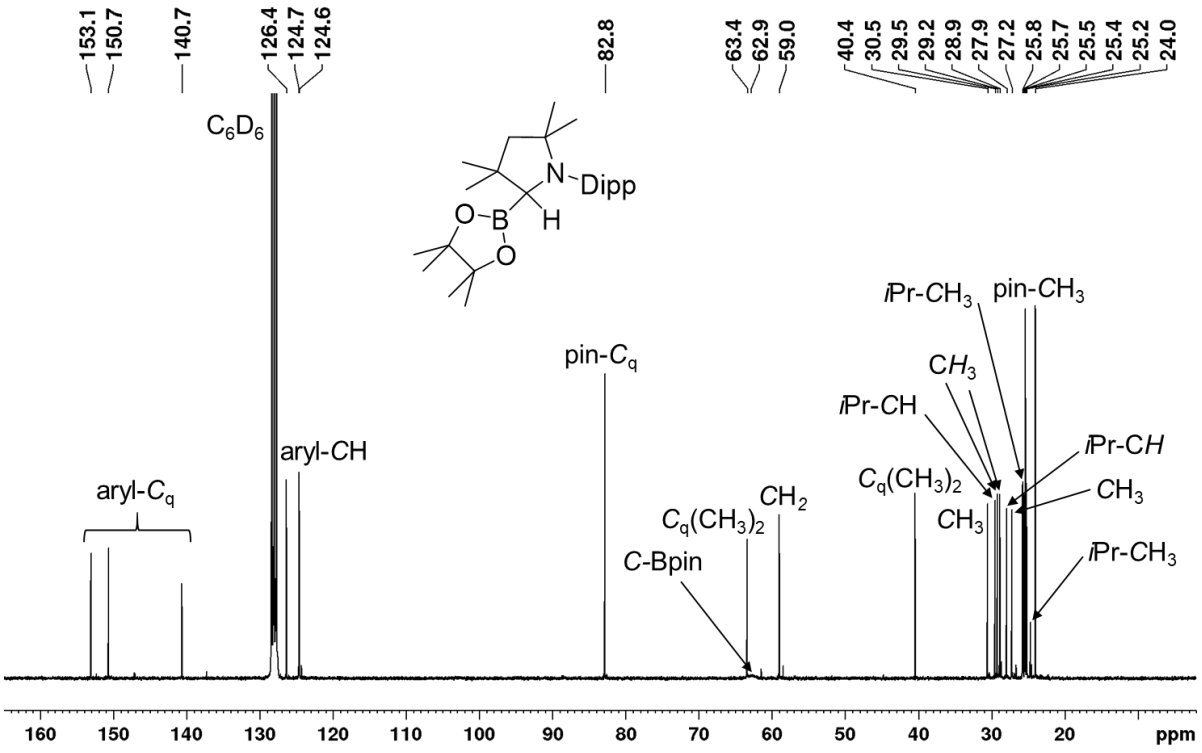

Figure 9.23 $^{13}C\{^{1}H\}$ NMR spectrum of cAAC^{Me}(H)Bpin **29** recorded in C_6D_6 (100 MHz).

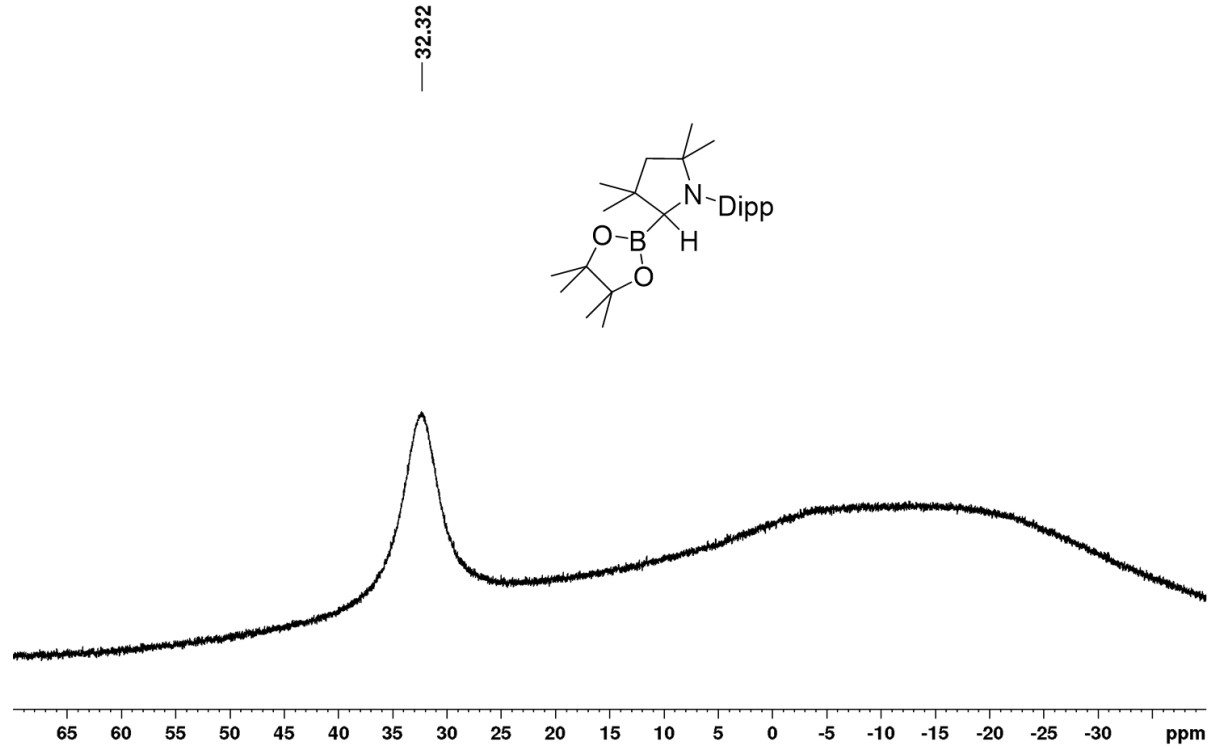

Figure 9.24 $^{11}B\{^{1}H\}$ NMR spectrum of cAAC^{Me}(H)Bpin **29** recorded in C_6D_6 (128 MHz).

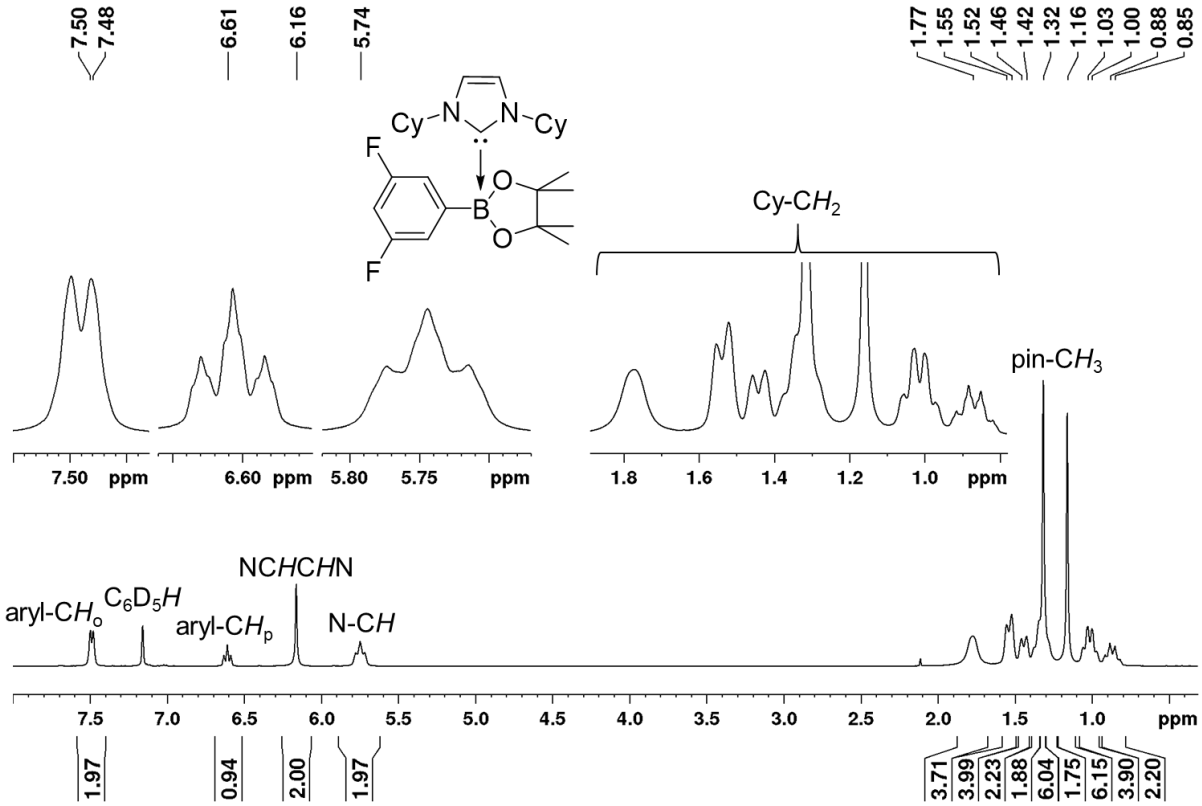

Figure 9.25 ^{1}H NMR spectrum of 3,5-$F_2C_6H_3$Bpin·Cy_2Im **30** recorded in C_6D_6 (500 MHz).

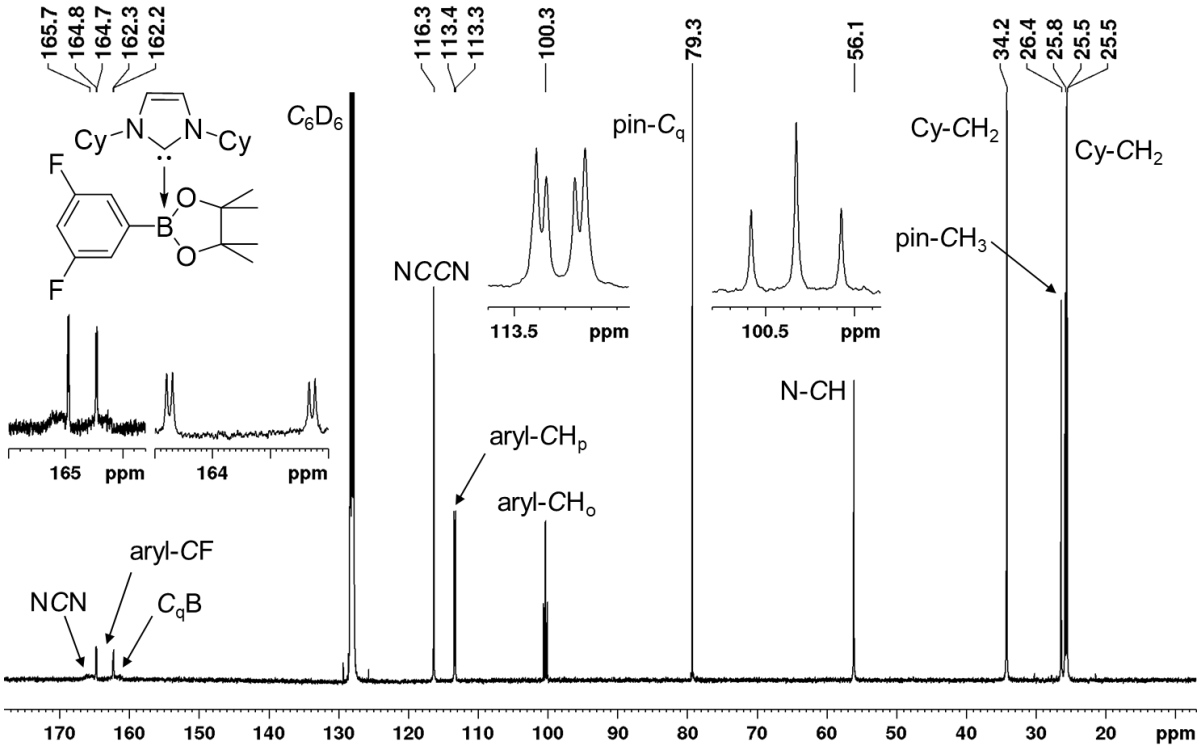

Figure 9.26 ^{13}C{^{1}H} NMR spectrum of 3,5-$F_2C_6H_3$Bpin·Cy_2Im **30** recorded in C_6D_6 (125 MHz).

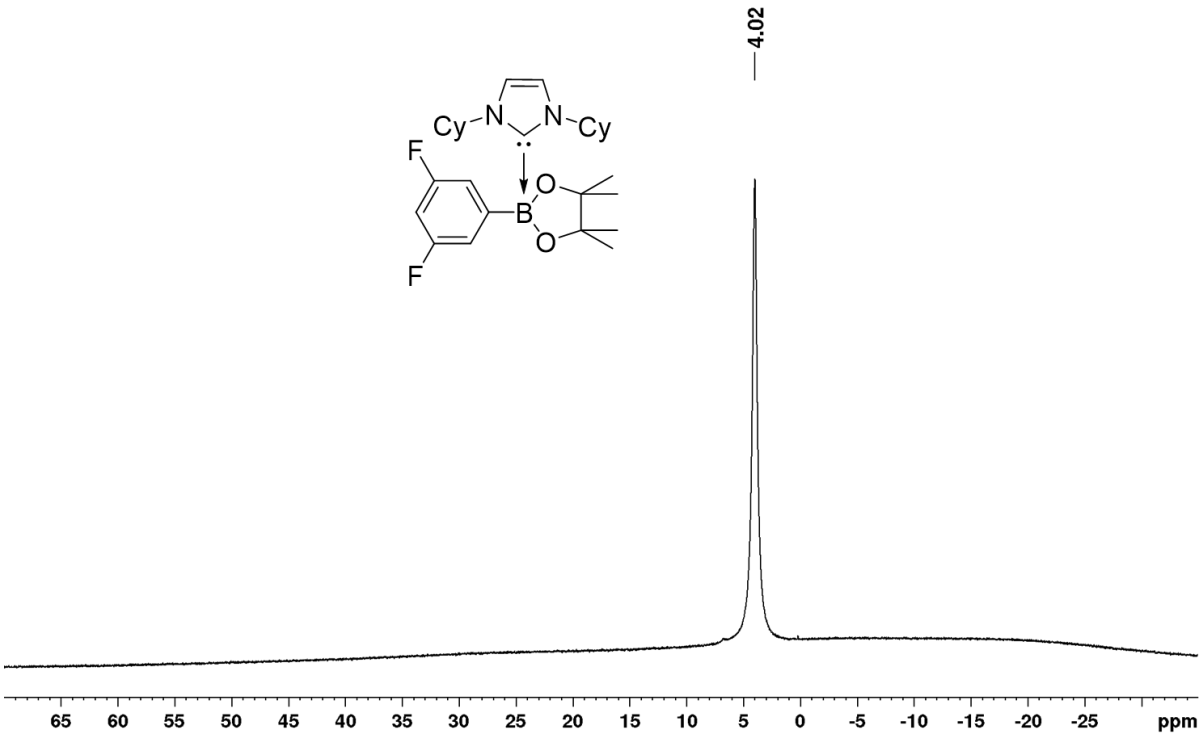

Figure 9.27 $^{11}B\{^{1}H\}$ NMR spectrum of 3,5-$F_2C_6H_3Bpin{\cdot}Cy_2Im$ **30** recorded in C_6D_6 (160 MHz).

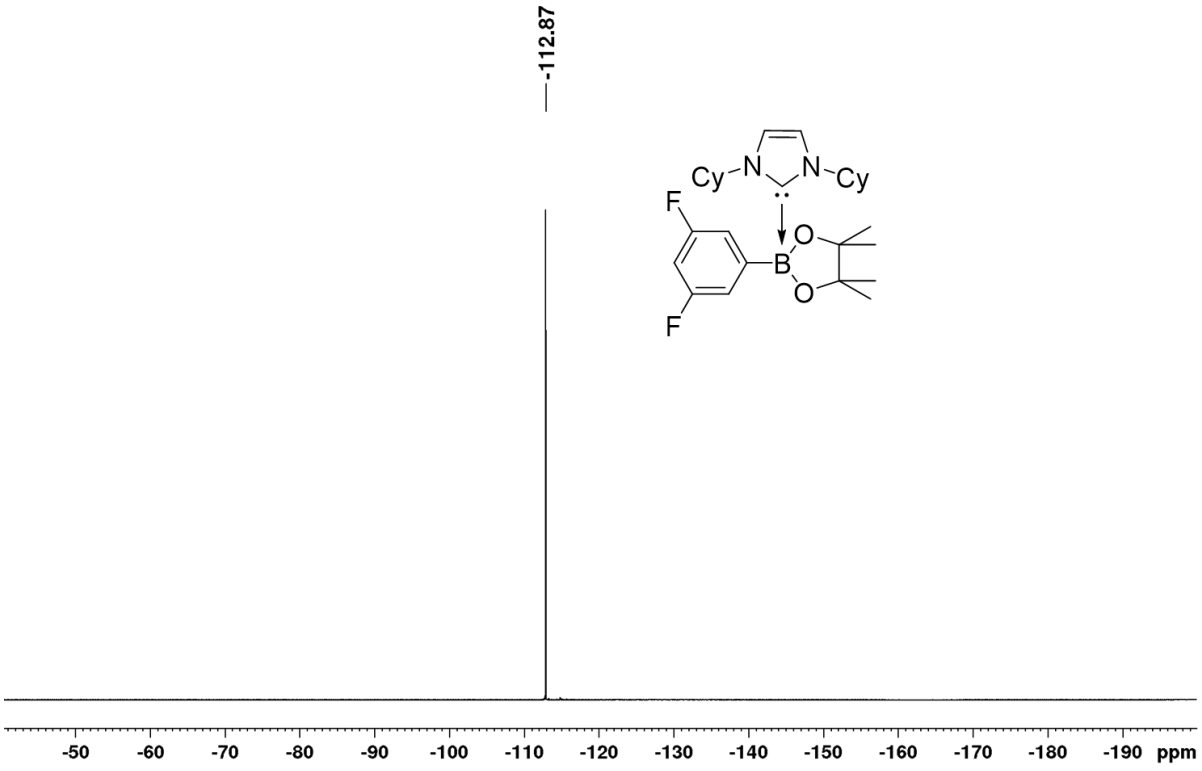

Figure 9.28 $^{19}F\{^{1}H\}$ NMR spectrum of 3,5-$F_2C_6H_3Bpin{\cdot}Cy_2Im$ **30** recorded in C_6D_6 (471 MHz).

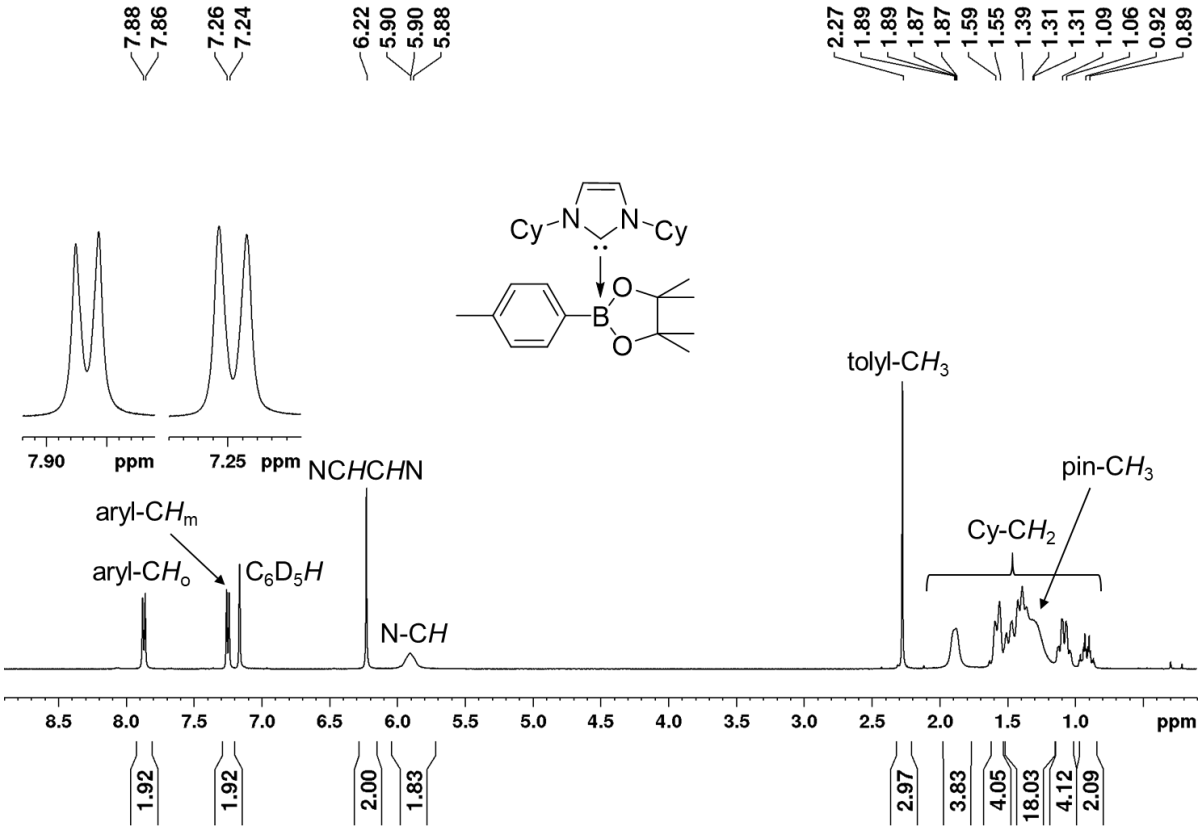

Figure 9.29 ^{1}H NMR spectrum of 4-CH_3-C_6H_4Bpin·Cy_2Im **31** recorded in C_6D_6 (500 MHz).

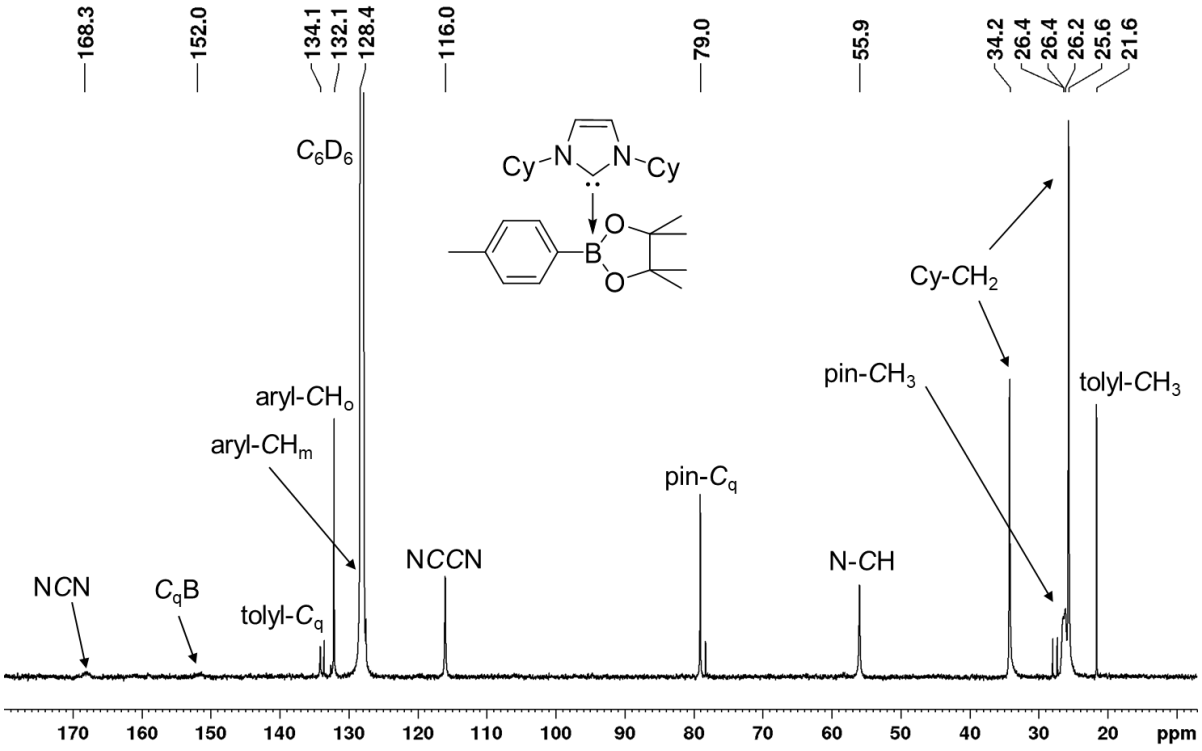

Figure 9.30 $^{13}C\{^{1}H\}$ NMR spectrum of 4-CH_3-C_6H_4Bpin·Cy_2Im **31** recorded in C_6D_6 (125 MHz).

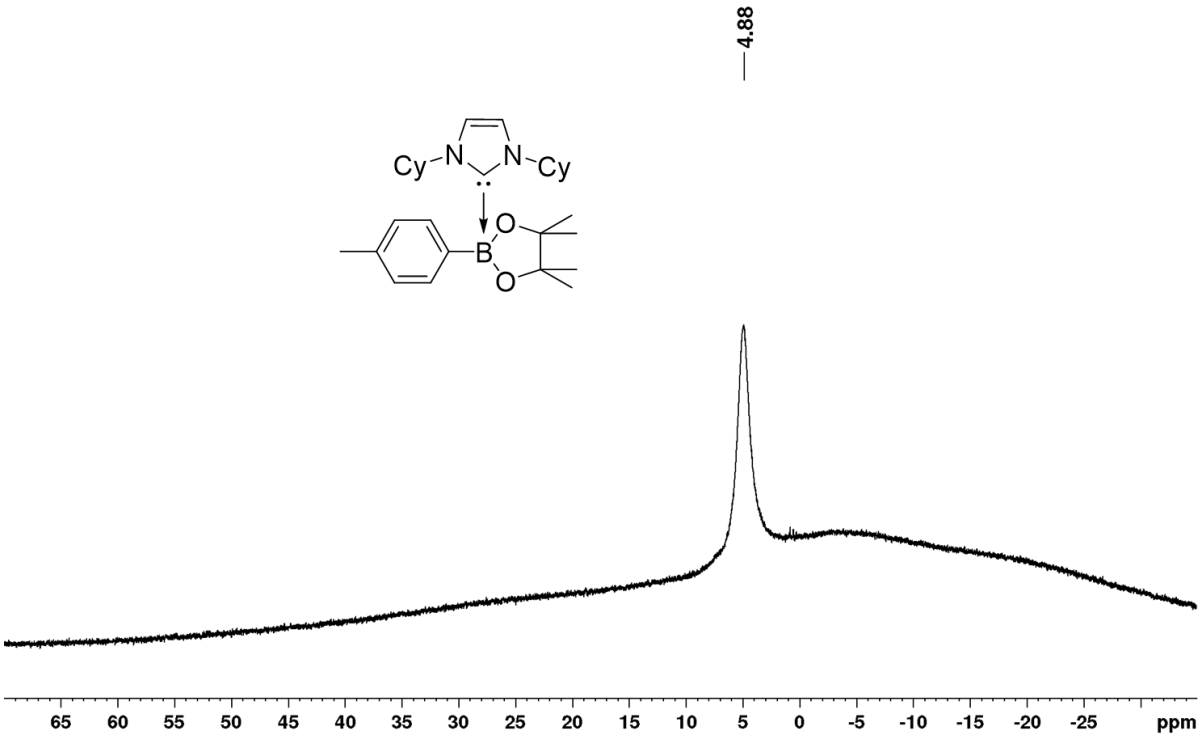

Figure 9.31 $^{11}B\{^1H\}$ NMR spectrum of 4-CH_3-C_6H_4Bpin·Cy_2Im **31** recorded in C_6D_6 (160 MHz).

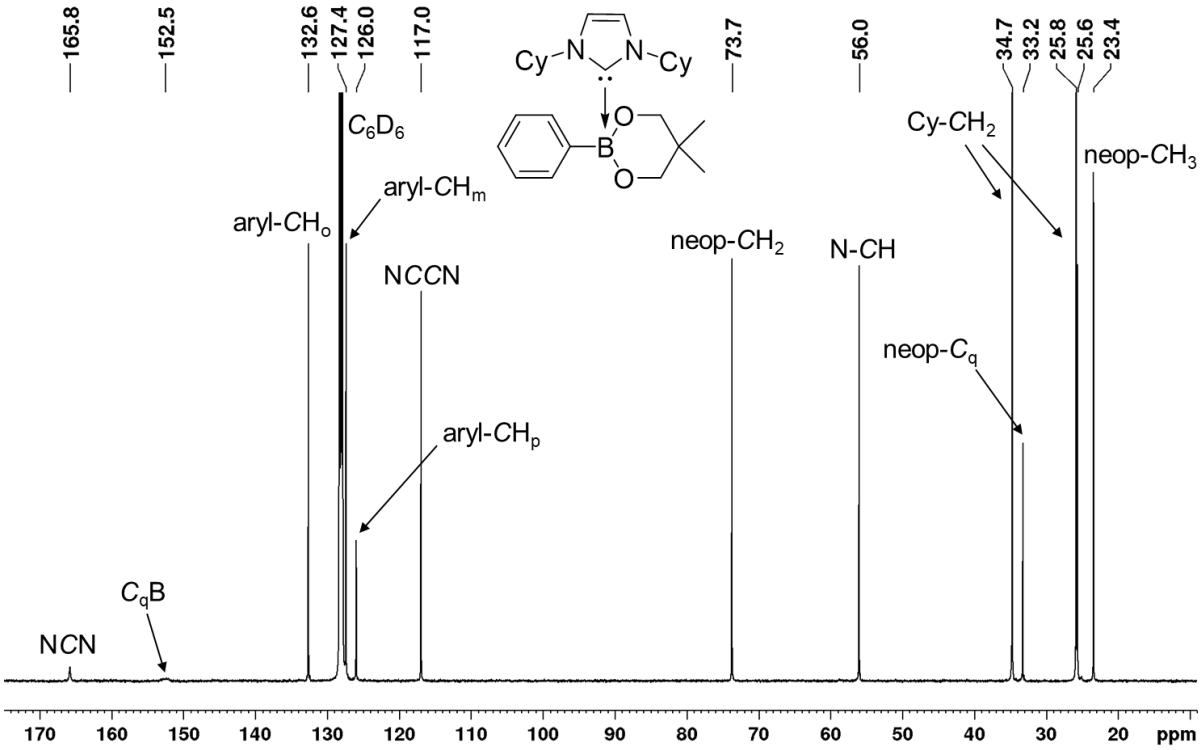

Figure 9.32 $^{13}C\{^1H\}$ NMR spectrum of C_6H_5Bneop·Cy_2Im **32** recorded in C_6D_6 (125 MHz).

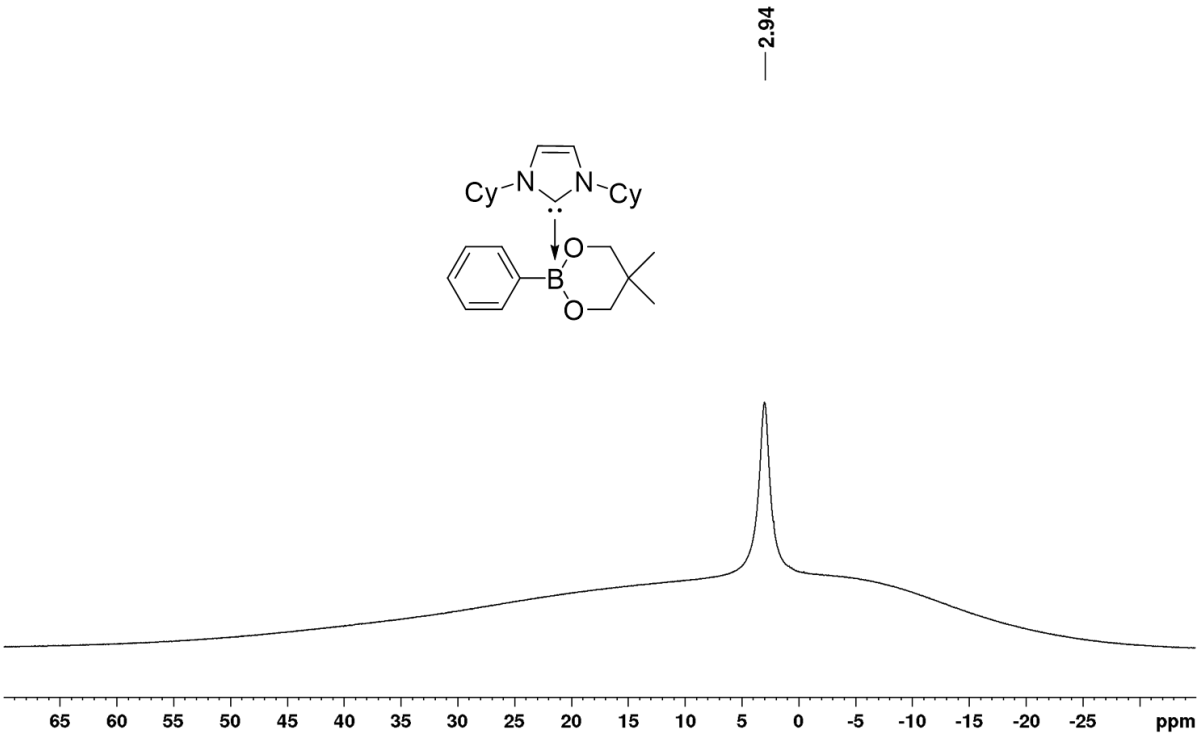

Figure 9.33 $^{11}B\{^{1}H\}$ NMR spectrum of C_6H_5Bneop·Cy_2Im **32** recorded in C_6D_6 (160 MHz).

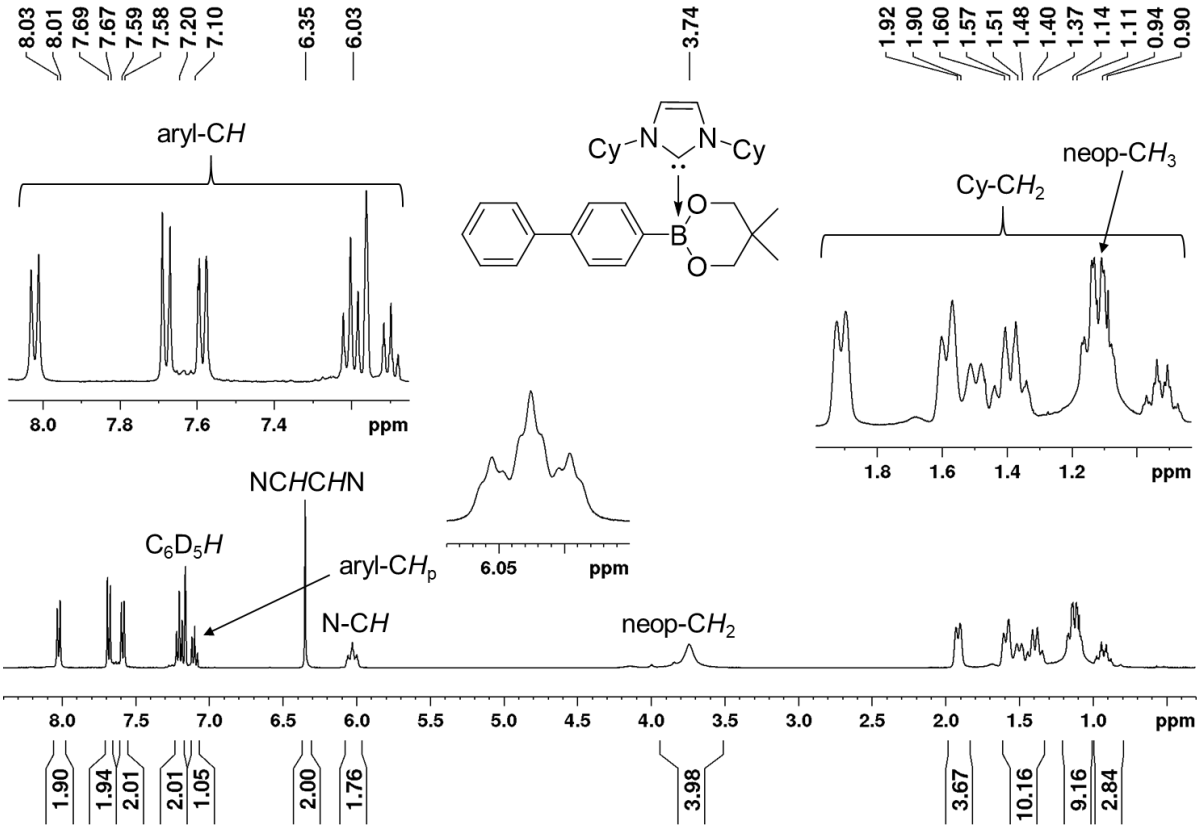

Figure 9.34 ^{1}H NMR spectrum of biphenylBneop·Cy_2Im **33** recorded in C_6D_6 (400 MHz).

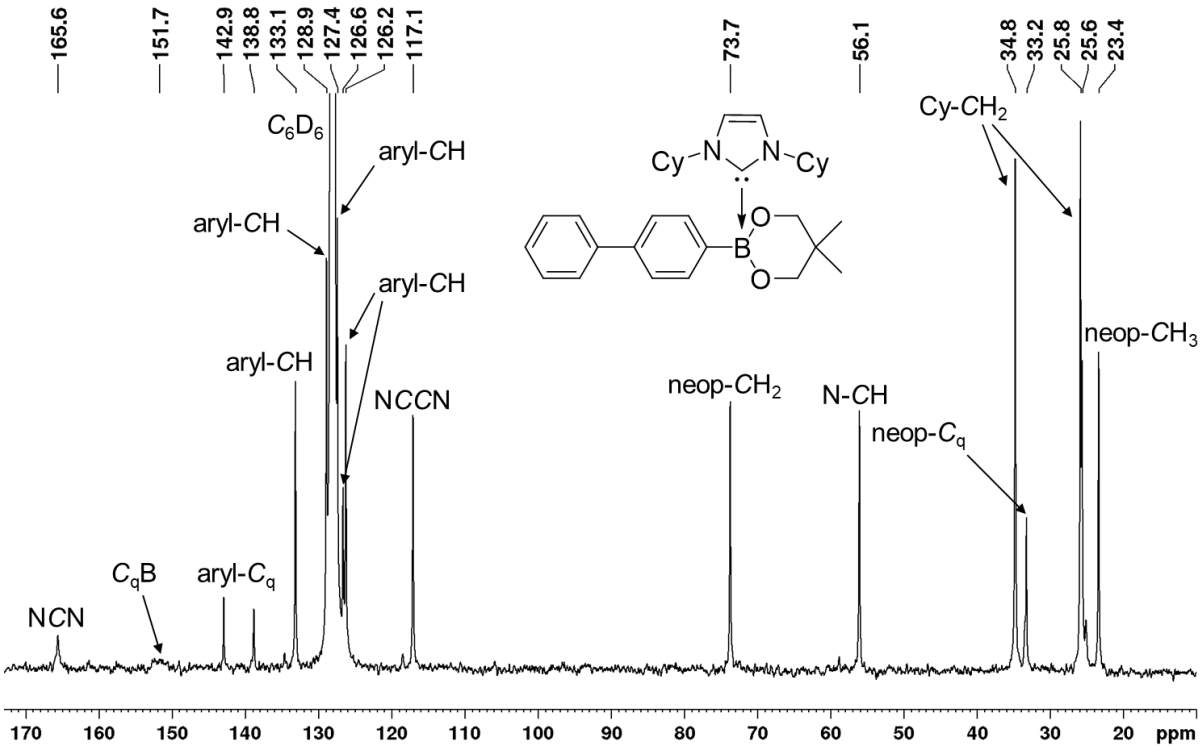

Figure 9.35 $^{13}C\{^{1}H\}$ NMR spectrum of biphenylBneop·Cy_2Im **33** recorded in C_6D_6 (100 MHz).

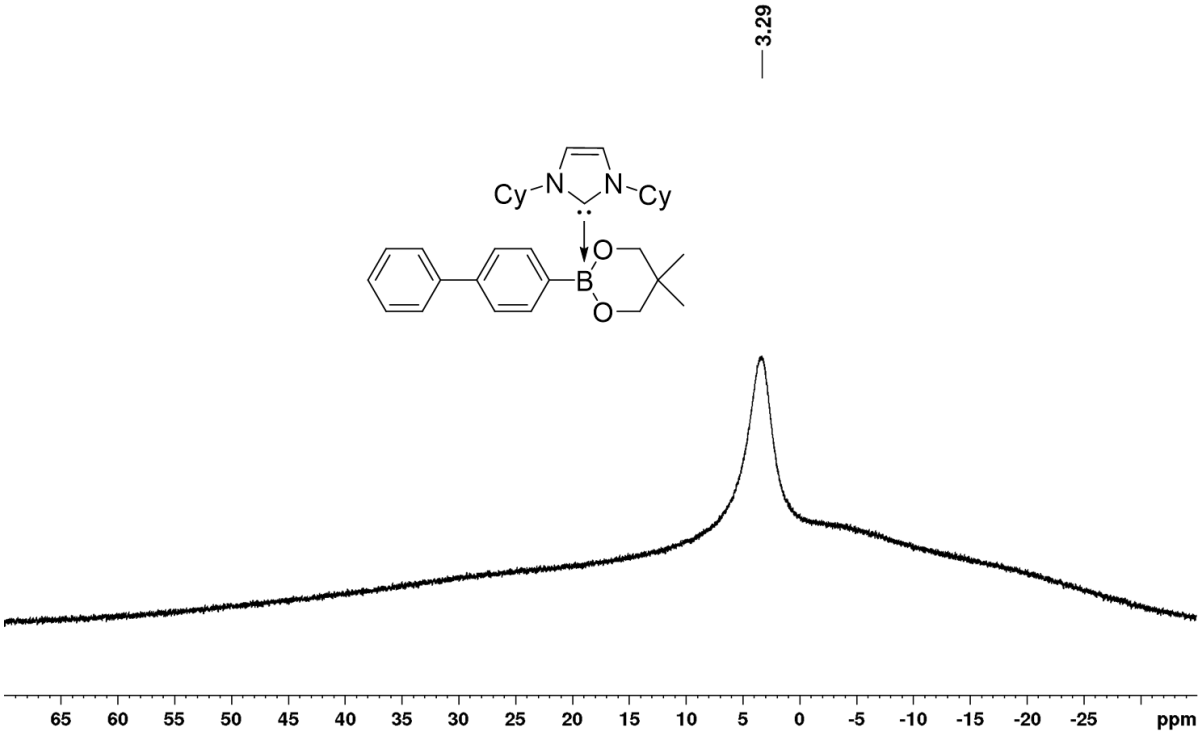

Figure 9.36 $^{11}B\{^{1}H\}$ NMR spectrum of biphenylBneop·Cy_2Im **33** recorded in C_6D_6 (128 MHz).

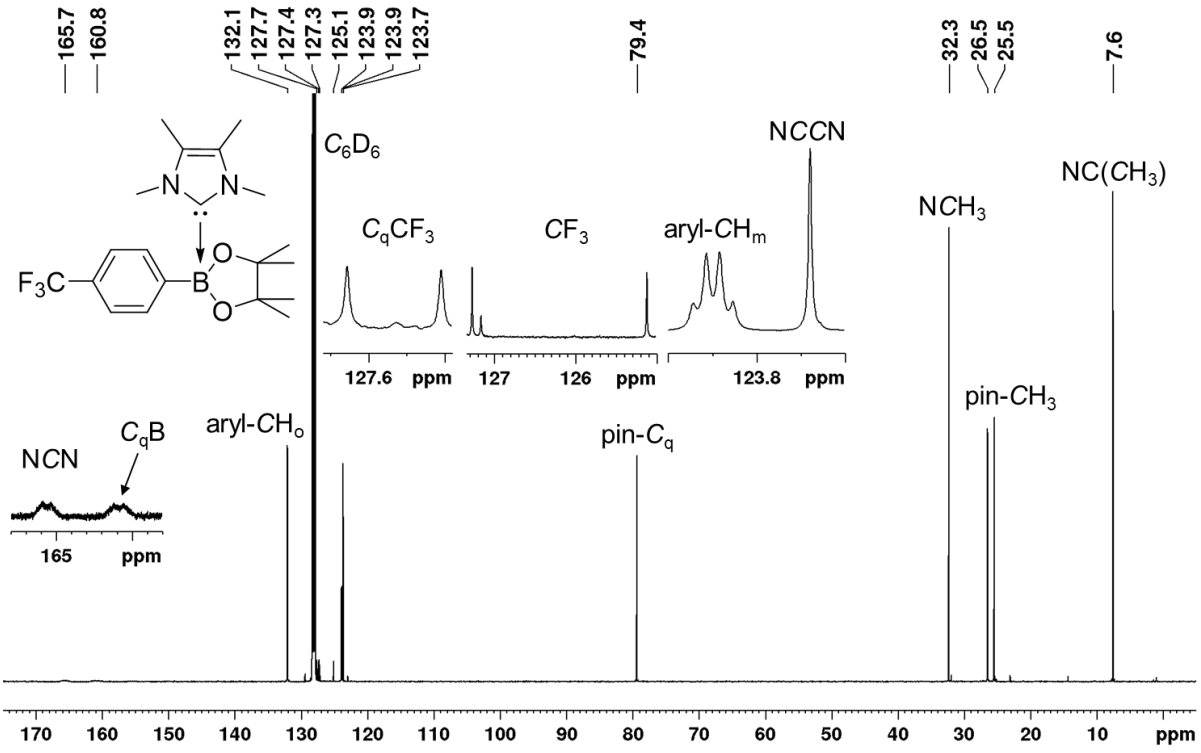

Figure 9.37 $^{13}C\{^{1}H\}$ NMR spectrum of 4-F_3C-C_6H_4Bpin·Me_2Im^{Me} **34** recorded in C_6D_6 (100 MHz).

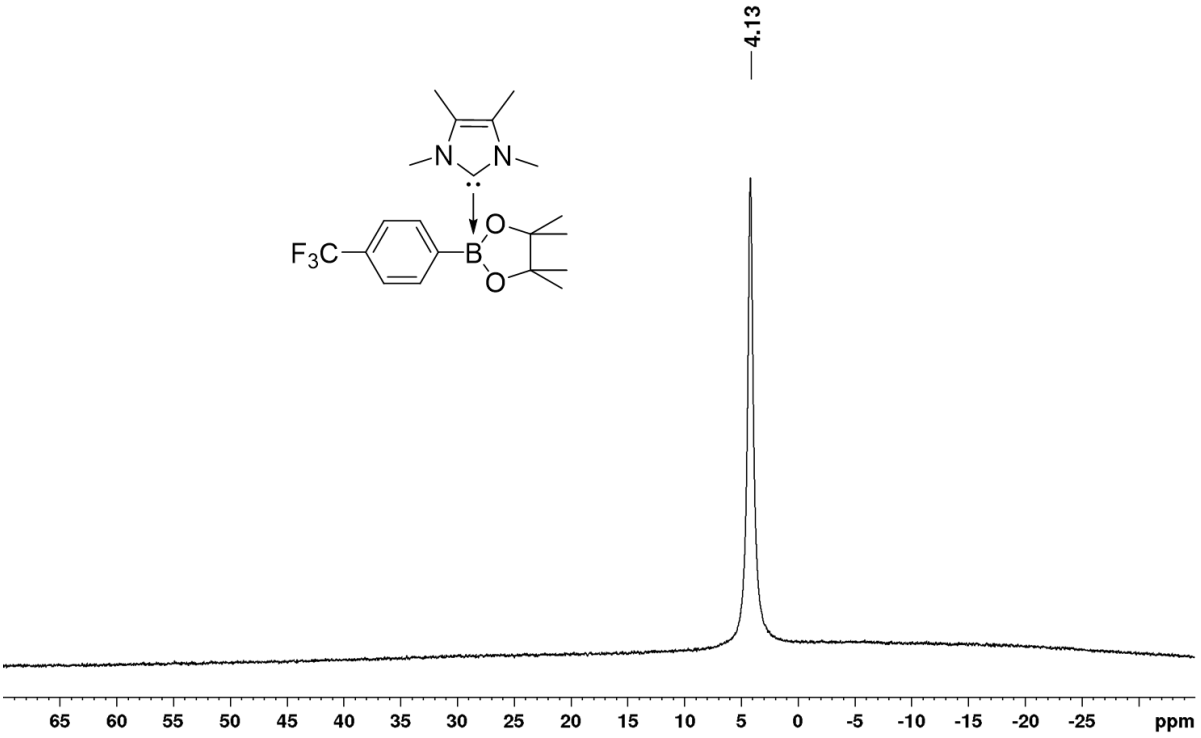

Figure 9.38 $^{11}B\{^{1}H\}$ NMR spectrum of 4-F_3C-C_6H_4Bpin·Me_2Im^{Me} **34** recorded in C_6D_6 (128 MHz).

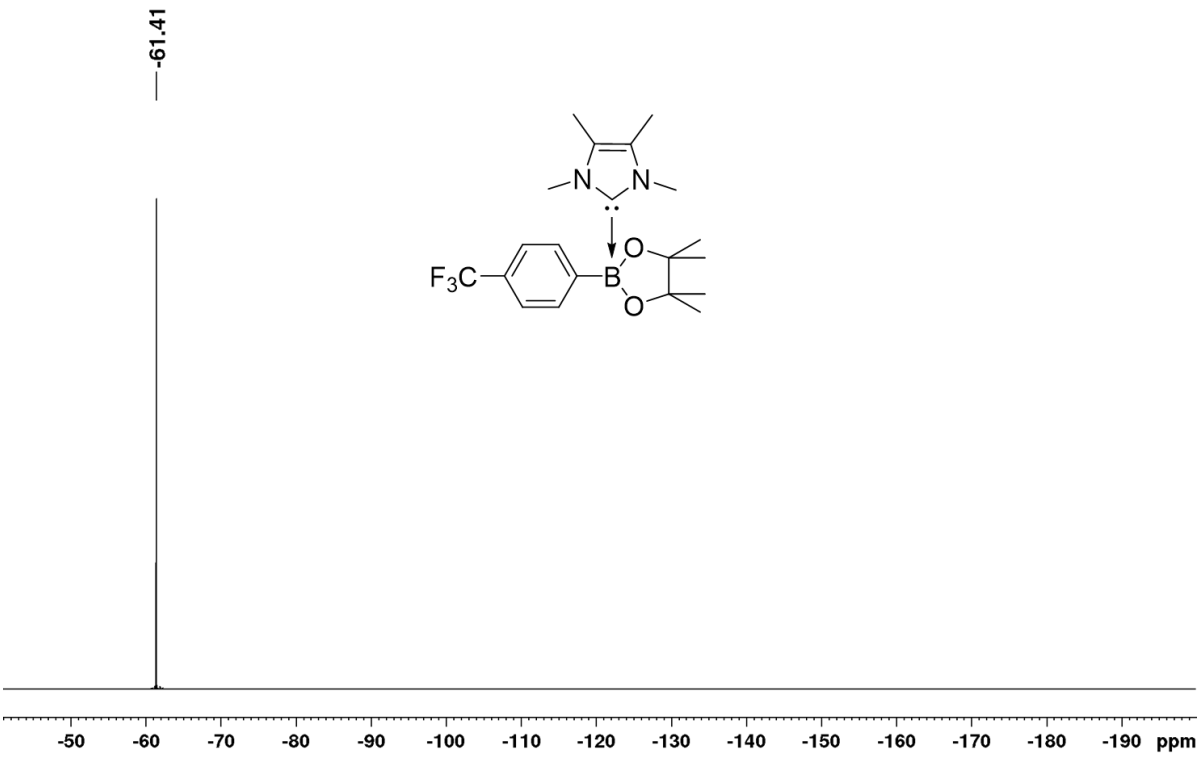

Figure 9.39 $^{19}F\{^{1}H\}$ NMR spectrum of 4-F_3C-C_6H_4Bpin·Me_2Im^{Me} **34** recorded in C_6D_6 (376 MHz).

9.4 PERMISSION

PERMISSION OF WILEY-VCH

Stoichiometric and Catalytic Aryl−Cl Activation and Borylation using NHC-stabilized Nickel(0) Complexes

This Agreement between Institut für Anorganische Chemie, Universität Würzburg -- Laura Kuehn ("You") and John Wiley and Sons ("John Wiley and Sons") consists of your license details and the terms and conditions provided by John Wiley and Sons and Copyright Clearance Center.

License Number	4855270777117
License date	Jun 24, 2020
Licensed Content Publisher	John Wiley and Sons
Licensed Content Publication	Chemistry - A European Journal
Licensed Content Title	Stoichiometric and Catalytic Aryl−Cl Activation and Borylation using NHC-stabilized Nickel(0) Complexes
Licensed Content Author	Laura Kuehn, Dominik G. Jammal, Katharina Lubitz, et al
Licensed Content Date	Apr 11, 2019
Licensed Content Volume	25
Licensed Content Issue	40
Licensed Content Pages	8
Type of use	Dissertation/Thesis
Requestor type	Author of this Wiley article
Format	Print and electronic
Portion	Full article
Will you be translating?	No

Title	Earth-Abundant Metal Catalyzed and Transition Metal-Free Borylation of Aryl Halides
Institution name	Julius-Maximilians-Universität Würzburg
Expected presentation date	Jul 2020
Requestor Location	Universität Würzburg Am Hubland Würzburg, Bayern 97074 Germany Attn: Institut für Anorganische Chemie, Universität Würzburg
Publisher Tax ID	EU826007151
Total	0.00 EUR

Terms and Conditions

TERMS AND CONDITIONS

This copyrighted material is owned by or exclusively licensed to John Wiley & Sons, Inc. or one of its group companies (each a"Wiley Company") or handled on behalf of a society with which a Wiley Company has exclusive publishing rights in relation to a particular work (collectively "WILEY"). By clicking "accept" in connection with completing this licensing transaction, you agree that the following terms and conditions apply to this transaction (along with the billing and payment terms and conditions established by the Copyright Clearance Center Inc., ("CCC's Billing and Payment terms and conditions"), at the time that you opened your RightsLink account (these are available at any time at http://myaccount.copyright.com).

Terms and Conditions

- The materials you have requested permission to reproduce or reuse (the "Wiley Materials") are protected by copyright.
- You are hereby granted a personal, non-exclusive, non-sub licensable (on a stand-alone basis), non-transferable, worldwide, limited license to reproduce

the Wiley Materials for the purpose specified in the licensing process. This license, **and any CONTENT (PDF or image file) purchased as part of your order,** is for a one-time use only and limited to any maximum distribution number specified in the license. The first instance of republication or reuse granted by this license must be completed within two years of the date of the grant of this license (although copies prepared before the end date may be distributed thereafter). The Wiley Materials shall not be used in any other manner or for any other purpose, beyond what is granted in the license. Permission is granted subject to an appropriate acknowledgement given to the author, title of the material/book/journal and the publisher. You shall also duplicate the copyright notice that appears in the Wiley publication in your use of the Wiley Material. Permission is also granted on the understanding that nowhere in the text is a previously published source acknowledged for all or part of this Wiley Material. Any third party content is expressly excluded from this permission.

- With respect to the Wiley Materials, all rights are reserved. Except as expressly granted by the terms of the license, no part of the Wiley Materials may be copied, modified, adapted (except for minor reformatting required by the new Publication), translated, reproduced, transferred or distributed, in any form or by any means, and no derivative works may be made based on the Wiley Materials without the prior permission of the respective copyright owner. **For STM Signatory Publishers clearing permission under the terms of the STM Permissions Guidelines only, the terms of the license are extended to include subsequent editions and for editions in other languages, provided such editions are for the work as a whole in situ and does not involve the separate exploitation of the permitted figures or extracts,** You may not alter, remove or suppress in any manner any copyright, trademark or other notices displayed by the Wiley Materials. You may not license, rent, sell, loan, lease, pledge, offer as security, transfer or assign the Wiley Materials on a stand-alone basis, or any of the rights granted to you hereunder to any other person.

- The Wiley Materials and all of the intellectual property rights therein shall at all times remain the exclusive property of John Wiley & Sons Inc, the Wiley

Companies, or their respective licensors, and your interest therein is only that of having possession of and the right to reproduce the Wiley Materials pursuant to Section 2 herein during the continuance of this Agreement. You agree that you own no right, title or interest in or to the Wiley Materials or any of the intellectual property rights therein. You shall have no rights hereunder other than the license as provided for above in Section 2. No right, license or interest to any trademark, trade name, service mark or other branding ("Marks") of WILEY or its licensors is granted hereunder, and you agree that you shall not assert any such right, license or interest with respect thereto

- NEITHER WILEY NOR ITS LICENSORS MAKES ANY WARRANTY OR REPRESENTATION OF ANY KIND TO YOU OR ANY THIRD PARTY, EXPRESS, IMPLIED OR STATUTORY, WITH RESPECT TO THE MATERIALS OR THE ACCURACY OF ANY INFORMATION CONTAINED IN THE MATERIALS, INCLUDING, WITHOUT LIMITATION, ANY IMPLIED WARRANTY OF MERCHANTABILITY, ACCURACY, SATISFACTORY QUALITY, FITNESS FOR A PARTICULAR PURPOSE, USABILITY, INTEGRATION OR NON-INFRINGEMENT AND ALL SUCH WARRANTIES ARE HEREBY EXCLUDED BY WILEY AND ITS LICENSORS AND WAIVED BY YOU.

- WILEY shall have the right to terminate this Agreement immediately upon breach of this Agreement by you.

- You shall indemnify, defend and hold harmless WILEY, its Licensors and their respective directors, officers, agents and employees, from and against any actual or threatened claims, demands, causes of action or proceedings arising from any breach of this Agreement by you.

- IN NO EVENT SHALL WILEY OR ITS LICENSORS BE LIABLE TO YOU OR ANY OTHER PARTY OR ANY OTHER PERSON OR ENTITY FOR ANY SPECIAL, CONSEQUENTIAL, INCIDENTAL, INDIRECT, EXEMPLARY OR PUNITIVE DAMAGES, HOWEVER CAUSED, ARISING OUT OF OR IN CONNECTION WITH THE DOWNLOADING, PROVISIONING, VIEWING OR USE OF THE MATERIALS REGARDLESS OF THE FORM OF ACTION, WHETHER FOR BREACH OF CONTRACT, BREACH OF WARRANTY,

TORT, NEGLIGENCE, INFRINGEMENT OR OTHERWISE (INCLUDING, WITHOUT LIMITATION, DAMAGES BASED ON LOSS OF PROFITS, DATA, FILES, USE, BUSINESS OPPORTUNITY OR CLAIMS OF THIRD PARTIES), AND WHETHER OR NOT THE PARTY HAS BEEN ADVISED OF THE POSSIBILITY OF SUCH DAMAGES. THIS LIMITATION SHALL APPLY NOTWITHSTANDING ANY FAILURE OF ESSENTIAL PURPOSE OF ANY LIMITED REMEDY PROVIDED HEREIN.

- Should any provision of this Agreement be held by a court of competent jurisdiction to be illegal, invalid, or unenforceable, that provision shall be deemed amended to achieve as nearly as possible the same economic effect as the original provision, and the legality, validity and enforceability of the remaining provisions of this Agreement shall not be affected or impaired thereby.

- The failure of either party to enforce any term or condition of this Agreement shall not constitute a waiver of either party's right to enforce each and every term and condition of this Agreement. No breach under this agreement shall be deemed waived or excused by either party unless such waiver or consent is in writing signed by the party granting such waiver or consent. The waiver by or consent of a party to a breach of any provision of this Agreement shall not operate or be construed as a waiver of or consent to any other or subsequent breach by such other party.

- This Agreement may not be assigned (including by operation of law or otherwise) by you without WILEY's prior written consent.

- Any fee required for this permission shall be non-refundable after thirty (30) days from receipt by the CCC.

- These terms and conditions together with CCC's Billing and Payment terms and conditions (which are incorporated herein) form the entire agreement between you and WILEY concerning this licensing transaction and (in the absence of fraud) supersedes all prior agreements and representations of the parties, oral or written. This Agreement may not be amended except in writing signed by both parties. This Agreement shall be binding upon and inure to the

benefit of the parties' successors, legal representatives, and authorized assigns.

- In the event of any conflict between your obligations established by these terms and conditions and those established by CCC's Billing and Payment terms and conditions, these terms and conditions shall prevail.
- WILEY expressly reserves all rights not specifically granted in the combination of (i) the license details provided by you and accepted in the course of this licensing transaction, (ii) these terms and conditions and (iii) CCC's Billing and Payment terms and conditions.
- This Agreement will be void if the Type of Use, Format, Circulation, or Requestor Type was misrepresented during the licensing process.
- This Agreement shall be governed by and construed in accordance with the laws of the State of New York, USA, without regards to such state's conflict of law rules. Any legal action, suit or proceeding arising out of or relating to these Terms and Conditions or the breach thereof shall be instituted in a court of competent jurisdiction in New York County in the State of New York in the United States of America and each party hereby consents and submits to the personal jurisdiction of such court, waives any objection to venue in such court and consents to service of process by registered or certified mail, return receipt requested, at the last known address of such party.

WILEY OPEN ACCESS TERMS AND CONDITIONS

Wiley Publishes Open Access Articles in fully Open Access Journals and in Subscription journals offering Online Open. Although most of the fully Open Access journals publish open access articles under the terms of the Creative Commons Attribution (CC BY) License only, the subscription journals and a few of the Open Access Journals offer a choice of Creative Commons Licenses. The license type is clearly identified on the article.

The Creative Commons Attribution License

The Creative Commons Attribution License (CC-BY) allows users to copy, distribute and transmit an article, adapt the article and make commercial use of the article. The CC-BY license permits commercial and non-

Creative Commons Attribution Non-Commercial License

The Creative Commons Attribution Non-Commercial (CC-BY-NC)License permits use, distribution and reproduction in any medium, provided the original work is properly cited and is not used for commercial purposes.(see below)

Creative Commons Attribution-Non-Commercial-NoDerivs License

The Creative Commons Attribution Non-Commercial-NoDerivs License (CC-BY-NC-ND) permits use, distribution and reproduction in any medium, provided the original work is properly cited, is not used for commercial purposes and no modifications or adaptations are made. (see below)

Use by commercial "for-profit" organizations

Use of Wiley Open Access articles for commercial, promotional, or marketing purposes requires further explicit permission from Wiley and will be subject to a fee.

Further details can be found on Wiley Online Library
http://olabout.wiley.com/WileyCDA/Section/id-410895.html

Other Terms and Conditions:
v1.10 Last updated September 2015
Questions? customercare@copyright.com or +1-855-239-3415 (toll free in the US) or +1-978-646-2777.

PERMISSION OF THE ROYAL SOCIETY OF CHEMISTRY

Chapter 3 is partly reproduced and slightly adapted from “L. Kuehn, M. Huang, U. Radius and T. B. Marder, *Org. Biomol. Chem.* **2019**, *17*, 6601; DOI: 10.1039/C9OB01244C.” with permission from The Royal Society of Chemistry. Figures, Schemes, and Tables in Chapter 3 are reproduced from “L. Kuehn, M. Huang, U. Radius and T. B. Marder, *Org. Biomol. Chem.* **2019**, *17*, 6601; DOI: 10.1039/C9OB01244C.” by permission of The Royal Society of Chemistry.

10 ACKNOWLEDGEMENTS

Dear Todd, Dear Udo,

First of all, I want to thank both of you for giving me the opportunity to do my PhD thesis in a collaboration in your groups and for being such good supervisors.

Todd, thank you for your help, the endless discussions (sometimes a bit off topic → Brexit, US elections...), for all the support and the trust you had in me. Thank you for always having good advice, sharing your knowledge and also for all the good laughs and your house parties (also thanks to Anne). It was a pleasure to be part of your group.

Udo, thank you for all your trust, support, sharing your knowledge and for always having an open door for all kinds of questions and problems. It was a pleasure to do all of my three theses under your supervision and being part of your great group for such a long time. Thank you for your friendly and uncomplicated manner and for the nice time we had in Florenz and Hirschegg.

Merci to **Dr. Emmanuel Lacôte** for the endless discussions in Todd's office and your help with polymerization and radicals.

Lieber **AK Radius**, danke für die tolle Zeit mit euch. Sowohl im ehemaligen dritten Stock mit den ganzen Stockkollegen als auch im neuen Gebäude. Ich hätte mich nirgends wohler fühlen können. Ich möchte mich bei den Ehemaligen **Flötz**, **Heidi**, **Rumpel**, **Toniii**, **Sabrina** und **Ulli** bedanken. Danke, dass ihr mich auch ein zweites Mal (nach der Bachelorarbeit) so nett aufgenommen habt und ich euch immer jede noch so dumme Frage stellen konnte. **Katha**, **Kuntze**, **Mirjam**, **Andi**, **Steffen**, **Michi**, **Lukas** und **Güü** (der neue Mitarbeiter des Monats!!)…vielen vielen Dank für die gemeinsame Zeit, den Zusammenhalt (vorallem beim Umzug) und die entspannte Atmosphäre nach Feierabend mit Themen vorallem auch abseits von Chemie (der wichtige Karpfenkalender, Sprunghefe, Stoffhosen…). Danke für die tollen Tagungen mit euch, bei denen wir einige Höhenmeter zurückgelegt und die ein oder andere Buttermilch getrunken haben. Das „enge" Beisammensein, die Codenames-Runden und der Prinzschnaps von dem man wirklich kein Kopfweh bekommt (entweder Dank Michis großzügiger Versorgung mit Elotrans oder der frischen Bergluft!?). Michi wurde im Gegenzug ja auch gut mit Krapfen versorgt. Der Tisch an dem Aperol aus Nudeln getrunken wird ist einfach immer der lustigere. Kollegen wie euch kann man sich für

die Zukunft nur wünschen. Danke **Katha**, **Kuntze** und **Matti** (die Hotel Medici Gang aus der Via Medici) für die lustige Zeit in Florenz. **Luis** (der schnellste Fußgänger), **Christian** und **Martin** (Luft!?) danke auch euch für die letzte gemeinsame Zeit zusammen, ihr seid auf jeden Fall eine weitere Bereicherung für den AK Radius.

I also want to thank **Jan Lorkowski** for the funny time when you were in Würzburg, we miss the upper drawer in your desk and the drinkable honey (Guys, see you the day after tomorrow!!!).

Katha, **Kuntze**, **Mirjam** und **Andi** gilt nochmal mein besonderer Dank für das Aufsetzen und Lösen von Kristallstrukturen. **Katha**, dir auch nochmal Danke für das Korrekturlesen meiner deutschen Zusammenfassung, als mich mein Deutsch schon im Stich gelassen hatte.

Next, I want to thank the whole **Marder group** for the good time in the lab, at the Christmas market, the wine festivals, and the house parties at Todd's! **Julia**, vielen Dank erstmal für das gewissenhafte Korrekturlesen dieser Arbeit. Danke auch für die schöne gemeinsame Zeit, ob beim Langhantel oder Spinning im Lifestyle oder Gassi gehen mit Loki. **Martin Eck**, Danke für deine anfängliche Hilfe bei meinem Thema und für deine immer nette Art (und für den tollen Plattenspieler). **Jan**, vielen Dank für die N64- (und ALLE anderen Konsolen) und Spieleabende. **Maria**, vielen Dank für die ganze Hilfe bei organisatorischen Dingen und für die vielen netten Gespräche zwischendurch. Vielen Dank auch an **Sabine** für deine Hilfe, vorallem auch bei der Kugelrohrdestillation und für die Einführung und Hilfe bei SPS Fragen. **Jiang**, thank you for the nice time after work, the discussion and the ONE beer (which is okay I guess!?).

Außerdem möchte ich mich beim alten und zum Teil neuen **AK Finze** bedanken, insbesondere bei **Michel**, **Shorty**, **Matti**, **Landmann**, **Raphael**, **Philipp**, **Tatjana**, **Jarno**, **Nils**, **Ludwig** und **Kristina**. Danke für die lustigen Mittagspausen und oft auch Feierabende!

Weiterhin möchte ich meinen Praktikanten **Simon Rachor**, **Michi** (jetzt mögen wir dich doch alle…!!!), **Maximilian Rist**, **Sebastian Halupczok**, **Dominik Jammal**, **Martin Stang**, **Christian Luz**, **Yvonne Vonhausen**, **Franziska Leimeister** und **Ludwig Zapf** danken. An dieser Stelle möchte ich mich ganz besonders bei **Dominik Jammal** für die lustige Zeit und deine stetige Motivation bedanken (außer am Tag nach meinem

Geburtstag als es für dich nur Reis gab!), bei **Martin Stang** für die ewige Praktikumszeit, deine Motivation und die vielen Diskussionen und bei **Ludwig Zapf** für das Aufsetzen und Lösen von Kristallen als Praktikant(!) und die CV-Messungen.

Vielen Dank an **Dr. Ivo Krummenacher** für die ESR- und CV-Messungen und die Hilfe bei der Auswertung, sowie für das Korrekturlesen der jeweiligen Abschnitte in meiner Arbeit. **Dr. Alexandra Friedrich**, vielen Dank für deine schnelle und ausführliche Hilfe bei Problemen mit Kristallstrukturen. Vielen Dank an **Dr. Rüdiger Bertermann**, **Marie-Luise Schäfer** und **Laura Wolz** für die zahlreichen NMR-Messungen und die Geduld bei den Tieftemperaturmessungen. Danke **Dr. Rüdiger Bertermann** für die Festkörper-NMR-Messungen. Danke auch an **Dr. Stefan Wagner** für die Hilfe rund um die Massenspektrometrie, die Hilfe bei Problemen mit dem Thermo Fischer GC-MS und auch die Hilfe beim Umzug des Geräts. Vielen Dank **Christoph** für die vielen, und oft auch spontanen HRMS Messungen. Des Weiteren möchte ich **Liselotte Michels** und **Sabine Timmroth** für die Anfertigung zahlreicher Elementaranalysen danken und für die freundliche Stimmung bei euch. Vielen Dank an **Johanna** für die GPC Messungen bei dir unten an der Zahnklinik. Einen großen Dank auch an **Cornelia Walter** für die ganze Unterstützung in allen organisatorischen Fragen und deine immerwährende Freundlichkeit, zu dir kommt man immer gerne! Vielen Dank an **Gertrud Wunderling** für die unendliche Geduld beim Chaos in der Küche, sowie **Alfred Scherzer** für die stetige Hilfe in allen möglichen Bereichen! Ohne euch würde es hier ganz anders zugehen! Danke auch den Mitarbeitern der Werkstätten **Alois Ruf**, **Manfred Reinhard** und **Wolfgang Obert**. Außerdem möchte ich mich bei den Glasbläsern **Berthold Fertig** und **Bernhard Werner** für die schnelle Reparatur wichtiger Glasgeräte bedanken.

Vielen Dank auch an **Dr. Justin Wolf** für die entspannte Zeit im AC2, dein abschließendes Erdbeereis-Event und die Mittwochsrunde „um die Ecke gedacht“! Es hat sehr viel Spaß gemacht und ich habe viel von dir gelernt.

Für die tolle Zeit während der Promotion möchte ich mich bei **Katha**, **Valerie**, **Anna**, **Tatjana**, **Lena**, **Jacqui** und **Juli** bedanken! Ihr seid mir echt sehr wichtig geworden und es wäre schön, wenn man sich nicht aus den Augen verliert. Natürlich möchte ich mich auch bei allen anderen Mitgliedern vom **Mittwochsstammtisch** bedanken (wir haben noch lange nicht alle Lokalitäten von Würzburg durch!).

An dieser Stelle nochmal extra Danke an **Dr. Lena Winner** für die tollen letzten Jahre, ob beim Spinning im Lifestyle (ohne dich ist es nicht mehr das gleiche) mit entspannten Saunagängen, Spieleabenden oder einem Besuch in der Probierstube!

Ein fast AK Radius Mitglied, **Raphael**, oder besser gesagt Raphood…danke, dass du ein so guter Freund für mich geworden bist über die letzten Jahre. 11 Uhr kochen war immer ein Lichtblick im manchmal dunklen Laboralltag für mich, auch wenn ich nur der Handlanger des „Directeur de Cuisine“ war. Danke für deine Kochskills… montags Spaghetti Carbonara sollte fest eingeführt werden! Danke für die vielen Gespräche über Sinnloses, Ernstes, aber auch Gott und die Welt, für deinen Humor und die unendliche Unterstützung bei allen PC Problemen.

Johanna, **Mosi**, **Moby**, **Alex**, **Uwe**, **Domi**, **Paddy** und **Matze** ich bin so froh, dass wir uns im ersten Semester unter all den Leuten kennengelernt und uns das ganze Studium über nicht aus den Augen verloren haben. Ohne euch wäre es echt fraglich gewesen, ob ich das alles so durchgezogen hätte. Die Lernphasen in der Bib und unser sonntaglicher TC/PC-Übungsblätter-Abend mit anschließender Knoblauchkartoffel-Belohnung vom Schlemmereck (rückblickend wirkt das gar nicht mehr so schlimm)… Ich danke euch auch für die lustige Zeit außerhalb der Uni und für unseren Urlaub in Sveti Petar u Šumi. Danke für eure immerwährende Freundschaft auch wenn man sich mal länger nicht gesehen hat!

Ein besonderer Dank gilt auch meinen Mädels von zu Hause **Tanja**, **Lisa**, **Katha**, **Sabrina** und **Michelle**, danke für eure bedingungslose Freundschaft und dass ihr immer für mich da seid!

Von ganzem Herzen möchte ich **meiner Familie** danken, dafür dass ihr immer hinter mir standet und steht und mich immer unterstützt. Ohne euch wäre das nicht möglich gewesen, ich bin froh, dass ich euch habe!

Matze, dir danke ich ganz besonders, dafür dass du immer für mich da bist und immer das Positive siehst, auch wenn ich das manchmal nicht kann. Danke für deine bedingungslose Liebe, deine Fürsorge, deine Gelassenheit und Hilfe...vor allem in der letzten Zeit. Ich freue mich auf alles was kommt und bin froh, dass ich dich hab!

11 REFERENCES

[1] A. B. Morgan, J. L. Jurs, J. M. Tour, *J. Appl. Polym. Sci.* **2000**, *76*, 1257-1268.

[2] T. Ishiyama, M. Murata, N. Miyaura, *J. Org. Chem.* **1995**, *60*, 7508-7510.

[3] B. M. Rosen, C. Huang, V. Percec, *Org. Lett.* **2008**, *10*, 2597-2600.

[4] C. Moldoveanu, D. A. Wilson, C. J. Wilson, P. Corcoran, B. M. Rosen, V. Percec, *Org. Lett.* **2009**, *11*, 4974-4977.

[5] C. Moldoveanu, D. A. Wilson, C. J. Wilson, P. Leowanawat, A.-M. Resmerita, C. Liu, B. M. Rosen, V. Percec, *J. Org. Chem.* **2010**, *75*, 5438-5452.

[6] P. Leowanawat, A.-M. Resmerita, C. Moldoveanu, C. Liu, N. Zhang, D. A. Wilson, L. M. Hoang, B. M. Rosen, V. Percec, *J. Org. Chem.* **2010**, *75*, 7822-7828.

[7] D. A. Wilson, C. J. Wilson, C. Moldoveanu, A.-M. Resmerita, P. Corcoran, L. M. Hoang, B. M. Rosen, V. Percec, *J. Am. Chem. Soc.* **2010**, *132*, 1800-1801.

[8] M. Murata, T. Sambommatsu, T. Oda, S. Watanabe, Y. Masuda, *Heterocycles* **2010**, *80*, 213-218.

[9] M. Murata, Y. Sogabe, T. Nimikoshi, S. Watanabe, *Heterocycles* **2012**, *86*, 133-138.

[10] Y. Sogabe, T. Namikoshi, S. Watanabe, M. Murata, *Synthesis* **2012**, *44*, 1233-1236.

[11] D. Adhikari, J. C. Huffman, D. J. Mindiola, *Chem. Commun.* **2007**, 4489-4491.

[12] T. Yamamoto, T. Morita, J. Takagi, T. Yamakawa, *Org. Lett.* **2011**, *13*, 5766-5769.

[13] G. A. Molander, L. N. Cavalcanti, C. García-García, *J. Org. Chem.* **2013**, *78*, 6427-6439.

[14] J. Dong, H. Guo, Q. S. Hu, *Eur. J. Org. Chem.* **2017**, *2017*, 7087-7090.

[15] A. Kumar, L. P. Bheeter, M. K. Gangwar, J.-B. Sortais, C. Darcel, P. Ghosh, *J. Organomet. Chem.* **2015**, *786*, 63-70.

[16] L. P. Bheeter, D. Wei, V. Dorcet, T. Roisnel, P. Ghosh, J. B. Sortais, C. Darcel, *Eur. J. Inorg. Chem.* **2015**, *2015*, 5226-5231.

[17] J. R. Coombs, R. A. Green, F. Roberts, E. M. Simmons, J. M. Stevens, S. R. Wisniewski, *Organometallics* **2018**, *38*, 157-166.

[18] X.-W. Liu, J. Echavarren, C. Zarate, R. Martin, *J. Am. Chem. Soc.* **2015**, *137*, 12470-12473.

[19] T. Niwa, H. Ochiai, Y. Watanabe, T. Hosoya, *J. Am. Chem. Soc.* **2015**, *137*, 14313-14318.

[20] J. Zhou, M. W. Kuntze-Fechner, R. Bertermann, U. S. D. Paul, J. H. J. Berthel, A. Friedrich, Z. Du, T. B. Marder, U. Radius, *J. Am. Chem. Soc.* **2016**, *138*, 5250-5253.

[21] T. Schaub, U. Radius, *Chem. Eur. J.* **2005**, *11*, 5024-5030.

[22] T. Schaub, M. Backes, U. Radius, *J. Am. Chem. Soc.* **2006**, *128*, 15964-15965.

[23] T. Schaub, M. Backes, U. Radius, *Eur. J. Inorg. Chem.* **2008**, *2008*, 2680-2690.

[24] T. Schaub, P. Fischer, A. Steffen, T. Braun, U. Radius, A. Mix, *J. Am. Chem. Soc.* **2008**, *130*, 9304-9317.

[25] P. Fischer, K. Götz, A. Eichhorn, U. Radius, *Organometallics* **2012**, *31*, 1374-1383.

[26] J. Zhou, J. H. J. Berthel, M. W. Kuntze-Fechner, A. Friedrich, T. B. Marder, U. Radius, *J. Org. Chem.* **2016**, *81*, 5789-5794.

[27] Y.-M. Tian, X.-N. Guo, M. W. Kuntze-Fechner, I. Krummenacher, H. Braunschweig, U. Radius, A. Steffen, T. B. Marder, *J. Am. Chem. Soc.* **2018**, *140*, 17612-17623.

[28] C. Sieck, M. G. Tay, M. H. Thibault, R. M. Edkins, K. Costuas, J. F. Halet, A. S. Batsanov, M. Haehnel, K. Edkins, A. Lorbach, *Chem. Eur. J.* **2016**, *22*, 10523-10532.

[29] S. Pietsch, E. C. Neeve, D. C. Apperley, R. Bertermann, F. Mo, D. Qiu, M. S. Cheung, L. Dang, J. Wang, U. Radius, Z. Lin, C. Kleeberg , T. B. Marder, *Chem. Eur. J.* **2015**, *21*, 7082-7098.

[30] L. Kuehn, M. Stang, S. Würtemberger-Pietsch, A. Friedrich, H. Schneider, U. Radius, T. B. Marder, *Faraday Discussions* **2019**, *220*, 350-363.

[31] Z. Wang, S. Bachman, A. S. Dudnik, G. C. Fu, *Angew. Chem. Int. Ed.* **2018**, *57*, 14529-14532; *Angew. Chem.* **2018**, *130*, 14737-14740.

[32] H. Zhang, S. Hagihara, K. Itami, *Chem. Lett.* **2015**, *44*, 779-781.

[33] T. Furukawa, M. Tobisu, N. Chatani, *Chem. Commun.* **2015**, *51*, 6508-6511.

[34] T. Ishiyama, J. Takagi, K. Ishida, N. Miyaura, N. R. Anastasi, J. F. Hartwig, *J. Am. Chem. Soc.* **2002**, *124*, 390-391.

[35] T. J. Mazzacano, N. P. Mankad, *J. Am. Chem. Soc.* **2013**, *135*, 17258-17261.

[36] J. V. Obligacion, S. P. Semproni, P. J. Chirik, *J. Am. Chem. Soc.* **2014**, *136*, 4133-4136.

[37] S. R. Tamang, A. Singh, D. K. Unruh, M. Findlater, *ACS Catal.* **2018**, *8*, 6186-6191.

[38] M. Tobisu, K. Nakamura, N. Chatani, *J. Am. Chem. Soc.* **2014**, *136*, 5587-5590.

[39] H. Zhang, S. Hagihara, K. Itami, *Chem. Eur. J.* **2015**, *21*, 16796-16800.

[40] C. H. Basch, K. M. Cobb, M. P. Watson, *Org. Lett.* **2016**, *18*, 136-139.

[41] J. Hu, H. Sun, W. Cai, X. Pu, Y. Zhang, Z. Shi, *J. Org. Chem.* **2016**, *81*, 14-24.

[42] J. Hu, Y. Zhao, J. Liu, Y. Zhang, Z. Shi, *Angew. Chem. Int. Ed.* **2016**, *55*, 8718-8722; *Angew. Chem.* **2016**, *128*, 8860-8864.

[43] K. Huang, D.-G. Yu, S.-F. Zheng, Z.-H. Wu, Z.-J. Shi, *Chem. Eur. J.* **2011**, *17*, 786-791.

[44] X. Pu, J. Hu, Y. Zhao, Z. Shi, *ACS Catal.* **2016**, *6*, 6692-6698.

[45] L. Guo, M. Rueping, *Chem. Eur. J.* **2016**, *22*, 16787-16790.

[46] C. Zarate, R. Manzano, R. Martin, *J. Am. Chem. Soc.* **2015**, *137*, 6754-6757.

[47] M. Tobisu, J. Zhao, H. Kinuta, T. Furukawa, T. Igarashi, N. Chatani, *Adv. Synth. Catal.* **2016**, *358*, 2417-2421.

[48] Q. Zhou, H. D. Srinivas, S. Zhang, M. P. Watson, *J. Am. Chem. Soc.* **2016**, *138*, 11989-11995.

[49] L. J. Murphy, H. Hollenhorst, R. McDonald, M. Ferguson, M. D. Lumsden, L. Turculet, *Organometallics* **2017**, *36*, 3709-3720.

[50] M. Suginome, H. Nakamura, Y. Ito, *Chem. Commun.* **1996**, 2777-2778.

[51] M. Suginome, T. Matsuda, Y. Ito, *Organometallics* **1998**, *17*, 5233-5235.

[52] M. Suginome, A. Yamamoto, M. Murakami, *J. Am. Chem. Soc.* **2003**, *125*, 6358-6359.

[53] M. Suginome, A. Yamamoto, M. Murakami, *J. Organomet. Chem.* **2005**, *690*, 5300-5308.

[54] M. Suginome, M. Shirakura, A. Yamamoto, *J. Am. Chem. Soc.* **2006**, *128*, 14438-14439.

[55] S. Mannathan, M. Jeganmohan, C. H. Cheng, *Angew. Chem. Int. Ed.* **2009**, *48*, 2192-2195; *Angew. Chem.* **2009**, *121*, 2226-2229.

[56] M. Daini, A. Yamamoto, M. Suginome, *Asian J. Org. Chem.* **2013**, *2*, 968-976.

[57] M. Suginome, Y. Ito, *J. Organomet. Chem.* **2003**, *680*, 43-50.

[58] R. J. Ely, J. P. Morken, *Org. Lett.* **2010**, *12*, 4348-4351.

[59] H. Y. Cho, J. P. Morken, *J. Am. Chem. Soc.* **2008**, *130*, 16140-16141.

[60] S. Ogoshi, K.-i. Tonomori, M.-a. Oka, H. Kurosawa, *J. Am. Chem. Soc.* **2006**, *128*, 7077-7086.

[61] H. Y. Cho, J. P. Morken, *J. Am. Chem. Soc.* **2010**, *132*, 7576-7577.

[62] H. Y. Cho, Z. Yu, J. P. Morken, *Org. Lett.* **2011**, *13*, 5267-5269.

[63] P. Zhang, I. A. Roundtree, J. P. Morken, *Org. Lett.* **2012**, *14*, 1416-1419.

[64] C. M. Macaulay, S. J. Gustafson, J. T. Fuller III, D.-H. Kwon, T. Ogawa, M. J. Ferguson, R. McDonald, M. D. Lumsden, S. M. Bischof, O. L. Sydora, D. H. Ess, M. Stradiotto, L. Turculet, *ACS Catal.* **2018**, *8*, 9907-9925.

[65] M. Suginome, T. Matsuda, T. Yoshimoto, Y. Ito, *Organometallics* **2002**, *21*, 1537-1539.

[66] Y. Sumida, H. Yorimitsu, K. Oshima, *Org. Lett.* **2008**, *10*, 4677-4679.

[67] Y. Sumida, H. Yorimitsu, K. Oshima, *J. Org. Chem.* **2009**, *74*, 3196-3198.

[68] S. Crotti, F. Bertolini, F. Macchia, M. Pineschi, *Org. Lett.* **2009**, *11*, 3762-3765.

[69] K. Hirano, H. Yorimitsu, K. Oshima, *Org. Lett.* **2007**, *9*, 5031-5033.

[70] V. Lillo, M. J. Geier, S. A. Westcott, E. Fernández, *Org. Biomol. Chem.* **2009**, *7*, 4674-4676.

[71] J. Zhou, G. C. Fu, *J. Am. Chem. Soc.* **2003**, *125*, 14726-14727.

[72] A. S. Dudnik, G. C. Fu, *J. Am. Chem. Soc.* **2012**, *134*, 10693-10697.

[73] J. Yi, J. H. Liu, J. Liang, J. J. Dai, C. T. Yang, Y. Fu, L. Liu, *Adv. Synth. Catal.* **2012**, *354*, 1685-1691.

[74] M. S. Cheung, F. K. Sheong, T. B. Marder, Z. Lin, *Chem. Eur. J.* **2015**, *21*, 7480-7488.

[75] D. G. Hall, *Boronic Acids: Preparation and Applications in Organic Synthesis, Medicine and Materials, 2nd ed. (Ed.: D. G. Hall), Wiley-VCH, Weinheim* **2011**.

[76] E. C. Neeve, S. J. Geier, I. A. I. Mkhalid, S. A. Westcott, T. B. Marder, *Chem. Rev.* **2016**, *116*, 9091-9161.

[77] A. B. Cuenca, R. Shishido, H. Ito, E. Fernández, *Chem. Soc. Rev.* **2017**, *46*, 415-430.

[78] I. A. I. Mkhalid, J. H. Barnard, T. B. Marder, J. M. Murphy, J. F. Hartwig, *Chem. Rev.* **2010**, *110*, 890-931.

[79] J. F. Hartwig, *Chem. Soc. Rev.* **2011**, *40*, 1992-2002.

[80] J. F. Hartwig, *Acc. Chem. Res.* **2012**, *45*, 864-873.

[81] A. Ros, R. Fernández, J. M. Lassaletta, *Chem. Soc. Rev.* **2014**, *43*, 3229-3243.

[82] M. Murata, *Heterocycles* **2012**, *85*, 1795-1819.

[83] W. K. Chow, O. Y. Yuen, P. Y. Choy, C. M. So, C. P. Lau, W. T. Wong, F. Y. Kwong, *RSC Adv.* **2013**, *3*, 12518-12539.

[84] W. Zhu, D. Ma, *Org. Lett.* **2006**, *8*, 261-263.

[85] C. Kleeberg, L. Dang, Z. Lin, T. B. Marder, *Angew. Chem. Int. Ed.* **2009**, *48*, 5350-5354; *Angew. Chem.* **2009**, *121*, 5454-5458.

[86] S. K. Bose, T. B. Marder, *Org. Lett.* **2014**, *16*, 4562-4565.

[87] S. K. Bose, A. Deißenberger, A. Eichhorn, P. G. Steel, Z. Lin, T. B. Marder, *Angew. Chem. Int. Ed.* **2015**, *54*, 11843-11847; *Angew. Chem.* **2015**, *127*, 12009-12014.

[88] T. Yoshida, L. Ilies, E. Nakamura, *ACS Catal.* **2017**, *7*, 3199-3203.

[89] W. Yao, H. Fang, S. Peng, H. Wen, L. Zhang, A. Hu, Z. Huang, *Organometallics* **2016**, *35*, 1559-1564.

[90] P. K. Verma, S. Mandal, K. Geetharani, *ACS Catal.* **2018**, *8*, 4049-4054.

[91] V. Lillo, A. Bonet, E. Fernández, *Dalton Trans.* **2009**, 2899-2908.

[92] K. Semba, T. Fujihara, J. Terao, Y. Tsuji, *Tetrahedron* **2015**, *71*, 2183-2197.

[93] V. Ritleng, M. Henrion, M. J. Chetcuti, *ACS Catal.* **2016**, *6*, 890-906.

[94] K. Kubota, H. Iwamoto, H. Ito, *Org. Biomol. Chem.* **2017**, *15*, 285-300.

[95] H. Yoshida, *ACS Catal.* **2016**, *6*, 1799-1811.

[96] J. V. Obligacion, P. J. Chirik, *Nat. Rev. Chem.* **2018**, *2*, 15-34.

[97] D. Hemming, R. Fritzemeier, S. A. Westcott, W. L. Santos, P. G. Steel, *Chem. Soc. Rev.* **2018**, *47*, 7477-7494.

[98] T. Schaub, C. Döring, U. Radius, *Dalton Trans.* **2007**, 1993-2002.

[99] T. Schaub, M. Backes, U. Radius, *Chem. Commun.* **2007**, 2037-2039.

[100] T. Zell, M. Feierabend, B. Halfter, U. Radius, *J. Organomet. Chem.* **2011**, *696*, 1380-1387.

[101] T. Schaub, P. Fischer, T. Meins, U. Radius, *Eur. J. Inorg. Chem.* **2011**, *2011*, 3122-3126.

[102] T. Zell, U. Radius, *Z. Anorg. Allg. Chem.* **2011**, *637*, 1858-1862.

[103] T. Zell, P. Fischer, D. Schmidt, U. Radius, *Organometallics* **2012**, *31*, 5065-5073.

[104] T. Zell, U. Radius, *Z. Anorg. Allg. Chem.* **2013**, *639*, 334-339.

[105] T. Schaub, M. Backes, U. Radius, *Organometallics* **2006**, *25*, 4196-4206.

[106] T. Schaub, M. Backes, O. Plietzsch, U. Radius, *Dalton Trans.* **2009**, 7071-7079.

[107] T. Zell, T. Schaub, K. Radacki, U. Radius, *Dalton Trans.* **2011**, *40*, 1852-1854.

[108] C. Dai, G. Stringer, T. B. Marder, A. J. Scott, W. Clegg, N. C. Norman, *Inorg. Chem.* **1997**, *36*, 272-273.

[109] C. Kleeberg, C. Borner, *Organometallics* **2018**, *37*, 4136-4146.

[110] W. Drescher, C. Borner, D. J. Tindall, C. Kleeberg, *RSC Adv.* **2019**, *9*, 3900-3911.

[111] N. Miyaura, T. Yanagi, A. Suzuki, *Synth. Commun.* **1981**, *11*, 513-519.

[112] N. Miyaura, A. Suzuki, *Chem. Rev.* **1995**, *95*, 2457-2483.

[113] K.-T. Wong, Y.-Y. Chien, Y.-L. Liao, C.-C. Lin, M.-Y. Chou, M.-k. Leung, *J. Org. Chem.* **2002**, *67*, 1041-1044.

[114] T. Ishiyama, N. Miyaura, *J. Organomet. Chem.* **2003**, *680*, 3-11.

[115] N. Miyaura, *Bull. Chem. Soc. Jpn.* **2008**, 1535-1553.

[116] T. Ishiyama, Y. Itoh, T. Kitano, N. Miyaura, *Tetrahedron Lett.* **1997**, *38*, 3447-3450.

[117] M. Murata, S. Watanabe, Y. Masuda, *J. Org. Chem.* **1997**, *62*, 6458-6459.

[118] M. Murata, T. Oyama, S. Watanabe, Y. Masuda, *J. Org. Chem.* **2000**, *65*, 164-168.

[119] O. Baudoin, D. Guénard, F. Guéritte, *J. Org. Chem.* **2000**, *65*, 9268-9271.

[120] A. Fürstner, G. Seidel, *Org. Lett.* **2002**, *4*, 541-543.

[121] L. Zhu, J. Duquette, M. Zhang, *J. Org. Chem.* **2003**, *68*, 3729-3732.

[122] A. Wolan, M. Zaidlewicz, *Org. Biomol. Chem.* **2003**, *1*, 3274-3276.

[123] N. PraveenGanesh, P. Y. Chavant, *Eur. J. Org. Chem.* **2008**, *2008*, 4690-4696.

[124] W. Tang, S. Keshipeddy, Y. Zhang, X. Wei, J. Savoie, N. D. Patel, N. K. Yee, C. H. Senanayake, *Org. Lett.* **2011**, *13*, 1366-1369.

[125] W. K. Chow, C. M. So, C. P. Lau, F. Y. Kwong, *Chem. Eur. J.* **2011**, *17*, 6913-6917.

[126] G. A. Molander, S. L. J. Trice, S. D. Dreher, *J. Am. Chem. Soc.* **2010**, *132*, 17701-17703.

[127] G. A. Molander, S. L. J. Trice, S. M. Kennedy, S. D. Dreher, M. T. Tudge, *J. Am. Chem. Soc.* **2012**, *134*, 11667-11673.

[128] G. A. Molander, S. L. J. Trice, S. M. Kennedy, *J. Org. Chem.* **2012**, *77*, 8678-8688.

[129] G. A. Molander, S. L. J. Trice, S. M. Kennedy, *Org. Lett.* **2012**, *14*, 4814-4817.

[130] W. K. Chow, O. Y. Yuen, C. M. So, W. T. Wong, F. Y. Kwong, *J. Org. Chem.* **2012**, *77*, 3543-3548.

[131] H. D. S. Guerrand, L. D. Marciasini, M. Jousseaume, M. Vaultier, M. Pucheault, *Chem. Eur. J.* **2014**, *20*, 5573-5579.

[132] V. Pandarus, O. Marion, G. Gingras, F. Béland, R. Ciriminna, M. Pagliaro, *ChemCatChem* **2014**, *6*, 1340-1348.

[133] L. Xu, P. Li, *Chem. Commun.* **2015**, *51*, 5656-5659.

[134] T. Iwai, T. Harada, R. Tanaka, M. Sawamura, *Chem. Lett.* **2014**, *43*, 584-586.

[135] H. D. S. Guerrand, M. Vaultier, S. Pinet, M. Pucheault, *Adv. Synth. Catal.* **2015**, *357*, 1167-1174.

[136] T. Ishiyama, N. Miyaura, *Chem. Rec.* **2004**, *3*, 271-280.

[137] P. J. Chirik, *Acc. Chem. Res.* **2015**, *48*, 1687-1695.

[138] S. Ando, H. Matsunaga, T. Ishizuka, *J. Org. Chem.* **2015**, *80*, 9671-9681.

[139] L. Kuehn, A. F. Eichhorn, T. B. Marder, U. Radius, *J. Organomet. Chem.* **2019**, *881*, 25-33.

[140] S. Díez-González, E. C. Escudero-Adán, J. Benet-Buchholz, E. D. Stevens, A. M. Z. Slawin, S. P. Nolan, *Dalton Trans.* **2010**, *39*, 7595-7606.

[141] N. Sakai, K. Fujii, S. Nabeshima, R. Ikeda, T. Konakahara, *Chem. Commun.* **2010**, *46*, 3173-3175.

[142] M. Eck, *PhD Thesis, Julius-Maximilians-Universität Würzburg,* **2017**.

[143] N. P. Mankad, D. S. Laitar, J. P. Sadighi, *Organometallics* **2004**, *23*, 3369-3371.

[144] D. S. Laitar, P. Müller, J. P. Sadighi, *J. Am. Chem. Soc.* **2005**, *127*, 17196-17197.

[145] T. Ohishi, M. Nishiura, Z. Hou, *Angew. Chem. Int. Ed.* **2008**, *47*, 5792-5795; *Angew. Chem.* **2008**, *120*, 5876-5879.

[146] C. Kleeberg, A. G. Crawford, A. S. Batsanov, P. Hodgkinson, D. C. Apperley, M. S. Cheung, Z. Lin, T. B. Marder, *J. Org. Chem.* **2012**, *77*, 785-789.

[147] R. D. Dewhurst, E. C. Neeve, H. Braunschweig, T. B. Marder, *Chem. Commun.* **2015**, *51*, 9594-9607.

[148] P. Nguyen, C. Dai, N. J. Taylor, W. P. Power, T. B. Marder, N. L. Pickett, N. C. Norman, *Inorg. Chem.* **1995**, *34*, 4290-4291.

[149] W. Clegg, C. Dai, F. J. Lawlor, T. B. Marder, P. Nguyen, N. C. Norman, N. L. Pickett, W. P. Power, A. J. Scott, *J. Chem. Soc., Dalton Trans.* **1997**, 839-846.

[150] W. Haubold, J. Hrebicek, G. Sawitzki, *Z. Naturforsch.* **1984**, *39b*, 1027-1031.

[151] I. A. Cade, W. Y. Chau, I. Vitorica-Yrezabal, M. J. Ingleson, *Dalton Trans.* **2015**, *44*, 7506-7511.

[152] D. Curtis, M. J. Gerald Lesley, N. C. Norman, A. Guy Orpen, J. Starbuck, *J. Chem. Soc., Dalton Trans.* **1999**, 1687-1694.

[153] T. B. Marder, N. C. Norman, A. Guy Orpen, M. J. Quayle, C. R. Rice, *J. Chem. Soc., Dalton Trans.* **1999**, 2127-2132.

[154] M. Gao, S. B. Thorpe, W. L. Santos, *Org. Lett.* **2009**, *11*, 3478-3481.

[155] M. Gao, S. B. Thorpe, C. Kleeberg, C. Slebodnick, T. B. Marder, W. L. Santos, *J. Org. Chem.* **2011**, *76*, 3997-4007.

[156] S. B. Thorpe, X. Guo, W. L. Santos, *Chem. Commun.* **2011**, *47*, 424-426.

[157] K.-s. Lee, A. R. Zhugralin, A. H. Hoveyda, *J. Am. Chem. Soc.* **2009**, *131*, 7253-7255.

[158] K.-s. Lee, A. R. Zhugralin, A. H. Hoveyda, *J. Am. Chem. Soc.* **2010**, *132*, 12766-12766.

[159] S. Pietsch, U. Paul, I. A. Cade, M. J. Ingleson, U. Radius, T. B. Marder, *Chem. Eur. J.* **2015**, *21*, 9018-9021.

[160] M. Eck, S. Würtemberger-Pietsch, A. Eichhorn, J. H. J. Berthel, R. Bertermann, U. S. D. Paul, H. Schneider, A. Friedrich, C. Kleeberg, U. Radius, T. B. Marder, *Dalton Trans.* **2017**, *46*, 3661-3680.

[161] P. Nguyen, G. Lesley, N. J. Taylor, T. B. Marder, N. L. Pickett, W. Clegg, M. R. J. Elsegood, N. C. Norman, *Inorg. Chem.* **1994**, *33*, 4623-4624.

[162] S.-H. Ueng, A. Solovyev, X. Yuan, S. J. Geib, L. Fensterbank, E. Lacôte, M. Malacria, M. Newcomb, J. C. Walton, D. P. Curran, *J. Am. Chem. Soc.* **2009**, *131*, 11256-11262.

[163] J. C. Walton, M. M. Brahmi, L. Fensterbank, E. Lacôte, M. Malacria, Q. Chu, S.-H. Ueng, A. Solovyev, D. P. Curran, *J. Am. Chem. Soc.* **2010**, *132*, 2350-2358.

[164] M.-A. Tehfe, M. Makhlouf Brahmi, J.-P. Fouassier, D. P. Curran, M. Malacria, L. Fensterbank, E. Lacôte, J. Lalevée, *Macromolecules* **2010**, *43*, 2261-2267.

[165] M.-A. Tehfe, J. Monot, M. M. Brahmi, H. Bonin-Dubarle, D. P. Curran, M. Malacria, L. Fensterbank, E. Lacôte, J. Lalevée, J.-P. Fouassier, *Polym. Chem.* **2011**, *2*, 625-631.

[166] M.-A. Tehfe, J. Monot, M. Malacria, L. Fensterbank, J.-P. Fouassier, D. P. Curran, E. Lacôte, J. Lalevée, *ACS Macro Lett.* **2012**, *1*, 92-95.

[167] J. Lalevée, S. Telitel, M. A. Tehfe, J. P. Fouassier, D. P. Curran, E. Lacôte, *Angew. Chem. Int. Ed.* **2012**, *51*, 5958-5961; *Angew. Chem.* **2012**, *124*, 6060-6063.

[168] S. Telitel, S. Schweizer, F. Morlet-Savary, B. Graff, T. Tschamber, N. Blanchard, J. P. Fouassier, M. Lelli, E. Lacôte, J. Lalevée, *Macromolecules* **2013**, *46*, 43-48.

[169] S. Würtemberger-Pietsch, H. Schneider, T. B. Marder, U. Radius, *Chem. Eur. J.* **2016**, *22*, 13032-13036.

[170] G. D. Frey, J. D. Masuda, B. Donnadieu, G. Bertrand, *Angew. Chem. Int. Ed.* **2010**, *49*, 9444-9447; *Angew.Chem.* **2010**, *122*, 9634–9637.

[171] A. F. Eichhorn, S. Fuchs, M. Flock, T. B. Marder, U. Radius, *Angew. Chem. Int. Ed.* **2017**, *56*, 10209-10213; *Angew. Chem.* **2017**, *129*, 10343-10347.

[172] A. F. Eichhorn, L. Kuehn, T. B. Marder, U. Radius, *Chem. Commun.* **2017**, *53*, 11694-11696.

[173] W. Clegg, A. J. Scott, F. E. S. Souza, T. B. Marder, *Acta Cryst.* **1999**, *C55*, 1885-1888.

[174] J. Zhang, H.-H. Wu, J. Zhang, *Eur. J. Org. Chem.* **2013**, *2013*, 6263-6266.

[175] S. Würtemberger-Pietsch, *PhD Thesis, Julius-Maximilians-Universität Würzburg,* **2016**.

[176] L. L. Cao, D. W. Stephan, *Organometallics* **2017**, *36*, 3163-3170.

[177] S. Yanagisawa, K. Ueda, T. Taniguchi, K. Itami, *Org. Lett.* **2008**, *10*, 4673-4676.

[178] G. Deng, K. Ueda, S. Yanagisawa, K. Itami, C.-J. Li, *Chem. Eur. J.* **2009**, *15*, 333-337.

[179] D. J. Brauer, H. Bürger, G. Pawelke, W. Weuter, J. Wilke, *J. Organomet. Chem.* **1987**, *329*, 293-304.

[180] W. E. Piers, S. C. Bourke, K. D. Conroy, *Angew. Chem. Int. Ed.* **2005**, *44*, 5016-5036; *Angew. Chem.* **2005**, *117*, 5142-5163.

[181] O. J. Metters, A. M. Chapman, A. P. M. Robertson, C. H. Woodall, P. J. Gates, D. F. Wass, I. Manners, *Chem. Commun.* **2014**, *50*, 12146-12149.

[182] C. Ollivier, P. Renaud, *Chem. Rev.* **2001**, *101*, 3415-3434.

[183] T. Ramnial, I. McKenzie, B. Gorodetsky, E. M. W. Tsang, J. A. C. Clyburne, *Chem. Commun.* **2004**, 1054-1055.

[184] G. Yan, D. Huang, X. Wu, *Adv. Synth. Catal.* **2018**, *360*, 1040-1053.

[185] F. W. Friese, A. Studer, *Chem. Sci.* **2019**, *10*, 8503-8518.

[186] T. Taniguchi, *Eur. J. Org. Chem.* **2019**, *2019*, 6308-6319.

[187] K. Oshima, T. Ohmura, M. Suginome, *Chem. Commun.* **2012**, *48*, 8571-8573.

[188] T. Ohmura, Y. Morimasa, M. Suginome, *J. Am. Chem. Soc.* **2015**, *137*, 2852-2855.

[189] G. Wang, H. Zhang, J. Zhao, W. Li, J. Cao, C. Zhu, S. Li, *Angew. Chem. Int. Ed.* **2016**, *55*, 5985-5989; *Angew. Chem.* **2016**, *128*, 6089-6093.

[190] G. Wang, J. Cao, L. Gao, W. Chen, W. Huang, X. Cheng, S. Li, *J. Am. Chem. Soc.* **2017**, *139*, 3904-3910.

[191] J. Cao, G. Wang, L. Gao, X. Cheng, S. Li, *Chem. Sci.* **2018**, *9*, 3664-3671.

[192] R. Xu, G.-p. Lu, C. Cai, *New J. Chem.* **2018**, *42*, 16456-16459.

[193] L. Zhang, L. Jiao, *J. Am. Chem. Soc.* **2017**, *139*, 607-610.

[194] L. Zhang, L. Jiao, *Chem. Sci.* **2018**, *9*, 2711-2722.

[195] L. Zhang, L. Jiao, *J. Am. Chem. Soc.* **2019**, *141*, 9124-9128.

[196] S. Pinet, V. Liautard, M. Debiais, M. Pucheault, *Synthesis* **2017**, *49*, 4759-4768.

[197] W.-M. Cheng, R. Shang, B. Zhao, W.-L. Xing, Y. Fu, *Org. Lett.* **2017**, *19*, 4291-4294.

[198] A. Yoshimura, Y. Takamachi, L.-B. Han, A. Ogawa, *Chem. Eur. J.* **2015**, *21*, 13930-13933.

[199] A. Yoshimura, Y. Takamachi, K. Mihara, T. Saeki, S.-i. Kawaguchi, L.-B. Han, A. Nomoto, A. Ogawa, *Tetrahedron* **2016**, *72*, 7832-7838.

[200] Y. Cheng, C. Mück-Lichtenfeld, A. Studer, *Angew. Chem. Int. Ed.* **2018**, *57*, 16832-16836; *Angew. Chem.* **2018**, *130*, 17074-17078.

[201] Y. Cheng, C. Mück-Lichtenfeld, A. Studer, *J. Am. Chem. Soc.* **2018**, *140*, 6221-6225.

[202] P. P. Power, *Chem. Rev.* **2003**, *103*, 789-810.

[203] E. Krause, H. Polack, *Ber. Dtsch. Chem. Ges. (A and B Series)* **1926**, *59*, 777-785.

[204] T. L. Chu, T. J. Weismann, *J. Am. Chem. Soc.* **1956**, *78*, 23-26.

[205] C. D. Martin, M. Soleilhavoup, G. Bertrand, *Chem. Sci.* **2013**, *4*, 3020-3030.

[206] S. Kundu, S. Sinhababu, V. Chandrasekhar, H. W. Roesky, *Chem. Sci.* **2019**, *10*, 4727-4741.

[207] C.-W. Chiu, F. P. Gabbaï, *Angew. Chem. Int. Ed.* **2007**, *46*, 1723-1725; *Angew. Chem.* **2007**, *119*, 1753-1755.

[208] T. Matsumoto, F. P. Gabbaï, *Organometallics* **2009**, *28*, 4252-4253.

[209] P. Bissinger, H. Braunschweig, A. Damme, I. Krummenacher, A. K. Phukan, K. Radacki, S. Sugawara, *Angew. Chem. Int. Ed.* **2014**, *53*, 7360-7363; *Angew. Chem.* **2014**, *126*, 7488-7491.

[210] M. F. Silva Valverde, P. Schweyen, D. Gisinger, T. Bannenberg, M. Freytag, C. Kleeberg, M. Tamm, *Angew. Chem. Int. Ed.* **2017**, *56*, 1135-1140; *Angew. Chem.* **2017**, *129*, 1155-1160.

[211] F. Dahcheh, D. Martin, D. W. Stephan, G. Bertrand, *Angew. Chem. Int. Ed.* **2014**, *53*, 13159-13163; *Angew. Chem.* **2014**, *126*, 13375-13379.

[212] S.-H. Ueng, M. Makhlouf Brahmi, É. Derat, L. Fensterbank, E. Lacôte, M. Malacria, D. P. Curran, *J. Am. Chem. Soc.* **2008**, *130*, 10082-10083.

[213] S.-H. Ueng, L. Fensterbank, E. Lacôte, M. Malacria, D. P. Curran, *Org. Lett.* **2010**, *12*, 3002-3005.

[214] D. P. Curran, A. Solovyev, M. Makhlouf Brahmi, L. Fensterbank, M. Malacria, E. Lacôte, *Angew. Chem. Int. Ed.* **2011**, *50*, 10294-10317; *Angew. Chem*. **2011**, *123*, 10476-10500.

[215] J. C. Walton, M. M. Brahmi, J. Monot, L. Fensterbank, M. Malacria, D. P. Curran, E. Lacôte, *J. Am. Chem. Soc.* **2011**, *133*, 10312-10321.

[216] T. Watanabe, D. Hirose, D. P. Curran, T. Taniguchi, *Chem. Eur. J.* **2017**, *23*, 5404-5409.

[217] S.-C. Ren, F.-L. Zhang, J. Qi, Y.-S. Huang, A.-Q. Xu, H.-Y. Yan, Y.-F. Wang, *J. Am. Chem. Soc.* **2017**, *139*, 6050-6053.

[218] J. Qi, F.-L. Zhang, Y.-S. Huang, A.-Q. Xu, S.-C. Ren, Z.-Y. Yi, Y.-F. Wang, *Org. Lett.* **2018**, *20*, 2360-2364.

[219] J.-K. Jin, F.-L. Zhang, Q. Zhao, J.-A. Lu, Y.-F. Wang, *Org. Lett.* **2018**, *20*, 7558-7562.

[220] K. Takahashi, M. Shimoi, T. Watanabe, K. Maeda, S. J. Geib, D. P. Curran, T. Taniguchi, *Org. Lett.* **2020**, *22*, 2054-2059.

[221] Y.-S. Huang, J. Wang, W.-X. Zheng, F.-L. Zhang, Y.-J. Yu, M. Zheng, X. Zhou, Y.-F. Wang, *Chem. Commun.* **2019**, *55*, 11904-11907.

[222] S. Stoll, A. Schweiger, *J. Magn. Reson.* **2006**, *178*, 42-55.

[223] F. Furche, R. Ahlrichs, C. Hättig, W. Klopper, M. Sierka, F. T. Weigend, *WIREs Comput. Mol. Sci* **2014**, *4*, 91-100.

[224] R. Ahlrichs, M. Bär, M. Häser, H. Horn, C. Kölmel, *Chem. Phys. Lett.* **1989**, *162*, 165-169.

[225] M. Häser, R. Ahlrichs, *J. Comput. Chem.* **1989**, *10*, 104-111.

[226] O. Treutler, R. Ahlrichs, *J. Chem. Phys. C* **1995**, *102*, 346-354.

[227] M. Von Arnim, R. Ahlrichs, *J. Comput. Chem.* **1998**, *19*, 1746-1757.

[228] F. Weigend, *Phys. Chem. Chem. Phys.* **2002**, *4*, 4285-4291.

[229] M. Sierka, A. Hogekamp, R. Ahlrichs, *J. Chem. Phys.* **2003**, *118*, 9136-9148.

[230] Y. Zhao, D. G. Truhlar, *Theor. Chem. Acc.* **2008**, *120*, 215-241.

[231] A. Schäfer, H. Horn, R. Ahlrichs, *J. Chem. Phys.* **1992**, *97*, 2571-2577.

[232] A. Schäfer, C. Huber, R. Ahlrichs, *J. Chem. Phys.* **1994**, *100*, 5829-5835.

[233] K. Eichkorn, O. Treutler, H. Oehm, M. Häser, R. Ahlrichs, *Chem. Phys. Lett.* **1995**, *242*, 652-660.

[234] K. Eichkorn, F. Weigend, O. Treutler, R. Ahlrichs, *Theor. Chem. Acc.* **1997**, *97*, 119-124.

[235] F. Weigend, *Phys. Chem. Chem. Phys.* **2006**, *8*, 1057-1065.

[236] F. Weigend, R. Ahlrichs, *Phys. Chem. Chem. Phys.* **2005**, *7*, 3297-3305.

[237] P. Deglmann, K. May, F. Furche, R. Ahlrichs, *Chem. Phys. Lett.* **2004**, *384*, 103-107.

[238] D. J. Krysan, P. B. Mackenzie, *J. Org. Chem.* **1990**, *55*, 4229-4230.

[239] W. A. Herrmann, G. Gerstberger, M. Spiegler, *Organometallics* **1997**, *16*, 2209-2212.

[240] A. J. Arduengo III, S. F. Gamper, J. C. Calabrese, F. Davidson, *J. Am. Chem. Soc.* **1994**, *116*, 4391-4394.

[241] K. Öfele, W. A. Herrmann, D. Mihalios, M. Elison, E. Herdtweck, W. Scherer, J. Mink, *J. Organomet. Chem.* **1993**, *459*, 177-184.

[242] C. A. Citadelle, E. L. Nouy, F. Bisaro, A. M. Z. Slawin, C. S. J. Cazin, *Dalton Trans.* **2010**, *39*, 4489-4491.

[243] H. Braunschweig, W. C. Ewing, T. Kramer, J. D. Mattock, A. Vargas, C. Werner, *Chem. Eur. J.* **2015**, *21*, 12347-12356.

[244] G. A. Bowmaker, S. E. Boyd, J. V. Hanna, R. D. Hart, P. C. Healy, B. W. Skelton, A. H. White, *J. Chem. Soc., Dalton Trans.* **2002**, 2722-2730.

[245] K. Semba, T. Fujihara, T. Xu, J. Terao, Y. Tsuji, *Adv. Synth. Catal.* **2012**, *354*, 1542-1550.

[246] F. Graf, L. Hupfer, **1981***, DE2940709A1*.

[247] A. J. Arduengo III, **1991***, US5077414*.

[248] A. J. Arduengo III, H. V. R. Dias, R. L. Harlow, M. Kline, *J. Am. Chem. Soc.* **1992**, *114*, 5530-5534.

[249] R. Jazzar, R. D. Dewhurst, J. B. Bourg, B. Donnadieu, Y. Canac, G. Bertrand, *Angew. Chem. Int. Ed.* **2007**, *46*, 2899-2902; *Angew. Chem.* **2007**, *119*, 2957-2960.

[250] H. Braunschweig, F. Guethlein, *Angew. Chem. Int. Ed.* **2011**, *50*, 12613-12616; *Angew. Chem.* **2011**, *123*, 12821-12824.

[251] H. Braunschweig, F. Guethlein, **2013***, EP2554547A1*.

[252] C. N. Welch, S. G. Shore, *Inorg. Chem.* **1968**, *7*, 225-230.

[253] R. Brotherton, A. McCloskey, J. Boone, H. Manasevit, *J. Am. Chem. Soc.* **1960**, *82*, 6245-6248.

[254] K. O. Christe, W. W. Wilson, R. D. Wilson, R. Bau, J. A. Feng, *J. Am. Chem. Soc.* **1990**, *112*, 7619-7625.

[255] W. A. Herrmann, C. Köcher, L. J. Gooßen, G. R. Artus, *Chem. Eur. J.* **1996**, *2*, 1627-1636.

[256] J.-Y. Cho, C. N. Iverson, M. R. Smith, *J. Am. Chem. Soc.* **2000**, *122*, 12868-12869.

[257] H. Kinuta, M. Tobisu, N. Chatani, *J. Am. Chem. Soc.* **2015**, *137*, 1593-1600.

[258] W. Xie, S. Chang, *Angew. Chem. Int. Ed.* **2016**, *55*, 1876-1880; *Angew. Chem.* **2016**, *128*, 1908-1912.

[259] T. Kawamoto, A. Sato, I. Ryu, *Org. Lett.* **2014**, *16*, 2111-2113.

[260] Y. Wu, P. Y. Choy, F. Y. Kwong, *Org. Biomol. Chem.* **2014**, *12*, 6820-6823.

[261] P. W. Betteridge, J. R. Carruthers, R. I. Cooper, K. Prout, D. J. Watkin, *J. Appl. Crystallogr.* **2003**, *36*.

[262] G. M. Sheldrick, *Acta Crystallogr. Sect. A* **2008**, *64*, 112-122.

[263] L. J. Farrugia, *J. Appl. Crystallogr.* **1997**, *30*, 565-565.

[264] K. Brandenburg, Diamond (version 4.4.0) - Crystal and Molecular Structure Visualization, Crystal Impact H. Putz & K. Brandenburg GbR, Bonn (Germany), **2017**.

[265] L. J. Farrugia, *J. Appl. Crystallogr.* **1999**, *32*, 837-838.

[266] P. Van der Sluis, A. Spek, *Acta Crystallogr. Sect. A* **1990**, *46*, 194-201.